# Examining Serine Hydrolase Small Molecule Inhibitors as Regulators of Hepatitis C Virus Life Cycle

**David Lefebvre**

**A thesis submitted**
**in partial fulfillment of the requirements for the**
**Master's Degree of Science in Chemistry**

**Department of Chemistry and Biomolecular Sciences**

**Faculty of Science**

**University of Ottawa**

**Abstract**

Hepatitis C virus (HCV) is a hepatotropic positive-sense RNA virus of the Flaviviridae virus family and is a major cause of chronic liver disease worldwide. Like all obligate parasites, HCV relies on host pathways to enable its pathogenesis. HCV, in particular, has a clear link with hepatic lipid metabolism, promoting a lipid-rich environment for its proliferation. This manifests as liver steatosis in many patients harboring chronic HCV infection. Based on our recent findings regarding an immunometabolic and HCV antiviral microRNA (miRNA), miRNA-185 targeting and down regulating serine hydrolases (SH) involved in lipid and endocannabinoid metabolism, here we investigate HCV and its dependency on certain metabolic serine hydrolases involved in lipid and endocannabinoid metabolism.

Serine hydrolases are one of the largest and most diverse enzyme families. This enzyme family has emerged as a center of therapeutic potential due to its implications in many metabolic roles. Here, we demonstrate that pharmacological inhibition of metabolic serine hydrolases alpha-beta hydrolyzing domain 6 (ABHD6), carboxylesterase 1 (CES1), and monoacylglycerol lipase (MGLL), enzymes involved in the hydrolysis of the endogenous cannabinoid receptor 1 (CB1) agonist 2-arachidonoyl glycerol (2-AG) are potently antiviral against HCV. Serine hydrolase inhibition with the MGLL inhibitor MJN110 paired with endocannabinoid signaling antagonization led to additive antiviral effects against HCV and has revealed modulation of the viral pathogenic phenotype to be its key course of action. MGLL inhibitor MJN110 transcriptomic characterization revealed modulations in humoral immunity and phagocytosis and acts antiviraly against HCV independent of CB1 antagonization. This provides an avenue for future investigation, assessing the viability of CB1 antagonization, and MGLL as a key host targeted antiviral factor in affecting HCV viral life cycle.

**Statement of Work**

The work presented in this thesis is my own and I take full responsibility for its content. All experiments and analysis were prepared by me, except for the HCV JFH1$_T$ 2a infected, KT195, WWL113, and MJN110 treated HuH7.5 dose curves which were performed by Roxana Filip in chapter 2, and the 2-BP treated HuH7.5 PAFAH1B3 ABPP which was performed by Dr. Geneviève Desrochers in chapter 3.

**Acknowledgments**

Firstly, I would like to express my deepest gratitude to my principal investigator, Dr. John Pezacki for his insight, guidance, enthusiastic encouragement, and useful critiques of this research work. You have been imperative to my success as a scientist and I strive to become a better one going forward.

I would like to extend my gratitude to people who have contributed to the completion of my graduate studies. To all the members of the Pezacki lab, both past and present, thank you for the unending support you provided during my graduate studies. Specifically, I would like to thank my many in-lab mentors, Ph.D. candidate Roxana Filip, Ph.D. candidate Rhea Alonzi, Dr. Geneviève Desrochers, Dr. David Prescott, MSc. Candidate Kaitlyn Morrill, MSc. Candidate Gabriel Sullivan, Ph.D. candidate Nadine Ahmed, and Ph.D. candidate Noreen Ahmed for their endless expertise and help during my studies. To my other lab members, thank you for the help you provided me during these past few years including the many presentations I had done for developing my skills as a presenter and speaker.

I would like to also thank Dr. Cory Harris from the University of Ottawa for collaborating on this project by providing access to CB1 agonist, and synthetic cannabinoid HU210 and the necessary facilities for the use of this small molecule under current Canadian Government standards. Additionally, I would like to thank Dr. Benjamin Cravatt from the Scripps Institute for the gifting of the serine hydrolase small molecules which started this investigation.

I would also like to thank the professors who have taken part in my Thesis Advisory Committee, Drs. Cory Harris, François-Xavier Campbell-Valois and John Pezacki. All of you have provided invaluable insight and direction to my projects and were imperative to the completion of this thesis. I would also like to thank the many class professors who helped me in the advancement

of my skills as a scientist, a presenter, and a thinker during my time here at the University of Ottawa.

I wish to thank my family and friends for their support and encouragement throughout my studies. To my many Dungeons and Dragon players and friends outside the lab, the social time we spent together kept me sane. To my brother, Cory Lefebvre, you have supported me throughout my studies, struggles, and give me the motivation to strive to heights I never thought I could achieve. Thank you for being a rock in my life and for being there through the thick of it all. To my chosen family, Waylon Desnoyers, Audra Thompson, both of you have taken me into your families and without that, I would not have been able to succeed in my studies otherwise. Your encouragement and love were instrumental to my success and I do not know what I would have done without either of you. Thank you and never change!

## Table of Contents

**List of Figures**

**List of Tables**

**Table 1:** List of abbreviations

| Abbreviation | Description |
|---|---|
| 2-AG | 2-arachidonoyl glycerol |
| 2-BP | 2-bromopalmitate |
| AA | arachidonic acid |
| AADAC | arylacetamide deacetylase |
| ABHD | alpha-beta hydrolyzing-domain |
| ABHD12 | alpha/beta-Hydrolase domain containing 12 |
| ABHD6 | alpha/beta-Hydrolase domain containing 6 |
| ABPP | Activity-based protein profiling |
| AC | adenylyl cyclase |
| ACC1 | acetyl-CoA carboxylase |
| ACOT1 | acyl-CoA thioesterase 1 |
| AEA | N-arachidonoyl-ethanolamine, ananamide |
| AMPK | AMP-activated protein kinase |
| ANOVA | analysis of variance |
| cAMP | cyclic adenosine monophosphate |
| CB1 | cannabinoid receptor 1 |
| CB2 | cannabinoid receptor 2 |
| CD | circular dichroism |
| CES1 | carboxylesterase 1 |
| CHC | chronic hepatitis C |
| CLDN1 | Claudilin-1 |
| CNS | central nervous system |
| CPT1a | carnitine palmitoyltransferase |
| CPVL | carboxypeptidase vitellogenic like |
| CTSA | cathepsin A |
| Cys | cysteine |
| DAA | direct-acting antivirals |
| DHA | docosahexaenoic acid |
| EC50 | calculated half-maximal effective concentration |
| EMCV | encephalomyocarditis virus |
| Endocannabinoid | endogenously produced cannabinoid |
| EPA | eicosapentaenoic acid |
| ER | endoplasmic reticulum |
| FASN | fatty acid synthase |
| FGR | full genomic replicon |
| FP | fluorphosphonate |
| FP-Biotin | fluorophosphonate-Biotin |
| GIRK | G protein-coupled inwardly-rectifying potassium channel |
| GO | Gene Ontology |
| GPCR | G-protein coupled receptor |
| HCV | Hepatitis C virus |
| HSA | highest single agent |

| | |
|---|---|
| HSD17B14 | 17-beta-hydroxysteroid dehydrogenase 14 |
| IRES | internal ribosme entry site |
| JFH | Japanese Fulminant Hepatitis |
| MAG | monoacylglycerol |
| MAPK | mitogen-activated protein kinase |
| MGLL | monoacylglycerol lipase |
| miRNA | microRNA |
| MW | membranous web |
| ncRNA | non-coding RNA |
| NHS | N-Hydroxysuccinimidyl |
| NSP | non-structural protein |
| ORF | open reading frame |
| PAFAH1B3 | platelet-activating factor acetylhydrolase 1b catalytic subunit 3 |
| pAMPK | phosphorylated AMPK |
| PAT | protein acyl transferases |
| PDI | protein disulfide isomerase |
| PKA | protein kinase A |
| PPAR | peroxisome proliferator-activated receptor |
| PPARα | peroxisome proliferator-activated receptor alpha |
| PREP | prolyl endopeptidase |
| PRR | pattern recognition receptors |
| PTM | post-translational modification |
| PUFA | polyunsaturated fatty acids |
| RISC | RNA induced silencing complex |
| RNA-Seq | RNA sequencing |
| SCD1 | steroyl-CoA desaturase 1 |
| SGR | sub genomic replicon |
| SH | serine hydrolase |
| siRNA | silencing RNA |
| SREBP1 | sterol regulatory element-binding protein 1 |
| THC | Δ9-tetrahydrocannabinol |
| UPS | ubiquitin-proteasome system |
| UTR | untranslated regions |
| UV | Ultraviolet |
| ZIP | zero interaction potency |

# Chapter 1: General introduction

## Introduction

### 1.1 Serine Hydrolases

Serine Hydrolases (SH) are one of the largest and most diverse enzyme families containing approximately 240 members in humans[2]. Making up approximately 1% of the human proteome, many serine hydrolases have emerged as targets of therapeutic potential with key roles in blood clotting, digestion, nervous system signaling, inflammation, and cancer [3–9]. They have also been reported to play important roles in bacterial and viral life cycle progression, virulence, and drug resistance [1,10–12]. SH enzyme family members span many catalytic roles such as lipases, esterases, amidases, thioesterases, peptidases, and proteases. As a result of their broad-reaching enzymatic roles, SHs are involved in the regulation of intracellular triglyceride and cholesterol ester stores [2]. These enzymatic roles can be sub divided further into two subgroups, serine proteases (~ 125 members) and metabolic serine hydrolases (~115 members) with the latter affecting a far more diverse array of substrates and thus, are the most structurally diverse set of the two groups.

SH all function through a base-activated serine nucleophile for their cleaving activities through a covalent acyl-enzyme intermediate[13]. All serine hydrolases are united by a shared common catalytic mechanism that begins with the activation of a conserved serine nucleophile for the attack on a substrate ester/thioester/amide bond to form an acyl-enzyme intermediate, followed by water-catalyzed hydrolysis of this intermediate to liberate the product. An example of this can be seen in **Figure 1.1** with SH MGLL and 2-AG.

### 1.2 Hepatitis C virus

Hepatitis C virus (HCV) is a hepatotropic positive-sense RNA virus of the Flaviviridae virus family that causes progressive liver damage which can result in liver cirrhosis and hepatocellular carcinoma[14]. It is estimated around 130 to 170 million people are infected worldwide with this

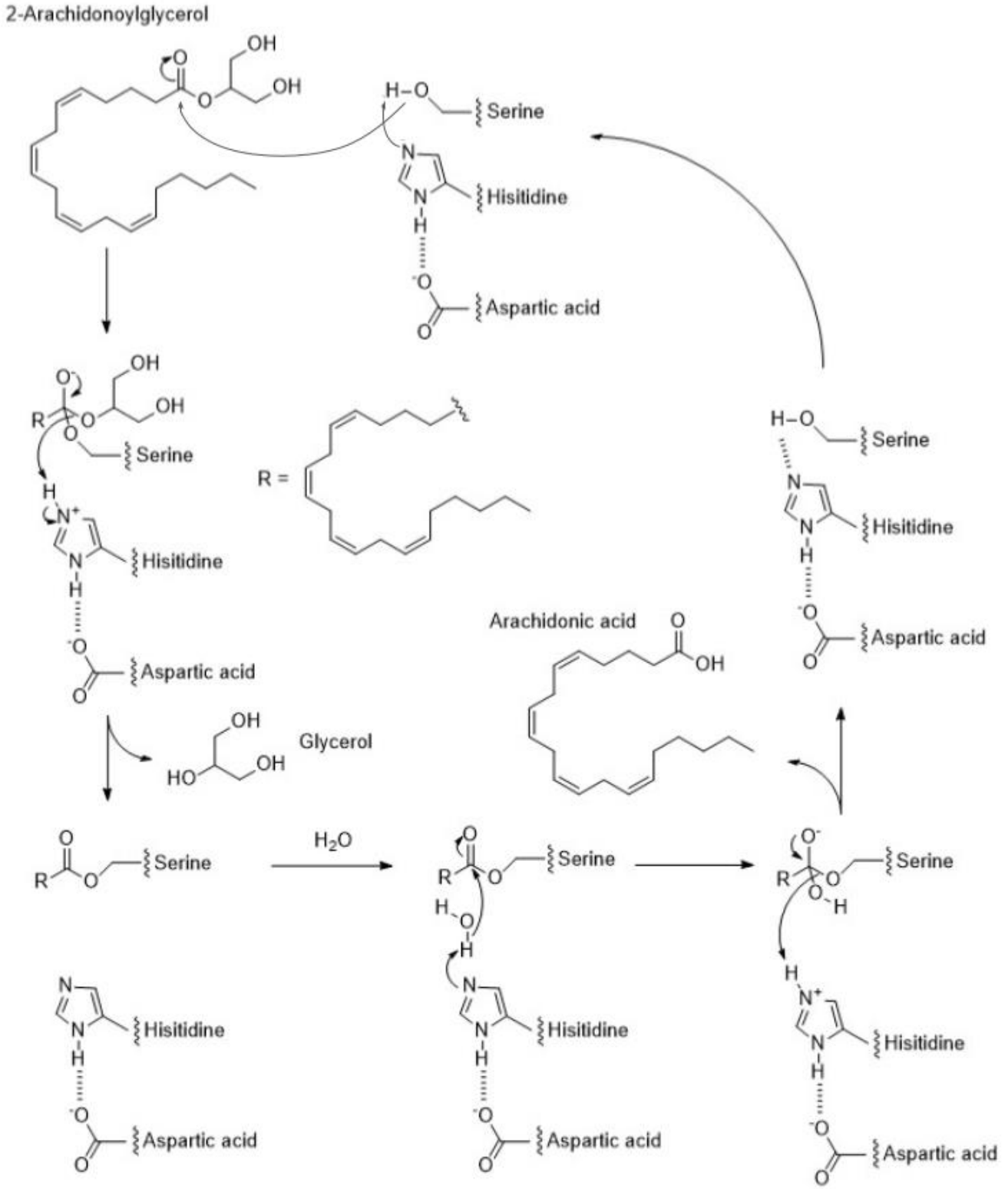


**Figure 1.1: Catalytic triad/processing of 2-AG by serine hydrolase MGLL**
First, the enzyme's activated nucleophilic serine attacks the carbonyl of 2-AG to form a covalently linked acyl-enzyme intermediate and release its first product, glycerol. This intermediate is then attacked by the activated nucleophilic hydroxyl of water, which result in hydrolysis of the substrate, release of the second product, arachidonic acid from the enzyme active site and regeneration of the nucleophilic serine for further catalysis. Adapted from Simon et al., 2010.

pathogen[15]. Of those acutely infected 80% progress to persistent infection which can result in this aforementioned liver cirrhosis and hepatocellular carcinoma[16]. To date, there is no effective vaccine, however, cocktails of direct-acting antivirals (DAAs) show promise as effective therapeutics[17]. DAAs are a class of drugs that inhibit specific portions of the HCV viral life cycle by targeting essential viral proteins necessary for viral life cycle progression. Current DAAs on the market target the HCV non-structural proteins NS3/4a protease, NS5A replication complex assembler, and the NS5b RNA dependant RNA polymerase (RdRp) [18,19]. Though current DAAs are widely available for HCV, other classes of DAAs targeting other disease-causing viruses remain elusive and demand further discovery.

### 1.2.1 HCV genome and lifecycle

HCV has an RNA genome of 9.6 kilobases in size flanked by 5‘- and 3’-untranslated regions (UTRs). The HCV genome encodes a polyprotein-coding open reading frame (ORF) encoding structural proteins at the N-terminus and non-structural proteins (NSPs) at the C terminus of the genome. The HCV encoded polyprotein is co-transcriptionally and post-translational processed by cellular and viral proteases to form its three structural proteins (core, E1, and E2), an ion channel (p7), and six NSPs (NS2, NS3a, NS4A, NS4B, NS5A, and NS5B) (**Figure 1.2 A**)[20]. HCV is a non-lytic virus that infects cells, replicates inside them using host and viral factors then gets released into the extracellular matrix without disrupting cell integrity[21]. The HCV life cycle can be generally divided into 4 steps: (1) virus entry; (2) genome translation and polyprotein processing; (3) genome replication, and (4) particle assembly and release from the host cell (**Figure 1.2 B**)[20,22,23]. HCV, in particular, has a clear link with hepatic lipid metabolism, promoting a lipid-rich environment; forming endoplasmic reticulum (ER) localized membranous webs (MWs) that contain the sites of viral replication and assembly for the virus. MWs also serve a protective role against cytoplasmic pattern recognition receptors (PRRs) preventing activation of cellular innate immune responses as well [24–27]. Many patients harboring chronic HCV infection

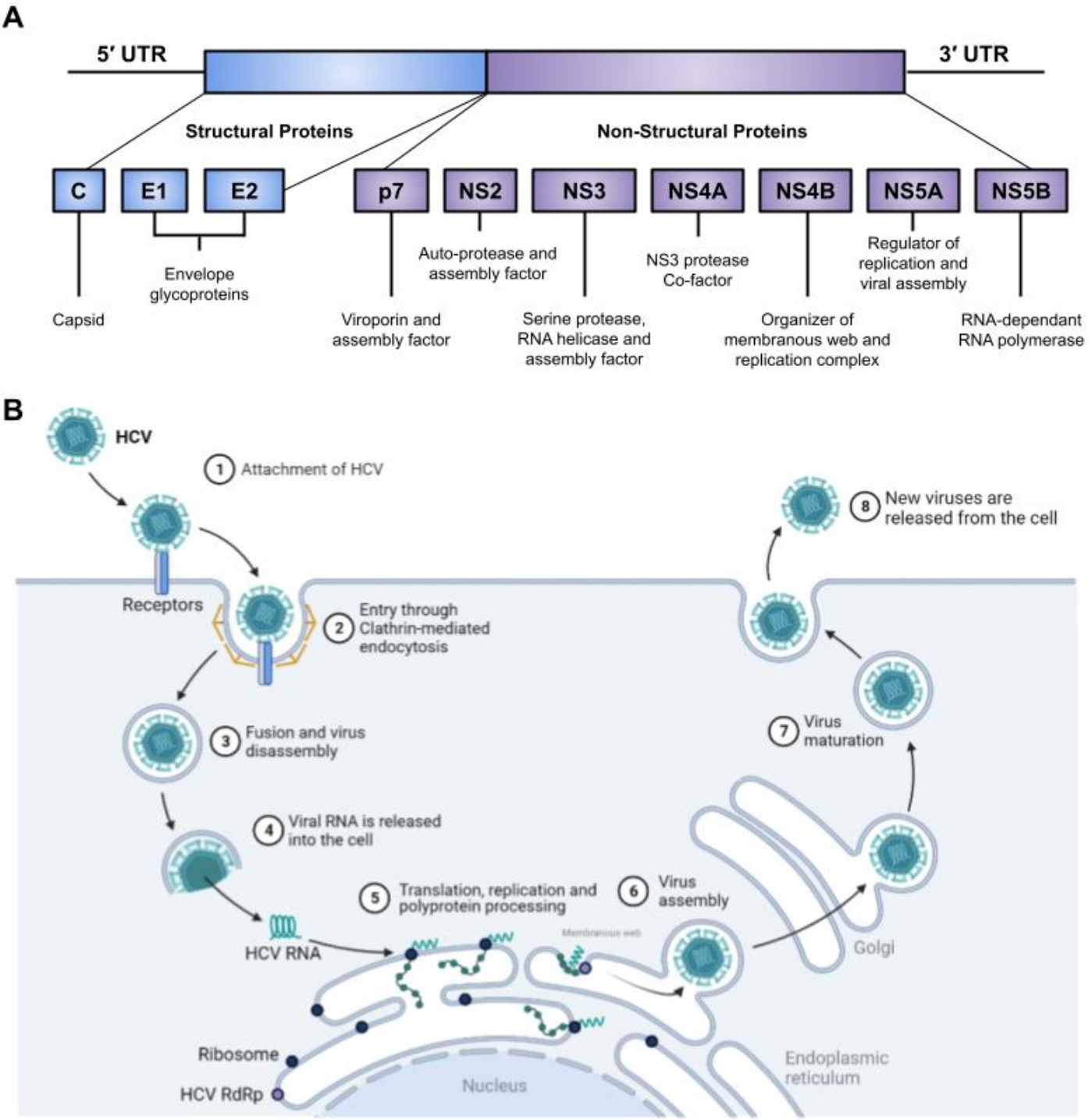


**Figure 1.2: HCV genome and viral life cycle**

(A) The HCV genome, flanked by 5-prime and 3-prime untranslated regions consists of is three structural proteins, core, Envelope proteins 1 and 2 (E1, E2), an ion channel, p7 and six non-structural proteins, NS2, NS3a, NS4A, NS4B, NS5A, and NS5B. Their associated roles in the HCV viral life cycle are outlined below. (B) HCV lipo viral particles interact with cell surface receptors (1) and initiates the entry process through clathrin-mediated endocytosis (2). After pH-dependant fusion and uncoating (3), the released HCV genomic RNA (4) is translated, and copied in ER-derived membranous webs (5). Core protein is transferred from cytoplasmic lipid droplets to form nucleocaspids that when assisted with NS5A, are loaded with replication complex associated HCV genomic RNA (6). HCV virion morphogenesis is linked with the VLDL secretory pathway (7) and ultimately form lipo viral particles for non-lytic release of further nascent infection (8). Adapted from Scheel et al., 2013

of some particular genotypes often manifest liver steatosis as a result of chronic infection. The virus itself is heterogenous and has been classified into 7 different genotypes so far, differing by as much as 33% over the whole viral genome [28].

### 1.2.2 HCV models

Recently, Harvey J. Alter, Michael Houghton, and Charles M. Rice were all jointly awarded the 2020 Nobel Prize in Physiology or Medicine for the discovery of Hepatitis C virus [29]. After the identification of HCV as the causative agent of non-A or non-B hepatitis in 1989 [30], advances in HCV was stunted by the inability to achieve efficient nascent viral replication for study [15]. Initial attempts to culture HCV in immortalized cell lines and primary hepatocytes resulted in low levels of viral replication. It was not until 10 years later that an efficient HuH-7 cell culture system that is based on the transfection of cloned viral consensus genome sequences was developed derived from a genotype 1b HCV consensus isolate. [31]. Since then, many HCV replicon systems have been developed to investigate HCV further. Bicistronic constructs were created containing an HCV internal ribosomal entry site (IRES) driving neomycin resistance gene (G418) and an encephalomyocarditis virus (EMCV) IRES driving HCV protein expression. This was incorporated successfully into HuH-7 cells encoding rather the full genomic replicon (FGR) or the sub-genomic replicon (SGR) [31,32]. Further work in HCV characterization led to the development of HuH-7.5 cells [33]. HuH-7.5 cells are more permissive to HCV infection due to a mutation in the cytosolic dsRNA sensor, RIG-I [34]. RIG-I lacking cells allow HCV to bypass the cellular innate immune response during infection. Compared to the replicon systems that are representative of HCV replication; advancements in assessing the full HCV viral life cycle were initially stunted. It was not until characterization of a Japanese fulminant hepatitis (JFH) genotype 2a HCV isolate that the full HCV virus life cycle could be assessed The $JFH1_T$ 2astrain was determined to be the first clinical isolate to replicate without replication enhancing mutations and recapitulate the entire HCV lifecycle in HuH7 cells[35, 36,37]. In my work, we utilized

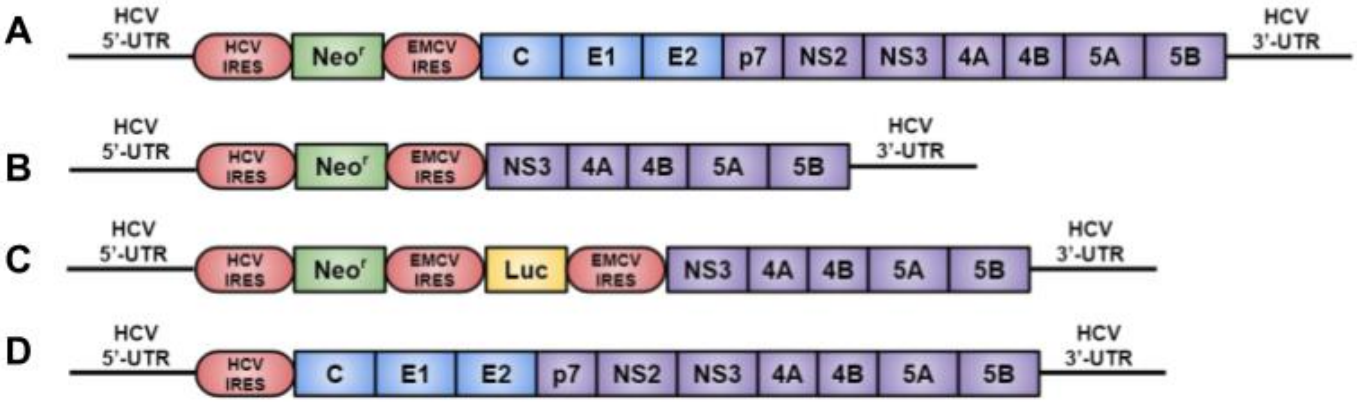


**Figure 1.3: HCV models**
The HuH7-SGR-Luc cell line (C) was derived from human hepatoma cells, HuH7s. The full genomic replicon HuH7.5-FGR (A) encodes all HCV structural (blue) and non-structural (purple) proteins. Sub-genomic replicons HuH7-SGR (B), HuH7-SGR-Luc (C) encodes non-structural proteins necessary to form the replication complex. HuH7-SGR-Luc encodes a luciferase enzyme (yellow) for quantification of replicon levels. This replicon also contains the EMCV IRES (red) and neomycin resistance (green) to ensure stable selection of the autonomously expressing HCV-cell lines. The full genomic model, HCV $JFH1_T$ 2a (D) is a fully infectious model of the virus and is not-stably expressed within hepatoma cells. Adapted from Singaravelu et al., 2014.

two models to assess the viability of SH small-molecule inhibition in the context of HCV: the HuH7-SGR-Luc model which reports on replicon levels through a constitutively expressed luciferase reporter in addition to the full HCV $JFH1_T$ 2a genotype which reports on the full virus lifecycle from entry to release (**Figure 1.3**) [15].

### 1.3 The cannabinoid system

The CB1 receptor is one of the most abundant GPCR in the central nervous system (CNS) and is involved in an array of different pathophysiological functions such as emotion, cognition, energy balance, pain sensation, and neuro-inflammation [38,39]. GPCRs are the largest family of signaling proteins. Structurally, most GPCRs contain an extracellular N-terminus, seven trans-membrane spanning α-helices, an intracellular C-terminus, and variable extracellular and intracellular elements [40]. GPCRs have been divided into 6 classes with class A, rhodopsin-like receptors being the most common. Class A GPCRs have a ligand-binding pocket between the seven helices, which could be either close to the extracellular surface or buried almost to half the depth of the anchored membrane [41]. CB1, a type-A GPCR though highly abundant in the mammalian human brain, is also present at much lower, but functionally relevant levels in many peripheral tissues and is involved in metabolism, including in adipose tissue, liver, skeletal muscle, and the pancreatic tissues [42].

#### 1.3.1 CB1 discovery

The plant *Cannabis sativa,* better known as marijuana, had its first reported uses as a medicinal plant tracing back to ancient China around 5000 years ago, where it was used as a cramp and pain relief agent [43]. The widely-documented uses of marijuana include anti-nociception, anti-inflammation, anticonvulsant, anti-emetic, as well as recreational use, which has largely limited its medical application [43]. It was not until approximately 50 years ago that the main psychoactive component of *Cannabis Sativa*, Δ9-tetrahydrocannabinol (THC) was identified among ~70 other

phytocannabinoids [42]. This discovery led to the generation of many synthetic cannabinoids which ultimately resulted in the subsequent identification and cloning of the GPCR CB1 [39,44,45]. Many other GPCRs, ion channels, and nuclear receptors have since been reported to interact with cannabinoids. This includes the aforementioned CB2, GPCR55, GPCR18, and GPCR119 [46–49].

### 1.3.2 Peripheral CB1

CB1 has been implicated in the pathogenesis of several metabolic diseases such as alcoholic and metabolic steatosis, liver fibrogenesis, insulin resistance, and non-alcoholic fatty liver disease; all a result of peripheral enhancement of CB1 [50]. Recent findings relate the alleviation of hepatic steatosis through the down-regulation of lipid droplet binding protein perilipin 2 (PLIN2) [51]. Pharmacological agonisation and antagonization of CB1 resulted also in the induction and reduction of PLIN2 respectively revealing a new signaling association between CB1 and PLIN2 perhaps [51]. Overall, this suggests that selective targeting of peripheral CB1 and/or peripheral specific CB1 ligands may be an efficient therapeutic strategy for the management of NAFLD and other metabolic diseases [50]. This was recently confirmed with the development of AM6545, an orally bioavailable CB1 antagonist with limited brain penetrance which demonstrated a reversal of steatosis as well as improved dyslipidemia and glycemic control [52]. In parallel, CB1 antagonists have also been shown to be novel and potent inhibitors of HCV, due to the virus' heavy link with hepatic lipid metabolism [53].

### 1.3.3 CB1 signaling

CB1's link to lipid metabolism lies within its downstream signaling. CB1 antagonization is known to inhibit heterotrimeric G-protein recruitment to the CB1 receptor. Demonstrated with CB1 antagonist Rimonabant, inhibition of G-protein $G\alpha_{i/o}$ enables adenylyl cyclase activity which increases cyclic adenosine monophosphate (cAMP) stores. This, in turn, activates protein

kinase A (PKA) which is responsible for LXRα inhibitor phosphorylation and activation of liver kinase B1 (LKB1), a key upstream kinase of AMP-activated protein kinase (AMPK) [54]. All this taken together activates AMPK, a master regulator of cellular homeostasis.

AMPK is a heterotrimeric complex evolved to sense low cellular ATP levels. A key regulator of both lipid and glucose metabolism, several factors lead to AMPK activation: mitochondrial poisons, oxygen or glucose starvation, low ATP: AMP ratios, as well as exercise. AMPK activation leads to the rewiring of cellular metabolism to decrease anabolic processes involving ATP consumption and increase catabolic processes that create ATP to restore the cell to a more favorable energy state. During AMPK activation processes such as fatty acid and sterol synthesis, ribosome biogenesis, protein translation, glycogen storage, and gluconeogenesis are all subsequently down-regulated while processes such as lipid β-oxidation, lipolysis, glucose uptake, glycolysis, autophagy initiation, autophagy progression, and mitochondrial biogenesis are all unregulated [55]. This highlights the importance of the development of peripheral centric CB1 antagonists for the treatment of not only metabolic diseases but now viral pathogenesis.

CB1 agonism, by comparison, results in none of the previously described antagonistic states. Instead, activation of CB1 inhibits adenylyl cyclase by coupling to the pertussis toxin (PTX)-sensitive G-protein (Gαi/o) and increases the phosphorylation of extracellular signal-regulated kinase 1/2 (pERK1/2) through G-protein dependent and β-arrestin1 dependent pathways [56]. Decrease in cAMP activates G-protein-coupled inwardly-rectifying potassium channels (GIRKs) and inhibits N-type and P/Q type voltage-gated calcium channels. This is most prevalent in neurons resulting in the inhibition of pre-synaptic neurotransmitter release. CB1 activation also leads to the phosphorylation and activation of mitogen-activated protein kinases (MAPK), such as p38 MAPK and c-Jun N-terminal kinase, which can regulate nuclear transcription. It is known that CB1 couples mainly to Gαi/o type G-proteins. However, coupling to other G-protein types under special circumstances has been also reported [56]. Interestingly, chronic CB1 agonism has

been shown to result in receptor desensitization and receptor internalization leading to a functionally antagonistic state of signaling [57–60]. The CB2 receptor appears predominantly in the CNS and immune cells with its primary role involved in immune responses [61–63].

Of the more well-characterized cannabinoid receptors, CB1, CB2, and novel cannabinoid receptors GPCR55, GPCR18, and GPCR119 [46,47], Expression Atlas gene expression data revealed only CB1 to be lowly expressed in HuH7s, the parental line to the HuH7.5s [64]. As a result, work assessing the effects of endocannabinoid metabolism was reviewed in the perspective of CB1 exclusively.

### 1.3.4 Endocannabinoids

Looking to endogenously produced cannabinoids (endocannabinoids), N-arachidonoyl-ethanolamine (AEA; anandamide) and 2-arachidonoylglycerol (2-AG) were some of the first endocannabinoids to be discovered and have been reported to serve as the endogenous agonists of the cannabinoid receptors. They remain the best-studied endocannabinoids to date and are both derivatives of arachidonic acid [42]. AEA is a high-affinity, partial agonist of CB1, and is almost inactive at CB2; whereas 2-AG acts as a full agonist at both CBRs with moderate-to-low affinity [45,65]. Canonically, though AEA and 2-AG have different receptor selectivity, both are produced in response to cellular $Ca^{2+}$ levels [66,67]. CB1 was first discovered in the brain and was found to be one of the most widely expressed GPCR [68]. Similarly, basal levels of 2-AG are approximately 1000 times larger than AEA in the brain [69].

### 1.3.5 CB1 and HCV

In peripheral tissues, CB1 is distributed in a region-specific manner [68]. Normally the expression of CB1 in the liver is very low [70]. However, under specific metabolic conditions, the expression of CB1 in several types of hepatic cells is remarkably increased. It is proposed that CB1 actively

contributes to hepatic insulin resistance, fibrosis, and lipogenesis [71]. Additionally, it is known that during HCV infection, in both a chronic hepatitis C (CHC) patient context and an *in vitro* context, there is enrichment in CB1 mRNA expression suggesting that this receptor is an HCV-inducible gene [72]. Similarly, in line with this observation, ECs are increased in plasma of patients with CHC and might reveal immunosuppressive and profibrogenic effects [73]. Due to the putative link between HCV, the cannabinoid system, and miRNA-185, we were interested in investigating this subset of endocannabinoid-altering enzymes: ABHD6, MGLL, and CES1. Serine hydrolases alpha/beta-hydrolase domain containing 6 (ABHD6), monoacylglycerol lipase (MGLL), and carboxylesterase 1 (CES1) are all metabolic serine hydrolases that have been reported to be responsible for the degradation of 2-arachidonoyl glycerol (2-AG) into arachidonic acid and glycerol in the brain (**Figure 1.1**) [74,75]. 2-AG is an endocannabinoid derived from arachidonic acid and is the primary agonist to the CB1 and CB2 receptors and is one of the most extensively studied monoacylglycerols [76–78].

### 1.4 MicroRNAs

MicroRNAs (miRNAs) are small non-protein-coding RNAs, with an average length of 22 nucleotides that post-transcriptionally regulate gene expression. A single guide strand is incorporated into the RNA-induced silencing complex (RISC) for targeting complementary RNAs. The level of complementarity between the guide and mRNA target determines which silencing mechanism will be employed; cleavage of target messenger RNA (mRNA) with subsequent degradation or translational repression [79].

#### 1.4.1 MicroRNA biogenesis

In one of our most recent reports, we demonstrated that the HCV antiviral effects observed by miRNA-185 transfection was a result of the changes observed in a subset of serine hydrolases involved in lipid and endocannabinoid metabolism, both in terms of abundance and activity as

determined through activity-based protein profiling, transcriptomics and lipidomic analyses [1]. This further cements this link between the cannabinoid system and HCV and requires further investigation.

### 1.4.2 MicroRNA function

Most studies to date have shown that miRNAs bind to a specific sequence usually at the 3' UTR of their target mRNA guided by their seed sequence, a sequence of six to eight nucleotides at the 5' end of the miRNA to induce translational repression, mRNA deadenylation and decapping [80,81]. miRNA binding to other mRNA regions have been reported, including the 5' UTR, protein-coding regions, as well as promoter regions [82]. The binding of miRNAs to 5′ UTR and coding regions have silencing effects on gene expression [83,84] while miRNA interaction with the DNA promoter region has been reported to induce transcription as well [85].

### 1.4.3 MicroRNA implications

MicroRNAs have been implicated in a diverse range of biological processes such as cellular differentiation, metabolism, immunity, and intracellular signaling [86–88]. Given the broad physiological reach of miRNAs, it is not surprising either that they play a key role in disease. Since their discovery and shift towards characterization in the literature, the link between miRNAs and disease has become increasingly established [89,90]. Often, miRNA expression patterns are tissue-specific and in many ways define the transcriptome of the cell. This was illustrated when the gene expression profile of a non-neuron cell became more like that of a neuron when the neuron-specific microRNA, miR-124 was exogenously expressed. Following along a similar train of thought, certain miRNA expression patterns could be disease-specific and hold great prognostic value as a result [90,91].

In our attempts to create a miRNA-185 like drug cocktail, we sought o characterize MGLL inhibition and CB1 antagonism co-treatment as a valid treatment regime, assessing the

downstream mRNA expression state of the cell in response to these treatments and the relative level of added inhibition during drug co-treatment. We were able to recapitulate portions of our previously reported miRNA-185 antiviral profile.

In our most recent publication, we used MGLL inhibitor MJN110 and CES1 inhibitor WWL113 to demonstrate that pharmacological inhibition of these key miRNA-185 endocannabinoid related SH targets leads to similar antiviral fates, noting their importance in the miRNA's antiviral profile.

### 1.5 Outline of work

The purpose of the work described herein was to demonstrate the use of metabolic serine hydrolase inhibitors as regulators of HCV viral life cycle. Furthermore, we also sought to investigate the viability of drug co-treatments to mimic miRNA-185's antiviral and SH targeting qualities.

First, we used irreversible small molecule inhibitors KT195, WWL113, and MJN110 for the pharmacological inhibition of ABHD6, CES1, and MGLL respectively, and tested these small molecules as antiviral treatments in two different HCV models; a replication model using the HuH7-SGR-Luc replicon system and a full viral lifecycle model using the HCV JFH1T 2a genotype virus. Anti-viral dose-response curves were determined of metabolic serine hydrolase inhibitor-treated replicon and infected hepatoma cells.

Secondly, the effectiveness of CB1 antagonization with AM251 was assessed in the two previously mentioned HCV models. HU210 was also used in testing an agonist-induced desensitization hypothesis of the CB1 receptor leading to HCV antiviral effects in both previously mentioned HCV models. Anti-viral dose-response curves were similarly determined.

It was discovered the downstream CB1 phosphorylation profiles of MGLL inhibitor MJN110 did not match the antagonistic, or functionally antagonistic kinomic profiles of AM251 and HU210 induced CB1 signaling respectively. As a result, to further delineate the antiviral action of MJN110, we sought to compare the transcriptomes of MJN110 and AM251 treated hepatocytes and discovered these molecules were antiviral through independent routes suggesting MJN110's antiviral course of action is independent of CB1 antagonization.

We initially assessed the effectiveness of serine hydrolase inhibitor cocktails to mimic the HCV antiviral effects of miRNA-185 but found drug co-treatment with MGLL inhibitor MJN110 and CB1 antagonistic AM251 to reveal additive HCV antiviral effects when used together. Gene

expression changes in response to MJN110:AM251 drug co-treatment was assessed and compared to the established miRNA-185 antiviral targeting profile.

Throughout this study, MGLL degradation was observed in our work by MGLL small molecule inhibitor MJN110 and thus was more thoroughly investigated.

Lastly, we assessed the dependency of proper lipidation on serine hydrolase abundance and activity through the use of a broad palmitoylation inhibitor, 2-bromopalmitate (2-BP) using activity-based protein profiling (ABPP) with fluorophosphonate-Biotin (FP-Biotin).

## 1.6 References


1. Filip R, Desrochers GF, Lefebvre DM, et al. Profiling of microRNA targets using activity-based protein profiling: linking enzyme activity to microRNA-185 function. *Cell Chem Biol*. 2021. doi:10.1016/j.chembiol.2020.12.009
2. Long JZ, Cravatt BF. The metabolic serine hydrolases and their functions in mammalian physiology and disease. *Chem Rev*. 2011. doi:10.1021/cr200075y
3. Davie EW, Ratnoff OD. Waterfall sequence for intrinsic blood clotting. *Science (80- )*. 1964. doi:10.1126/science.145.3638.1310
4. Whitcomb DC, Lowe ME. Human pancreatic digestive enzymes. *Dig Dis Sci*. 2007;52.
5. Lane RM, Potkin SG, Enz A. Targeting acetylcholinesterase and butyrylcholinesterase in dementia. *Int J Neuropsychopharmacol*. 2006;9.
6. Bonventre J V. Reduced fertility and postischaemic brain injury in mice deficient in cytosolic phospholipase A2. *Nature*. 1997;390.
7. Menendez JA, Lupu R. Fatty acid synthase and the lipogenic phenotype in cancer pathogenesis. *Nat Rev Cancer*. 2007;7.
8. Simon GM, Cravatt BF. Activity-based proteomics of enzyme superfamilies: Serine hydrolases as a case study. *J Biol Chem*. 2010. doi:10.1074/jbc.R109.097600
9. Nomura DK. Monoacylglycerol lipase regulates a fatty acid network that promotes cancer pathogenesis. *Cell*. 2010;140.
10. Steuber H, Hilgenfeld R. Recent advances in targeting viral proteases for the discovery of novel antivirals. *Curr Top Med Chem*. 2010;10.
11. White MJ. The HtrA-like serine protease PepD interacts with and modulates the Mycobacterium tuberculosis 35-kDa antigen outer envelope protein. *PLoS One*. 2011;6.
12. Damblon C. The catalytic mechanism of β-lactamases: NMR titration of an active-site lysine residue of the TEM-1 enzyme. *Proc Natl Acad Sci USA*. 1996;93.
13. Bachovchin DA, Cravatt BF. The pharmacological landscape and therapeutic potential of serine hydrolases. *Nat Rev Drug Discov*. 2012. doi:10.1038/nrd3620
14. Lavanchy D. Evolving epidemiology of hepatitis C virus. *Clin Microbiol Infect*. 2011;17(2). doi:10.1111/j.1469-0691.2010.03432.x
15. Lohmann V, Bartenschlager R. On the history of hepatitis C virus cell culture systems. *J Med Chem*. 2014;57(5). doi:10.1021/jm401401n
16. Hoofnagle JH. Course and outcome of hepatitis C. In: *Hepatology*. Vol 36. ; 2002. doi:10.1053/jhep.2002.36227
17. Jazwinski AB, Muir AJ. Direct-acting antiviral medications for chronic hepatitis C virus infection. *Gastroenterol Hepatol*. 2011;7(3).
18. Vermehren J, Park JS, Jacobson IM, Zeuzem S. Challenges and perspectives of direct antivirals for the treatment of hepatitis C virus infection. *J Hepatol*. 2018;69(5). doi:10.1016/j.jhep.2018.07.002
19. Asselah T, Boyer N, Saadoun D, Martinot-Peignoux M, Marcellin P. Direct-acting antivirals for the treatment of hepatitis C virus infection: Optimizing current IFN-free treatment and future perspectives. *Liver Int*. 2016;36. doi:10.1111/liv.13027
20. Manns MP, Buti M, Gane E, et al. Hepatitis C virus infection. *Nat Rev Dis Prim*. 2017;3(1):17006. doi:10.1038/nrdp.2017.6
21. Kim CW, Chang KM. Hepatitis C virus: virology and life cycle. *Clin Mol Hepatol*. 2013;19(1). doi:10.3350/cmh.2013.19.1.17
22. Gerold G, Pietschmann T. The HCV life cycle: In vitro tissue culture systems and therapeutic targets. *Dig Dis*. 2014;32(5). doi:10.1159/000360830
23. Scheel TKH, Rice CM. Understanding the hepatitis C virus life cycle paves the way for highly effective therapies. *Nat Med*. 2013;19(7). doi:10.1038/nm.3248

24. Popescu CI, Riva L, Vlaicu O, Farhat R, Rouillé Y, Dubuisson J. Hepatitis C virus life cycle and lipid metabolism. *Biology (Basel)*. 2014;3(4). doi:10.3390/biology3040892
25. Hofmann S, Krajewski M, Scherer C, et al. Complex lipid metabolic remodeling is required for efficient hepatitis C virus replication. *Biochim Biophys Acta - Mol Cell Biol Lipids*. 2018;1863(9). doi:10.1016/j.bbalip.2018.06.002
26. Bassendine MF, Sheridan DA, Bridge SH, Felmlee DJ, Neely RDG. Lipids and HCV. *Semin Immunopathol*. 2013;35(1). doi:10.1007/s00281-012-0356-2
27. Neufeldt CJ, Joyce MA, Van Buuren N, et al. The Hepatitis C Virus-Induced Membranous Web and Associated Nuclear Transport Machinery Limit Access of Pattern Recognition Receptors to Viral Replication Sites. *PLoS Pathog*. 2016;12(2). doi:10.1371/journal.ppat.1005428
28. Zein NN. Clinical significance of hepatitis C virus genotypes. *Clin Microbiol Rev*. 2000;13(2). doi:10.1128/CMR.13.2.223-235.2000
29. The Nobel Assembly at Karolinska Institutet. Press release: The Nobel Prize in Physiology or Medicine 2020. Nobelförsamlingen: The Nobel Assembly at Karolinska Institutet. https://www.nobelprize.org/prizes/medicine/2020/press-release/. Accessed July 10, 2021.
30. Choo QL, Kuo G, Weiner AJ, Overby LR, Bradley DW, Houghton M. Isolation of a cDNA clone derived from a blood-borne non-A, non-B viral hepatitis genome. *Science (80- )*. 1989;244(4902). doi:10.1126/science.2523562
31. Lohmann V, Körner F, Koch JO, Herian U, Theilmann L, Bartenschlager R. Replication of subgenomic hepatitis C virus RNAs in a hepatoma cell line. *Science (80- )*. 1999;285(5424). doi:10.1126/science.285.5424.110
32. Blight KJ, Kolykhalov AA, Rice CM. Efficient initiation of HCV RNA replication in cell culture. *Science (80- )*. 2000;290(5498). doi:10.1126/science.290.5498.1972
33. Blight KJ, McKeating JA, Rice CM. Highly Permissive Cell Lines for Subgenomic and Genomic Hepatitis C Virus RNA Replication. *J Virol*. 2002;76(24). doi:10.1128/jvi.76.24.13001-13014.2002
34. Sumpter R, Loo Y-M, Foy E, et al. Regulating Intracellular Antiviral Defense and Permissiveness to Hepatitis C Virus RNA Replication through a Cellular RNA Helicase, RIG-I. *J Virol*. 2005;79(5). doi:10.1128/jvi.79.5.2689-2699.2005
35. Kato T, Furusaka A, Miyamoto M, et al. Sequence analysis of hepatitis C virus isolated from a fulminant hepatitis patient. *J Med Virol*. 2001;64(3). doi:10.1002/jmv.1055
36. Kato T, Date T, Miyamoto M, et al. Efficient Replication of the Genotype 2a Hepatitis C Virus Subgenomic Replicon. *Gastroenterology*. 2003;125(6). doi:10.1053/j.gastro.2003.09.023
37. Wakita T, Pietschmann T, Kato T, et al. Production of infectious hepatitis C virus in tissue culture from a cloned viral genome. *Nat Med*. 2005;11(7). doi:10.1038/nm1268
38. Herkenham M, Lynn AB, Little MD, et al. Cannabinoid receptor localization in brain. *Proc Natl Acad Sci U S A*. 1990;87(5). doi:10.1073/pnas.87.5.1932
39. Devane WA, Dysarz FA, Johnson MR, Melvin LS, Howlett AC. Determination and characterization of a cannabinoid receptor in rat brain. *Mol Pharmacol*. 1988;34(5).
40. Gurevich V V., Gurevich E V. GPCR signaling regulation: The role of GRKs and arrestins. *Front Pharmacol*. 2019;10(FEB). doi:10.3389/fphar.2019.00125
41. Fredriksson R, Lagerström MC, Lundin LG, Schiöth HB. The G-protein-coupled receptors in the human genome form five main families. Phylogenetic analysis, paralogon groups, and fingerprints. *Mol Pharmacol*. 2003;63(6). doi:10.1124/mol.63.6.1256
42. Pacher P, Bátkai S, Kunos G. The endocannabinoid system as an emerging target of pharmacotherapy. *Pharmacol Rev*. 2006. doi:10.1124/pr.58.3.2
43. Pertwee RG. Cannabinoid pharmacology: The first 66 years. *Br J Pharmacol*. 2006;147(SUPPL. 1). doi:10.1038/sj.bjp.0706406

44. Matsuda LA, Lolait SJ, Brownstein MJ, Young AC, Bonner TI. Structure of a cannabinoid receptor and functional expression of the cloned cDNA. *Nature*. 1990;346(6284). doi:10.1038/346561a0
45. Pertwee RG, Howlett AC, Abood ME, et al. Cannabinoid Receptors and Their Ligands : Beyond CB 1 and CB 2. *Pharmacol Rev*. 2010;62(4).
46. Brown AJ. Novel cannabinoid receptors. *Br J Pharmacol*. 2007;152(5). doi:10.1038/sj.bjp.0707481
47. McHugh D, Hu SSJ, Rimmerman N, et al. N-arachidonoyl glycine, an abundant endogenous lipid, potently drives directed cellular migration through GPR18, the putative abnormal cannabidiol receptor. *BMC Neurosci*. 2010;11. doi:10.1186/1471-2202-11-44
48. Munro S, Thomas KL, Abu-Shaar M. Molecular characterization of a peripheral receptor for cannabinoids. *Nature*. 1993;365(6441). doi:10.1038/365061a0
49. Kano M, Ohno-Shosaku T, Hashimotodani Y, Uchigashima M, Watanabe M. Endocannabinoid-mediated control of synaptic transmission. *Physiol Rev*. 2009;89(1). doi:10.1152/physrev.00019.2008
50. Mallat A, Teixeira-Clerc F, Deveaux V, Manin S, Lotersztajn S. The endocannabinoid system as a key mediator during liver diseases: New insights and therapeutic openings. *Br J Pharmacol*. 2011;163(7). doi:10.1111/j.1476-5381.2011.01397.x
51. Irungbam K, Churin Y, Matono T, et al. Cannabinoid receptor 1 knockout alleviates hepatic steatosis by downregulating perilipin 2. *Lab Investig*. 2020;100(3). doi:10.1038/s41374-019-0327-5
52. Cluny NL, Vemuri VK, Chambers AP, et al. A novel peripherally restricted cannabinoid receptor antagonist, AM6545, reduces food intake and body weight, but does not cause malaise, in rodents. *Br J Pharmacol*. 2010;161(3). doi:10.1111/j.1476-5381.2010.00908.x
53. Shahidi M, Tay ESE, Read SA, et al. Endocannabinoid CB1 antagonists inhibit hepatitis C virus production, Providing a novel class of antiviral host-targeting agents. *J Gen Virol*. 2014. doi:10.1099/vir.0.067231-0
54. Wu HM, Yang YM, Kim SG. Rimonabant, a CB1 Inverse Agonist, Inhibits Hepatocyte Lipogenesis by Activating LKB1 and AMPK Axis Downstream of G{alpha}i/o Inhibition 2137. *MolPharmacol*. 2011;(1521-0111 (Electronic)).
55. Herzig S, Shaw RJ. AMPK: Guardian of metabolism and mitochondrial homeostasis. *Nat Rev Mol Cell Biol*. 2018;19(2). doi:10.1038/nrm.2017.95
56. Al-Zoubi R, Morales P, Reggio PH. Structural insights into cb1 receptor biased signaling. *Int J Mol Sci*. 2019;20(8). doi:10.3390/ijms20081837
57. Schlosburg JE, Blankman JL, Long JZ, et al. Chronic monoacylglycerol lipase blockade causes functional antagonism of the endocannabinoid system. *Nat Neurosci*. 2010. doi:10.1038/nn.2616
58. Ibsen MS, Finlay DB, Patel M, Javitch JA, Glass M, Grimsey NL. Cannabinoid CB1 and CB2 receptor-mediated arrestin translocation: Species, subtype, and agonist-dependence. *Front Pharmacol*. 2019;10(APR). doi:10.3389/fphar.2019.00350
59. Hsieh C, Brown S, Derleth C, Mackie K. Internalization and recycling of the CB1 cannabinoid receptor. *J Neurochem*. 1999;73(2). doi:10.1046/j.1471-4159.1999.0730493.x
60. Wu DF, Yang LQ, Goschke A, et al. Role of receptor internalization in the agonist-induced desensitization of cannabinoid type 1 receptors. *J Neurochem*. 2008;104(4). doi:10.1111/j.1471-4159.2007.05063.x
61. S. Onaivi E. Commentary: Functional Neuronal CB2 Cannabinoid Receptors in the CNS. *Curr Neuropharmacol*. 2011;9(1). doi:10.2174/157015911795017416
62. Atwood BK, Straiker A, MacKie K. CB2 cannabinoid receptors inhibit synaptic transmission when expressed in cultured autaptic neurons. *Neuropharmacology*. 2012;63(4). doi:10.1016/j.neuropharm.2012.04.024

63. Cabral G. A. G-TL. Emerging Role of the CB2 Cannabinoid Receptor in Immune Regulation and Therapeutic Prospects. *Expert Rev Mol Med*. 2009;11(804).
64. Barretina J, Caponigro G, Stransky N, et al. The Cancer Cell Line Encyclopedia enables predictive modelling of anticancer drug sensitivity. *Nature*. 2012;483(7391). doi:10.1038/nature11003
65. Di Marzo V, De Petrocellis L. Why do cannabinoid receptors have more than one endogenous ligand? *Philos Trans R Soc B Biol Sci*. 2012;367(1607). doi:10.1098/rstb.2011.0382
66. Castillo PE, Younts TJ, Chávez AE, Hashimotodani Y. Endocannabinoid Signaling and Synaptic Function. *Neuron*. 2012;76(1). doi:10.1016/j.neuron.2012.09.020
67. Katona I, Freund TF. Endocannabinoid signaling as a synaptic circuit breaker in neurological disease. *Nat Med*. 2008;14(9). doi:10.1038/nm.f.1869
68. Mackie K. Distribution of cannabinoid receptors in the central and peripheral nervous system. *Handb Exp Pharmacol*. 2005;168. doi:10.1007/3-540-26573-2_10
69. Buczynski MW, Parsons LH. Quantification of brain endocannabinoid levels: Methods, interpretations and pitfalls. *Br J Pharmacol*. 2010;160(3). doi:10.1111/j.1476-5381.2010.00787.x
70. Miller LK, Devi LA. The highs and lows of cannabinoid receptor expression in disease: Mechanisms and their therapeutic implications. *Pharmacol Rev*. 2011;63(3). doi:10.1124/pr.110.003491
71. Maccarrone M, Bab I, Bíró T, et al. Endocannabinoid signaling at the periphery: 50 years after THC. *Trends Pharmacol Sci*. 2015;36(5). doi:10.1016/j.tips.2015.02.008
72. van der Poorten D, Shahidi M, Tay E, et al. Hepatitis C virus induces the cannabinoid receptor 1. *PLoS One*. 2010;5(9). doi:10.1371/journal.pone.0012841
73. Patsenker E, Sachse P, Chicca A, et al. Elevated levels of endocannabinoids in chronic hepatitis c may modulate cellular immune response and hepatic stellate cell activation. *Int J Mol Sci*. 2015. doi:10.3390/ijms16047057
74. Baggelaar MP, Maccarrone M, van der Stelt M. 2-Arachidonoylglycerol: A signaling lipid with manifold actions in the brain. *Prog Lipid Res*. 2018;71. doi:10.1016/j.plipres.2018.05.002
75. Savinainen JR, Saario SM, Laitinen JT. The serine hydrolases MAGL, ABHD6 and ABHD12 as guardians of 2-arachidonoylglycerol signalling through cannabinoid receptors. *Acta Physiol*. 2012. doi:10.1111/j.1748-1716.2011.02280.x
76. Ahn K, McKinney MK, Cravatt BF. Enzymatic pathways that regulate endocannabinoid signaling in the nervous system. *Chem Rev*. 2008;108(5). doi:10.1021/cr0782067
77. Murataeva N, Straiker A, MacKie K. Parsing the players: 2-arachidonoylglycerol synthesis and degradation in the CNS. *Br J Pharmacol*. 2014;171(6). doi:10.1111/bph.12411
78. Sugiura T, Kondo S, Kishimoto S, et al. Evidence that 2-arachidonoylglycerol but not N-palmitoylethanolamine or anandamide is the physiological ligand for the cannabinoid CB2 receptor. Comparison of the agonistic activities of various cannabinoid receptor ligands in HL-60 cells. *J Biol Chem*. 2000;275(1). doi:10.1074/jbc.275.1.605
79. MacFarlane L-A, R. Murphy P. MicroRNA: Biogenesis, Function and Role in Cancer. *Curr Genomics*. 2010;11(7). doi:10.2174/138920210793175895
80. Huntzinger E, Izaurralde E. Gene silencing by microRNAs: Contributions of translational repression and mRNA decay. *Nat Rev Genet*. 2011;12(2). doi:10.1038/nrg2936
81. Ipsaro JJ, Joshua-Tor L. From guide to target: Molecular insights into eukaryotic RNA-interference machinery. *Nat Struct Mol Biol*. 2015;22(1). doi:10.1038/nsmb.2931
82. Xu W, Lucas AS, Wang Z, Liu Y. Identifying microRNA targets in different gene regions. *BMC Bioinformatics*. 2014;15. doi:10.1186/1471-2105-15-S7-S4
83. Forman JJ, Legesse-Miller A, Coller HA. A search for conserved sequences in coding regions reveals that the let-7 microRNA targets Dicer within its coding sequence. *Proc*

*Natl Acad Sci U S A*. 2008;105(39). doi:10.1073/pnas.0803230105
84. Zhang J, Zhou W, Liu Y, Liu T, Li C, Wang L. Oncogenic role of microRNA-532-5p in human colorectal cancer via targeting of the 5'UTR of RUNX3. *Oncol Lett*. 2018;15(5). doi:10.3892/ol.2018.8217
85. Dharap A, Pokrzywa C, Murali S, Pandi G, Vemuganti R. MicroRNA miR-324-3p induces promoter-mediated expression of RelA gene. *PLoS One*. 2013;8(11). doi:10.1371/journal.pone.0079467
86. Yang M, Liu W, Pellicane C, et al. Identification of miR-185 as a regulator of de novo cholesterol biosynthesis and low density lipoprotein uptake. *J Lipid Res*. 2014. doi:10.1194/jlr.M041335
87. Jonas S, Izaurralde E. Towards a molecular understanding of microRNA-mediated gene silencing. *Nat Rev Genet*. 2015;16(7). doi:10.1038/nrg3965
88. Song L, Tuan RS. MicroRNAs and cell differentiation in mammalian development. *Birth Defects Res Part C - Embryo Today Rev*. 2006;78(2). doi:10.1002/bdrc.20070
89. Ardekani AM, Naeini MM. The role of microRNAs in human diseases. *Avicenna J Med Biotechnol*. 2010;2(4).
90. Li Y, Kowdley K V. MicroRNAs in Common Human Diseases. *Genomics, Proteomics Bioinforma*. 2012;10(5). doi:10.1016/j.gpb.2012.07.005
91. Sood P, Krek A, Zavolan M, Macino G, Rajewsky N. Cell-type-specific signatures of microRNAs on target mRNA expression. *Proc Natl Acad Sci U S A*. 2006;103(8). doi:10.1073/pnas.0511045103

# Chapter 2: Examining serine hydrolase small molecule inhibitors of endocannabinoid metabolism as regulators of Hepatitis C virus life cycle

## 2.1 Introduction

### 2.1.1 Small molecule inhibition of protein targets

Small molecules inhibitors inhibit their targets according to the molecule's inherent binding and dissociative properties to the target. This is usually defined for non-covalent inhibitors with the constant Ki. The Ki inhibition constant represents a dissociation constant of the small molecule inhibitor from the enzyme target. The binding equilibrium described by Ki depends on the kinetic mechanism of inhibition. Common schemes include competitive, uncompetitive, non-competitive, and mixed inhibition which all describe how the small molecule inhibitor inhibits the enzymatic system. In competitive inhibition, the inhibitor binds only to free enzyme (E), not to the enzyme-substrate complex (ES). In uncompetitive inhibition, the inhibitor binds only to the enzyme-substrate complex and not to free enzyme. Mixed inhibition involves inhibitor binding to both free enzyme and enzyme-substrate complex with different binding constants (Ki and αKi, where $\alpha = 1+[S]/K_m$). Lastly, non-competitive inhibition is a special case of mixed inhibition where substrate binding does not affect inhibitor binding ($\alpha = 1$). Overall, Ki values only accurately report a binding constant when the kinetic mechanism is correctly identified [1].

Covalent inhibitors are another class of protein targeting ligands that can produce very specific effects with excellent biochemical and cellular potencies, even in the presence of high concentrations of endogenous completive ligand [2]. Other benefits of covalent inhibitors include a sustained duration of action, increased ligand efficiency, enhanced capability of targeting shallow binding sites previously deemed "undruggable", and increased ability to evade resistant mutations [3]. Most covalent inhibitors function through a two-step mechanism, initially forming a reversible protein-inhibitor complex and resolving into the formation of a covalent bond between the enzyme and the inhibitor. See **Scheme 2.1** below for the complete details.

**Scheme 2.1: Covalent inhibition of a protein target through a two-step mechanism**
Adapted from Strelow et al. 2017. A two-step mechanism of inhibition is described where P reflects the target protein, I is the inhibitor, P•I is the reversibly bound protein inhibitor complex, and P-I reflects the formation of a covalent bond between the target protein and inhibitor. The potency of the first reversible binding event is defined by $K_I$, and the maximum potential rate of inactivation is defined by kinact. Taken together, the $k_{inact}/K_I$ is a second-order rate constant describing the efficiency of the overall conversion of free P to the covalent P-I complex.

Though covalent inhibitors provide many benefits, they also have many reported disadvantages including covalent modification of off-target proteins, nucleic acids, or other small molecules through non-selective reaction, adverse drug responses, inappropriate levels of inhibition of enzymes where partial or short-duration inhibition is desired, the lack of some of the advantages noted above if the targeted enzyme is rapidly degraded and resynthesized [3]. This rapid degradation was observed in MGLL inhibitor MJN110 treated hepatocytes and thus was further investigated in this chapter.

### 2.1.2 The proteasome system

Proteolysis is the breakdown of proteins into smaller polypeptides or amino acids usually by cellular proteases. Proteolysis provides a mechanism of quality control during and after protein folding, an ability to rapidly respond to changing cellular stimuli, and a mechanism to modulate the pool of available amino acids at a rapid and systematic level [4,5].

### 2.1.3 Protein degradation

The majority of proteins undergo degradation through the ubiquitin-proteasome system (UPS). The UPS operates through a collection of regulated and orchestrated steps in which proteins are marked for degradation by covalent post-translational modification (PTM) with the protein ubiquitin. Ubiquitination of proteins is carried out by a cascade of three enzymes: the E1, a ubiquitin-activating enzyme, E2, responsible for transthiolation of the ubiquitin intermediate, and E3, a ubiquitin ligase that forms an iso-peptide bond between the carboxy-terminus of ubiquitin

and a lysine side chain of the target. This process is catalytically cyclic generating poly-ubiquitin chains on its target that ultimately directs it for proteasomal degradation. The eukaryotic 26S proteasome is a 2.5 MDa proteolytic complex that consists of two main subcomplexes: the 20S core particle (20S CP) and the 19S regulatory particle (19S RP). The 19S RP is responsible for substrate recognition, deubiquitination, and unfolding of the protein target. The 20S CP is responsible primarily for the protein target's degradation [4].

### 2.1.4 Degrons

A pressing question regarding intracellular proteolysis is: how are specific proteins recognized by the proteolytic machinery and degraded under specific conditions with highly characteristic degradation rates? Early work suggested that global structural features determine the metabolic stability of individual proteins. For example, mutant proteins or proteins that had incorporated amino-acid analogs during their synthesis were found to have shorter half-lives in vivo than their wild-type counterparts [6,7]. However, later analyses revealed that these correlations with gross protein properties did not generally hold true, and although abnormal proteins were frequently short-lived, this need not reflect a change in their global structure.

Most short-lived proteins are distinguished by localized structure determinants that target them to the ubiquitin-ligase machinery or directly to the proteasome. These degradation signals, or 'degrons', are usually defined as a minimal element within a protein that is sufficient for recognition and degradation by the 26S proteasome. Degrons can vary as short amino acid sequences, structural motifs within a protein, or specific and exposed amino acids (usually Lysine and arginine) [8–10]. Here in this chapter, we explore this unique method of regulation of MGLL by inhibitor MJN110.

### 2.1.5 Drug-drug interactions

Drug combination treatments have become a standard therapy for many complex diseases such as tuberculosis, malaria, HIV, and most advanced cancers [11–15]. Drug combination therapies often enable therapeutic benefits by enhancing treatment efficacy, avoiding the acquisition of mono-therapy resistance, and enabling multidrug treatment regimens at lower and physiologically relevant drug concentrations. To evaluate the pre-clinical significance of drug combination treatments, functional screening assays that probe combination effects in a dose-response matrix assay are commonly performed [16]. This led to the development of the web tool application SynergyFinder in 2017, and later on updated to SynergyFinder2.0 from the Institute for Molecular Medicine Finland (FIMM), the University of Helsinki by Ianevski et al. [16,17].

### 2.1.6 SynergyFinder 2.0

SynergyFinder2.0 is an interactive web-based application for the analysis and visualization of drug combination screening data. Since its release in 2017, SynergyFinder has become a widely used tool for both the discovery of novel synergistic drug combinations but also to better understand the mechanisms of combination treatment efficacy or resistance, especially in cancer [17]. The degree of synergy or antagonism of a drug combination is determined by comparing the observed drug combination response against the expected response, calculated using a reference model that assumes no interaction between the drugs (**Figure 2.3 A**).

### 2.1.7 Synergy models

The most commonly used reference models include the highest single agent (HSA) [18], Bliss [19], Loewe [20], and zero interaction potency (ZIP) models [21]. These models quantify the degree of synergy between a drug combination either as the excess over the maximum single dose-response (HSA), the multiplicative effect of single drugs as they act independently (Bliss), the expected response corresponding to an additive effect if the single drugs were the same compound (Loewe), and the expected response corresponding to the effect as if the single drug

did not alter the potency of each other (ZIP) [17]. A synergy score represented by δ is defined as the average access in response due to drug-drug interactions. A synergy score less than -10 between two drugs is likely to be antagonistic; a synergy score between -10 and 10 between two drugs is likely to be additive; while and a synergy score larger than 10 between two drugs is likely to be synergistic.

### 2.1.8 Microarrays

Transcriptomic technologies are used to study an organism's transcriptome, a sum of all its RNA transcripts. RNA transcripts transcribed from an organism's genome can be divided into messenger RNAs (mRNA), and non-coding RNAs (ncRNAs) [22–24]. First attempts to study the whole transcriptome began in the early 1990s, and with technological advances in the late 1990s, transcriptomics has become a widely practiced discipline [25]. To date, two contemporary techniques are widely used: microarrays, which quantify a set of predetermined sequences, and RNA sequencing (RNA-Seq), which uses high throughput sequencing to capture all RNA sequences. Measuring the expression of an organism's genes has been instrumental in the understanding of human disease, and pathogenesis. An analysis of gene expression in its entirety allows detection of broad coordinated trends which cannot be discerned normally by more targeted assays.

Microarrays use short nucleotide oligomers, known as probes, which are arrayed on a solid substrate. Transcript abundance is measured by hybridization of fluorescently labeled RNA transcripts to these probes. The intensity of fluorescence at each probe indicates the relative abundance for that probe sequence. The primary challenge with the use of microarray is that prior knowledge of the organism of interest, through the form of an annotated genome library is required. This information is essential for the generation of the many probes of the array. Transcriptomic methods require often significant computation to produce meaningful data.

## 2.2 Objective

Inspired by the broad serine hydrolase targeting aspect of microRNA-185, we sought to create a broad, serine hydrolase targeting drug co-treatment regimen as a possible antiviral cocktail against HCV. Firstly, we sought to characterize these irreversible metabolic serine hydrolase small molecule inhibitors (KT195, WWL113, and MJN110) in our two previously described HCV models. Similarly, we wanted to assess if agonism and antagonism of CB1 (HU210, and AM251) were equally antiviral against HCV in these aforementioned HCV models, perhaps relating the antiviral nature of these serine hydrolase inhibitors to CB1 functional antagonism and antagonism respectively. After this, we created broad serine hydrolase targeting inhibitor cocktail combinations with SH inhibitors ABHD6 inhibitor KT195, CES1 inhibitor WWL113, MGLL inhibitor MJN110 and AADAC inhibitor Yoshio3 under a Loewe drug distribution hypothesis to mimic the SH targeting quality of miRNA-185[20]. We observed heavy cytotoxicity in these serine hydrolase cocktails. To further understand the antiviral effects of MGLL inhibitor MJN110, we thought to investigate the transcriptome of MJN110 treated HuH7.5s and compare it to the transcriptome of CB1 antagonist AM251 treated HuH7.5s in hopes of relating MJN110's antiviral action to CB1 antagonization. We discovered however that MJN110 was, in fact, antiviral independent of CB1 antagonism and so we combined MGLL inhibitor MJN110 with CB1 antagonist AM251 since CB1 antagonism has been reported previously to be HCV antiviral, and as it targets similar SH factors to that of miRNA-185. Through SynergyFinder2.0, we sought to assess any potential synergistic effects co-treatment with these two small molecules might have against HCV. Along a similar vein, we sought to assess the gene signaling changes in response to this co-treatment, linking the observed gene changes back to the miRNA-185 antiviral profile.

Lastly, we sought to further demystify this loss in MGLL protein abundance during MGLL inhibitor MJN110 treatment in our HuH7.5s.

## 2.3 Results

### 2.3.1 Small molecule inhibition of metabolic serine hydrolases ABHD6, MGLL, and CES1 is potently antiviral against Hepatitis C Virus

Our investigation began by assessing the inhibitory effects that a subset of small molecule inhibitors may have on HCV related to miRNA-185. This set of inhibitors included the monoacylglycerol lipase (MGLL) inhibitor MJN110, alpha/beta-hydrolase domain containing 6 (ABHD6) inhibitor KT195, carboxylesterase 1 (CES1) inhibitor WWL113, arylacetamide deacetylase (AADAC) inhibitor Yoshio-3, carboxypeptidase vitellogenic like (CPVL) inhibitor ABC110, and platelet-activating factor acetylhydrolase 1b catalytic subunit 3 (PAFAH1B3) inhibitor P11, metabolic serine hydrolases with implications to HCV. MGLL inhibitor MJN110, ABHD6 inhibitor KT195, and CES1 inhibitor WWL113 demonstrated potent inhibition of HuH7-SGR-Luc replicon levels initially and as a result, were more thoroughly characterized in the HuH7-SGR-Luc HCV replicon model and the full infectious HCV $JFH1_T$ 2a model to assess any HCV antiviral dose-response relationships with these small molecule inhibitors.

Sub-genomic replicon levels of ABHD6 and CES-1 inhibitor-treated HuH7-SGR-Luc cells were measured by assessing the relative, protein normalized chemiluminescence produced from the oxidation of luciferin into oxyluciferin by firefly luciferase of the HuH7-SGR-Luc replicon (**Figure 1.3**). ABHD6 inhibitor KT195 treated HuH7-SGR-Luc demonstrated a dose-dependent decrease of replicon levels both at 24 and 72 hours of treatment with a calculated half-maximal effective concentration ($EC_{50}$) of 3.8 and 2.5 µM respectively (**Figure 2.1 A**). CES1 inhibitor WWL113 treated HuH7-SGR-Luc demonstrated a dose-dependent decrease of replicon levels both at 24 and 72 hours of treatment with a calculated $EC_{50}$ of 13.1 and 15.6 µM respectively (**Figure 2.1 B**). Conversely, CES1 inhibitor WWL113, HCV $JFH1_T$ 2a infected HuH7.5s did not demonstrate dose-dependent inhibition of HCV $JFH1_T$ 2a IRES levels (**Supplemental Figure S2.2 A)**.

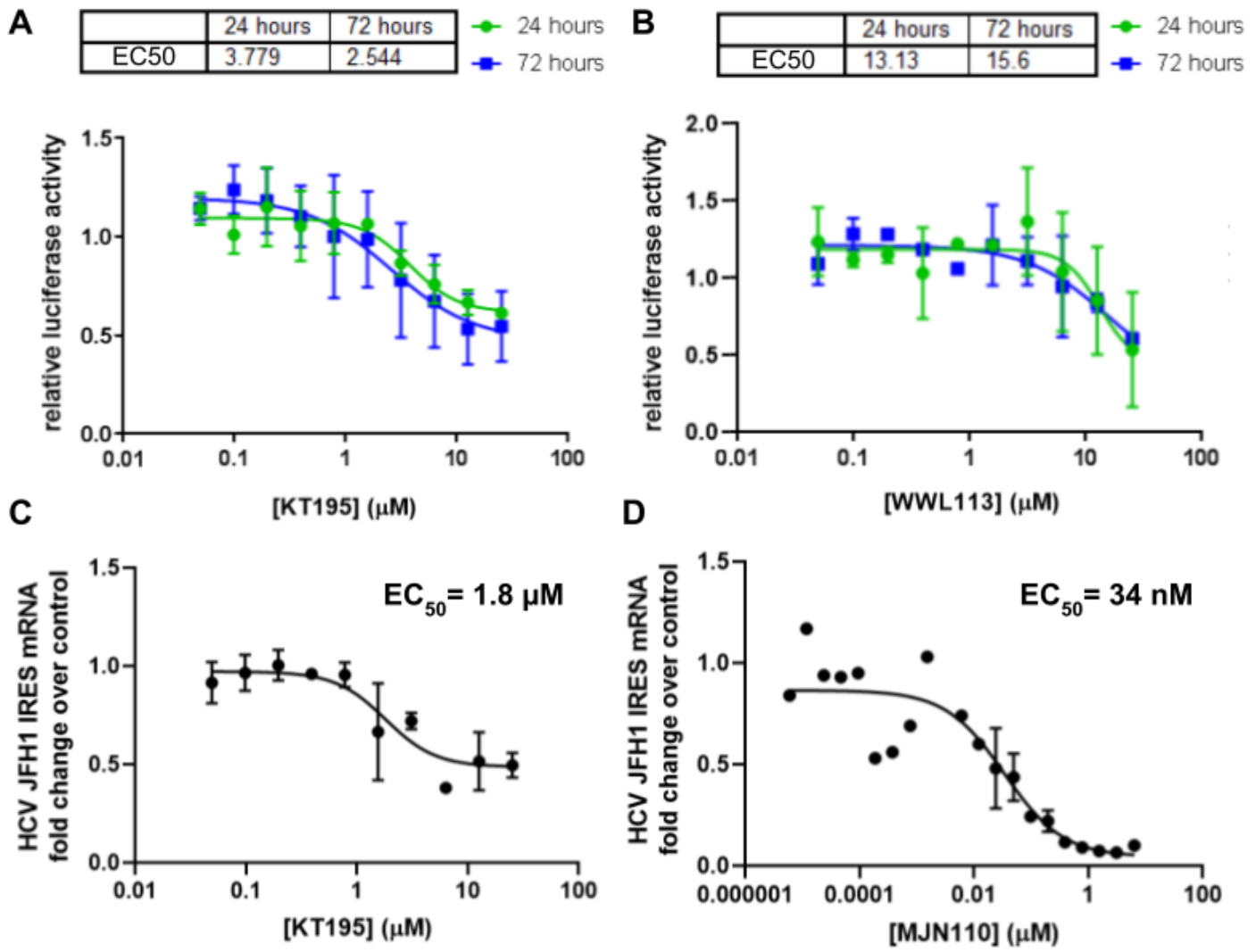


**Figure 2.1: Small molecule inhibition of metabolic serine hydrolases ABHD6, MGLL, and CES1 are potently antiviral against Hepatitis C Virus**

(A) The ABHD6 inhibitor KT195 inhibits the HCV-SGR in a dose-dependent manner with an $EC_{50}$ (half-maximal effective concentration) of 3.8 μM at 24 hours and 2.5 μM at 72 hours as measured by the protein concentration normalized firefly luciferase signal to the loading control, DMSO. Subgenomic replicon harbouring cells were seeded, 24 hours after which the medium was changed for fresh medium containing the corresponding small molecule, followed by a 24 or 72 hour incubation. n=3.

(B) The CES-1 inhibitor WWL113 inhibits the HCV-SGR in a dose-dependent manner with an $EC_{50}$ (half-maximal effective concentration) of 13.1 μM at 24 hours and 15.6 μM at 72 hours as measured by the protein concentration normalized firefly luciferase signal to the vehicle control. Subgenomic replicon harbouring cells were seeded, 24 hours after which the medium was changed for fresh medium containing the corresponding small molecule, followed by a 24 or 72 hour incubation. n=3.

(C) The ABHD6 inhibitor KT195 inhibits HCV $JFH1_T$ 2a infection in a dose-dependent manner with an $EC_{50}$ (half-maximal effective concentration) of 1.8 μM as measured by RT-qPCR of the HCV internal ribosome entry site (IRES). Cells were infected with HCV $JFH1_T$ 2a for 5 hours, after which the medium was changed for fresh medium containing the corresponding small molecule, followed by a 72 hour incubation. n=2.

(D) The MGLL inhibitor MJN110 inhibits HCV $JFH1_T$ 2a infection in a dose-dependent manner with an $EC_{50}$ (half-maximal effective concentration) of 34 nM as measured by RT-qPCR of the HCV internal ribosome entry site (IRES). Cells were infected with HCV $JFH1_T$ 2a for 5 hours, after which the medium was changed for fresh medium containing the corresponding small molecule, followed by a 72 hour incubation. n=3.

This suggests the replicative effects observed in the HuH7-SGR-Luc are not potent enough to elicit a lingering antiviral effect in the full virus model or simply, it is not effective against genotype 2 HCV. HCV RNA levels of HCV $JFH1_T$ 2a Infected ABHD6 and MGLL inhibitor-treated HuH7.5s were assessed using RT-qPCR of the HCV $JFH1_T$ 2a internal ribosome entry site (IRES) against control mRNA transcript levels. Cells were infected with HCV $JFH1_T$ 2a for 5 hours, after which the medium was changed to fresh medium containing the corresponding small molecule, followed by a 72-hour incubation. ABHD6 inhibitor KT195 treated, HCV $JFH1_T$2a infected HuH7.5s demonstrated a dose-dependent decrease of HCV $JFH1_T$ 2a IRES levels with a calculated $EC_{50}$ of 1.8 µM (**Figure 2.1 C**). MGLL inhibitor MJN110 treated, HCV $JFH1_T$ 2a infected HuH7.5s demonstrated a potent dose-dependent decrease of HCV $JFH1_T$ 2a IRES levels with a calculated $EC_{50}$ of 34 nM at 72 hours (**Figure 2.1 D**). This suggests that the MGLL inhibitor MJN110 functions not at the replication level but may have effects in other parts of the HCV life cycle such as entry, release, or assembly. Further investigation into the MGLL inhibitor MJN110 did not reveal dose-dependent effects of HCV inhibition in the HuH7-SGR-Luc replicon model suggesting this inhibitor may affect the HCV viral life cycle independent of replication or may be genotype 2a specific (**Supplemental Figure 2.2 B**).

To assess the viability of these small-molecule treatments and dose-response curves, the cytotoxicity of these small-molecule treatments was assessed. Cell viability of these small-molecule treated hepatocytes was first assessed through an MTT cell viability assay. Cell viability was assessed for 48 Hour MJN110 and KT195 treated HuH7.5s and for 72 Hour MJN110, KT195, and WWL113 treated HuH7.5s (**Supplemental figure 2.4 A-F**). Of all the small molecules, MJN110 was investigated further as its $EC_{90}$ of approximately 1 µM lay well within cell viability ranges of cell viability assays assessed (**Supplemental figure 2.4 C, F, Supplemental figure 2.5 A**).

ABHD6 inhibitor KT195, 72 hour treated HuH7.5s demonstrated a significant shift in cell viability starting at 12.5 µM treatment and higher (**Supplemental figure 2.4 A**). The chosen treatment concentration of 10 µM where we report approximately a 50 percent decrease in viral abundance in both tested models has been reported to demonstrate heavy fatty acid amide hydrolase off-targeting effects as visualized through FP-Rhodamine ABPP in rat brain homogenates [26]. As a result of its off-targeting effects at this HCV effective concentration, ABHD6 inhibitor KT195 was omitted from future studies. CES1 inhibitor WWL113's calculated $EC_{50}$ of 15.6 µM in the 72 hour treated HuH7-SGR-Luc reporter system closely resembled the calculated $LD_{50}$ of the MTT assay curve presented here of 13.6 µM (**Figure 2.1 D, Supplemental figure 2.4 B**). WWL113 did not demonstrate any dose-dependent inhibition of HCV levels in $JFH1_T$ 2a HCV infected HuH7.5s and thus was omitted from future studies (**Supplemental figure 2.2 A**).

Here we demonstrated the effectiveness of metabolic serine hydrolases ABHD6, CES1, and MGLL as key pharmacological targets for viral inhibition of HCV. Using both HCV models, the HuH7-SGR-Luc and full HCV $JFH1_T$ 2a, allowed us to further demystify what part of the HCV viral life cycle these serine hydrolases particularly affect to create these observed antiviral effects.

### 2.3.2 CB1 agonism and antagonism are potently antiviral against HCV

Of the set of metabolic serine hydrolases that demonstrated antiviral effects in the tested HCV models, ABHD6, CES1, and MGLL all serve to hydrolyze 2-AG, the primary endogenous agonist of CB1 to different extents [27]. It is hypothesized that during inhibition of these 2-AG hydrolyzing enzymes, increases in 2-AG would occur, ultimately resulting in the activation of the CB1 receptor and downstream signaling effectors such as MAPK and AMPK [28]. Chronic CB1 agonism has been shown to result in receptor desensitization and internalization [29–32]. This

signaling fate even in the presence of constant agonism leads to a functionally antagonistic state in terms of CB1 signaling. As a result, CB1 antagonist AM251 was initially acquired to mirror the effects that were hypothesized to occur during MGLL chronic administration. AM251 is a CB1 antagonist that demonstrates its HCV antiviral effects mostly through AMPK activation and modulation of lipogenesis and β-oxidation genes such as sterol regulatory element-binding protein 1 (SREBP-1), stearoyl-CoA desaturase 1 (SCD1), fatty acid synthase (FASN), peroxisome proliferator, activated receptor alpha (PPARα), and acetyl-CoA carboxylase (ACC) [33].

It has been reported previously that CB1 antagonism through administration of 10 μM AM251 is potently antiviral in a CB1 dependant manner in $JFH1_T$ 2a HCV infected HuH7s [33]. CB1 antagonist AM251 treated HuH7-SGR-Luc did not demonstrate a strong dose-dependent decrease of replicon levels after 48 hours of treatment (**Figure 2.2 A**). CB1 antagonist AM251 treated HCV $JFH1_T$ 2a infected HuH7.5s demonstrated a potent dose-dependent decrease of HCV $JFH1_T$ 2a IRES levels with a calculated $EC_{50}$ of 5.3 μM at 72 hours (**Figure 2.2 B**). To assess further whether agonism of the CB1 receptor is antiviral against HCV, CB1 agonist and synthetic cannabinoid 1,1-Dimethylheptyl- 11-hydroxy- tetrahydrocannabinol, HU210 was used.

Compared to the partial CB1 agonist THC from cannabis, HU210 is a synthetic cannabinoid and is reported to be 100 to 800 times more potent as a CB1 agonist and has an extended duration of action [34]. CB1 agonist HU210 treated HuH7-SGR-Luc cells demonstrated a dose-dependent decrease of replicon levels after 72 hours of treatment with calculated $EC_{50s}$ of 4.7 μM (**Figure 2.2 C**). CB1 agonist HU210 treated, HCV $JFH1_T$ 2a infected HuH7.5s demonstrated a potent decrease of HCV $JFH1_T$ 2a IRES levels at the high levels of treatment. A significant and potently antiviral effect was observed at 10 μM of CB1 agonist treatment (**Figure 2.2D**).

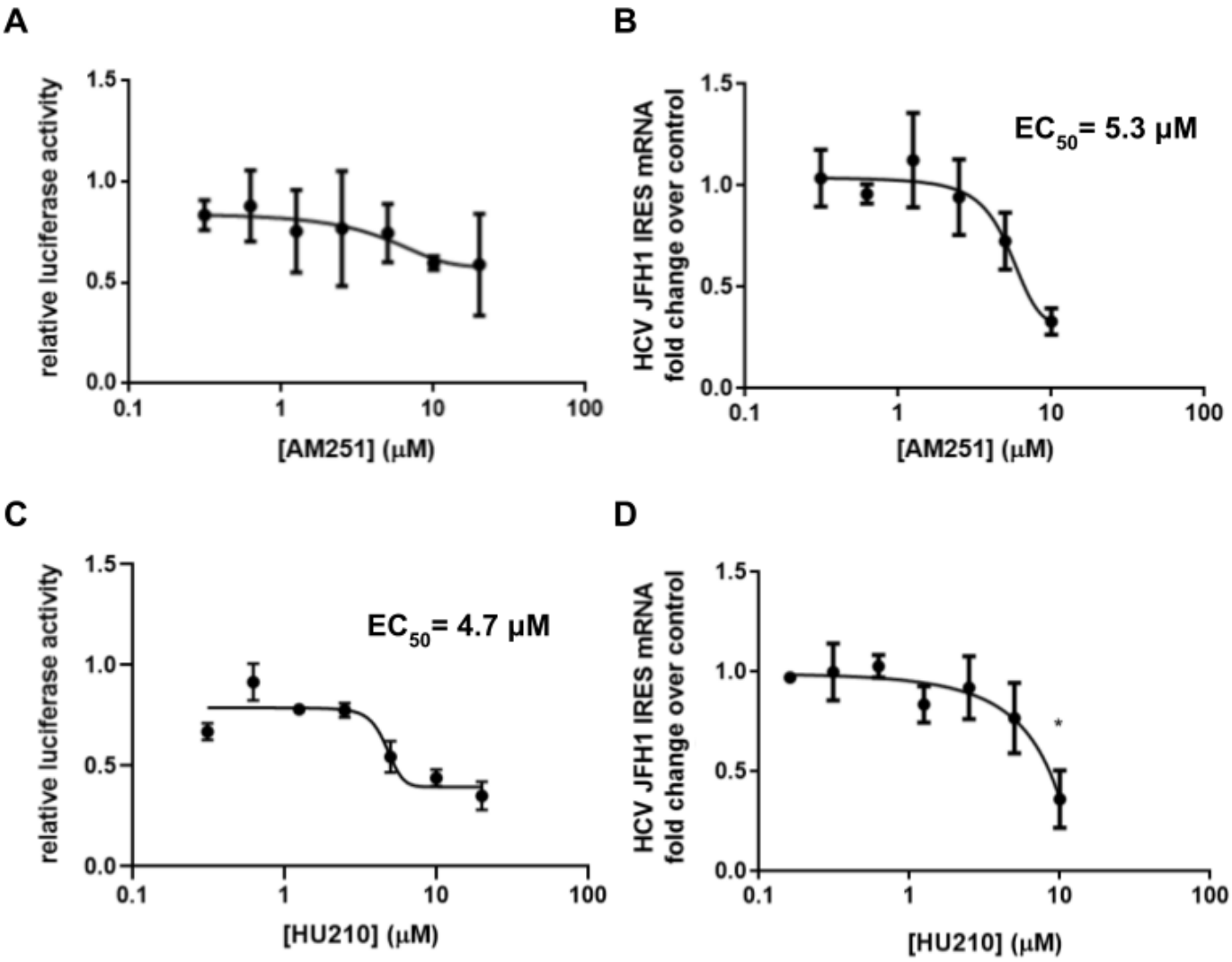


**Figure 2.2: CB1 agonism and antagonism are potently antiviral against HCV**
(A) The CB1 antagonist AM251 inhibits the HCV-SGR in a dose-dependent manner as measured by the protein concentration normalized firefly luciferase signal to the loading control, DMSO. Subgenomic replicon harbouring cells were seeded, 24 hours after which the medium was changed for fresh medium containing the corresponding small molecule, followed by a 48 hour incubation. n=3.
(B) The CB1 agonist HU210 inhibits the HCV-SGR in a dose-dependent manner with an $EC_{50}$ (half-maximal effective concentration) of 4.7 μM at 72 hours as measured by the protein concentration normalized firefly luciferase signal to the loading control, DMSO. Subgenomic replicon harbouring cells were seeded, 24 hours after which the medium was changed for fresh medium containing the corresponding small molecule, followed by a 72 hour incubation. n=2.
(C) The CB1 antagonist AM251 inhibits HCV $JFH1_T$ 2a infection in a dose-dependent manner with an $EC_{50}$ (half-maximal effective concentration) of 5.3 μM as measured by RT-qPCR of the HCV internal ribosome entry site (IRES). Cells were infected with HCV $JFH1_T$ 2a for 5 hours, after which the medium was changed for fresh medium containing the corresponding small molecule, followed by a 72 hour incubation. n=3.
(D) The CB1 agonist HU210 inhibits HCV $JFH1_T$ 2a infection as measured by RT-qPCR of the HCV internal ribosome entry site (IRES). Cells were infected with HCV $JFH1_T$ 2a for 5 hours, after which the medium was changed for fresh medium containing the corresponding small molecule, followed by a 72 hour incubation. Significant downregulation occurs at a 10 μM treatment. n=3. Significance assessed with two-tailed, unpaired student's t test, *$p < 0.05$.

This highlights CB1 agonism as an antiviral route in need of further investigation in the context of HCV.

Overall, these findings highlight the importance of the cannabinoid system as an attractive therapeutic target for HCV. Going forward, the assessment of MJN110's capacity to induce CB1 antagonism requires further assessment to identify the molecule's antiviral course of action.

### 2.3.3 MGLL inhibitor MJN110 antiviral effects are unrelated to CB1 antagonism

Initially comparing 1 µM MJN110 and 10 µM AM251 treated hepatocytes revealed differential phosphorylation profiles downstream of CB1 (Data not shown). This suggested that MJN110's antiviral capacity might not act through CB1 antagonization. To further delineate MJN110's antiviral course of action, we performed transcriptomics of 1 µM MJN110 and 10 µM AM251 treated HuH7.5s to assess global gene changes for each small molecule treatment to compare the transcriptomic profiles of each drug to each other.

siRNA mediated knock-down of MGLL mRNA expression, and pharmacological inhibition of MGLL by MJN110 led to strong antiviral responses in HCV $JFH1_T$ 2a infected HuH7.5s only after 72 hours of treatment (**Figure 2.1**) [35]. With this in mind, we assessed the broad gene expression changes that occur during MGLL inhibitor MJN110 treatment using microarray after 72 hours of treatment.

Changes in transcript abundance of 72 hour 1 µM MGLL inhibitor MJN110 treated HuH7.5s were assessed using the Affymetrix GeneChip™ Human Gene 2.0 ST Array, n = 2. Significance was assessed through analysis of variance (ANOVA) with the empirical Bayes correction using Thermofisher's Transcriptome Analysis Console Software. Significant fold changes ($p < 0.05$) less than -1.5 and greater than 1.5 are displayed (**Supplemental Table 2.9**).

Using transcriptomics, we wanted to identify key antiviral factors or modulated pathways that play a role in the observed antiviral profile during MGLL inhibitor MJN110 treatment. To do this, we performed candidate gene prioritization based on functional annotations through the ToppGene Suite [36]. ToppGene analysis of the 72 hour MJN110 treated HuH7.5 transcriptome revealed modulation in biological processes involved in gene silencing by miRNAs. These processes share the same hit list of 12 altered miRNAs with miRNA-449a and miRNA-708 having been previously related to HCV (**Table 2.1**, **Supplemental Table 2.12**) [37–39].

**Table 2.1**: Summary of GO: Molecular Function and Biological Processes of the AM251 and MJN110 transcriptomes

| Drug treatment | Incubation time (Hours) | Up or down-regulated | Altered GO: Molecular Function and Biological Processes |
|---|---|---|---|
| AM251 | 72 | Up | Amino acid transport and flux |
| | | Down | Lipid binding, lipid metabolism, lipid signaling, and sterol metabolism |
| MJN110 | 72 | Up | Gene silencing by miRNAs |
| | | Down | Gene silencing by miRNAs |
| | 24 | Up | Immunoglobulin and antigen-binding |
| | | Down | Phagocytosis, humoral immunity, complement activation, B-cell activation |

Overall, the hypothesis of MJN110 inducing changes in miRNAs did not reveal many clear avenues for further investigation. We further hypothesized that the antiviral effects observed at 72 hours could be a result of gene signaling changes that occur earlier on during treatment. Respectively, we performed a microarray analysis of 24-hour MGLL inhibitor MJN110 treated HuH7.5s (**Supplemental table 2.8**) followed by ToppGene gene ontology analysis (**Supplemental Table 2.11**). Transcriptomic changes were assessed as previously described.

ToppGene analysis of the 24 hour MJN110 treated HuH7.5s transcriptome revealed modulation in biological processes involved in immunoglobulin mediated humoral response, extracellular membrane remodeling, and olfactory pathway transduction (**Supplemental Table 2.11**). More

specifically, ToppGene analysis of all significantly down-regulated 24 hour 1 µM MGLL inhibitor MJN110 treated HuH7.5s microarray hits revealed down-regulation in GO: Biological processes such as B cell receptor signaling, phagocytosis, B cell activation, plasma membrane invagination, and classical complement activation, and humoral immunity (**Table 2.1**). MJN110 mediated negative regulation of phagocytosis and plasma membrane invagination dynamics might have implications in affecting HCV entry.

Due to MGLL's putative link to the cannabinoid system, our initial hypothesis to the observed antiviral effects was concerning a CB1 functional antagonization model due to increases in 2-AG lipid species caused by MGLL inhibition. To assess if MGLL inhibition and CB1 antagonization are related, the transcriptome of AM251 treated HuH7.5s was assessed. We performed a microarray analysis of 72-hour CB1 antagonist AM251 treated HuH7.5s (**Supplemental Table 2.10**) followed by ToppGene gene ontology analysis (**Table 2.1**, **Supplemental Table 2.13**). Transcriptomic changes were assessed as previously described.

Unsurprisingly, ToppGene analysis of all significantly down-regulated 72 hour 10 µM CB1 antagonist AM251 treated HuH7.5s microarray hits revealed down-regulation in GO: Molecular functions and Biological Processes of lipid binding, phospholipid binding, lipid transporter activity, cellular lipid metabolic processes, and steroid metabolic processes (**Table 2.1, Supplemental Table 2.13**).

Comparing the AM251 transcriptome to either MJN110 transcriptome, they shared no related ToppGene GO hits (**Table 2.1**). Similarly, comparing the AM251 transcriptome to either MJN110 transcriptome demonstrated few related significantly altered microarray hits, all seemingly unrelated to the cannabinoid system (**Figure 2.3**).

Comparison of all significantly altered microarray hits between the 72 hour treated MJN110 and AM251 transcriptomes showed six parallel transcript changes of three microRNAs:

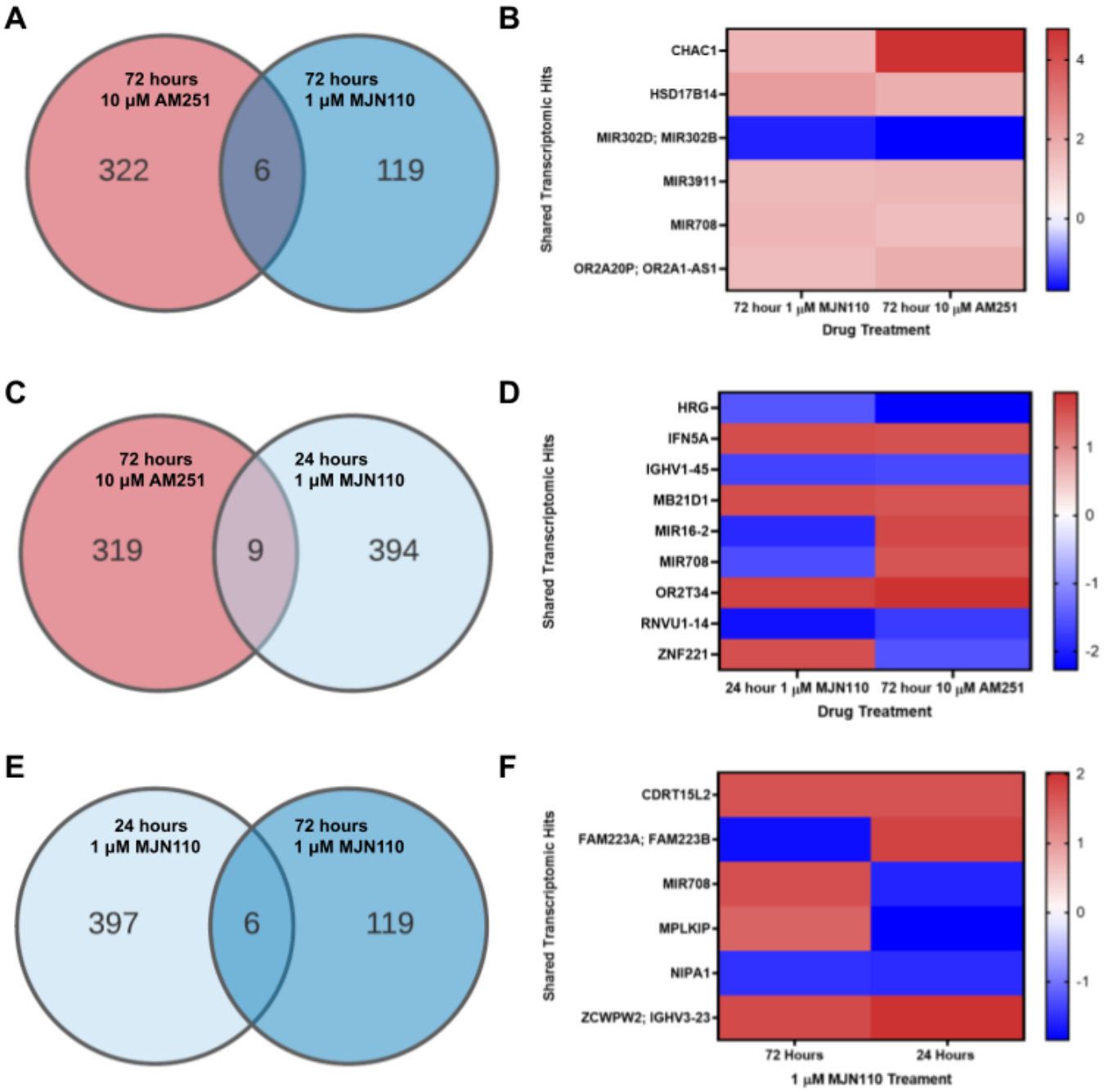


**Figure 2.3: Analysis of all shared transcriptomic hits between the MJN110 and AM251 transcriptomes demonstrate MJN110's antiviral effects are unrelated to CB1 antagonism**

All significantly up and down-regulated 1.5 fold change microarray hits of 24 and 72 hour 1 μM MJN110 treated HuH7.5s and 72 hour 10 μM AM251 treated HuH7.5s were compared.

(A) Venn diagram representing all shared transcriptomic hits between the 72 hour 10 μM AM251 treated HuH7.5 transcriptome, and the 72 hour 1 μM MJN110 treated HuH7.5 transcriptome. Fold change intensity of the related gene hits can be seen in the heat map adjacent (B).

(C) Venn diagram representing all shared transcriptomic hits between the 72 hour 10 μM AM251 treated HuH7.5 transcriptome, and the 24 hour 1 μM MJN110 treated HuH7.5 transcriptome. Fold change intensity of the related gene hits can be seen in the heat map adjacent (D).

(E) Venn diagram representing all shared transcriptomic hits between the 24 and 72 hour 1 μM MJN treated HuH7.5 transcriptomes. Fold change intensity of the related gene hits can be seen in the heat map adjacent (F).

miR302D;miR302B, miR3911, miR708, 17-beta-hydroxysteroid dehydrogenase 14 (HSD17B14) which oxidizes both estradiol and testosterone into their less bioactive steroid metabolites estrone and androstenedione, Glutathione-specific gamma-glutamylcyclotransferase 1 (CHAC1) which cleaves glutathione into 5-oxo-L-proline and a Cys-Gly dipeptide, important for apoptosis initiation and execution, and an olfactory receptor 2A1/2A42 (OR2A1-AS1) a GPCR responsible for the perception of a smell (**Figure 2.3 A, B**).

Comparison of all significantly altered microarray hits between the 24 hour treated MJN110 and 72 hour treated AM251 transcriptomes showed six parallel and three divergent transcript level changes. Parallel changes in histidine-rich glycoprotein (HRG), interferon-alpha 5 (IFN5A), immunoglobulin heavy variable 1-45 (IGHV1-45), cyclic GMP-AMP synthase (MB21D1), olfactory receptor 2T34 (OR2T34), and RNA variant U1 small nuclear 14 (RNVU1-14) transcript levels were observed, while divergent changes in two miRNAs: miR16-2, miR-708 and zinc finger protein 221 (ZNF221) transcript levels were observed (**Figure 2.3 C, D**).

Comparison between the MJN110 treated HuH7.5 transcriptomes reveals few conserved hits, suggesting dramatic transcriptomic changes throughout MJN110 treatment. Of the shared transcriptomic hits, three demonstrated parallel and three demonstrated divergent transcript level changes. Parallel changes in CMT1A duplicated region transcript 15 protein-like protein (CDRT15L2), NIPA Magnesium Transporter 1 (NIPA1), and zinc finger CW-type and PWWP domain containing 2 (ZCWPW2) transcript levels were observed, while divergent changes in FAM223A; FAM223B, miR708, and MPLKIP transcript levels were observed (**Figure 2.3 E, F**).

Overall, transcriptomic analysis of MJN110 and AM251 treated hepatocytes revealed MJN110 serves its HCV antiviral function through routes unrelated to CB1 antagonism. Additionally, the MJN110 transcriptome changes dramatically throughout MJN110 treatment and suggests early

on, MJN110 might serve its antiviral function by negatively affecting HCV viral entry through the negative regulation of genes involved in phagocytosis and plasma membrane dynamics.

### 2.3.4 MGLL inhibitor, MJN110, and CB1 antagonist, AM251, co-treatment acts additively against Hepatitis C virus

We managed to demonstrate that targeting SHs of the endocannabinoid system, CES1, and MGLL, targets of miRNA-185 recapitulated the miRNA's antiviral phenotype (**Figure 2.1 B, D**). We hypothesized, to further recapitulate the miR-185 phenotype; we could create a drug cocktail that mimics the broad SH targeting capabilities of miRNA-185. We first created a serine hydrolase irreversible small molecule inhibitor cocktail for the treatment of HCV (**Supplemental figure 2.3 A-C**). However, of all tested cocktails, few revealed promising results likely due to the broad cytotoxic effects when combining these irreversible small molecule inhibitors. So instead, we sought to combine our highest acting SH inhibitor, MGLL inhibitor MJN110 with another factor to mimic the effects of miRNA-185.

We discovered that MGLL inhibitor MJN110, our highest inhibiting SH inhibitor, serves its antiviral function independent of CB1 antagonism (**Table 2.1**, **Figure 2.3 A-F**). With this in mind, we combined MJN110 and CB1 antagonist AM251 instead to broadly target these key serine hydrolase targets. Together, these small molecules affect MGLL (through MJN110), and downstream effectors of CB1 antagonism, AMPK signaling: SREBP-1, SCD-1, FASN, PPARα (through AM251), effectors targeted similarly by miRNA-185 [35].

The degree of synergy or antagonism was determined by comparing the observed drug combination response against the expected response, calculated using a reference model that assumes no interaction between the drugs (**Figure 2.4 A**). SynergyFinder2.0 was used to assess the drug combination of MJN110 and AM251 in the context of HCV inhibition. Here we report a dose-response matrix of HCV inhibition of HCV $JFH1_T$ 2a infected, MGLL inhibitor

MJN110 and CB1 antagonist AM251 treated HuH7.5s (**Figure 2.4 B**). Inhibition of HCV $JFH1_T$ 2a was determined by RT-qPCR of the HCV IRES.

Of the most commonly used reference models: highest single agent (HSA) [18], Bliss [19], Loewe [20], and zero interaction potency (ZIP) models[21]. Here, using the HSA reference model through SynergyFinder 2.0, we calculated a synergy score of δ = 7.43 (**Figure 2.4 C, D**) for the entire plot and a calculated synergy score of the most synergistic 3-by-3 dose-response area of δ = 8.56 (MJN110: 0.01-1 µM, AM251: 2-8 µM, **Supplemental figure 2.8 C**). A synergy score is defined as the average percentage increase in response due to drug-drug interactions. Other synergy models (Loewe, Bliss, ZIP) were deemed as less representative of this drug dose-response matrix but can be found in Appendix A (**Supplemental figures 2.7-2.10**). A Loewe synergy scoring model was discarded as each drug's (MJN110 and AM251) HCV $JFH1_T$ 2a antiviral dose-response curve displayed magnitudes of difference in their respective $EC_{50}$ values, and therefore potencies, at 34 nm and 5.3 µM respectively (**Figure 2.1 D**, **Figure 2.2 B**). The Bliss and ZIP scoring models were similarly discarded as each model assumes independent drug interactions for their respective synergy calculations. The MJN110:AM251 co-treatment has 2 ways in which the drugs affect the potency of each other: firstly, MGLL inhibition leads to increases in 2-AG lipid species that might act in competition against AM251 CB1 receptor binding. Secondly, it was later discovered that AM251 administration affects MGLL mRNA transcript abundance significantly during HCV JFH1T 2a infection therefore affecting MJN110 potency.

All drug treatments within the MJN110:AM251 drug dose-response matrix demonstrate significant down-regulation of HCV viral abundance except for the 0.01 µM MJN110 treatment as determined through two-tailed, unpaired student's t-tests (**Figure 2.4 B**). Inhibition

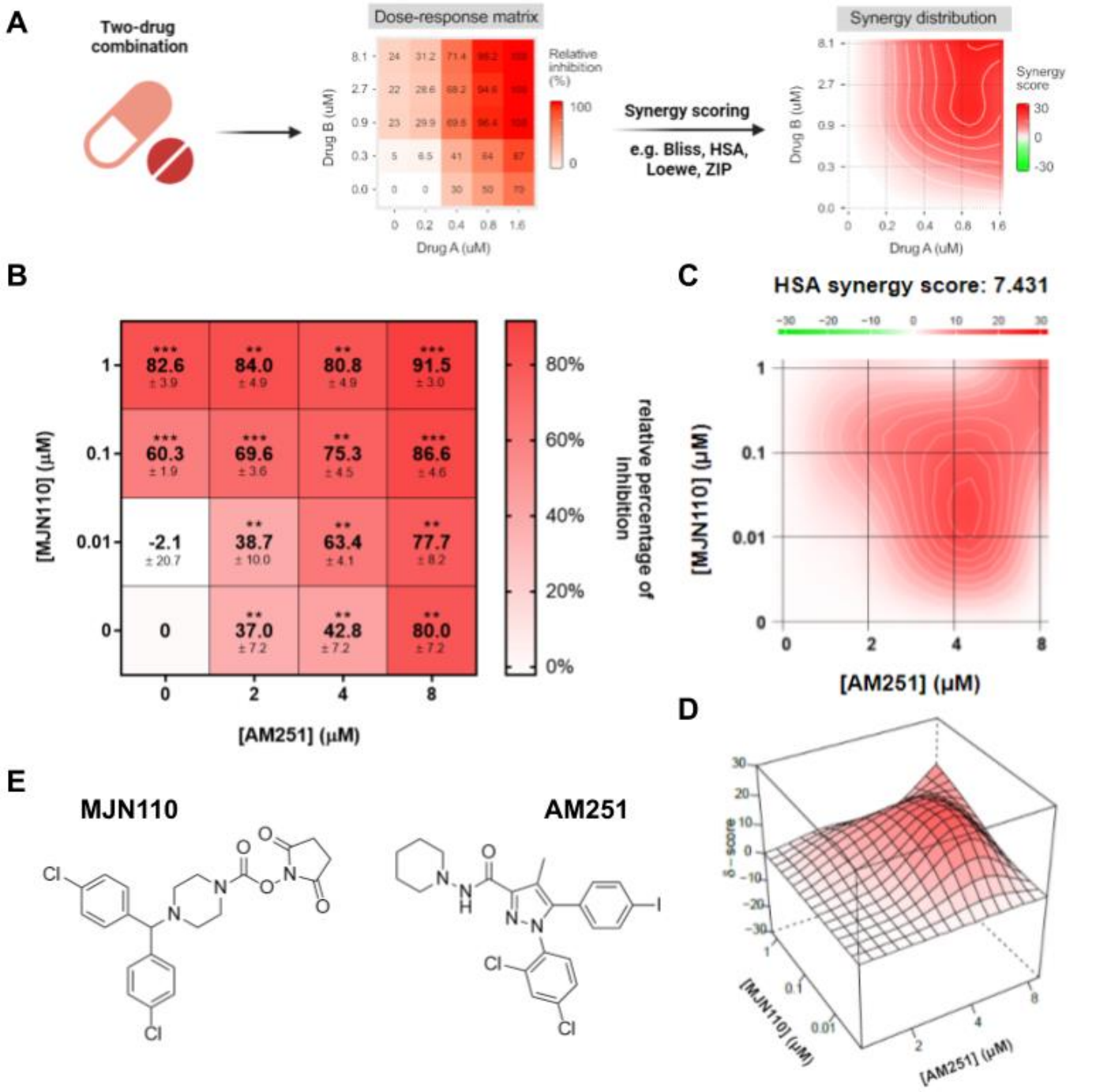


**Figure 2.4: MGLL inhibitor, MJN110, CB1 antagonist, AM251, co-treatment acts additively against HCV**
(A) Workflow for Synergy Finder 2.0 analysis from data collection to analysis for a two drug combination adjusted from Ianevski et al., 2020.
(B) MJN110:AM251 four-by-four drug matrix reporting on HCV inhibition. Inhibition of HCV $JFH1_T$ 2a was determined by RT-qPCR of the HCV internal ribosome entry site (IRES). Cells were infected with HCV $JFH1_T$ 2a for 5 hours, after which the medium was changed for fresh medium containing the corresponding MJN110:AM251 co-treatments, followed by a 72 hour incubation. n = 3. Significance assessed with two-tailed, unpaired student's t test, *p < 0.05, **p < 0.01, ***p < 0.001.
(C) Calculated topological synergy map using synergy finder 2.0, two-dimensional representation. Calculated synergy score of the MJN110:AM251 matrix, δ = 7.43.
(D) Calculated topological synergy map using synergy finder 2.0, three-dimensional representation. Calculated synergy score of the MJN110:AM251 matrix, δ = 7.43.
(E) Structure of MJN110 (left) and AM251 (right).

of HCV JFH1$_T$ 2a was determined by RT-qPCR of the HCV IRES. From the calculated topological synergy map of the MJN110:AM251 drug matrix through SynergyFinder2.0, there appears to be 2 highly synergistic drug treatment combinations areas. These areas appear at concentrations of 0.01 µM:4 µM and 1 µM:8 µM in the MJN110:AM251 drug matrix (**Figure 2.4 B**). As previously stated, no significant change in HCV viral abundance was observed with 0.01 µM MJN110 treated HCV JFH1$_T$ 2a infected HuH7.5s, while 4 µM AM251 treated HCV JFH1$_T$ 2a infected HuH7.5s demonstrated a modest 40% decrease in viral abundance compared to control levels. However, speaking to the additive quality of this drug combination, when treated with both 0.01 µM MJN110 and 4 µM AM251, we see a significant increase in HCV down-regulation compared to the 0.01 µM MJN110 drug treatment alone (**Figure 2.5 E**).

Overall, with a calculated synergy score of δ = 7.43, we report an additive, 7.4 percent increase of inhibition against Hepatitis C virus due to drug-drug interactions when co-treating with MGLL inhibitor MJN110 and CB1 antagonist AM251. We sought next to assess key downstream SH targets of miRNA-185 and relate the antiviral capacity of this drug co-treatment to miRNA-185.

### 2.3.5 MGLL inhibitor, MJN110 and CB1 antagonist, AM251, co-treatment recapitulates partly the miR-185 phenotype

miRNA-185 transfection in HuH7.5s, as determined with RT-qPCR, significantly decreases arylacetamide deacetylase (AADAC), acyl-CoA thioesterase 1 (ACOT1), carboxylesterase-1 (CES1), fatty acid synthase (FASN), monoacylglycerol lipase (MGLL), and peroxisome proliferator-activated receptor alpha (PPARα) mRNA transcript levels. We demonstrated that pharmacological inhibition of endocannabinoid-related two serine hydrolase targets, MGLL and CES1, were antiviral in HCV JFH1$_T$ 2a infected HuH7.5s and in the HuH7-SGR-Luc replicon model respectively (**Figure 2.1 B, D**). Looking to the MJN110:AM251 drug co-treatment, in

attempts to mimic the antiviral and SH targeting qualities of miRNA-185, we sought to assess a subset of these miRNA-185 down-regulated SH targets during this drug co-treatment.

mRNA signaling changes of this 72-hour drug combination study was determined using RT-qPCR of HCV JFH1$_T$ 2a infected drug combination-treated HuH7.5s. Cells were infected with HCV JFH1$_T$ 2a for 5 hours, after which the medium was changed to fresh medium containing the corresponding MJN110:AM251 co-treatments, followed by a 72-hour incubation. Here we principally report the signaling changes of the highest drug concentration co-treatment:1 µM MJN110, 8 µM AM251 and their respective solo treatments (**Figure 2.5 A-D**).

Significant increases in CPT1a mRNA levels were previously reported by Shahidi *et al.* in 12, 24, and 48 hour 10 µM AM251 treated HCV JFH1$_T$ 2a infected HuH7s. A non-significant up-regulation of CPT1a mRNA levels of 72 hour treated HCV JFH1$_T$ 2a infected HuH7.5s can be observed with all treatments with the highest level of up-regulation, a 2.5 fold increase occurring with the MJN110:AM251 co-treatment array (**Figure 2.5 A**).

As expected, decreases in FASN mRNA levels were observed in 72 hour 8 µM AM251 treated HCV JFH1$_T$ 2a infected HuH7.5s. This mimics what has previously been reported in 12, 24, and 48 hour 10 µM AM251 treated HCV JFH1$_T$ 2a infected HuH7s [33]. 1 µM MJN110 treatment alone did not lead to any significant changes in FASN expression. As expected, co-treatment of CB1 antagonist AM251 and MGLL inhibitor MJN110 reveals similar significant FASN down-regulation of mRNA levels at 72 hours (**Figure 2.5 B**). This decrease in FASN gene expression affects *de novo* lipogenesis, acts negatively against HCV, and recapitulated what's been observed previously during miRNA-185 transfection.

mRNA expression changes of PPARα and MGLL in response to MJN110:AM251 co-treatment were by far the most interesting. AM251 treatment of HCV JFH1$_T$ 2a infected HuH7s resulted in

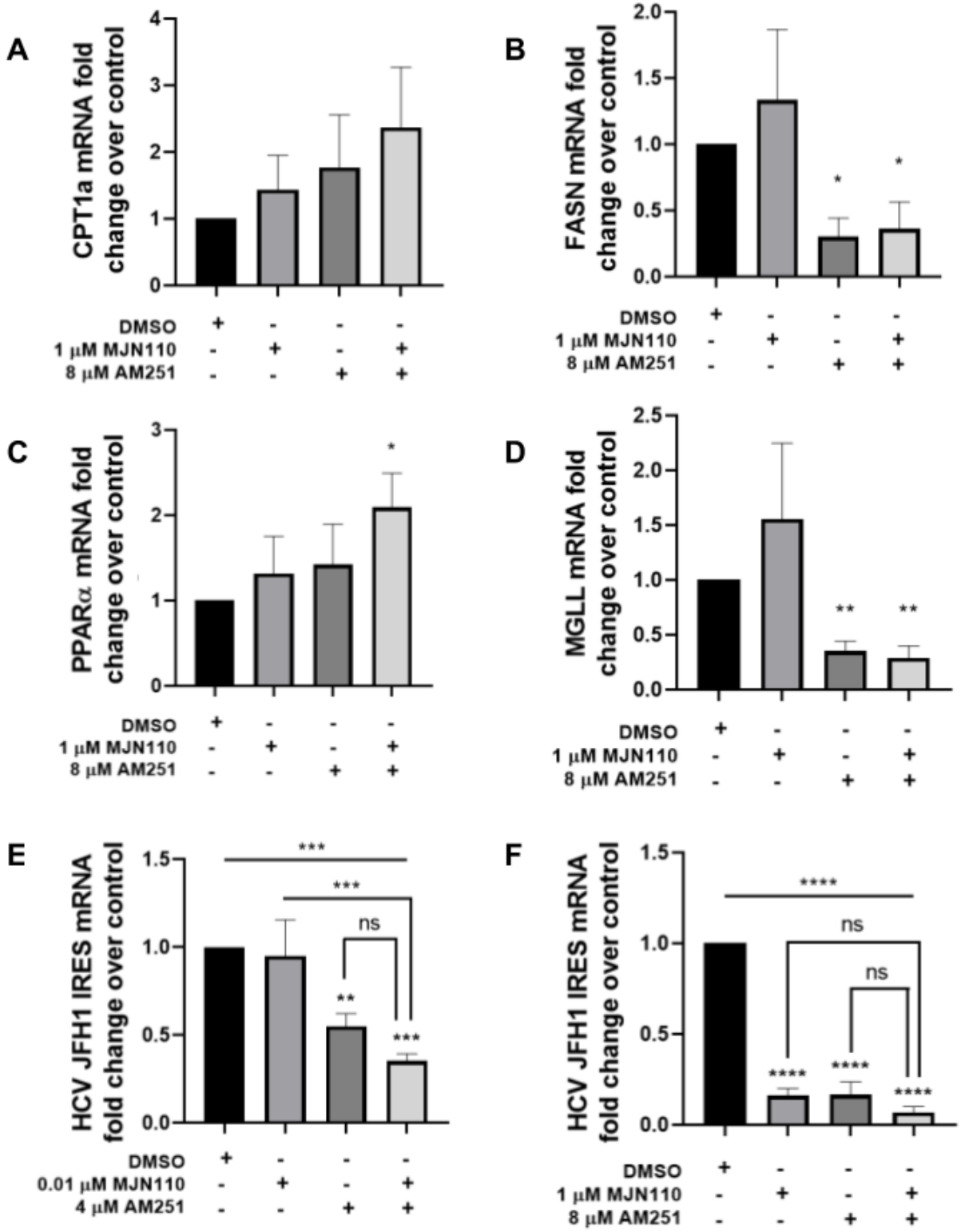


**Figure 2.5: MGLL inhibitor, MJN110, CB1 antagonist, AM251, co-treatment recapitulates partly the miR-185 phenotype**

mRNA fold change of as determined by RT-qPCR for (A) CPT1a, (B) FASN, (C) PPARα, (D) MGLL, and (E,F) HCV JFH1$_T$ 2a IRES. Cells were infected with HCV JFH1$_T$ 2a for 5 hours, after which the medium was changed for fresh medium containing the corresponding small molecule treatments, followed by a 72 hour incubation. n = 3. Significance assessed (A-D) with two-tailed, unpaired student's t test, *p < 0.05, **p < 0.01, ***p < 0.001. Significance assessed (E,F) with a one-way ANOVA, with multiple comparisons post hoc tests, *p < 0.05, **p < 0.01, ***p < 0.001, ****p < 0.0001.

significant up-regulation of PPARα after 48 hours of treatment [33]. Regarding the reported matrix, each drug treatment alone of MJN110 and AM251, demonstrated no significant up-regulation after 72 hours of treatment in PPARα mRNA levels in HCV $JFH1_T$ 2a infected HuH7.5s. However, co-treatment of MJN110 and AM251 together in HCV $JFH1_T$ 2a infected HuH7.5s after 72 hours did demonstrate significant up-regulation of PPARα mRNA levels (**Figure 2.5 C**). An upwards non-significant trend in CPT1a mRNA levels was also observed demonstrating a similar increase in expression of fatty acid oxidation genes in these co-treated cells (**Figure 2.5 A**). This demonstrates the additive effects that each small molecule can contribute together in creating a more potent anti-viral profile in increasing fatty acid catabolism.

Interestingly, CB1 antagonism with CB1 antagonist AM251 appears to affect MGLL mRNA abundance significantly in HCV $JFH1_T$ 2a infected HuH7.5s after 72 hours of treatment (**Figure 2.5 D**). This has not been previously reported in the induction of its HCV antiviral phenotype suggesting AM251 is antiviral through AMPK activation and MGLL antagonization [33]. Surprisingly in the case of the HCV $JFH1_T$ 2a infected AM251:MJN110 drug matrix treated HuH7.5s, there is a compounding inhibitory effect on MGLL with each of these small molecule treatments. We know from previous work and from current reports here that MGLL inhibitor MJN110 administration inhibits MGLL. We now report that CB1 antagonist AM251 affects MGLL mRNA expression levels during HCV $JFH1_T$ infection as well. This suggests a two-pronged attack on MGLL, this key host targeted antiviral factor. 10 µM AM251 treatment of non-infected HuH7.5s demonstrate a small but significant drop in MGLL abundance after 72 hours of treatment (**Supplemental figure 2.12 A, B**). MGLL mRNA abundance of non-infected HuH7.5s also revealed a similar but non-significant negative regulatory trend (**Supplemental figure 2.11 C**). Expectedly, MGLL mRNA expression of HCV $JFH1_T$ 2a infected 1 µM MJN110 treated HuH7.5s demonstrated no significant changes in transcript abundance, nor did the MGLL

mRNA levels of 24 hour 1 µM MJN110 treated non-infected HuH7.5s (**Figure 2.5 C, Supplemental figure 2.11 C**).

Overall, we have observed changes in gene expression that align with current knowledge on CB1 antagonization with AM251. Interestingly, significant changes in gene expression were observed regarding PPARα mRNA levels during drug co-treatments with MJN110 and AM251 and speak to the additive nature of this drug dose-response matrix. We have discovered that CB1 antagonist AM251 alters MGLL expression levels and may serve to add to AM251's antiviral profile. Overall we have managed to recapitulate inhibitory effects on serine hydrolases MGLL, and FASN with this drug matrix but contrastingly to miRNA185, instead promote fatty acid oxidation through PPARα.

### 2.3.6 MGLL inhibitor MJN110 degrades MGLL through the 26S proteasome

MJN110 is a NHS carbamate inhibitor of the serine hydrolase MGLL. As an NHS carbamate inhibitor, these small molecule species usually result in the covalent modification and inhibition of the active site of their target, in this case, MGLL. As a result, modulation of protein abundance or mRNA expression is not usually expected to change throughout small molecule treatment. NHS carbamate inhibitors have recently been identified as a promising class of serine hydrolase inhibitors that shows minimal cross-reactivity with other proteins in the proteome [40]. In parallel with our most recent report [35], we see a decrease in MGLL abundance throughout MJN110 treatment. 1 µM MJN110 treatment in HuH7.5s showing significant down-regulation of MGLL abundance after 6 hours of treatment with maximal down-regulation reported at 24 hours (**Figure 2.6 A, B**). This suggests MGLL is undergoing an abundance shift through rather proteasomal degradation or autophagy fates when treated with the MGLL inhibitor MJN110. As a result, we thought to utilize the proteasome inhibitor MG132 to inquire further about MGLL's shift in abundance in response to MJN110 inhibition.

Carbobenzoxy-Leu-Leu-leucinal, MG132 (**Figure 2.6 C**) is a synthetic peptide aldehyde, transition-state inhibitor ($K_i$ = 4 nM) primarily of the chymotrypsin-like activity of the proteasome. This inhibitor blocks the proteolytic activity of the 26S proteasome without influencing its ATPase or isopeptidase activities [41–43]. Six-hour 1 µM MJN110 treated HuH7.5s demonstrates again a significant decrease in MGLL abundance (**Figure 2.6 D, E**). A six-hour time treatment was chosen to prevent the induction of apoptosis that occurs during multi-day MG132 administration [44]. Interestingly, co-treatment of the MGLL inhibitor MJN110, and the proteasome inhibitor MG132, yielded a significant rescue of MGLL abundance back to control levels (**Figure 2.6 D, E**). This rescue suggests MGLL is degraded through the 26S proteasome and is not a result of autophagosomal mediated lysosomal degradation. 5 µM MG132 treatments alone yielded no significant changes in MGLL abundance after 6 hours of treatment further validating our model of MGLL induced degradation by MJN110 binding through the 26S proteasome.

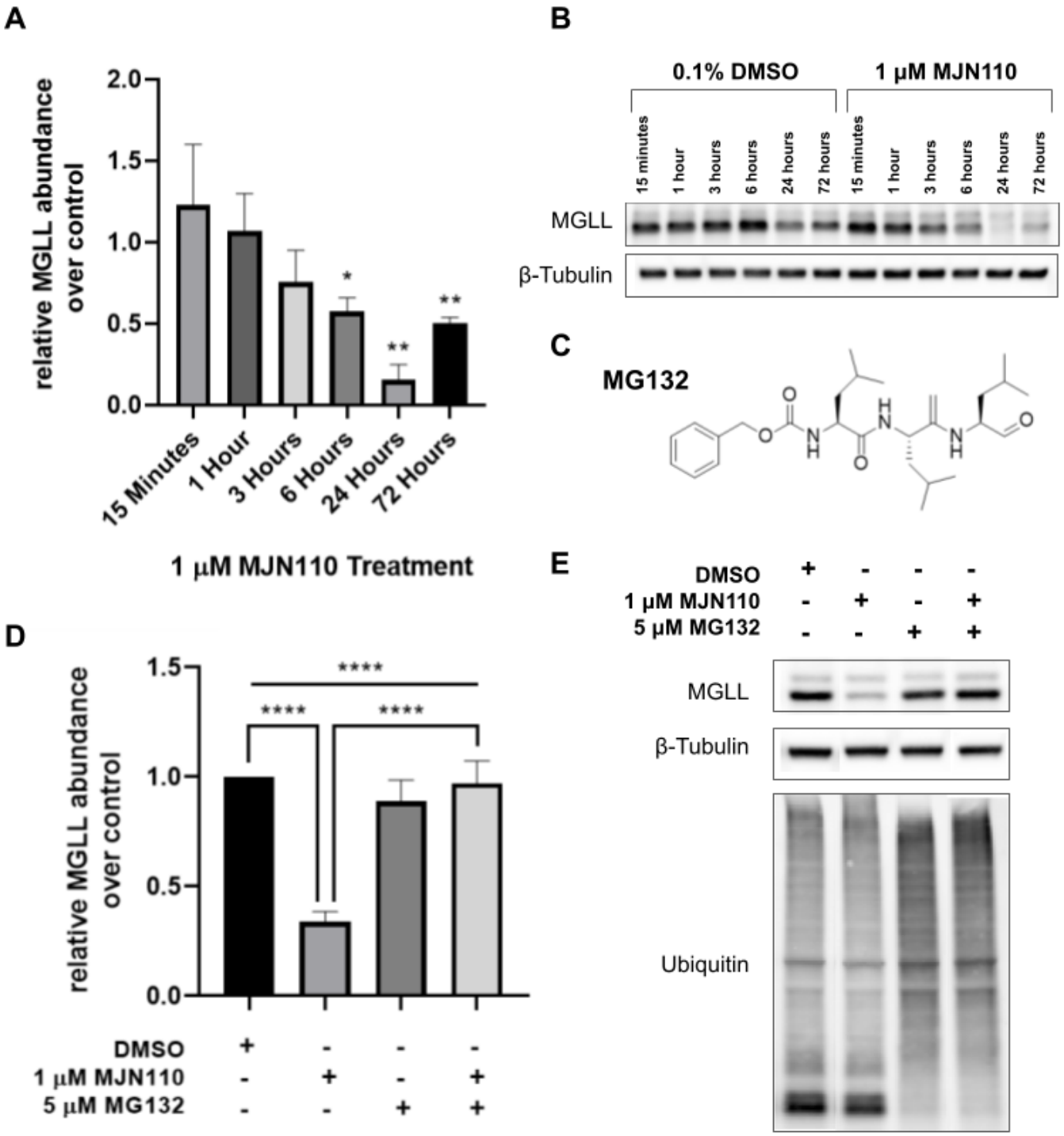


**Figure 2.6: MJN110 inhibited MGLL is degraded through the 26S proteasome**
(A) MJN110 treated HuH7.5s demonstrates changes in MGLL abundance over the course of treatment. n = 3. Significance assessed with two-tailed, unpaired student's t test, *p < 0.05, **p < 0.01.
(B) Representative blot of one of the biological replicates is shown of (A).
(C) Structure of proteasome inhibitor MG132.
(D) MJN110 treated HuH7.5s after 6 hours of treatment showed significant downregulation of relative MGLL abundance. Co-treatment with MGLL inhibitor MJN110, and proteasome inhibitor MG132 for 6 hours in HuH7.5s demonstrated a significant rescue in MGLL abundance back to control levels. n = 4. Significance assessed with a one-way ANOVA, with multiple comparison post hoc tests, *p < 0.05, **p < 0.01, ***p < 0.001, ****p < 0.0001.
(E) Representative blot of one of the biological replicates is shown of (D).

## 2.4 Discussion

This chapter and its investigations stemmed from our initial interests in miR-185 and its link to many serine hydrolases involved in lipid and endocannabinoid metabolism. This miRNA has been reported to have well-established roles in regulating immuno-lipidic metabolism and is also deemed antiviral against Hepatitis C virus [35,45,46]. Of the initially tested small-molecule inhibitor set, metabolic serine hydrolase inhibitors KT195, MJN110, and WWL113 all demonstrated dose-dependent antiviral effects in the HuH7-SGR-Luc replicon model and/or the fully infectious HCV $JFH1_T$ 2a genotype model, SHs all related to the endocannabinoid system.

ABHD6 is an integral membrane metabolic serine hydrolase with a 2-AG hydrolytic capacity that accounts for ~4% of 2-AG hydrolysis in the mouse brain, as well as a monoacylglycerols (MAGs) and bis(monoacylglycerol)phosphate (BMP) hydrolytic capacity [47–49]. Some reports suggest ABHD6 functions as a critical modulator of metabolic syndrome in peripheral tissues. Selective knockdown of ABHD6 protected mice from high-fat-diet-induced obesity, hepatic steatosis, and systemic insulin resistance principally by negatively affecting fatty acid metabolism [50]. ABHD6 inhibitor KT195 treatment leads to a moderate but dose-dependent decrease in replicon and HCV $JFH1_T$ 2a IRES mRNA levels (**Figure 2.1 A, C**). The HuH7-SGR-Luc replicon contains only NSPs necessary for the formation of the replication complex and lacks structural proteins to create any viable virus for further non-lytic infection (**Figure 1.3 C**)[51]. KT195 mediated inhibition of ABHD6, in theory, must affect HCV replication potently enough to translate into the full model of the virus across genotypes. ABHD6 inhibition should increase 2-AG levels, but with the abundance of other high contributing 2-AG hydrolyzing enzymes, especially MGLL, the HCV antiviral effects that ABHD6 inhibition demonstrates would likely not be a result of alterations in CB1 signaling. It could be hypothesized that ABHD6 inhibitor KT195 is potently antiviral, affecting viral replication through the down-regulation of fatty acid synthesis related genes. Contrastingly, ABHD6 siRNA knockdown experiment revealed an upregulation of

HCV IRES expression levels in HCV JFH1$_T$ 2a infected HuH7.5s 72 hours post-transfection [35]. This could likely be due to ABHD6's role in regulating BMP lipid species which are involved in the regulation of lysosomal stability and endosomal trafficking, pathways used by HCV for its egress, and release [52–54]. This puts into question ABHD6 inhibitor KT195's specificity and/or its observed antiviral effects. These inhibitory effects could be a response to the lowered cellular viability caused by the drug as well. KT195 was discontinued from further investigation due to its moderate cytotoxicity at its HCV-relevant concentration of 10 µM and for the aforementioned reasons above (**Figure 2.1 A, C, Supplemental figure 2.4 A**). ABHD6 was also not down-regulated in response to miRNA-185 transfection and thus is further cemented as an ideal candidate for the recapitulation of the miRNA-185 antiviral profile drug cocktail.

MGLL is a metabolic serine hydrolase that preferentially hydrolyzes MAGs into fatty acids and glycerol, and is the main SH responsible for the degradation of 2-AG in the brain [48,55,56]. MGLL inhibitor MJN110 treatment leads to a potent dose-dependent decrease of HCV JFH1$_T$ 2a IRES mRNA levels but not in the replicon suggesting MJN110 does not affect replication but other parts of the HCV viral life cycle (**Figure 2.1 B**). It was hypothesized that during MGLL inhibition by MJN110, increases in 2-AG would occur, ultimately resulting in the activation of the CB1 receptor and subsequent desensitization of the CB1 receptor due to its high 2-AG hydrolyzing contribution, activating AMPK. Changes in AMPK Thr172 phosphorylation however was not observed in MGLL inhibitor MJN110 treated non-infected HuH7.5s [35]. In parallel, changes in mRNA expression levels of downstream AMPK effectors such as SREBP1c, SCD1, FASN, carnitine palmitoyltransferase 1A (CPT1a) are all similarly not significantly altered in response to 24 hour MGLL inhibitor MJN110 treatment in uninfected HuH7.5s.(**Supplemental figure 2.11**). Overall, it appears that MGLL inhibitor MJN110 acts independently of AMPK signaling and potentially CB1 as a whole. Assessment of AMPK signaling during HCV infection and MJN110 treatment has yet to be performed though and might reveal AMPK signaling alterations since

CB1 expression and abundance is enhanced during HCV infection [57], perhaps playing a larger role in this antiviral profile. Instead, we think MGLL inhibition by MJN110 in the liver may exert its antiviral effects through reduced hydrolysis of 2-AG and other MAGs leading to broader effects on lipid homeostasis perhaps affecting HCV entry.

Analysis of MAG and free fatty acid species after 72 hours of treatment revealed a significant elevation in 18:1 MAG in MJN110 treated HuH7.5s. MGLL inhibitor MJN110 treated HuH7.5s also revealed the expected increase in 2-AG lipid species [35,40]. Unexpectedly, increases in arachidonic acid (AA) lipid species, a hydrolysis product of 2-AG metabolism was also observed in contrast to what has been reported in brain lipid tissue previously [35,40]. Several polyunsaturated fatty acids (PUFAs) including arachidonic acid (AA), docosahexaenoic acid (DHA), and eicosapentaenoic acid (EPA) can exert anti-HCV activities in HCV subgenomic replicon harboring systems [58,59]. AA, an eicosanoid precursor that can be catalyzed by at least three types of enzymes in the cell, generates numerous metabolites that can mediate diverse physiological and pathological responses in processes such as blood pressure, inflammation, phagocyte activation, pain, and fever [58]. Some reports demonstrate that in HCV-replicon harboring cells, the anti-viral activity observed is a result of AA lipid peroxidation. Parental HuH7 hepatocytes when administered AA by comparison do not demonstrate any significant levels of arachidonic acid lipid peroxidation [60]. Huang *et al.* concluded that in the presence of AA and the absence of lipid-soluble antioxidants, HCV replication induces lipid peroxidation that in turn decreases HCV RNA levels. Increases in AA levels is a potential avenue for further investigation in the context of MJN110 treated hepatocytes to explain MJN110's antiviral course of action.

CES1 is a lumen and ER-localized metabolic serine hydrolase that catalyzes ester- or amide-containing substrates into alcohols and/or carboxylic acids. CES1 inhibitor WWL113 treatment lead to a potent dose-dependent decrease of HCV replicon levels but not in HCV $JFH1_T$ 2a infected HuH7.5s (**Figure 2.1 D**). This suggests the inhibitive replicative effects are not potent

enough to elicit a persisting antiviral effect in the full virus model or WWL113/CES1 inhibition might not be effective against genotype 2 HCV. It was shown that WWL113's antiviral dose-response curve closely mimics our reported MTT cell viability curve perhaps suggesting the observed antiviral effects might be a consequence of the drop in cellular viability. As mentioned previously with the lowly 2-AG hydrolyzing SH ABHD6, in the presence of other high contributing 2-AG hydrolyzing enzymes, especially MGLL, the HCV antiviral effects that CES1 inhibition demonstrates would likely not be a result of alterations in CB1 signaling. WWL113 was discontinued from future investigation due to these aforementioned qualities.

Overall, we have managed to demonstrate the potency of targeting metabolic serine hydrolases ABHD6, CES1, and MGLL as HCV antiviral factors. To assess the putative link between these serine hydrolases and the cannabinoid system, we thought to test whether CB1 antagonism and agonism have antiviral effects against HCV.

CB1 antagonist AM251 treatment led to a small but dose-dependant decrease in HuH7-SGR-Luc replicon levels (**Figure 2.2 D**). Similarly, a dose-dependent decrease in HCV $JFH1_T$ 2a IRES mRNA levels was observed (**Figure 2.2 B**). When comparing the replicon versus the fully infectious model curve, the magnitude of inhibition was markedly lower in the replicon model. This is likely due to the lowered relative abundance of the CB1 receptor in the replicon system [57]. It has been shown previously that the antiviral properties of CB1 antagonist AM251 are a result of downstream CB1 antagonistic signaling resulting in the phosphorylation and activation of AMPK. AM251 mediated activation of AMPK resulted in the enhancement of genes involved in lipid oxidation such as CPT1a and PPARα while inhibiting genes involved in lipogenesis such as SREBP-1, FASN, SCD-1, and ACC-1. CB1 antagonist AM251's antiviral effect was determined to be not only CB1 dependant but somewhat AMPK dependant and have effects on HCV RNA, viral protein levels, particle production, and virus infectivity [33].

We assessed CB1 agonist and synthetic cannabinoid HU210 in the context of HCV in both of our previously reported models. CB1 agonist HU210 treatment demonstrated a dose-dependent decrease in HuH7-SGR-Luc replicon levels (**Figure 2.2 D**). A significant decrease in HCV $JFH1_T$ 2a IRES mRNA levels was observed though right-shifted compared to the replicon dose-response curve. (**Figure 2.2 B**). This suggests that during full infection, CB1 agonism with HU210 is not as potent of an antiviral regime, or might not be as effective versus genotype 2 HCV. It is reported that HU210 elicits a significant bias towards cAMP inhibition ($G_{\alpha i/o}$ stimulation) over pERK1/2 activation [61,62]. Though HU210 administration had a stimulatory effect on WT hypothalamic AMPK activity, reduction of AMPK activity in WT liver and visceral fat was reported as well[63]. With this in mind, we know CB1 antagonist AM251 acts principally through the activation of AMPK through the enrichment of genes involved in lipid oxidation and down-regulation of pro-lipogenic genes. The antiviral effects we are observing during HU210 administration may be a result of cAMP inhibition and not AMPK. Previously, inhibition of PKA activity in Huh7.5 cells induces peripheral membrane changes of CLDN1, a key HCV viral entry factor into intracellular vesicular location and activation of AMPK [64]. HCV infection in Huh7.5s increases cAMP levels and phosphorylated PKA substrates, supporting a model where infection activates PKA in a cAMP-dependent manner to promote virus release and transmission. HU210 treatment might abrogate this particular pathway leading to its antiviral effect, though this requires further investigation.

Due to MGLL's putative link to the cannabinoid system, initial hypotheses on the antiviral action of MJN110 relates to a CB1 functional antagonization model. We compared the transcriptomes of MJN110 and AM251 treated hepatocytes and showed they share no GO hits and few transcriptomic hits all seemingly unrelated to lipid and endocannabinoid metabolism. AM251 treated hepatocyte transcriptomics revealed alterations in cellular lipid binding, lipid metabolism, and lipid signaling, and sterol metabolism while the MJN110 treated hepatocyte transcriptome,

which changed dramatically during treatment, revealed changes in gene regulation by miRNAs, humoral immunity, and phagocytosis.

In line with previous findings, it was suggested that MJN110 doesn't affect HCV replication but other portions of the HCV life cycle. Here, a potential avenue of investigation is assessing MJN110's role in altering HCV entry and egress as transcriptomics revealed early onset inhibition of processes involved in phagocytosis, plasma membrane invagination, and internalization. HCV is known to induce the formation of autophagosome-like vesicles (also referred to as double-membrane vesicles (DMVs)) to enhance viral replication and non-lytic egress. Recent evidence suggests that DMVs are a central hub for the synthesis of viral genomic RNA spanning many viruses including enteroviruses, poliovirus, hepatitis C virus, noroviruses, and coronaviruses [67]. Interestingly enough, miRNA-185 serves to inhibit HCV replication through the regulation of lipid microenvironments. This includes MWs but also DMVs. MJN110 might also serve to similarly affect these pathways.

Key individual MJN110 microarray hits of interest include 17-beta-hydroxysteroid dehydrogenase 14 (HSD17B14) and miRNA708 (**Supplemental Table 2.9**). HSD17B14 is rather under characterized but has been reported to have a NAD-dependent 17-beta-hydroxysteroid dehydrogenase activity. HSD17B14 oxidizes both estradiol and testosterone into their less bioactive steroid metabolites estrone and androstenedione, respectively [68,69]. Our group reported recently the transcriptional profiling of a protein disulfide isomerase (PDI) inhibitor called Origamicin in the HuH7-SGR-Luc HCV model and noted changes in expression levels of genes involved in the oxidative ER stress response and the unfolded protein response [70]. Of this transcriptomic set, HSD17B14 was significantly up-regulated and was one of the top 25 genes up-regulated upon treatment with 50 µM Origamicin. Interestingly, HSD17B14 was also significantly up-regulated in response to 72-hour AM251 administration (**Supplemental**

**Table 2.10**). HSD17B14 might have further implications for HCV pathogenesis and ER stress that have yet to be explored.

miRNA708 has been implicated as a tumor suppressor miRNA of HCC, targeting SMAD3 as its main course of action. miR-708 expression was significantly decreased in HCC tissue, while ectopic expression of miR-708 suppressed HCC cell proliferation, migration, and invasion through SMAD3 targeting [37]. Both MJN110 and AM251 72 hour transcriptomes revealed enhancement of this miRNA (**Figure 2.5 B**) and might be a key target to these small molecule HCV antiviral profiles.

Knowing that MJN110 and AM251 are antiviral against HCV through independent routes, we thought to assess their cooperativity in inhibiting HCV, and ultimately their ability in mimicking miRNA-185's antiviral profile. Using SynergyFinder 2.0, we determined the level of HCV inhibition enhancement. Using the HSA reference model, we calculated for a 4-by-4 MGLL inhibitor MJN110: CB1 antagonist AM251 dose-response matrix a synergy score of $\delta = 7.43$, which represents an additive increase in inhibition of approximately 7.4% beyond expectation (**Figure 2.4 C, D**). We demonstrated this dose-response matrix negatively affects *de novo* lipogenesis, MAG lipolysis, but enhances fatty acid oxidation, and shows an unexpected and multifaceted inhibition of a key HCV antiviral factor of miRNA185, MGLL (**Figure 2.5 A-D**).

Fatty acid synthase is a metabolic serine hydrolase and multi-enzyme complex responsible for the synthesis of *de novo* fatty acids, mainly palmitate lipid species (C16:0). It has previously been reported to be up-regulated both in abundance and activity during HCV infection [71]. It is essential for HCV entry and production but also modulates HCV replication by direct interaction with the HCV RNA dependant RNA polymerase (RdRp) and non-structural protein NS5a [72,73]. We recapitulated the FASN down-regulation observed during miRNA-185 treatment with this drug co-treatment.

Peroxisome proliferator-activated receptors (PPARs) are a family of ligand-activated nuclear transcription factors that are involved in lipids, insulin sensitization, glucose metabolism, and fatty acid metabolism [74,75]. PPARα is a transcription factor and a major regulator of lipid metabolism in the liver. PPARα is activated normally by dietary fatty acids and eicosanoids and promotes uptake, utilization, and catabolism of fatty acids by up-regulation of genes involved in fatty acid transport, fatty acid binding, and activation, and peroxisomal and mitochondrial fatty acid β-oxidation [75]. It is hypothesized that increases in PPARα mRNA expression is caused by increases in AA, and other 20:4 lipid species in response to 72-hour MGLL inhibitor MJN110 treatment in HuH7.5s [35]. PPARα has also been shown previously to be activated during AM251 treatment, though the exact mechanism of this activation has yet to be elucidated. A possible mechanism of PPARα activation by CB1 antagonist AM251 observed here could be through the inhibition of MGLL mRNA expression. This likely will affect cellular 2-AG and AA lipid species stores which in turn might activate PPARα. Together, these two small molecules may act through MGLL to further enhance cellular lipid oxidation against HCV.

AM251 mediated decreases in MGLL mRNA expression have not been previously reported in the induction of AM251's HCV antiviral phenotype [33]. It was shown through AMPK antagonist Compound C administration to AM251 treated HCV $JFH1_T$ 2a infected cells that viral levels did not return entirely back to control levels suggesting secondary antiviral factors at play past AMPK activation. In this case, we hypothesize that AM251 affects MGLL mRNA abundance to benefit AM251's HCV antiviral profile. MGLL normally serves to terminate 2-AG endocannabinoid mediated CB1 signaling. Under the effects of CB1 antagonism, this decrease in MGLL mRNA expression will lead ultimately to decreased MGLL abundance but also decreased 2-AG hydrolysis. Increases in 2-AG levels would serve to activate CB1. This observation could be the cells attempting to re-initiate CB1 viability through 2-AG, leading to its internalization, recycling/degradation, and synthesis. We demonstrated that 10 μM AM251

treatment of non-infected HuH7.5s demonstrate a small but significant drop in MGLL abundance after 72 hours of treatment (**Supplemental figure 2.12: A, B**). MGLL mRNA abundance of non-infected HuH7.5s also revealed a similar but non-significant negative regulatory trend (**Supplemental figure 2.11 C**).

Using proteasome inhibitor MG132, we inquired further about MGLL's shift in abundance in response to MJN110 treatment. Co-treatment of the MGLL inhibitor MJN110 with proteasome inhibitor MG132 yielded a significant rescue of MGLL abundance back to control levels (**Figure 2.6 D, E**). This rescue suggests MGLL is degraded through the 26S proteasome and is not a result of autophagosomal mediated lysosomal degradation. To assess how MGLL, when treated with MGLL inhibitor MJN110 is proteasomally degraded, we were seeking to perform co-Immunoprecipitation of MGLL during MJN110 treatment. It is hypothesized that MJN110 active-site covalent modification of MGLL might allosterically alter MGLL for degron presentation for polyubiquitination, or direct proteasomal degradation through the 26S proteasome.

The superposition of previously published apo-MGLL and ligand-bound-MGLL structures revealed that the majority of the Cα atoms can be superimposed with very little difference. Only a small subset of the lid-domain (151–225), namely residues in the range of 151–173 display large variations to ligand binding [76,77]. During binding, the labile lid domain which consists primarily of α-helix A4 (residues 158–170 in the open conformation) rolls over the active site opening resulting in an almost 180° counter-clockwise rotation and closed (blocked active site hole) confirmation of the protein. Molecular docking experiments demonstrated 2-AG is best stabilized for hydrolysis while MGLL is in its closed confirmation [76,77]. Comparatively, *Bertrand et al,* demonstrated that during carbamate inhibitor SAR629 binding, MGLL remains in an open confirmation as α-helix A4 is displaced with no clear electron density, leaving the lid domain and catalytic tunnel surface solvent exposed. Two SAR629 inhibitors are present in the active site with one having irreversibly modified MGLL through the covalent attachment of SAR629 by loss

of the 1,2,4-triazole leaving group[77]. SAR629 is different from MJN110 in only two ways: firstly in the leaving group (the 1,2,4-triazole and 1-hydroxy-pyrrolidine-2,5-dione respectively), and secondly in the para-substituted halogens found on the diphenylmethylpiperazine, (fluorines and chlorines respectively) [78]. Overall, if MJN110 causes similar exposure of these domains, their associated solvent exposed lysine and arginine residues could be further polyubiquitinated. This could lead to subsequent sequestering and degradation of the MJN110-MGLL complex by the UPS.

Initial attempts at performing Co-IP of MGLL yielded undetectable immunoprecipitates, though positive control EGFR precipitates were readily visualized (Data not shown). Future efforts will be made to investigate this hypothesis further.

Overall, potential applications going forward could be to assess the effects of using combinations of direct-acting antivirals (DAAs) with these potent host-targeted antivirals such as MJN110. Especially about MGLL, this serine hydrolase has emerged as a center of therapeutic potential in the context of HCV. However, its antiviral course of action, perhaps affecting HCV entry and/or AA lipid peroxidation still requires further investigation. Combining MJN110 or other MGLL inhibitor analogs of a non-brain penetrating quality could benefit current therapies available for the treatment of HCV as well. Additionally, to better recapitulate the effects of miRNA185, a combination of MJN110 or another MGLL targeting factor with a PPARα specific antagonist or a pan-PPAR antagonist such as benzamide could be an interesting future route of investigation in a clinical context [79].

Looking to MJN110 mediated degradation of MGLL; ultraviolet (UV) circular dichroism (CD) spectroscopy will be performed to assess broad secondary structure changes in response to MJN110 drug treatment to further investigate this degron presentation hypothesis. UV CD spectroscopy is a method for the rapid determination of protein secondary structure and protein

folding using the unequal absorption of left-handed and right-handed circularly polarized light. Often, CD can be used to estimate the structure of unknown proteins and monitor conformational changes due to temperature, mutations, heat, denaturants, or binding interactions [80]. Here we plan to use this technique in the investigation of MGLL inhibitor MJN110 mediated MGLL degron presentation and ultimately its subsequent degradation through the UPS.

## 2.5 Conclusion

Overall, we have managed to demonstrate the effectiveness of irreversible serine hydrolase small molecule inhibitors as regulators of the HCV viral life cycle. We demonstrate that ABHD6 inhibitor KT195 serves to inhibit HCV likely by affecting HCV replication. MGLL inhibition with MJN110 inhibits HCV likely not through affecting HCV replication but perhaps entry. MJN110 administration significantly increases, as expected, 2-AG, and unexpectedly, AA lipid species in response to treatment which is an avenue for further investigation to explain these potent antiviral effects regarding AA peroxidation. CES1 inhibitor WWL113 administration reconfirmed our previous findings, reporting perturbation of CES1 to have effects on HCV replication. Investigating this putative link between the endocannabinoid system and HCV, we assessed CB1 agonism and antagonism as routes of therapeutic potential for HCV as well. We illustrated potent antiviral effects through CB1 antagonist AM251 administration with mRNA expression changes reflecting decreases in lipogenesis while increasing lipid oxidation processes. CB1 agonism through CB1 agonist and synthetic cannabinoid HU210 revealed similar antiviral effects against HCV suggesting that this agonist-mediated antiviral effect is a result of a functionally antagonistic state of CB1 signaling.

With interest to mimic the broad SH targeting qualities of a previously reported antiviral microRNA, miRNA-185, we created serine hydrolase irreversible covalent inhibitor drug cocktails. We concluded that these cocktails suffered from too much cytotoxicity and instead looked to a drug combination treatment of MJN110 with AM251 as a co-treatment regime against HCV which still exemplified some SH targeting capabilities that mimicked miRNA-185's antiviral SH targeting profile. Using SynergyFinder2.0, we determined this drug combination had an additive inhibitory effect of $\delta = 7.4$ against HCV as determined in $JFH1_T$ 2a HCV infected HuH7.5s which represents a 7.4 percent increase in HCV inhibition beyond expectation. Assessing gene expression changes in response to drug co-treatment revealed down-regulation

of lipogenesis through FASN down-regulation and increases in lipid oxidation genes as seen with PPARα and CPT1a. Though MGLL was already selected to be a key inhibited target of this drug co-treatment regime through the use of MJN110, we were surprised to discover that AM251 administration affects MGLL mRNA abundance as well, further down-regulating a potent host targetable antiviral factor with this two-pronged attack approach.

Transcriptomics analysis revealed that MJN110 does not act in any similar fashion to CB1 antagonist AM251. Instead of altering lipid metabolism, transport, and biogenesis, early MJN110 administration negatively alters humoral immunity and phagocytosis, perhaps hinting at a role for MJN110 in affecting HCV entry and egress.

Lastly, we observed that during MJN110 administration, MGLL abundance was significantly altered throughout treatment and that this MJN110-MGLL complex was degraded through the 26S proteasome.

## 2.6 Materials, experimental and statistical details

### 2.6.1 Cell Culture

HuH7.5 hepatocellular carcinoma cells were expanded in DMEM media (Gibco TM Cat. # 11995065) supplemented with FBS (10%, Wisent Cat. # 080-450) and 100 nM non-essential amino acids (Gibco Cat. #11140076). HuH 7-Hepatitis C virus sub-genomic replicon-Luciferase construct (Huh7-SGR-Luc) hepatocellular carcinoma cells were expanded in DMEM media (Gibco TM Cat. # 11995065) supplemented with FBS (10%, Wisent Cat. # 080-450), 100 nM non-essential amino acids (Gibco Cat. #11140076) and 500 ug/mL G418-Sulfate antibiotic, Geneticin (Gibco TM Cat. #11995065).

### 2.6.2 Cytotoxicity Assay: LDH

Cytotoxicity was measured using the Abcam LDH Assay Kit (Abcam, Cat.#: ab65393) as per the manufacturer's protocol.

### 2.6.3 Cytotoxicity Assay: MTT

Cytotoxicity was assessed by using 3-(4,5-dimethylthiazol-2-yl)-2,5-diphenyltetrazolium bromide (Thermo-Fisher Technologies: Cat.#: M6494, CAS# 298-93-1) concentrated to 2.5 mg/mL in 1x PBS. Cells seeded in a 96 well plate for cytotoxicity assessment were washed with 1x PBS. Spent washing medium was aspirated and 50 µL of 2.5 mg/mL 3-(4,5-dimethylthiazol-2-yl)-2,5-diphenyltetrazolium bromide diluted in 1x PBS was added to each well. Plates were then incubated at 37˚Celucius, 5.0% CO2 for 3 hours after which, excess reagent is aspirated and discarded. Precipitated formzan crystals were solubilized in 50 µL of DMSO, per well then absorbance was read at 562 nm using the SpectraMaxi3 ® i3x spectrophotometer (Molecular Devices, Cat.#: i3x).

### 2.6.4 Immunoblotting

Noninfected and infected cell lysate samples were resuspended in 30 µL of 6X Laemli SDS-PAGE loading buffer then heat prepped at 95°C for 10 minutes. The dyed lysates were then loaded onto a rather a 10% or 12% TGX Stain-Free™ FastCast™ Acrylamide gel (Bio-Rad Cat.# 1610182) loading 7 uL of the all blue protein ladder (Bio-Rad Cat.# 1610393) as protein weight standard. Proteins were transferred from the gel to a PVDF membrane using the Trans-Blot® Turbo™ Transfer System (Bio-Rad), blocked with 3% BSA in TBS-Tween-20 (pH 7.4, 0.05%) for 1 hour at room temperature, fluorescently imaged and then probed with the appropriate primary and secondary antibody dilutions as indicated in Supplementary Table 1.

### 2.6.5 Microarray 72 Hours

Huh7.5 cells were cultured as previously described. Huh7.5 cells were seeded at 100 000 cells/well in a 6 well plate. After 24 hours, cells were then treated for 72 hours with a subset of small molecules: DMSO (Control, CAS Number: 67-68-5), MJN110 (MGLL inhibitor, CAS Number:  1438416-21-7), and AM251 (CNR1 antagonist, CAS Number: 183232-66-8). RNA isolation was performed using the RNeasy (Qiagen, Cat.#: 74136) isolation kit according to the manufacturer's provided protocol. Expression profiling was performed in biological duplicate using the Affymetrix Human Gene ST.2.0 arrays. Normalization and analysis were performed using the Affymetrix Expression Console and the Transcriptome Analysis Console, both provided by Thermo Fisher Scientific.

### 2.6.6 Microarray 24 Hours

Huh7.5 cells were cultured as previously described. Huh7.5 cells were seeded at 1,500,000 cells/well respectively in a 10 cm plate. After 24 hours, cells were then treated for 24 hours with a subset of small molecules: DMSO (Control, CAS Number: 67-68-5) or MJN110 (MGLL inhibitor, CAS Number:  1438416-21-7). RNA isolation was performed using the RNeasy (Qiagen, Cat.#: 74136) isolation kit according to the manufacturer's provided protocol.

Expression profiling was performed in biological duplicate using the Affymetrix Human Gene ST.2.0 arrays. Normalization and analysis were performed using the Affymetrix Expression Console and the Transcriptome Analysis Console, both provided by Thermo Fisher Scientific.

### 2.6.7 Protein Assays: Bradford

Protein concentrations were determined using the Bradford Protein Assay Kit (Bio-Rad, Cat.#: 5000001) as per the manufacturer's protocol.

### 2.6.8 Protein Assays: DC

Protein concentrations were determined using the DC Protein Assay Kit (Bio-Rad, Cat.#: 5000116) as per the manufacturer's protocol.

### 2.6.9 Quantitative PCR

RNA isolation was performed using the RNeasy (Qiagen, Cat.#: 74136) isolation kit as per the manufacturer's protocol. RNA integrity and concentration were determined via Nanodropping (NanoDrop TM 1000 Spectrophotometer, Thermo Fisher Scientific). Reverse transcription was performed using the iScript cDNA Synthesis Kit (Bio-Rad) using 500 ng of RNA as per the manufacturer's protocol. Quantitative PCR (qPCR) was performed using SYBR Green Supermix (Bio-Rad) as per manufacturer's protocol on the CFX Real-Time PCR Detection System (Bio-Rad) with the primer sequences are listed in Supplementary Table 6. 18S rRNA was used for normalization and expression fold changes relative to mock treatments were calculated using the $2^{-\Delta\Delta Ct}$ method. Significance assessed with two-tailed, unpaired student's t-test where $p<0.05$ was considered significant.

### 2.6.10 RNA isolation and quantification

RNA isolation was performed using the RNeasy (Qiagen, Cat.#: 74136) isolation kit as per

the manufacturer's protocol. RNA integrity and concentration were determined via Nanodropping (NanoDrop TM 1000 Spectrophotometer, Thermo Fisher Scientific).

### 2.6.11 Single Luciferase

HuH7-SGR-Luc Cells were seeded at 20 000 cells/well in a 24 well plate. After 24 hours and 72 hours, cells were treated with equal volume amounts of DMSO solubilized small molecules. Cells are lysed after 96 hours post-seeding in 100 µL of Passive Lysis Buffer (Promega Cat.# E1941) and analyzed using a Lmax luminometer microplate reader (Molecular Devices). Relative chemiluminescence was measured through the normalization of firefly luciferase signal to cell lysate protein concentrations. Chemiluminescence was measured in duplicate. Protein lysate concentration was normally determined using Bradford protein assay. The Luciferase Assay solution was added volume-wise 1:1 Luciferase assay solution to cell lysate and consisted of the following components: 25 mM Glycylglycine, 15 mM KxPO4 (pH 8.0), 4mM EGTA, 2 mM ATP, 1 mM DTT, 15 mM MGSO4, 0.1 mM CoA, 75 uM luciferin.

### 2.6.12 Small Molecules

ABC110 (CAS Number: N/A), P11 (CAS Number: 942285-55-4), Yoshio 3 (CAS Number: N/A), and JP408 (CAS Number: N/A) were kind gifts from Dr. Benjamin Cravatt, of The Scripps Research Institute. HU210 (CAS Number: 112830-95-2) was provided by Dr. Cory Harris, of the University of Ottawa. KT195 (CAS Number: 1402612-58-1), WWL113 (CAS Number: 947669-86-5), MJN110 (CAS Number: 1438416-21-7), AM251 (CAS Number: 183232-66-8 were all purchased from Millipore-Sigma. All small molecules used in this investigation can be found in **Supplemental figure 2.1**.

### 2.6.13 Statistics

Error bars displayed in this investigation is the calculated standard deviation between related samples. Statistical significance in large was measured with two-tailed, unpaired student's t test, where *p < 0.05, **p < 0.01, ***p < 0.001 and ****p < 0.0001, except for figure 2.5 E,F and figure 2.6 D where statistical significance was measured with a one-way ANOVA, with multiple comparison post hoc tests, *p < 0.05, **p < 0.01, ***p < 0.001, ****p < 0.0001.

Statistical significance of supplemental tables 2.8 - 2.10 summarized in figure 2.3 was measured with the analysis of variance (ANOVA) statistical test with the empirical Bayes correction. p values < 0.05 are deemed significant. The significance of GO analyses in supplemental tables 2.11 - 2.13 summarized in table 2.1 was assessed through the probability density function with the Bonferroni correction. p values < 0.05 are deemed significant.

### 2.6.14 Curve fitting

Dose-response curves of the SH small molecule inhibitors, cocktails, CB1 antagonists, and agonists dose-response curves in the HuH7-SGR-Luc and/or HCV JFH1T 2a models were performed using GraphPad Prism 8.4.3 using the Nonlinear regression (curve fit); log(agonist) vs. response – Variable slope (four parameters) option. See 2.6.11.1 below:

**2.6.14.1** $$Y = Bottom + (Top - Bottom)/(1 + 10^{(LogEC50-X)*HillSlope})$$

### 2.6.15 SynergyFinder2.0 Curve fitting

Curve fitting of drug dose-response matrix data was performed according to the LL4 curve fitting option according to Synergy Finder 2.0; a four-parameter logistic regression curve-fitting algorithm used to fit single-drug dose-response curves.

### 2.6.16 Synergy Calculations

S refers to the measured synergy. EA, EB,..., EN are the measured responses of the single drugs, while a, b and n are the doses of the single drugs required to produce the combination effect EA, B,..., N. For the ZIP model, xN is the dose of Nth drug fitted with four-parameter log-logistic (4PL) function, whereas mN is the dose that produces the half-maximum effect (also known as relative $EC_{50}$ or $IC_{50}$, depending on the readout), and λN is the shape parameter indicating the slope of the dose-response curve. For individual equations corresponding to each drug interaction reference model, see **Supplemental figures 2.7–2.10** for the Bliss, HAS, Loewe, and ZIP models receptively and **Supplemental figure 2.6** for the SynergyFinder 2.0 drug dose-response curves and matrix report.

## 2.7 References


1. Rogers A, Gibon Y. Enzyme kinetics: Theory and practice. In: *Plant Metabolic Networks*. ; 2009. doi:10.1007/978-0-387-78745-9_4
2. Strelow JM. A Perspective on the Kinetics of Covalent and Irreversible Inhibition. *J Biomol Screen*. 2017;22(1). doi:10.1177/1087057116671509
3. Tuley A, Fast W. The Taxonomy of Covalent Inhibitors. *Biochemistry*. 2018;57(24). doi:10.1021/acs.biochem.8b00315
4. Livneh I, Cohen-Kaplan V, Cohen-Rosenzweig C, Avni N, Ciechanover A. The life cycle of the 26S proteasome: From birth, through regulation and function, and onto its death. *Cell Res*. 2016. doi:10.1038/cr.2016.86
5. Ravid T, Hochstrasser M. Diversity of degradation signals in the ubiquitin-proteasome system. *Nat Rev Mol Cell Biol*. 2008;9(9). doi:10.1038/nrm2468
6. Platt T, Miller JH, Weber K. In vivo degradation of mutant lac repressor. *Nature*. 1970;228(5277). doi:10.1038/2281154a0
7. Rabinovitz M. TRANSLATIONAL REPRESSION IN THE CONTROL OF GLOBIN CHAIN INITIATION BY HEMIN. *Ann N Y Acad Sci*. 1974;241(1). doi:10.1111/j.1749-6632.1974.tb21890.x
8. Cho S, Dreyfuss G. A degron created by SMN2 exon 7 skipping is a principal contributor to spinal muscular atrophy severity. *Genes Dev*. 2010;24(5). doi:10.1101/gad.1884910
9. Fortmann KT, Lewis RD, Ngo KA, Fagerlund R, Hoffmann A. A Regulated, Ubiquitin-Independent Degron in IκBα. *J Mol Biol*. 2015;427(17). doi:10.1016/j.jmb.2015.07.008
10. Varshavsky A. The N-end rule: Functions, mysteries, uses. *Proc Natl Acad Sci U S A*. 1996;93(22). doi:10.1073/pnas.93.22.12142
11. Davies G, Boeree M, Hermann D, Hoelscher M. Accelerating the transition of new tuberculosis drug combinations from Phase II to Phase III trials: New technologies and innovative designs. *PLoS Med*. 2019. doi:10.1371/journal.pmed.1002851
12. Adam I, Ibrahim Y, Gasim GI. Efficacy and safety of artemisinin-based combination therapy for uncomplicated Plasmodium falciparum malaria in Sudan: A systematic review and meta-Analysis. *Malar J*. 2018. doi:10.1186/s12936-018-2265-x
13. Properzi M, Magro P, Castelli F, Quiros-Roldan E. Dolutegravir-rilpivirine: first 2-drug regimen for HIV-positive adults. *Expert Rev Anti Infect Ther*. 2018. doi:10.1080/14787210.2018.1544491
14. Sun W, He S, Martínez-Romero C, et al. Synergistic drug combination effectively blocks Ebola virus infection. *Antiviral Res*. 2017. doi:10.1016/j.antiviral.2016.11.017
15. Gotwals P, Cameron S, Cipolletta D, et al. Prospects for combining targeted and conventional cancer therapy with immunotherapy. *Nat Rev Cancer*. 2017. doi:10.1038/nrc.2017.17
16. Ianevski A, He L, Aittokallio T, Tang J. SynergyFinder: A web application for analyzing drug combination dose-response matrix data. *Bioinformatics*. 2017;33(15). doi:10.1093/bioinformatics/btx162
17. Ianevski A, Giri AK, Aittokallio T. SynergyFinder 2.0: visual analytics of multi-drug combination synergies. *Nucleic Acids Res*. 2020. doi:10.1093/nar/gkaa216
18. Berenbaum MC. What is synergy? *Pharmacol Rev*. 1989.
19. BLISS CI. THE TOXICITY OF POISONS APPLIED JOINTLY. *Ann Appl Biol*. 1939. doi:10.1111/j.1744-7348.1939.tb06990.x
20. LOEWE S. The problem of synergism and antagonism of combined drugs. *Arzneimittelforschung*. 1953.
21. Yadav B, Wennerberg K, Aittokallio T, Tang J. Searching for Drug Synergy in Complex Dose-Response Landscapes Using an Interaction Potency Model. *Comput Struct*

*Biotechnol J*. 2015. doi:10.1016/j.csbj.2015.09.001
22. Mercer TR, Dinger ME, Mattick JS. Long non-coding RNAs: Insights into functions. *Nat Rev Genet*. 2009;10(3). doi:10.1038/nrg2521
23. MacFarlane L-A, R. Murphy P. MicroRNA: Biogenesis, Function and Role in Cancer. *Curr Genomics*. 2010;11(7). doi:10.2174/138920210793175895
24. Song L, Tuan RS. MicroRNAs and cell differentiation in mammalian development. *Birth Defects Res Part C - Embryo Today Rev*. 2006;78(2). doi:10.1002/bdrc.20070
25. Adams MD, Kelley JM, Gocayne JD, et al. Complementary DNA sequencing: Expressed sequence tags and human genome project. *Science (80- )*. 1991;252(5013). doi:10.1126/science.2047873
26. Buczynski MW, Herman MA, Hsu KL, et al. Diacylglycerol lipase disinhibits VTA dopamine neurons during chronic nicotine exposure. *Proc Natl Acad Sci U S A*. 2016;113(4). doi:10.1073/pnas.1522672113
27. Baggelaar MP, Maccarrone M, van der Stelt M. 2-Arachidonoylglycerol: A signaling lipid with manifold actions in the brain. *Prog Lipid Res*. 2018;71. doi:10.1016/j.plipres.2018.05.002
28. Ibsen MS, Connor M, Glass M. Cannabinoid CB 1 and CB 2 Receptor Signaling and Bias . *Cannabis Cannabinoid Res*. 2017. doi:10.1089/can.2016.0037
29. Schlosburg JE, Blankman JL, Long JZ, et al. Chronic monoacylglycerol lipase blockade causes functional antagonism of the endocannabinoid system. *Nat Neurosci*. 2010. doi:10.1038/nn.2616
30. Ibsen MS, Finlay DB, Patel M, Javitch JA, Glass M, Grimsey NL. Cannabinoid CB1 and CB2 receptor-mediated arrestin translocation: Species, subtype, and agonist-dependence. *Front Pharmacol*. 2019;10(APR). doi:10.3389/fphar.2019.00350
31. Hsieh C, Brown S, Derleth C, Mackie K. Internalization and recycling of the CB1 cannabinoid receptor. *J Neurochem*. 1999;73(2). doi:10.1046/j.1471-4159.1999.0730493.x
32. Wu DF, Yang LQ, Goschke A, et al. Role of receptor internalization in the agonist-induced desensitization of cannabinoid type 1 receptors. *J Neurochem*. 2008;104(4). doi:10.1111/j.1471-4159.2007.05063.x
33. Shahidi M, Tay ESE, Read SA, et al. Endocannabinoid CB1 antagonists inhibit hepatitis C virus production, Providing a novel class of antiviral host-targeting agents. *J Gen Virol*. 2014. doi:10.1099/vir.0.067231-0
34. Devane WA, Breuer A, Sheskin T, et al. A Novel Probe for the Cannabinoid Receptor. *J Med Chem*. 1992;35(11). doi:10.1021/jm00089a018
35. Filip R, Desrochers GF, Lefebvre DM, et al. Profiling of microRNA targets using activity-based protein profiling: linking enzyme activity to microRNA-185 function. *Cell Chem Biol*. 2021. doi:10.1016/j.chembiol.2020.12.009
36. Chen J, Bardes EE, Aronow BJ, Jegga AG. ToppGene Suite for gene list enrichment analysis and candidate gene prioritization. *Nucleic Acids Res*. 2009;37(SUPPL. 2). doi:10.1093/nar/gkp427
37. Li Q, Li S, Wu Y, Gao F. miRNA-708 functions as a tumour suppressor in hepatocellular carcinoma by targeting SMAD3. *Oncol Lett*. 2017;14(2). doi:10.3892/ol.2017.6429
38. Sarma NJ, Tiriveedhi V, Subramanian V, et al. Hepatitis C Virus Mediated Changes in miRNA-449a Modulates Inflammatory Biomarker YKL40 through Components of the NOTCH Signaling Pathway. *PLoS One*. 2012;7(11). doi:10.1371/journal.pone.0050826
39. Sarma NJ, Tiriveedhi V, Crippin JS, Chapman WC, Mohanakumar T. Hepatitis C Virus-Induced Changes in MicroRNA 107 (miRNA-107) and miRNA-449a Modulate CCL2 by Targeting the Interleukin-6 Receptor Complex in Hepatitis. *J Virol*. 2014;88(7). doi:10.1128/jvi.03060-13
40. Niphakis MJ, Cognetta AB, Chang JW, et al. Evaluation of NHS carbamates as a potent

and selective class of endocannabinoid hydrolase inhibitors. *ACS Chem Neurosci*. 2013. doi:10.1021/cn400116z
41. Lee DH. Proteasome inhibitors: Valuable new tools for cell biologists. *Trends Cell Biol*. 1998. doi:10.1016/S0962-8924(98)01346-4
42. Rock KL, Gramm C, Rothstein L, et al. Inhibitors of the proteasome block the degradation of most cell proteins and the generation of peptides presented on MHC class I molecules. *Cell*. 1994. doi:10.1016/S0092-8674(94)90462-6
43. Lee DH, Goldberg AL. Selective inhibitors of the proteasome-dependent and vacuolar pathways of protein degradation in Saccharomyces cerevisiae. *J Biol Chem*. 1996. doi:10.1074/jbc.271.44.27280
44. Han YH, Moon HJ, You BR, Park WH. The effect of MG132, a proteasome inhibitor on HeLa cells in relation to cell growth, reactive oxygen species and GSH. *Oncol Rep*. 2009;22(1). doi:10.3892/or_00000427
45. Wang L, Jia X-J, Jiang H-J, et al. MicroRNAs 185, 96, and 223 Repress Selective High-Density Lipoprotein Cholesterol Uptake through Posttranscriptional Inhibition. *Mol Cell Biol*. 2013. doi:10.1128/mcb.01580-12
46. Singaravelu R, O'Hara S, Jones DM, et al. MicroRNAs regulate the immunometabolic response to viral infection in the liver. *Nat Chem Biol*. 2015. doi:10.1038/nchembio.1940
47. Marrs WR, Blankman JL, Horne EA, et al. The serine hydrolase ABHD6 controls the accumulation and efficacy of 2-AG at cannabinoid receptors. *Nat Neurosci*. 2010. doi:10.1038/nn.2601
48. Blankman JL, Simon GM, Cravatt BF. A comprehensive profile of brain enzymes that hydrolyze the endocannabinoid 2-arachidonoylglycerol. *Chem Biol*. 2007;14.
49. Pribasnig MA, Mrak I, Grabner GF, et al. α/β hydrolase domain-containing 6 (ABHD6) degrades the late Endosomal/Lysosomal lipid Bis(Monoacylglycero)phosphate. *J Biol Chem*. 2015;290(50). doi:10.1074/jbc.M115.669168
50. Thomas G, Betters JL, Lord CC, et al. The Serine Hydrolase ABHD6 Is a Critical Regulator of the Metabolic Syndrome. *Cell Rep*. 2013. doi:10.1016/j.celrep.2013.08.047
51. Robinson M, Yang H, Sun SC, et al. Novel hepatitis C virus reporter replicon cell lines enable efficient antiviral screening against genotype 1a. *Antimicrob Agents Chemother*. 2010;54(8). doi:10.1128/AAC.00289-10
52. Lai C-K, Jeng K-S, Machida K, Lai MMC. Hepatitis C Virus Egress and Release Depend on Endosomal Trafficking of Core Protein. *J Virol*. 2010;84(21). doi:10.1128/jvi.00587-10
53. Petersen NHT, Olsen OD, Groth-Pedersen L, et al. Transformation-Associated Changes in Sphingolipid Metabolism Sensitize Cells to Lysosomal Cell Death Induced by Inhibitors of Acid Sphingomyelinase. *Cancer Cell*. 2013;24(3). doi:10.1016/j.ccr.2013.08.003
54. Hullin-Matsuda F, Luquain-Costaz C, Bouvier J, Delton-Vandenbroucke I. Bis(monoacylglycero)phosphate, a peculiar phospholipid to control the fate of cholesterol: Implications in pathology. *Prostaglandins Leukot Essent Fat Acids*. 2009;81(5-6). doi:10.1016/j.plefa.2009.09.006
55. Sugiura T, Kondo S, Sukagawa A, et al. 2-arachidonoylglycerol: A possible endogenous cannabinoid receptor ligand in brain. *Biochem Biophys Res Commun*. 1995;215(1). doi:10.1006/bbrc.1995.2437
56. Mechoulam R, Ben-Shabat S, Hanus L, et al. Identification of an endogenous 2-monoglyceride, present in canine gut, that binds to cannabinoid receptors. *Biochem Pharmacol*. 1995;50(1). doi:10.1016/0006-2952(95)00109-D
57. van der Poorten D, Shahidi M, Tay E, et al. Hepatitis C virus induces the cannabinoid receptor 1. *PLoS One*. 2010;5(9). doi:10.1371/journal.pone.0012841
58. Leu GZ, Lin TY, Hsu JTA. Anti-HCV activities of selective polyunsaturated fatty acids. *Biochem Biophys Res Commun*. 2004;318(1). doi:10.1016/j.bbrc.2004.04.019
59. Kapadia SB, Chisari F V. Hepatitis C virus RNA replication is regulated by host

geranylgeranylation and fatty acids. *Proc Natl Acad Sci U S A*. 2005;102(7). doi:10.1073/pnas.0409834102
60. Huang H, Chen Y, Ye J. Inhibition of hepatitis C virus replication by peroxidation of arachidonate and restoration by vitamin E. *Proc Natl Acad Sci U S A*. 2007;104(47). doi:10.1073/pnas.0708423104
61. Khajehali E, Malone DT, Glass M, Sexton PM, Christopoulos A, Leach K. Biased agonism and biased allosteric modulation at the CB1 cannabinoid receptors. *Mol Pharmacol*. 2015;88(2). doi:10.1124/mol.115.099192
62. Glass M, Felder CC. Concurrent stimulation of cannabinoid CB1 and dopamine D2 receptors augments cAMP accumulation in striatal neurons: Evidence for a G(s) linkage to the CB1 receptor. *J Neurosci*. 1997;17(14). doi:10.1523/jneurosci.17-14-05327.1997
63. Lim CT, Kola B, Feltrin D, et al. Ghrelin and cannabinoids require the ghrelin receptor to affect cellular energy metabolism. *Mol Cell Endocrinol*. 2013;365(2). doi:10.1016/j.mce.2012.11.007
64. Farquhar MJ, Harris HJ, Diskar M, et al. Protein Kinase A-Dependent Step(s) in Hepatitis C Virus Entry and Infectivity. *J Virol*. 2008;82(17). doi:10.1128/jvi.00592-08
65. Hsu KL, Tsuboi K, Adibekian A, Pugh H, Masuda K, Cravatt BF. DAGLβ inhibition perturbs a lipid network involved in macrophage inflammatory responses. *Nat Chem Biol*. 2012;8(12). doi:10.1038/nchembio.1105
66. Dominguez E, Galmozzi A, Chang JW, et al. Integrated phenotypic and activity-based profiling links Ces3 to obesity and diabetes. *Nat Chem Biol*. 2014;10(2). doi:10.1038/nchembio.1429
67. Wolff G, Melia CE, Snijder EJ, Bárcena M. Double-Membrane Vesicles as Platforms for Viral Replication. *Trends Microbiol*. 2020;28(12). doi:10.1016/j.tim.2020.05.009
68. Lukacik P, Keller B, Bunkoczi G, et al. Structural and biochemical characterization of human orphan DHRS10 reveals a novel cytosolic enzyme with steroid dehydrogenase activity. *Biochem J*. 2007;402(3). doi:10.1042/BJ20061319
69. Sivik T, Vikingsson S, Gréen H, Jansson A. Expression patterns of 17β-hydroxysteroid dehydrogenase 14 in human tissues. *Horm Metab Res*. 2012;44(13). doi:10.1055/s-0032-1321815
70. Özcelik D, Seto A, Rakic B, Farzam A, Supek F, Pezacki JP. Gene Expression Profiling of Endoplasmatic Reticulum Stress in Hepatitis C Virus-Containing Cells Treated with an Inhibitor of Protein Disulfide Isomerases. *ACS Omega*. 2018;3(12). doi:10.1021/acsomega.8b02676
71. Yang W, Hood BL, Chadwick SL, et al. Fatty acid synthase is up-regulated during hepatitis C virus infection and regulates hepatitis C virus entry and production. *Hepatology*. 2008;48(5). doi:10.1002/hep.22508
72. Li X, Chen YT, Josson S, et al. MicroRNA-185 and 342 Inhibit Tumorigenicity and Induce Apoptosis through Blockade of the SREBP Metabolic Pathway in Prostate Cancer Cells. *PLoS One*. 2013. doi:10.1371/journal.pone.0070987
73. Menendez JA, Lupu R. Fatty acid synthase and the lipogenic phenotype in cancer pathogenesis. *Nat Rev Cancer*. 2007;7.
74. Dharancy S, Lemoine M, Mathurin P, Serfaty L, Dubuquoy L. Peroxisome proliferator-activated receptors in HCV-related infection. *PPAR Res*. 2009. doi:10.1155/2009/357204
75. Kersten S. Integrated physiology and systems biology of PPARα. *Mol Metab*. 2014;3(4). doi:10.1016/j.molmet.2014.02.002
76. Schalk-Hihi C, Schubert C, Alexander R, et al. Crystal structure of a soluble form of human monoglyceride lipase in complex with an inhibitor at 1.35 A ° resolution. *Protein Sci*. 2011;20(4). doi:10.1002/pro.596
77. Bertrand T, Augé F, Houtmann J, et al. Structural Basis for Human Monoglyceride Lipase Inhibition. *J Mol Biol*. 2010;396(3). doi:10.1016/j.jmb.2009.11.060

78. Deng H, Li W. Monoacylglycerol lipase inhibitors: modulators for lipid metabolism in cancer malignancy, neurological and metabolic disorders. *Acta Pharm Sin B*. 2020;10(4). doi:10.1016/j.apsb.2019.10.006
79. Rakic B, Sagan SM, Noestheden M, et al. Peroxisome proliferator-activated receptor α antagonism inhibits hepatitis C virus replication. *Chem Biol*. 2006. doi:10.1016/j.chembiol.2005.10.006
80. Greenfield NJ. Using circular dichroism spectra to estimate protein secondary structure. *Nat Protoc*. 2007;1(6). doi:10.1038/nprot.2006.202

# Chapter 3: Serine hydrolase ABPP screen of palmitoylation inhibitor 2-BP treated hepatoma cells

## 3.1 Introduction

### 3.1.1 Palmitoylation as a post-translational modification

The lipidation of proteins through thioester modification by palmitate (S-palmitoylation) is an abundant and common PTM present on hundreds of protein targets [1]. Palmitate is a 16-carbon saturated fatty acid synthesized *de novo* by FASN that can be post-translationally added to cysteine (Cys) residues of proteins through a reversible thioester linkage. Palmitoylation increases the hydrophobicity of palmitoylated proteins and facilitates their attachment to intracellular and dynamic plasma membranes. Palmitoylation further regulates their subcellular localization and functions as a result. Signaling molecules such as GPCRs, Ras GTPases, Src kinases, neurotransmitter receptors, and endothelial nitric oxide synthase are palmitoylated, and a dynamic palmitoylation and depalmitoylation system is essential for their individual function [2].

### 3.1.2 Palmitoylation inhibitor 2-bromopalmitate

2-bromopalmitate (2-BP) is an irreversible inhibitor to numerous membrane-associated enzymes [3]. Further characterization of 2-BP revealed a more broad and promiscuous activity but was later shown to block S-palmitoylation and microdomain recruitment of the Src and Fyn, families of non-receptor tyrosine kinases. This study established 2-BPs role as one of the few early pharmacological tools to inhibit protein S-palmitoylation [4]. 2-BP inhibition is thought to block protein palmitoylation by inhibiting a family of conserved protein acyl transferases (PATs) [5]. To date, there have been 23 distinct PAT enzymes that are presumed to regulate the profile of palmitoylated proteins by either PAT localization, protein interactions, or active site selectivity [5]. Current genetic models involving PATs implicate their roles widely in stem cell differentiation, learning, neurodegeneration, cancer progression, malignancy, and metastasis [6]. Over the past decade, the promiscuity of 2-BP has been overshadowed by the significant need for pharmacological tools to study protein palmitoylation. Several advancements in the

development of 2-BP clickable probes and even 2-BP activity-based probe analogs have been developed reporting on the dynamics of mitochondrial S-depalmitoylation and PAT enzyme activity respectively [1,2].

It has been shown that palmitoylation affects enzyme activity through its control of localization and membrane dynamics [6–8]. Due to the membrane-associated nature of many serine hydrolases, proper lipidation may be essential for their function. It has previously been demonstrated that insulin alters the protein palmitome. This group demonstrated insulin-stimulated palmitoylation without affecting PAFAH1B3 protein abundance.[8]. A member of our group, Dr. Geneviève Desrochers, PhD., demonstrated that with 20 µM 2-BP treatment for 6 hours of HuH7.5s, PAFAH1B3 activity was decreased nearly significantly as determined using ABPP with the chemical probe FP-Biotin without affecting PAFAH1B3 protein abundance (**Figure 3.2 A, B**). Significance was assessed using a Student's T-Test.

### 3.1.3 Activity-based protein profiling

Activity-based protein profiling (ABPP) is a functional proteomic technology that allows for the determination and readout of the functional state of a specific subset of related enzymes (**Figure 3.1**). Canonical ABPP probes target a large but manageable size of the human proteome often defined by the shared catalytic features of the targeted enzymatic group [9]. Most ABPP probes consist of three main components: a reactive group, a linker, and some sort of reporter tag. ABPP probes must demonstrate a certain level of promiscuity while still enabling a high level of intraclass coverage. This needs to be maintained all the while minimizing interclass cross-reactivity to report on the functional state of the targeted enzyme family. In the context of serine hydrolases, due to the great nucleophilicity of the catalytic serine, covalent modification by many electrophiles including fluorphosphonates (FPs), aryl phosphonates, sulfonyl fluorides, and carbamates are possible. FP reporter tagged ABPP probes have emerged as a stand out

for reporting on serine hydrolase activity [9–11]. Common ABPP reporter tags include fluorophores, biotin, and bio-orthogonal handles such as alkynes or azides, that can be modified using click chemistry to attach the desired reporter.

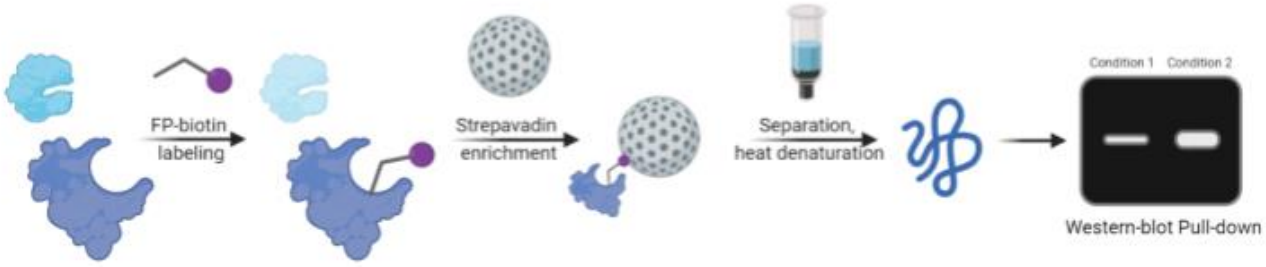


**Figure 3.1: ABPP workflow**
Schematic representation of an ABPP workflow. The active proteome is labelled with FP-Biotin. The biotinylated proteome is enriched with streptavidin, isolated and subsequently analyzed by western-blotting

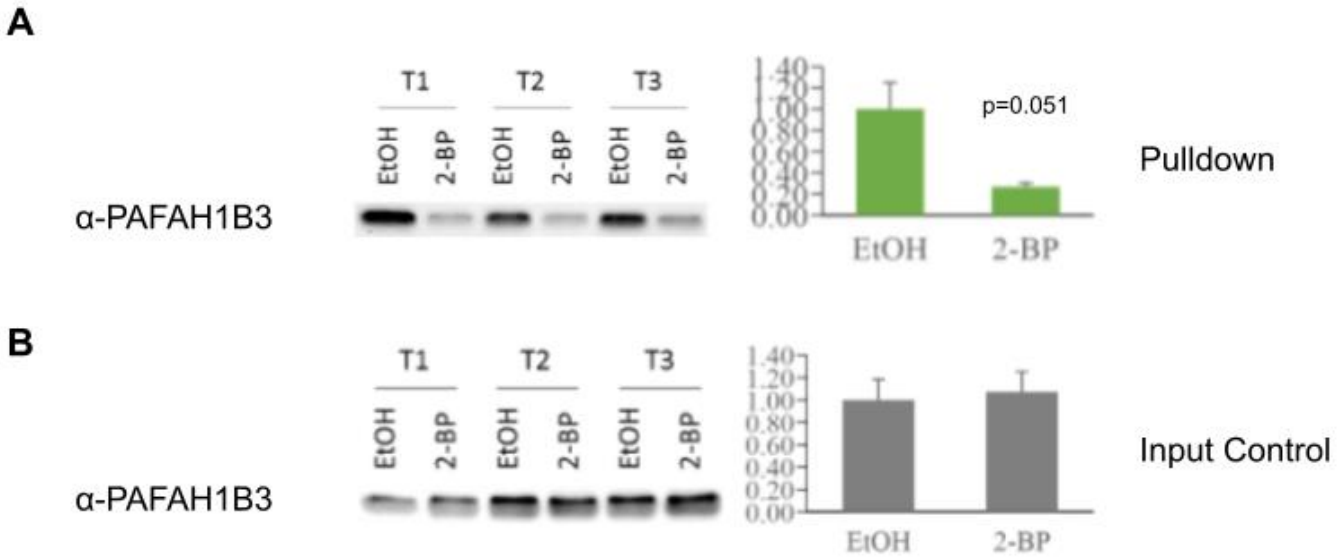


**Figure 3.2: PAFAH1B3 activity is down regulated in response to palmitoylation inhibition**
HuH7.5 cells were seeded. Seeding media was aspirated and replaced with media containing a 20 μM 2-BP concentration for 6 Hours. Cell lysates were collected and aliquots of each sample were taken and abundance was assessed using traditional western blotting techniques (Input Control). Following this, the active SH proteome was labelled with FP-Biotin. The biotinylated proteome was enriched with streptavidin, isolated and subsequently analyzed by western-blotting as well. Serine hydrolase PAFAH1B3 activity (A) and abundance (B) was assessed. A representative blot of the full biological triplicate is shown to the left. n = 3. Data was courtesy of Dr. Geneviève Desrochers, PhD.

### 3.2 Objectives

Due to the membrane-associated nature of many serine hydrolases, recent findings by Wei *et al.,* and within our group, proper lipidation may be an essential PTM for general serine hydrolase function. To assess whether protein palmitoylation is essential for serine hydrolase activity and function, we assessed a sub-set of serine hydrolases spanning different roles using FP-Biotin ABPP in response to protein palmitoylation inhibition using the palmitoylation inhibitor 2-BP.

## 3.3 Results

### 3.3.1 ABPP of 2-BP treated HuH7.5s reveals up-regulation of serine hydrolase activity and abundance

We assessed the activity of a greater sub-set of serine hydrolases in response to protein palmitoylation inhibition with the broad palmitoylation inhibitor 2-BP using FP-Biotin ABPP and conventional western blotting techniques. This subset of serine hydrolases includes alpha/beta hydrolase domain containing 6 (ABHD6), acyl-CoA thioesterase 1/2 (ACOT1/2), fatty acid synthase (FASN), monoacylglycerol lipase (MGLL), and prolyl endopeptidase (PREP) (**Figure 3.3 A-E**). Abundance was also determined for alpha/beta hydrolase domain containing 12 (ABHD12) and carboxypeptidase vitellogenic like (CPVL), and activity was determined for cathepsin A (CTSA) as well (**Figure 3.3 F-H**). HuH7.5 cells were treated with 20 µM of palmitoylation inhibitor 2-BP for rather 10 minutes or 6 hours. The 10 minute 2-BP treatment represents a competitive inhibition condition where 2-BP and endogenous free lipids compete for the PAT enzymes. The 6-hour treatment represents a condition instead where PAT enzymes are fully inhibited by 2-BP. Each of these conditions was compared against an untreated control. Aliquots were taken from each condition and abundance was assessed using traditional western blotting techniques. Following this, the active SH proteome was labeled using FP-Biotin. The biotinylated proteome was enriched with streptavidin, isolated, and subsequently analyzed by western blotting as well. Conversely to what was previously discovered with PAFAH1B3, changes in activity and abundance of tested serine hydrolases all shifted positively in response to 2-BP treatment.

Acyl-CoA thioesterases (ACOTs) catalyze the hydrolysis of acyl-CoA to form free fatty acids and Co-enzyme A (CoA). ACOT1 is responsible for this activity in the cytoplasm while ACOT2 is

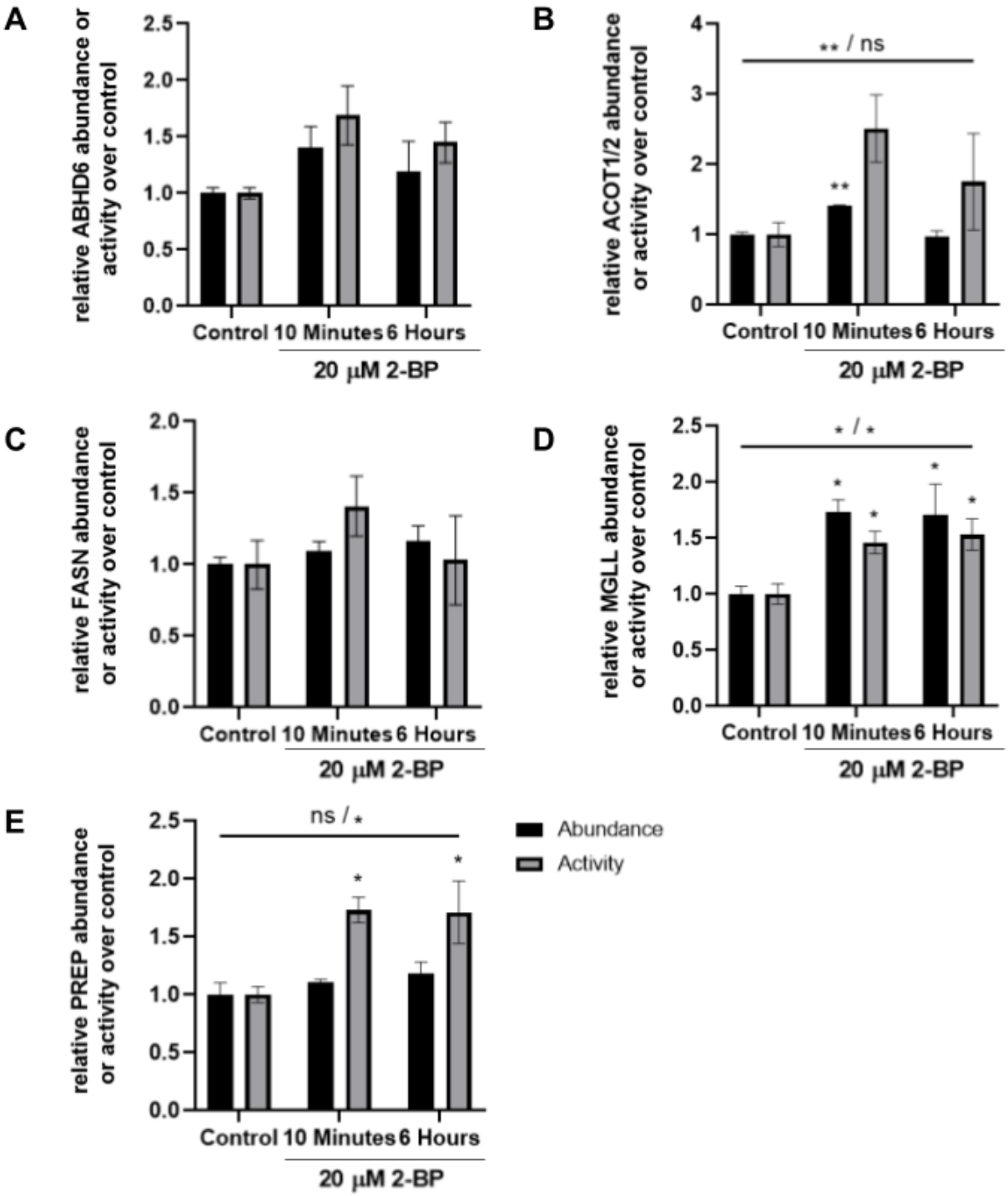


**Figure 3.3: Inhibition of palmitoylation demonstrates changes in activity and abundance in a subset of serine hydrolases**

HuH7.5 cells were seeded. Seeding media was aspirated and replaced with media containing a 20 μM 2-BP concentration for 6 Hours. Cell lysates were collected, one proteome was treated equally with a 20 μM concentration of 2-BP for 10 minutes. Aliquots were taken from each condition and abundance was assessed using traditional western blotting techniques. Following this, the active SH proteome was labelled with FP-Biotin. The biotinylated proteome was enriched with streptavidin, isolated and subsequently analyzed by western-blotting as well. Serine hydrolases: (A) ABHD6, (B) ACOT1/2, (C) FASN, (D) MGLL, and (E) PREP were assessed. n = 3. Significance was assessed with a one-way ANOVA, with multiple comparisons post hoc tests, *p < 0.05, **p < 0.01, ***p < 0.001, ****p < 0.0001. ANOVA p value: (abundance / activity)

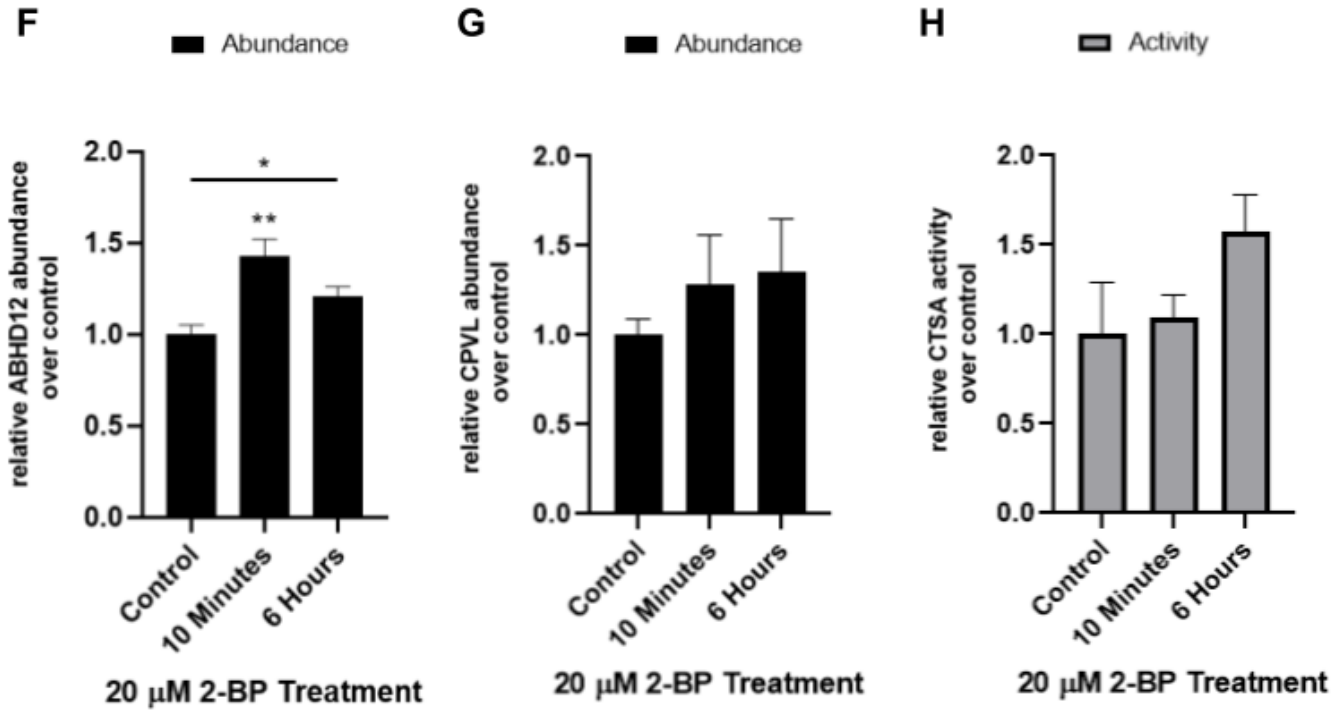


**Figure 3.3: Inhibition of palmitoylation demonstrates changes in activity and abundance in a subset of serine hydrolases (continued)**
HuH7.5 cells were seeded. Spent media was aspirated and replaced with media containing a 20 μM 2-BP concentration for 6 Hours.Cell lysates were collected, one proteome was treated equally with a 20 μM concentration of 2-BP for 10 minutes. Aliquots were taken from each condition and abundance was assessed using traditional western blotting techniques. Following this, the active SH proteome was labelled with FP-Biotin. The biotinylated proteome was enriched with streptavidin, isolated and subsequently analyzed by western-blotting as well. Serine hydrolases: (F) ABHD12, (G) CPVL, and (H) CTSA were assessed. n = 3. Significance was assessed with a one-way ANOVA, with multiple comparisons post hoc tests, *$p < 0.05$, **$p < 0.01$, ***$p < 0.001$, ****$p < 0.0001$.

mitochondrial in its localization [12]. Separating ACOT1/2 abundance and activity is challenging using conventional western blotting techniques as both ACOT1 and ACOT2 are virtually indistinguishable using conventional electrophoretic methods. ACOT1 and ACOT 2 both share extremely high sequence similarities and similar molecular weights. For this reason, the activity and abundance of these proteins were assessed together. ACOT1/2 abundance and activity were assessed in response to 2-BP treatment. A significant increase in ACOT1/2 abundance can be observed after 10 min of 20 µM 2-BP treatment. Non-significant increases in activity can also be seen at both time points, noticeably after 10 minutes and less so after 6 hours of treatment (**Figure 3.3 B**). Overall, palmitoylation affects ACOT1/2 activity throughout treatment. ACOT1/2 abundance is also significantly affected by palmitoylation inhibition in the short term but recovers back to control levels in the long term.

MGLL is a monoacylglycerol lipase, responsible for the degradation of MAGs and the primary CB1 endogenous agonist 2-AG in the brain [13]. Here, in response to 2-BP treatment, there is a significant up-regulation of MGLL abundance and activity during treatment (**Figure 3.3 D**).

PREP is a serine peptidase involved in the maturation and degradation of peptide hormones and neuropeptides [14]. Here we report 20 µM 2-BP treatment induces changes in PREP activity during treatment without significant shifts in abundance (**Figure 3.3 E**). Overall, palmitoylation inhibition affects PREP activity without modulating protein abundance.

ABHD12 participates in the breakdown of CB1 endogenous agonist 2-AG but also the hydrolysis of lysophosphatidylserines [15]. ABHD12 abundance levels shift significantly in response to 2-BP treatment though the magnitude of their changes is not large (**Figure 3.3 F**). Though palmitoylation affected ABHD12 abundance, activity of this serine hydrolase should be further assessed.

### 3.4 Discussion

We have shown that palmitoylation inhibition with 2-BP in HuH7.5 cells revealed significant changes in serine hydrolase activity and abundance. Using FP-Biotin ABPP and conventional western blotting techniques in response to protein palmitoylation inhibition with the broad palmitoylation inhibitor 2-BP, we were able to characterize these effects demonstrating significant changes in activity and/or abundance for serine hydrolases ABHD12, ACOT1/2, MGLL, and PREP. Conversely to what was previously discovered with PAFAH1B3, changes in activity and abundance of tested serine hydrolases all shifted positively in response to 2-BP treatment. The tested SHs have been organized according to their cellular localization. See **Figure 3.4** for this organization.

ABHD6 is a ~30 kDa hydrolase with a single transmembrane domain near the N-terminus and a cytosolically oriented catalytic domain. ABHD6 abundance and activity were increased non-significantly in response to 2-BP treatment. However, the increases in activity observed appeared to be a consequence of the increase in protein abundance (**Figure 3.3 A**).

MGLL is a ~33 kDa enzyme, responsible for the degradation of MAGs and the primary CB1 endogenous agonist 2-AG in the brain [13]. Here, in response to 2-BP treatment, there is a significant up-regulation of MGLL abundance and activity at both time points (**Figure 3.3 D**). In the long term, palmitoylation inhibition might serve to activate MGLL activity through its increase in protein abundance perhaps.

ABHD12 is a ~45 kDa transmembrane glycoprotein responsible for the breakdown of CB1 endogenous agonist 2-AG but also the hydrolysis of lysophosphatidylserines [15]. ABHD12 abundance levels shift significantly in response to 2-BP treatment though the magnitude of their changes is not large (**Figure 3.3 F**).

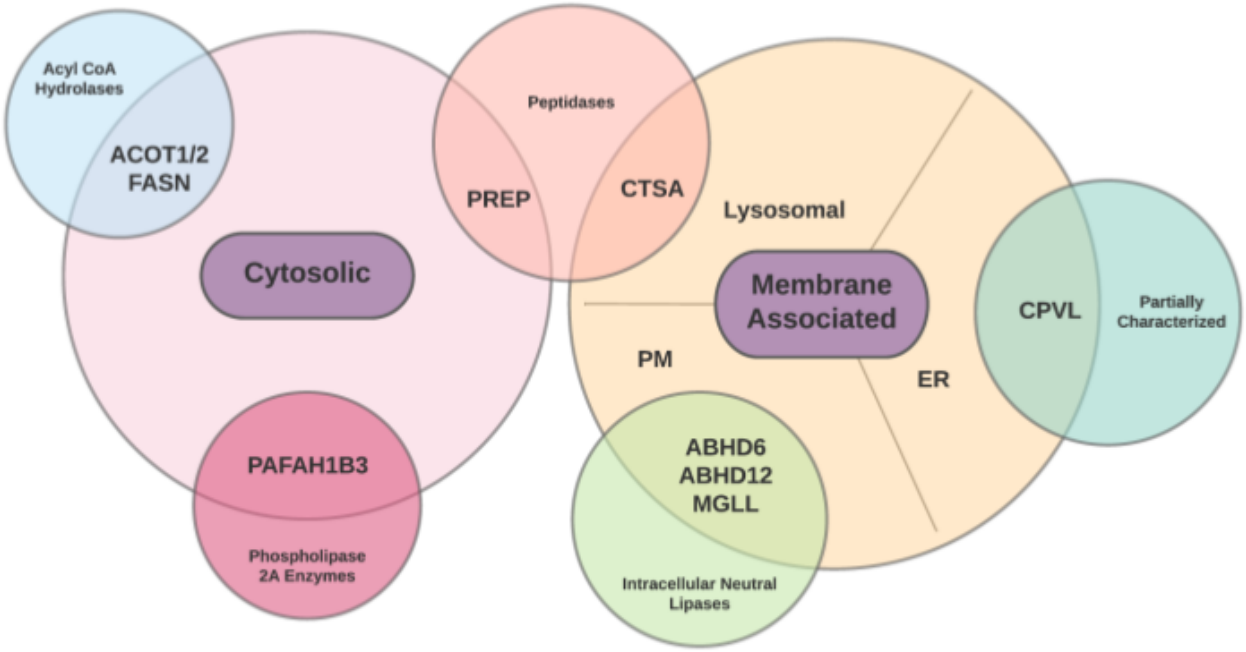


**Figure 3.4: Serine hydrolase localization in the cell varies widely based on function**
All tested serine hydrolases of 2-BP treated HuH7.5s are shown and localization organized according to their cytosolic and membrane associated nature. Serine hydrolases were organized initially by they cytosolic vs. membrane associated nature then by their respective serine hydrolase families. Membrane association was further subdivided into rather lysosomal, endoplasmic reticulum (ER), or plasma membrane (PM) protein associations.Serine hydrolases: alpha/beta-Hydrolase domain containing 6 (ABHD6), alpha/beta-Hydrolase domain containing 12 (ABHD12), Acyl-CoA thioesterase 1/2 (ACOT1/2), carboxypeptidase vitellogenic like (CPVL), cathepsin A (CTSA), fatty acid synthase (FASN), monoacylglycerol lipase (MGLL), platelet-activating factor acetylhydrolase IB subunit alpha1 (PAFAH1B3) and prolyl endopeptidase (PREP) are organized.

Interestingly, it appears all intracellular neutral lipases tested were increased in response to 2-BP treatment. It was hypothesized that the membrane association of these enzymes is essential for its function and perturbation of lipidation would cause alterations in activity. We see a response that overall activates these targets principally through alterations of abundance. Future investigations lie in the plasma membrane localization of these serine hydrolases in response to lipidation inhibition. Interestingly, all these targets play roles in the hydrolysis of the CB1 endocannabinoid and agonist, 2-AG. It has been reported that proper palmitoylation of CB1 at $Cys^{415}$ is necessary for proper membrane localization and signaling [16]. These changes in SH activity and abundance could be a consequence of CB1 perturbation. What we observe here might simply be a homeostatic response to re-enable CB1 receptor dynamics.

Looking to Acyl-CoA Hydrolases, FASN did not demonstrate significant changes in activity or abundance in response to 2-BP treatment. FASN is responsible for the synthesis of *de novo* fatty acids, mainly palmitate lipid species[17]. It was hypothesized; FASN might have a compensatory enhancement in activity or abundance to accommodate the altered palmitome but this is not the case at least after 6 hours. Perhaps FASN activity and abundance are altered in the long term instead. ACOT1/2 however did demonstrate significant changes in abundance after 10 minutes of 20 µM 2-BP administration. Similar non-significant trends of up-regulation in ACOT1/2 activity can be seen as well. Acyl-CoA thioesterases (ACOTs) catalyze the hydrolysis of acyl-CoA esters to form free fatty acids and Co-enzyme A (CoA). ACOT1 is responsible for this activity in the cytoplasm while ACOT2 is mitochondrial in its localization [12]. In this case, in response to 2-BP treatment, inhibition of palmitoylation enables ACOT1/2 activity in an attempt to increase free fatty acid and Acyl CoA stores. Early work on ACOTs referred to this enzyme family as Palmitoyl-CoA hydrolases [18]. A potential hypothesis to these results is an acute homeostatic response to regenerate palmitate and free fatty acids for proper lipidation of the proteome. FASN in this case, if its activity or abundance were equally and significantly up-

regulated could further support this hypothesis. Perhaps FASN might overtake ACOT1/2 in its role to generate free fatty acids in the long term.

Regarding the peptidases, they provide a unique opportunity to compare SH peptidases of different cellular localizations, cytosolic (PREP) and lysosomal (CTSA) specifically. Interestingly, PREP demonstrated significant changes in its activity in response to 2-BP administration throughout treatment (**Figure 3.3 E**). Comparatively, CTSA activity levels did not significantly change though there was a similar magnitude of change after 6 hours of treatment (**Figure 3.3 H**). PREP is a cytosolic serine peptidase involved in the maturation and degradation of peptide hormones and neuropeptides [14]. CTSA is classified as both a cathepsin and carboxypeptidase and has been reported to be an essential co-factor for the activity of beta-galactosidase and neuraminidase through protein-protein interactions [19]. CTSA abundance must be further investigated in response to 2-BP treatment for proper conclusions to be drawn. At this point, without knowledge on CTSA abundance, the shifts in abundance that might occur in response to 2-BP treatment would change the effects that palmitoylation inhibition may have on CTSA.

Overall, these findings further illustrate the relationship between these metabolic serine hydrolases and their requirements for proper lipidation for function. It should be noted, assessing the basal state of palmitoylation of these SH targets is essential for being able to put these results into context. Similarly, a certain possibility to these results regarding the up-regulation of activity and/or abundance of membrane-bound SHs could be a consequence of membrane-bound SHs becoming cytosolically available and free to react more readily in the cytosolic milieu. However, based on these findings, it appears that inhibition of palmitoylation does not significantly down-regulate the function of serine hydrolases regulating endocannabinoid metabolism and lipid synthesis. PAFAH1B3 is involved in lipid signaling during the immune response which might suggest proper palmitoylation is essential in these processes. Going forward, assessing whether there is a link between the endocannabinoid

system and the palmitoylation system might provide insights into lipid signaling dynamics that are not well characterized. Similarly, assessing the roles Acyl-CoA hydrolases have in regulating the palmitome requires further investigation.

### 3.5 Conclusion

We demonstrated that palmitoylation inhibitor-treated cells show enhancement of serine hydrolases ACOT1/2, MGLL, PREP, and ABHD12.

ACOT1/2 demonstrated significant shifts in abundance in response to palmitoylation inhibition with abundance levels returning to control levels in the long term. Palmitoylation inhibition appears to positively regulate MGLL abundance and activity. Inhibition of palmitoylation significantly increased PREP activity levels without affecting abundance throughout treatment. Lastly, palmitoylation inhibition significantly up-regulates ABHD12 abundance levels though activity levels remain to be investigated.

Overall, inhibition of palmitoylation does not significantly down-regulate the function of serine hydrolases regulating endocannabinoid metabolism and lipid synthesis**.** Interestingly, palmitoylation served to increase serine hydrolases involved in endocannabinoid signaling and metabolism. Assessing whether there is a link putative link between the cannabinoid system and the palmitoylation system might provide insights into the cross-talk these two systems might have in regulating the lipid and palmitome.

### 3.6 Materials, experimental and statistical details

#### 3.6.1 Active proteome labeling with fluorophosphonate-biotin

Protein lysates were diluted using a 1% Triton-X in phosphate-buffered saline, pH 7.4 lysis to 1 mL of 1 mg/ml for western-blots pull-down experiments and 2 mg/ml for mass-spectrometry. Fluorophosphonate-biotin probe (Santa Cruz Biotechnologies, Cat.# sc-215056A, CAS Number: 259270-28-5) or DMSO negative control was added to active proteome for a final concentration of 5 µM and incubated with rotation for 1 hour at 37°C. Proteins were precipitated in 5 times the volume of acetone for at least 15 minutes at -80°C and centrifuged for 5 minutes at 4500 g at 4°C. The acetone was removed and the protein pellets were washed with 750 µl of -20°C methanol in 3 alternating cycles of sonication (5 one-second pulses, 30% power) and centrifugation at 20 800 g for 5 minutes at 4°C. The protein pellets were then dissolved in 650 µl 2.5% SDS in PBS and sonicated for 15 one-second pulses at 30% power. The samples were then heated for 5 minutes at 60°C followed by centrifugation at 6500 g for 4 minutes to pellet any remaining contaminants. Aliquots of the supernatants were taken for input controls after which the samples were completed with 1x PBS for a final volume of 8 ml.

#### 3.6.2 Cell Culture

HuH7.5 hepatocellular carcinoma cells were expanded in DMEM media (Gibco TM Cat. # 11995065) supplemented with FBS (10%, Wisent Cat. # 080-450) and 100 nM non-essential amino acids (Gibco Cat. #11140076).

#### 3.6.3 Immunoblotting

Streptavidin beads were washed 3 times with PBS then resuspended in 1 mL of PBS. The resuspension was centrifuged down at 5000 g for 5 minutes at room temperature and the excess PBS was aspirated off. The beads were then resuspended in 45 µL of 2X SDS-PAGE

loading buffer then heat prepped at 95°C for 15 minutes. The resuspended samples were then heat denatured at 95°C for 15 minutes then loaded onto a 10% TGX Stain-Free™ FastCast™ Acrylamide gel (Bio-Rad Cat.# 1610182) loading 7 µL of the all blue protein ladder (Bio-Rad Cat.# 1610393) as protein weight standard. Proteins were transferred from the gel to a PVDF membrane using the Trans-Blot® Turbo™ Transfer System (Bio-Rad), blocked with 3% BSA in TBS-Tween 20 (pH 7.4, 0.05%) for 1 hour at room temperature, fluorescently imaged and then probed with the appropriate primary and secondary antibody dilutions as indicated in Supplementary Table 1.

### 3.6.4 Streptavidin enrichment

100 µL of streptavidin-agarose beads (ThermoFisher Scientific, Cat.# 20353) were washed 3 times with 1x PBS in Micro Bio-Spin™ Chromatography Columns (Bio-Rad Cat.# 7326204) and then transferred over to the protein samples. Protein samples were then incubated via rotation for 2 hours at room temperature. The beads were pelleted by centrifugation at 1400 g for 2 minutes at room temperature then transferred into Micro Bio-Spin™ Chromatography Columns (Bio-Rad Cat.# 7326204 ) and washed 3 times with 1% SDS followed by three washes with 6 M urea.

### 3.6.5 Statistics

Error bars displayed in this investigation is the calculated standard deviation between related samples. Statistical significance was measured with a one-way ANOVA, with multiple comparison post hoc tests, *$p < 0.05$, **$p < 0.01$, ***$p < 0.001$, ****$p < 0.0001$.

## 3.7 References


1. Kathayat RS, Cao Y, Elvira PD, et al. Active and dynamic mitochondrial S-depalmitoylation revealed by targeted fluorescent probes. *Nat Commun*. 2018;9(1). doi:10.1038/s41467-017-02655-1
2. Zheng B, Deran M, Li X, Liao X, Fukata M, Wu X. 2-Bromopalmitate analogues as activity-based probes to explore palmitoyl acyltransferases. *J Am Chem Soc*. 2013;135(19). doi:10.1021/ja311416v
3. Coleman RA, Rao P, Fogelsong RJ, Bardes ESG. 2-Bromopalmitoyl-CoA and 2-bromopalmitate: Promiscuous inhibitors of membrane-bound enzymes. *Biochim Biophys Acta (BBA)/Lipids Lipid Metab*. 1992;1125(2). doi:10.1016/0005-2760(92)90046-X
4. Webb Y, Hermida-Matsumoto L, Resh MD. Inhibition of protein palmitoylation, raft localization, and T cell signaling by 2-bromopalmitate and polyunsaturated fatty acids. *J Biol Chem*. 2000;275(1). doi:10.1074/jbc.275.1.261
5. Fukata M, Fukata Y, Adesnik H, Nicoll RA, Bredt DS. Identification of PSD-95 palmitoylating enzymes. *Neuron*. 2004;44(6). doi:10.1016/j.neuron.2004.12.005
6. Davda D, El Azzouny MA, Tom CTMB, et al. Profiling targets of the irreversible palmitoylation inhibitor 2-bromopalmitate. *ACS Chem Biol*. 2013;8(9). doi:10.1021/cb400380s
7. Linder ME, Deschenes RJ. Palmitoylation: Policing protein stability and traffic. *Nat Rev Mol Cell Biol*. 2007;8(1). doi:10.1038/nrm2084
8. Wei X, Song H, Semenkovich CF. Insulin-regulated protein palmitoylation impacts endothelial cell function. *Arterioscler Thromb Vasc Biol*. 2014;34(2). doi:10.1161/ATVBAHA.113.302848
9. Cravatt BF, Wright AT, Kozarich JW. Activity-based protein profiling: from enzyme chemistry to proteomic chemistry. *Annu Rev Biochem*. 2008;77.
10. Liu Y, Patricelli MP, Cravatt BF. Activity-based protein profiling: the serine hydrolases. *Proc Natl Acad Sci USA*. 1999;96.
11. Barglow KT, Cravatt BF. Activity-based protein profiling for the functional annotation of enzymes. *Nat Methods*. 2007;4(10). doi:10.1038/nmeth1092
12. Westin MAK, Alexson SEH, Hunt MC. Molecular cloning and characterization of two mouse peroxisome proliferator-activated receptor α (PPARα)-regulated peroxisomal acyl-CoA thioesterases. *J Biol Chem*. 2004;279(21). doi:10.1074/jbc.M313863200
13. Mulvihill MM, Nomura DK. Therapeutic potential of monoacylglycerol lipase inhibitors. In: *Life Sciences*. Vol 92. ; 2013. doi:10.1016/j.lfs.2012.10.025
14. Long JZ, Cravatt BF. The metabolic serine hydrolases and their functions in mammalian physiology and disease. *Chem Rev*. 2011. doi:10.1021/cr200075y
15. Savinainen JR, Saario SM, Laitinen JT. The serine hydrolases MAGL, ABHD6 and ABHD12 as guardians of 2-arachidonoylglycerol signalling through cannabinoid receptors. *Acta Physiol*. 2012. doi:10.1111/j.1748-1716.2011.02280.x
16. Oddi S, Stepniewski TM, Totaro A, et al. Palmitoylation of cysteine 415 of CB1 receptor affects ligand-stimulated internalization and selective interaction with membrane cholesterol and caveolin 1. *Biochim Biophys Acta - Mol Cell Biol Lipids*. 2017;1862(5). doi:10.1016/j.bbalip.2017.02.004
17. Menendez JA, Lupu R. Fatty acid synthase and the lipogenic phenotype in cancer pathogenesis. *Nat Rev Cancer*. 2007;7(10). doi:10.1038/nrc2222
18. OGIWARA H, TANABE T, NIKAWA J -i, NUMA S. Inhibition of Rat-Liver Acetyl-Coenzyme-A Carboxylase by Palmitoyl-Coenzyme A: Formation of Equimolar Enzyme-Inhibitor Complex. *Eur J Biochem*. 1978;89(1). doi:10.1111/j.1432-1033.1978.tb20893.x
19. Galjart NJ, Morreau H, Willemsen R, Gillemans N, Bonten EJ, d'Azzo A. Human

lysosomal protective protein has cathepsin A-like activity distinct from its protective function. *J Biol Chem*. 1991;266(22). doi:10.1016/s0021-9258(18)98751-x

20 Russell RS, Meunier JC, Takikawa S, et al. Advantages of a single-cycle production assay to study cell culture-adaptive mutations of hepatitis C virus. Proc Natl Acad Sci U S A. 2008;105(11). doi:10.1073/pnas.080042210521. Niphakis MJ, Cognetta AB, Chang JW, et al.

21. Niphakis MJ, Cognetta AB, Chang JW, et al. Evaluation of NHS carbamates as a potent and selective class of endocannabinoid hydrolase inhibitors. ACS Chem Neurosci. 2013. doi:10.1021/cn400116z

22. Rakic B, Sagan SM, Noestheden M, et al. Peroxisome proliferator-activated receptor α antagonism inhibits hepatitis C virus replication. Chem Biol. 2006. doi:10.1016/j.chembiol.2005.10.006

23. Ianevski A, Giri AK, Aittokallio T. SynergyFinder 2.0: visual analytics of multi-drug combination synergies. Nucleic Acids Res. 2020. doi:10.1093/nar/gkaa216

# Chapter 4: Future directions

### 4.1 Future directions

Assessing CB1 induction during HCV infection and what effects that might have in contributing to the MJN110 antiviral profile is vital. Namely, demonstrating a lack of AMPK activation in response to MJN110 administration during HCV infection is required to fully confirm a CB1 independent mechanism of HCV inhibition for MGLL inhibitor MJN110. This hypothesis also extends to other, 2-AG hydrolyzing metabolic serine hydrolases with links to the endocannabinoid system such as ABHD6, ABHD12, and CES1.

We have demonstrated the viability of MJN110 for drug co-treatment through our reported drug dose-response matrix of MJN110 and CB1 antagonist AM251. Investigating the therapeutic relevance of MGLL targeted host antivirals, and the combinatory effects they might have with currently available DAAs might prove beneficial for the treatment of HCV while awaiting other curative discoveries. Exploring the HCV antiviral effects of MJN110 and other MGLL inhibitors as potential pan-flavivirus targeting antivirals could present an interesting future route for MGLL host targeted antivirals past HCV due to reported herein, the effects MGLL inhibition by MJN110 has on extracellular membrane dynamics.

Regarding MJN110 pharmacodynamic characterization, MGLL irreversible inhibition by MJN110 reveals MGLL is swiftly degraded by the proteasome throughout treatment, a drawback of irreversible drug design. This would result in reduced MGLL inhibition over time as MGLL clearance and regeneration occur. Determining if MJN110 binding induces structural shifts in MGLL for degron presentation and subsequent degradation might prove invaluable for the development of longer-lasting, more temporally viable MGLL host targeted antivirals based on MJN110. This unique method of enzymatic down-regulation, though potent, would demonstrate long-term treatment issues in the clinic. Co-IP of MJN110 treated cells will be used to assess if this method of down-regulation is ubiquitin dependant while CD spectroscopy of MJN110

treated purified MGLL protein will be done to assess global protein changes for this degron presentation hypothesis for UPS mediated MGLL degradation.

Lastly, characterization of metabolic serine hydrolases in response to palmitoylation inhibition revealed only phospholipase 2A enzyme PAFAH1B3 requires proper lipidation for its function. Neutral lipases ABHD6, ABHD12, and MGLL, were all positively regulated in response to improper lipidation, suggesting it is not essential for its function but rather, might play an interesting role in cross-talk between the endocannabinoid system and the palmitoylation system. Assessing if the lack of CB1 palmitoylation induces the expression of endocannabinoid system-related serine hydrolases might demonstrate a unique method of lipid signaling and regulation that might span to other GPCRs.

# Appendix A – Supplemental figures for chapter 2

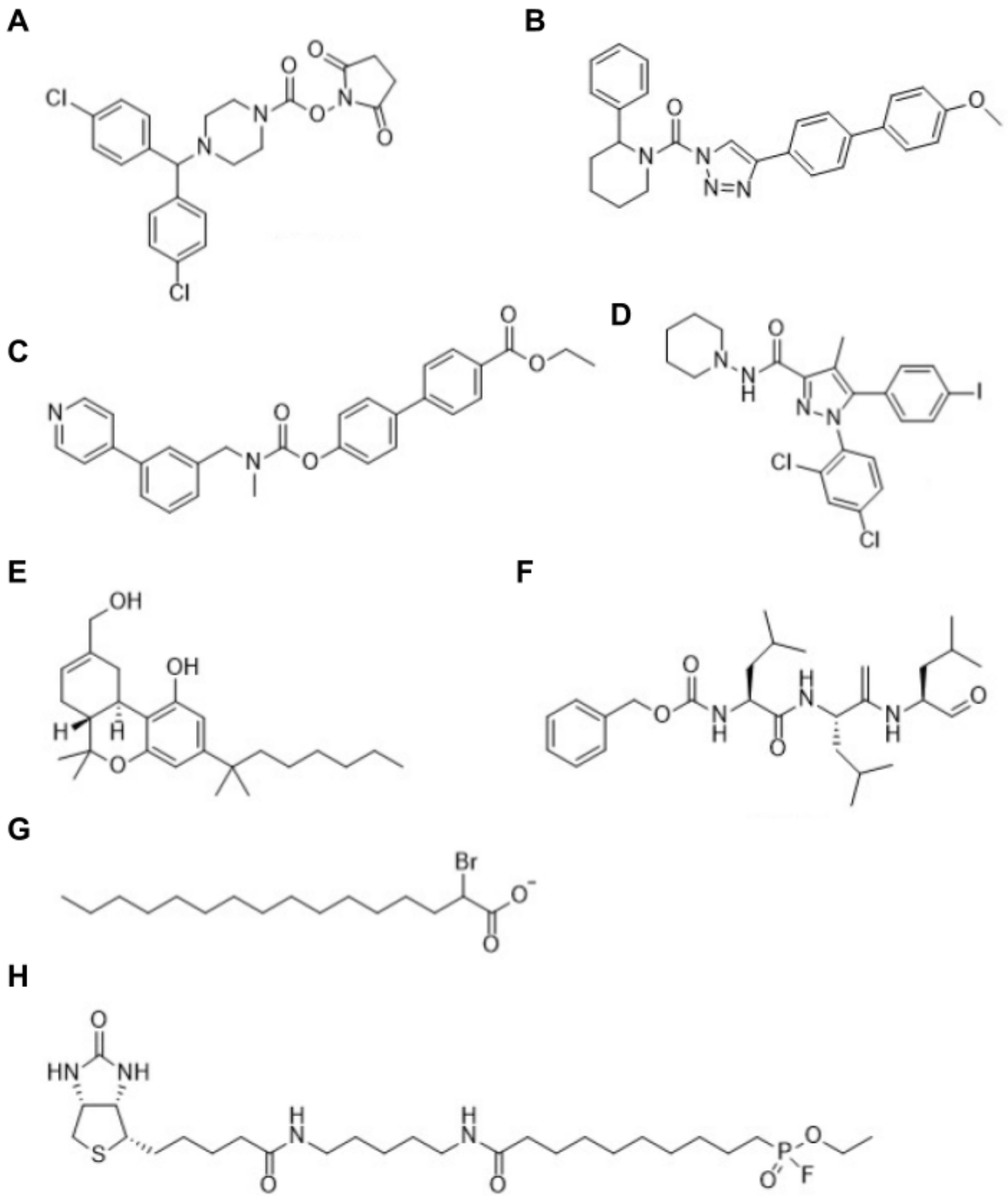


**Supplemental figure 2.1: Chemical structures of all small molecules used in this investigation**
Chemical structure of (A) MGLL inhibitor, MJN110, (B) ABHD6 inhibitor, KT195, (C) CES1 inhibitor, WWL113, (D) CB1 antagonist, AM251, (E) CB1 agonist, HU210, (F) proteasome inhibitor, MG132, (G) palmitoylation inhibitor. 2-bromopalmitate (2-BP), (H) serine hydrolase activity probe, FP-Biotin (Fluorophosphonate-Biotin

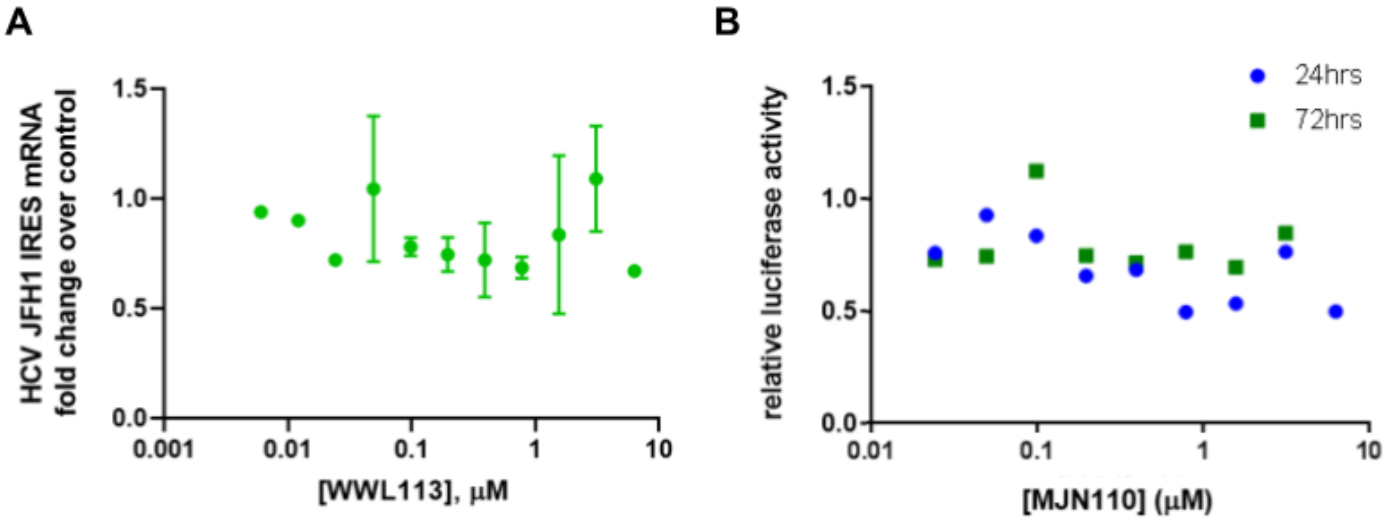


**Supplemental figure 2.2: Small molecule inhibition of metabolic serine hydrolases MGLL and CES1 have selective inhibitory profiles**

(A) The CES1 inhibitor WWL113 does not inhibit HCV $JFH1_T$ 2a infection as measured by RT-qPCR of the HCV internal ribosome entry site (IRES). Cells were infected with HCV $JFH1_T$ 2a for 5 hours, after which the medium was changed for fresh medium containing the corresponding small molecule, followed by a 72 hour incubation. n=2.

(B) The MGLL inhibitor MGLL does not inhibit the HCV-SGR as measured by the protein concentration normalized firefly luciferase signal to the vehicle control. Subgenomic replicon harbouring cells were seeded, 24 hours after which the medium was changed for fresh medium containing the corresponding small molecule, followed by a 24 or 72 hour incubation. n=1.

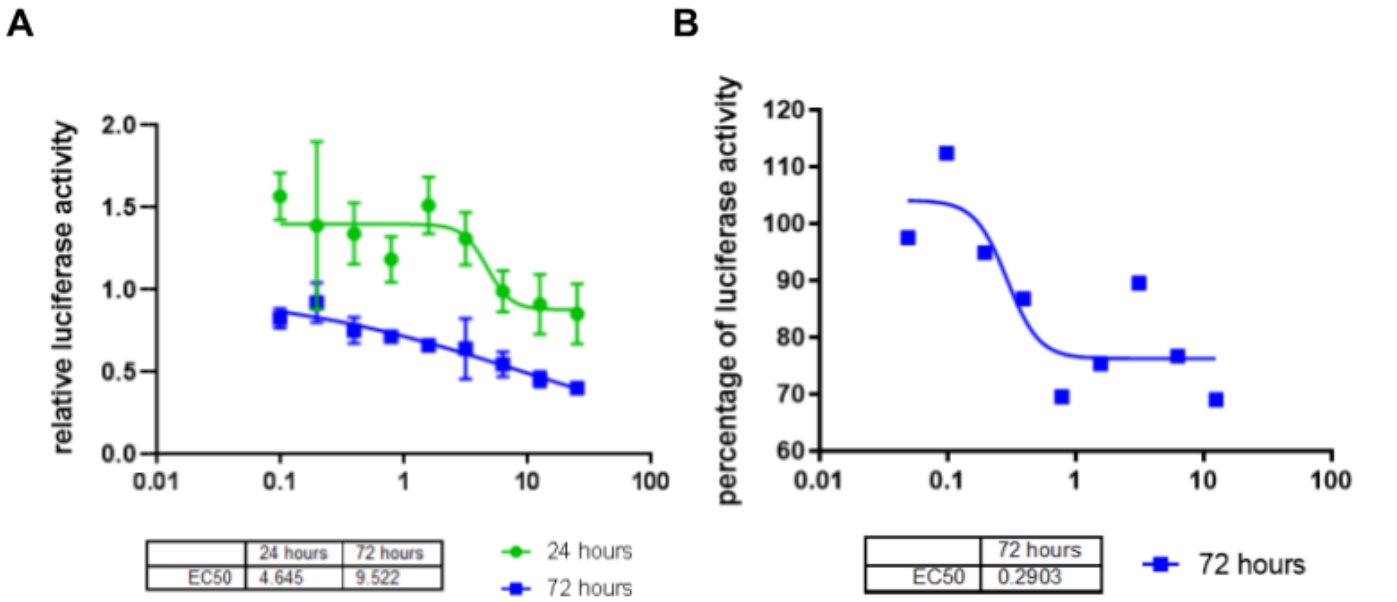


C

| Small Molecules | 72 Hour Treatment | | | | | | | | | | | | | | | | | | | 24 Hour Treatment | | | | | | | | | | |
|---|---|---|---|---|---|---|---|---|---|---|---|---|---|---|---|---|---|---|---|---|---|---|---|---|---|---|---|---|---|---|
| AADAC Inhibitor Yoshio 3 | | | | * | | | * | | * | * | | * | * | * | * | | | | * | | | * | | * | * | | * | * | * | * |
| ABHD6 Inhibitor KT195 | | | * | | | * | | * | | * | * | | * | * | * | | | * | | | * | | * | | * | * | | * | * | * |
| CES1 Inhibitor WWL113 | | * | | | * | | | * | * | | * | * | | * | * | | * | | | * | | | | * | * | | * | * | | * | * |
| MGLL Inhibitor MJN110 | * | | | | * | * | * | | | | * | * | * | | * | * | | | | * | * | * | | | | | * | * | * | | * |

**Supplemental figure 2.3: Loewe distributed small molecule serine hydrolase inhibitor cocktails**
(A) The ABHD6 inhibitor KT195, and CES1 inhibitor WWL113 co-treatment distributed under a Loewe hypothesis inhibits the HCV-SGR in a dose-dependent manner with an $EC_{50}$ (half-maximal effective concentration) of 4.6 μM at 24 hours and 9.5 μM at 72 hours as measured by the protein concentration normalized firefly luciferase signal to the loading control, DMSO. Subgenomic replicon harbouring cells were seeded, 24 hours after which the medium was changed for fresh medium containing the corresponding small molecules (1:1 ratio of KT195:WWL113 to the specified total concentration), followed by a 24 or 72 hour incubation. n=3.
(B) The AADAC inhibitor Yoshio 3 and MGLL inhibitor MJN110 co-treatment inhibits the HCV-SGR in a dose-dependent manner with an $EC_{50}$ (half-maximal effective concentration) of 0.29 μM at 72 hours as measured by the protein concentration normalized firefly luciferase signal to the vehicle control. Subgenomic replicon harbouring cells were seeded, 24 hours after which the medium was changed for fresh medium containing the corresponding small molecule (1:1 ratio of Yoshio 3:MJN110 to the specified total concentration), followed by a 72 hour incubation. n=3.
(C) Serine Hydrolase tested cocktail array. Each tested serine hydrolase cocktail were tested under the premise that the expected response corresponds to an additive effect as if the single drugs were the same compound (Loewe). That being said, serine hydrolase cocktails were tested in equal ratios of SH small molecules inhibitors up to the displayed concentration. Green squares represent cocktails that were able to curve fit while those that are red yielded no curve fitting capabilities.

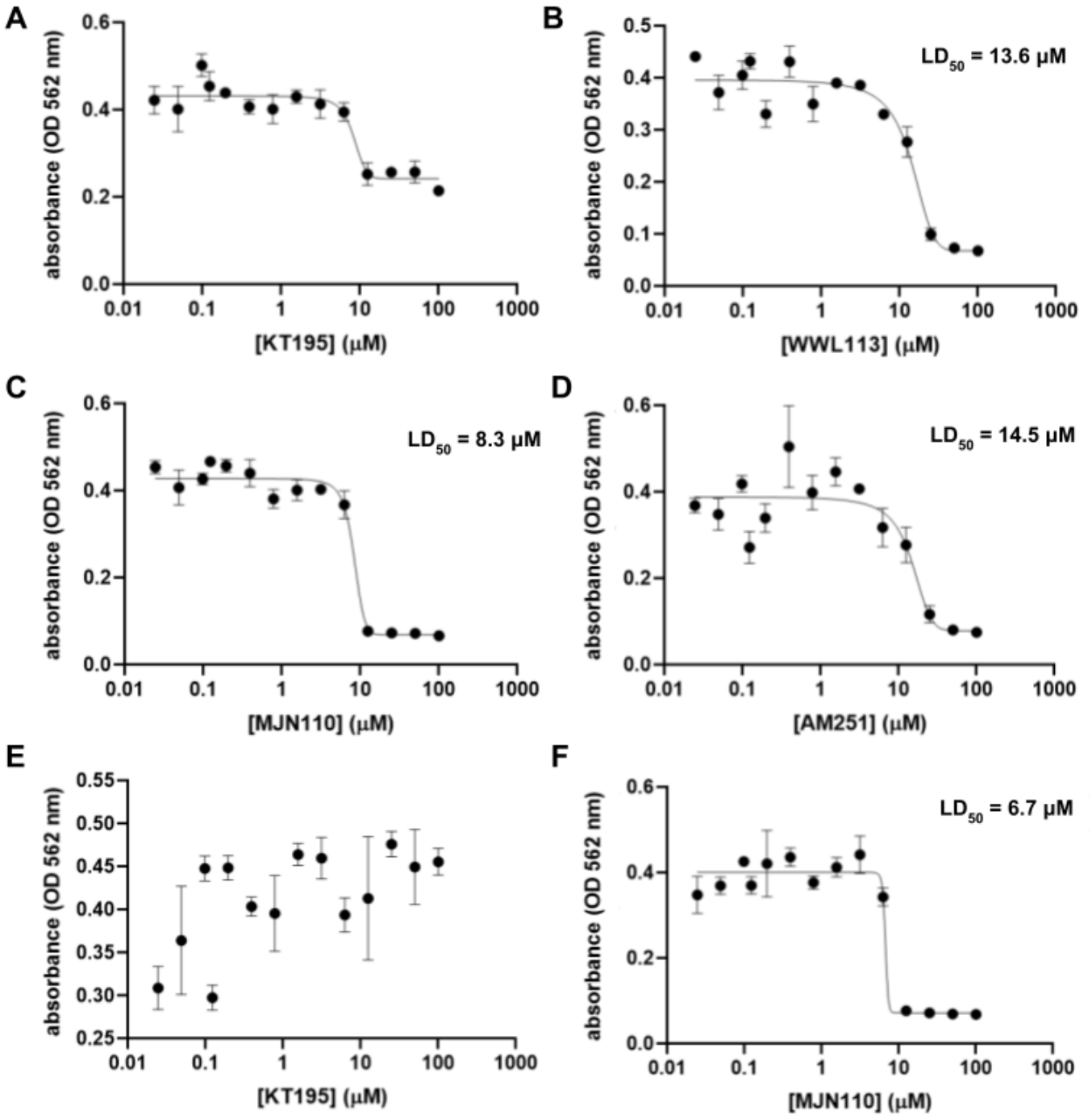


**Supplemental figure 2.4: Drug cell viability curves as determined though the MTT cell viability assay**
Drug cytotoxicity was assessed using a MTT cell viability assay. HuH7.5 cells were initially seeded in a 96-well plate, treated with the corresponding small molecule and incubated for the corresponding amount of time. At the end of incubation, spend media was aspirated, washed, and then treated with 50 uL of 2.5 mg/mL of MTT diluted in 1x PBS and incubated for 3 hours at 37°C, 5.0% $CO_2$. Spent MTT reagent is aspirated and the precipitated formzan crystals are solubilized in 50 uL DMSO. The plate is then read at 562 nm using the i3 spectrometer. Cell viability was assessed for (A) ABHD6 inhibitor KT195, (B) CES1 inhibitor WWL113 ($LD_{50}$ = 13.6 μM), (C) MGLL inhibitor MJN110 ($LD_{50}$ = 8.3 μM) and (D) CB1 antagonist AM251($LD_{50}$ = 14.5 μM) at 72 hours. Cell viability was also assessed for (E) ABHD6 inhibitor KT195 and (F) MGLL inhibitor MJN110 ($LD_{50}$ = 6.7 μM) at 48 hours. n = 3, error bars represent the standard deviation of a technical triplicate. $LD_{50}$ represents the lethal dose where a 50 reduction of cell viability is observed compared to control levels.

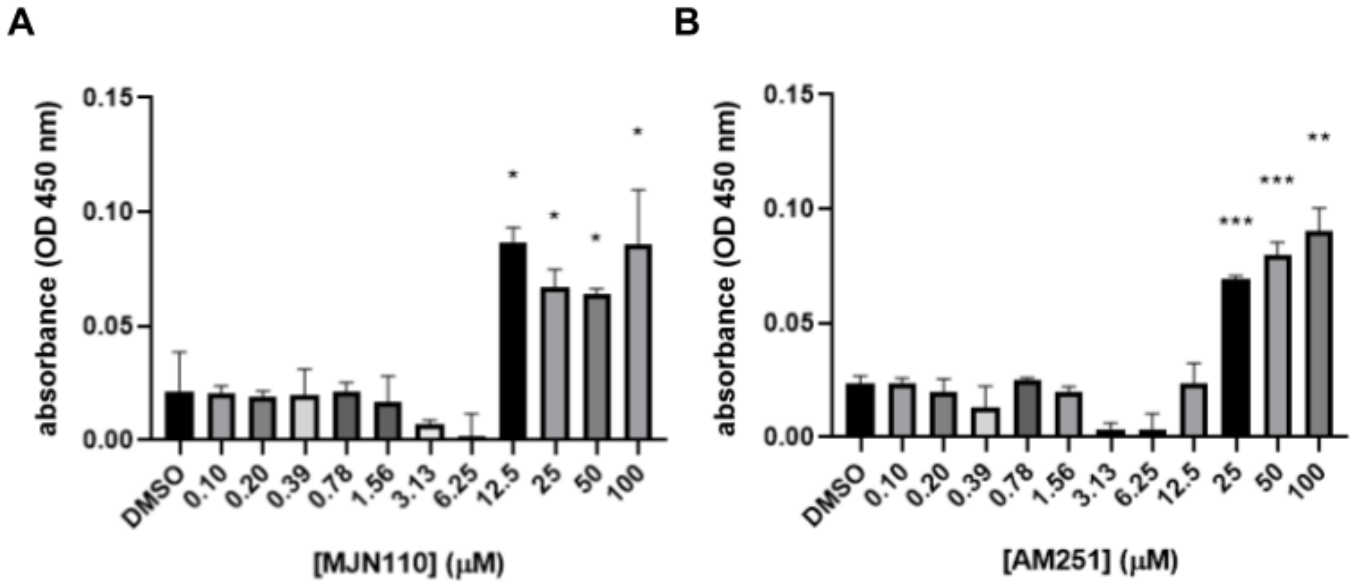


**Supplemental figure 2.5: Drug cell viability as determined through the lactate dehydrogenase cell viability assay**

Cell viability in response to (A) MGLL inhibitor MJN110 and (B) CB1 antagonist AM251 after 72 hours was assessed using an Abcam LDH cell viability assay kit. HuH7.5 cells were initially seeded in a 96-well plate, after which, the spent media was aspirated and replaced with media containing the corresponding small molecules for 72 hours at 37°C, 5.0% $CO_2$. Post incubation, 10 uL for each well was transferred into an optically clear 96-well plate. 100 uL of the LDH Reaction Mix was added and mixed in each well after which the plate was read at 450 nm for LDH concentration and 650 nm for it's normalization. Here represents the absorbance normalized treatment array.n = 3, error bars represent the standard deviation of a technical triplicate.Significance assessed with two-tailed, unpaired student's t test, *p < 0.05, **p < 0.01, ***p < 0.001.

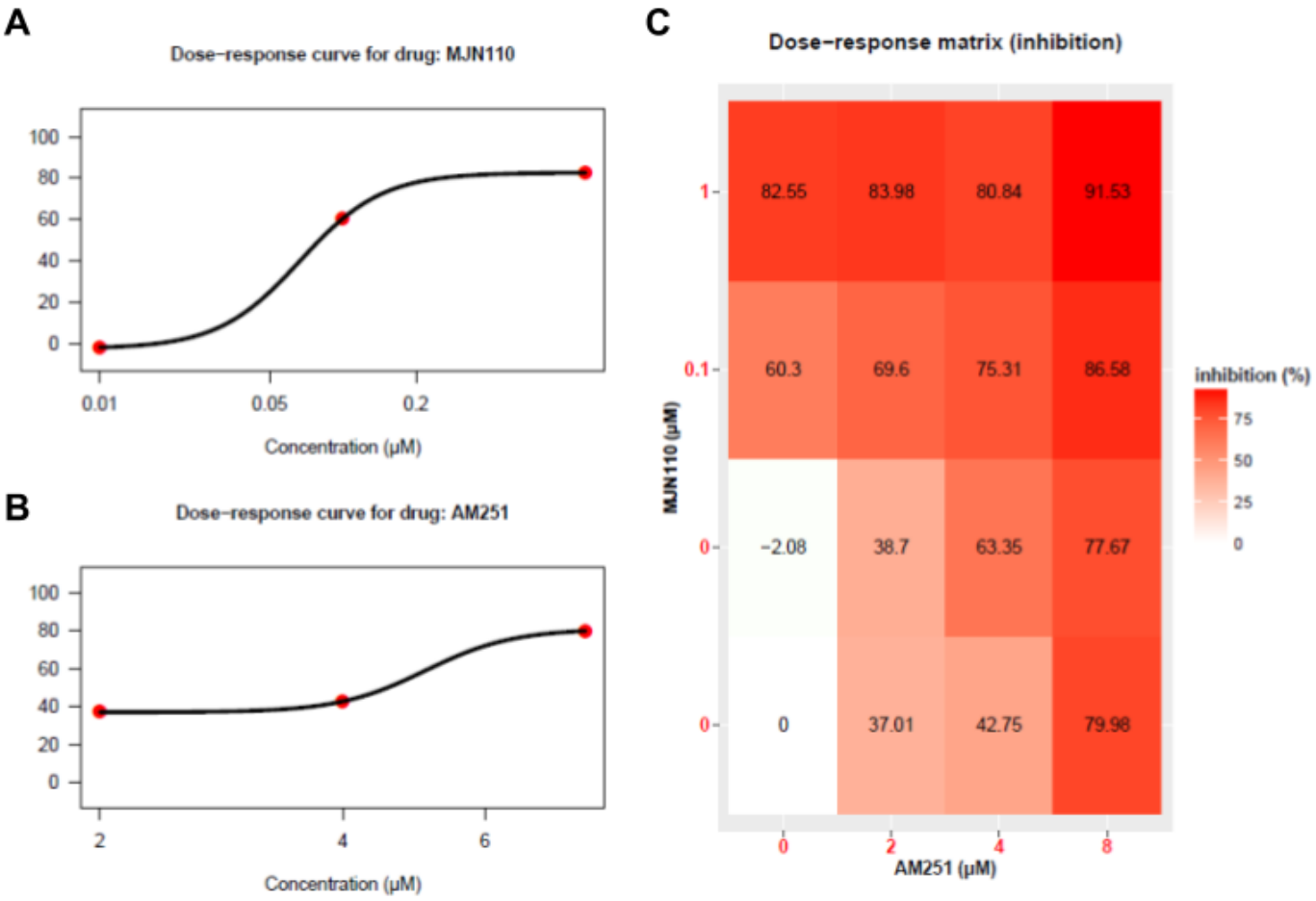


**Supplemental figure 2.6: Calculation and visualization of synergy scores for drug combination AM251:MJN110 individual Curves and matrix using SynergyFinder2.0**

SynergyFinder 2.0 brute analysis, static report. Inhibition of HCV $JFH1_T$ 2a was determined by RT-qPCR of the HCV internal ribosome entry site (IRES). Cells were infected with HCV $JFH1_T$ 2a for 5 hours, after which the medium was changed for fresh medium containing the corresponding MJN110:AM251 co-treatments, followed by a 72 hour incubation. n = 3. Individual Dose curves for (A) MJN110 and (B) AM251 Curves were fit using the LL4 curve fitting feature. (C) Inhibition dose response matrix for AM251:MJN110

A

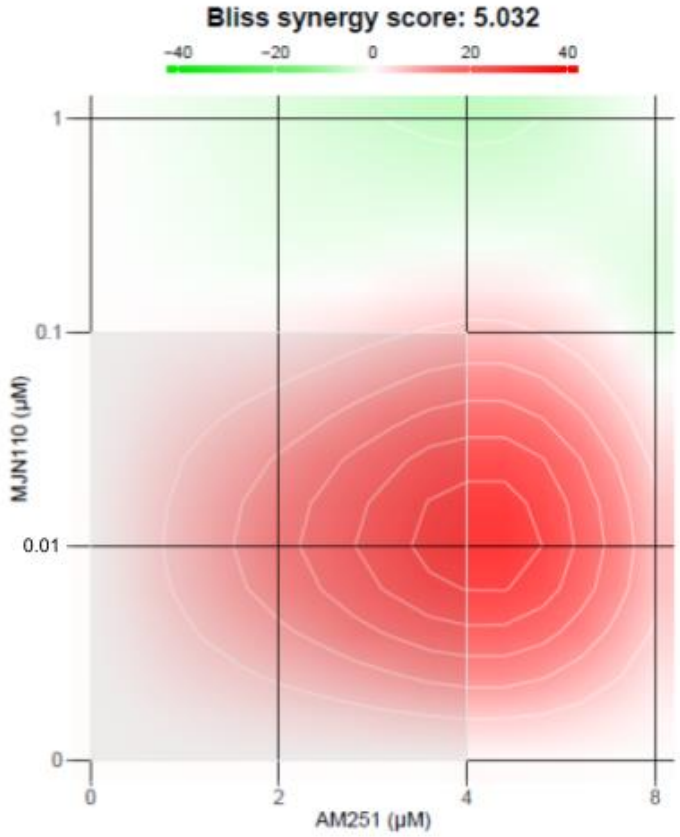


B

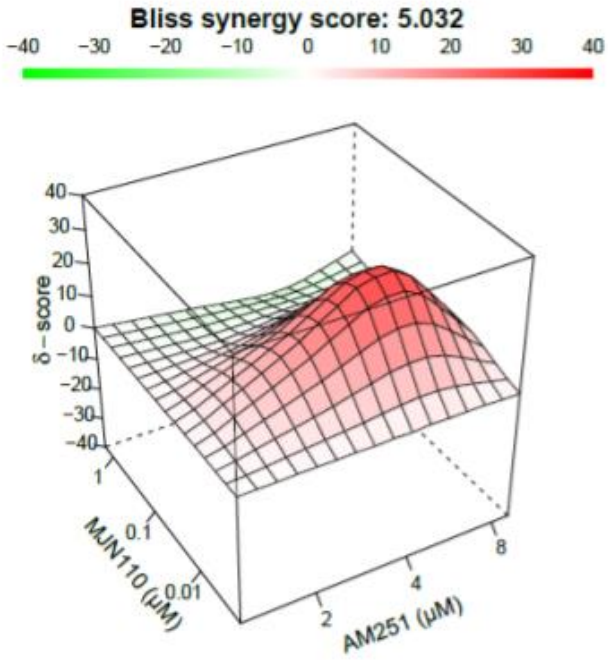


C

| Drug combination | Synergy score | Most synergistic area score | Method |
|---|---|---|---|
| AM251 - MJN110 | 5.03 | 6.16 | Bliss |

D

$$S_{BLISS} = E_{A,B,\ldots,N} - (E_A + E_B + \ldots + E_N - E_A E_b - E_A E_N - E_B E_N - \ldots - E_A E_B \ldots E_N).$$

**Supplemental figure 2.7: Calculation and visualization of synergy scores for drug combination AM251:MJN110 using SynergyFinder2.0, Bliss calculated synergy**

Bliss synergy is determined as the multiplicative effect of single drugs as they act independently of each other.
(A) Calculated topological Bliss synergy map using synergy finder 2.0, two-dimensional representation. Calculated synergy score of the MJN110:AM251 matrix, δ = 5.03. The greyed 3-by-3 area refers to the treatment range with the highest overall synergy, δ = 6.16.
(B) Calculated topological Bliss synergy map using synergy finder 2.0, three-dimensional representation. Calculated synergy score of the MJN110:AM251 matrix, δ = 5.032
(C) Overview of the calculated Bliss synergy
(D) Bliss synergy calculation equation. S refers to the measured synergy. $E_A$, $E_B$,..., $E_N$ are the measured responses of the single drugs or, the measured responses of multi drug combinations.

A

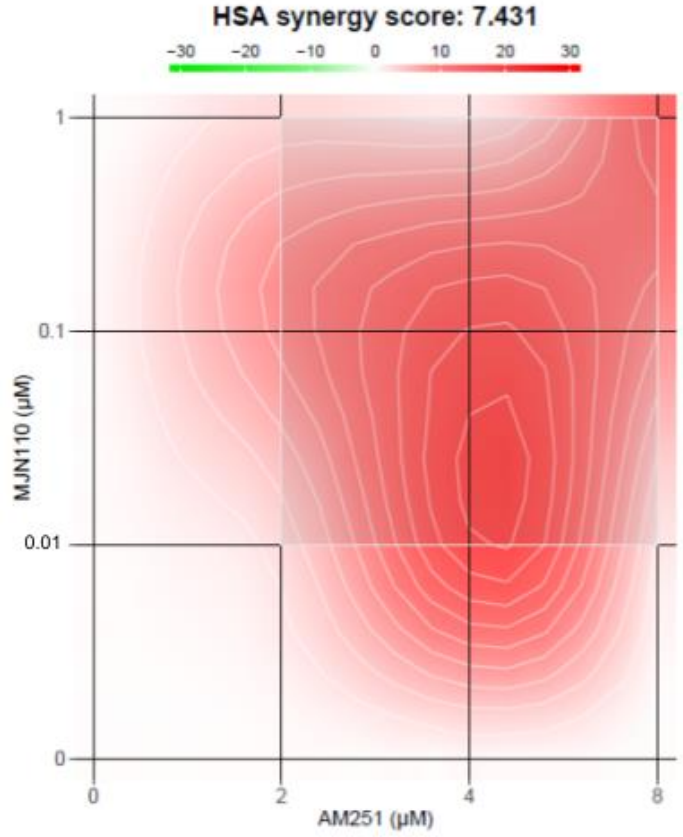


B

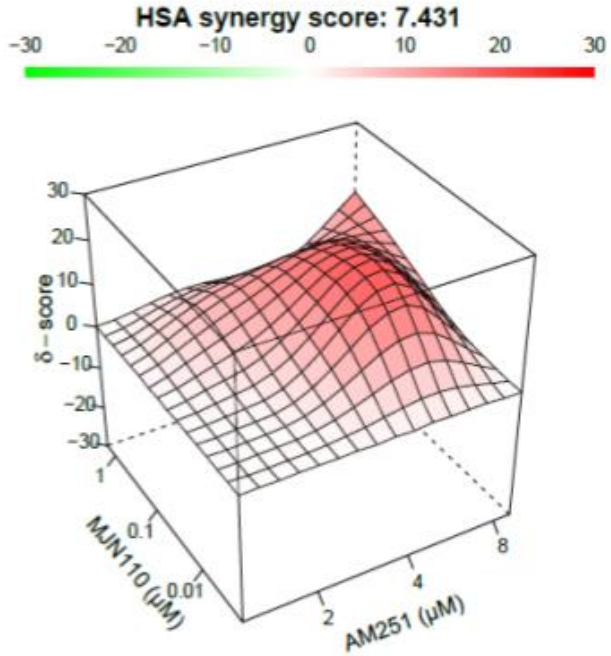


C

| Drug combination | Synergy score | Most synergistic area score | Method |
|---|---|---|---|
| AM251 - MJN110 | 7.43 | 8.56 | HSA |

D

$$S_{HSA} = E_{A,B,\ldots,N} - \max(E_A, E_B, \ldots, E_N).$$

**Supplemental figure 2.8: Calculation and visualization of synergy scores for drug combination AM251:MJN110 using SynergyFinder2.0, HSA calculated synergy**

Highest single agent (HSA) synergy is determined as the excess response over the maximum single dose response.

(A) Calculated topological HSA synergy map using synergy finder 2.0, two-dimensional representation. Calculated synergy score of the MJN110:AM251 matrix, δ = 7.43. The greyed 3-by-3 area refers to the treatment range with the highest overall synergy, δ = 8.56.

(B) Calculated topological HSA synergy map using synergy finder 2.0, three-dimensional representation. Calculated synergy score of the MJN110:AM251 matrix, δ = 7.43

(C) Overview of the calculated HSA synergy

(D) HSA synergy calculation equation. S refers to the measured synergy. $E_A$, $E_B$,..., $E_N$ are the measured responses of the single drugs or, the measured responses of multi drug combinations.

A

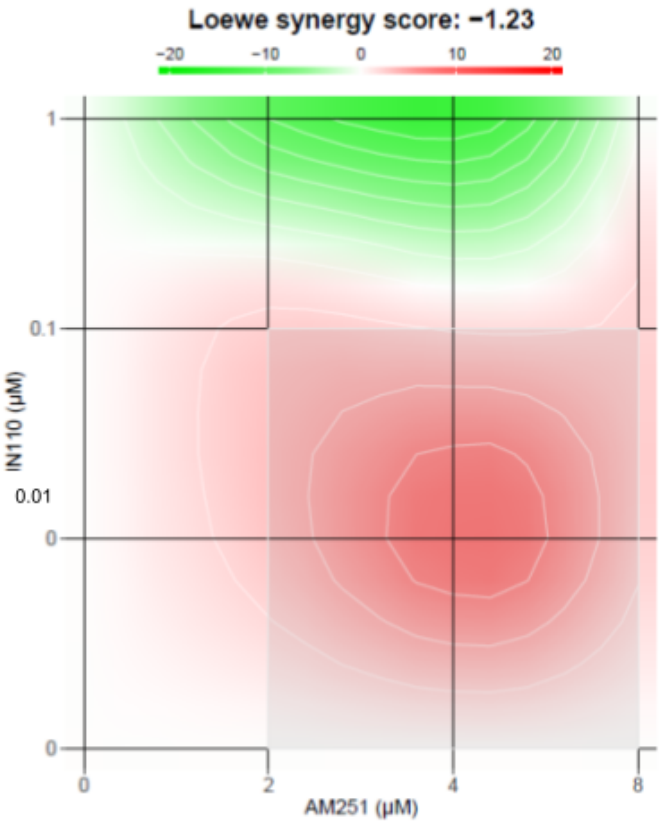


B

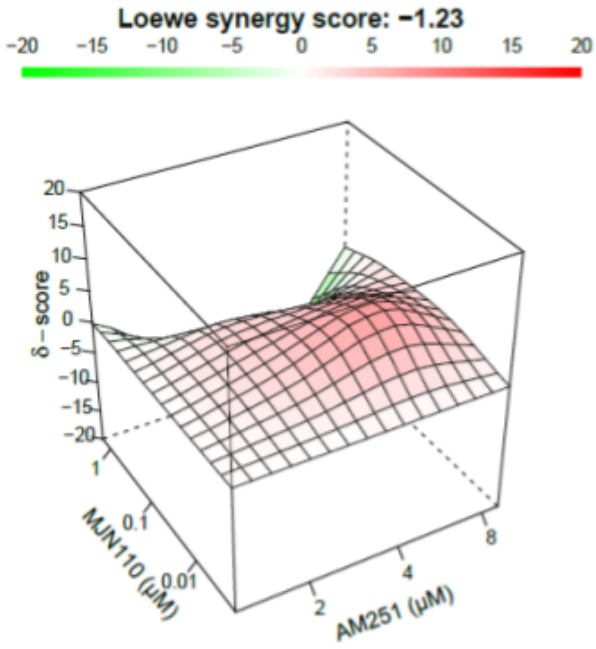


C

| Drug combination | Synergy score | Most synergistic area score | Method |
|---|---|---|---|
| AM251 - MJN110 | -1.23 | 2.40 | Loewe |

D

$$S_{LOEWE} = \frac{a}{A} + \frac{b}{B} + \ldots + \frac{n}{N}.$$

**Supplemental figure 2.9: Calculation and visualization of synergy scores for drug combination AM251:MJN110 using SynergyFinder2.0, Loewe calculated synergy**

Loewe synergy is determined as the expected response corresponding to an additive effect if the single drugs were the same compound.

(A) Calculated topological Loewe synergy map using synergy finder 2.0, two-dimensional representation. Calculated synergy score of the MJN110:AM251 matrix, δ = -1.23. The greyed 3-by-3 area refers to the treatment range with the highest overall synergy, δ = 2.40.

(B) Calculated topological Loewe synergy map using synergy finder 2.0, three-dimensional representation. Calculated synergy score of the MJN110:AM251 matrix, δ = -1.23

(C) Overview of the calculated Loewe synergy

(D) Loewe synergy calculation equation. S refers to the measured synergy. A, B and N are the doses of the single drugs required to produce the particular response. Loewe synergy assumes a monotonic additivity where linear ratios of drug combinations elicit the same level of response. E.g. 80% inhibition is achieved separately by 1 μM of drug A or 2 μM of drug B, a combination of 0.5 μM of A and 1 μM of B should also inhibit 80%

A

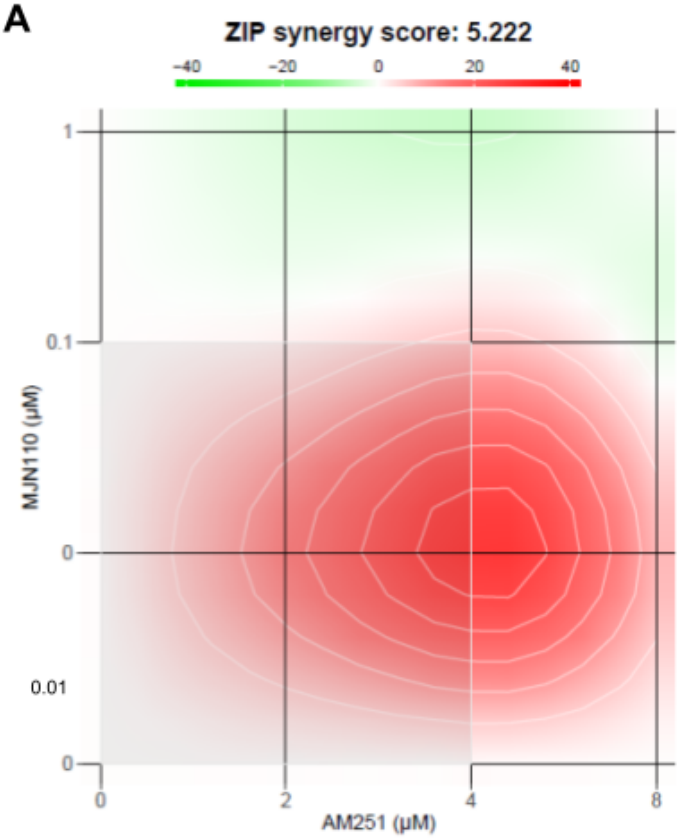


B

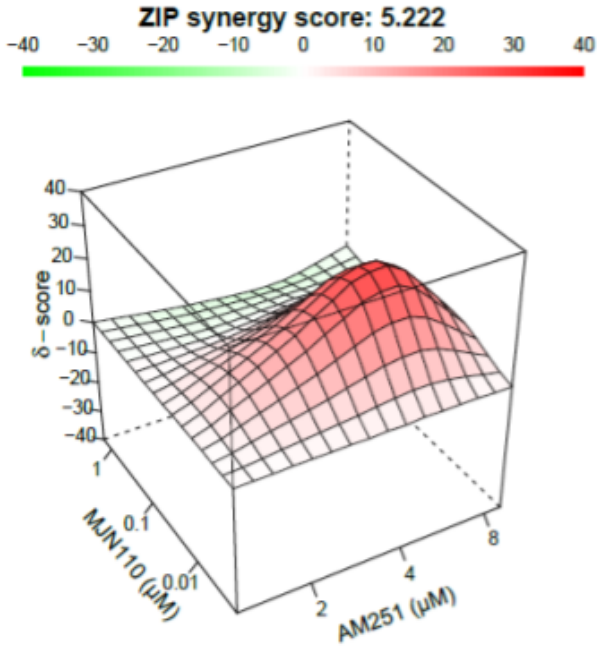


C

| Drug combination | Synergy score | Most synergistic area score | Method |
|---|---|---|---|
| AM251 - MJN110 | 5.22 | 6.16 | ZIP |

**Supplemental figure 2.10: Calculation and visualization of synergy scores for drug combination AM251:MJN110 using SynergyFinder2.0, ZIP calculated synergy**

Zero interaction potency (ZIP) synergy is determined as the expected response corresponding to the effect as if the single drug did not alter the potency of each other.

(A) Calculated topological ZIP synergy map using synergy finder 2.0, two-dimensional representation. Calculated synergy score of the MJN110:AM251 matrix, δ = 5.22. The greyed 3-by-3 area refers to the treatment range with the highest overall synergy, δ = 6.16.

(B) Calculated topological ZIP synergy map using synergy finder 2.0, three-dimensional representation. Calculated synergy score of the MJN110:AM251 matrix, δ = 5.22.

(C) Overview of the calculated ZIP synergy

**D**

$$S_{ZIP} = E_{A,B,\ldots,N} - \left( \frac{\left(\frac{x_A}{m_A}\right)^{\lambda_A}}{1+\left(\frac{x_A}{m_A}\right)^{\lambda_A}} + \frac{\left(\frac{x_B}{m_B}\right)^{\lambda_B}}{1+\left(\frac{x_B}{m_B}\right)^{\lambda_B}} + \ldots \right.$$
$$+ \frac{\left(\frac{x_N}{m_N}\right)^{\lambda_N}}{1+\left(\frac{x_N}{m_N}\right)^{\lambda_N}} - \frac{\left(\frac{x_A}{m_A}\right)^{\lambda_A}}{1+\left(\frac{x_A}{m_A}\right)^{\lambda_A}} \frac{\left(\frac{x_B}{m_B}\right)^{\lambda_B}}{1+\left(\frac{\mathrm{x}_B}{m_B}\right)^{\lambda_B}}$$
$$- \frac{\left(\frac{x_A}{m_A}\right)^{\lambda_A}}{1+\left(\frac{x_A}{m_A}\right)^{\lambda_A}} \frac{\left(\frac{x_N}{m_N}\right)^{\lambda_N}}{1+\left(\frac{x_N}{m_N}\right)^{\lambda_N}}$$
$$- \frac{\left(\frac{x_B}{m_B}\right)^{\lambda_B}}{1+\left(\frac{x_B}{m_B}\right)^{\lambda_B}} \frac{\left(\frac{x_N}{m_N}\right)^{\lambda_N}}{1+\left(\frac{x_N}{m_N}\right)^{\lambda_N}} - \ldots$$
$$\left. - \frac{\left(\frac{x_A}{m_A}\right)^{\lambda_A}}{1+\left(\frac{x_A}{m_A}\right)^{\lambda_A}} \frac{\left(\frac{x_B}{m_B}\right)^{\lambda_B}}{1+\left(\frac{x_B}{m_B}\right)^{\lambda_B}} \ldots \frac{\left(\frac{x_N}{m_N}\right)^{\lambda_N}}{1+\left(\frac{x_N}{m_N}\right)^{\lambda_N}} \right).$$

**Supplemental figure 2.10: Calculation and visualization of synergy scores for drug combination AM251:MJN110 using SynergyFinder2.0, ZIP calculated synergy (continued)**

Zero interaction potency (ZIP) synergy is determined as the expected response corresponding to the effect as if the single drug did not alter the potency of each other.

(D) ZIP synergy calculation equation. $x_N$ is the dose of $N^{th}$ drug fitted with four parameter log-logistic (4PL) function, whereas $m_N$ is the dose that produces the half-maximum effect (also known as relative $EC_{50}$ or $IC_{50}$, depending on the readout), and $\lambda_N$ is the shape parameter indicating the slope of the dose– response curve.

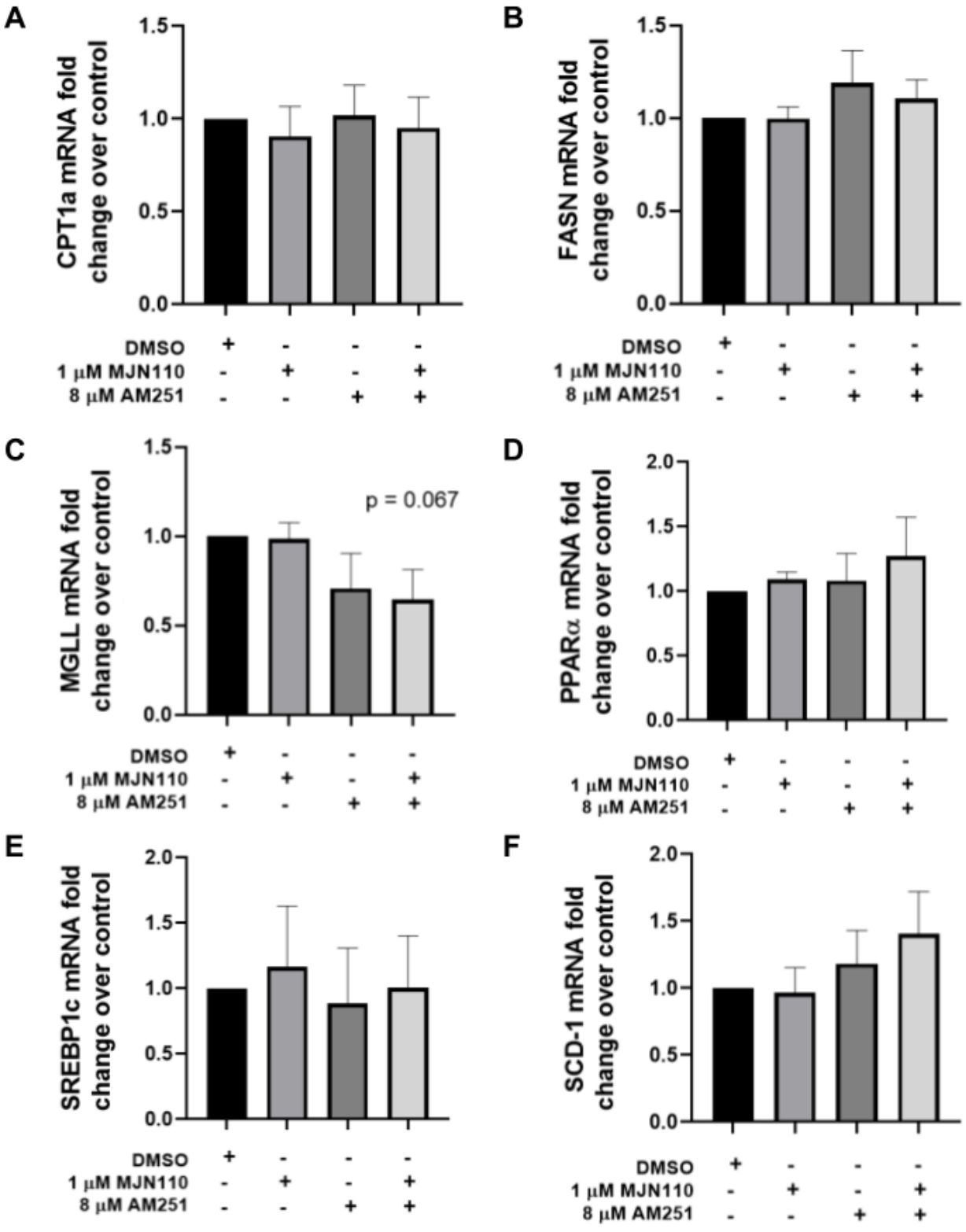


**Supplemental figure 2.11: MGLL inhibitor, MJN110, CB1 antagonist, AM251, co-treatment expression changes are dependent on HCV infection**

mRNA fold change of as determined by RT-qPCR of (A) CPT1a, (B) FASN, (C) MGLL, (D) PPARα, (E) SREBP1c, and (F) SCD-1. HuH7.5s Cells were seeded, after which medium was changed for fresh medium containing the corresponding small molecule treatments, followed by a 24 hour incubation. n = 3.

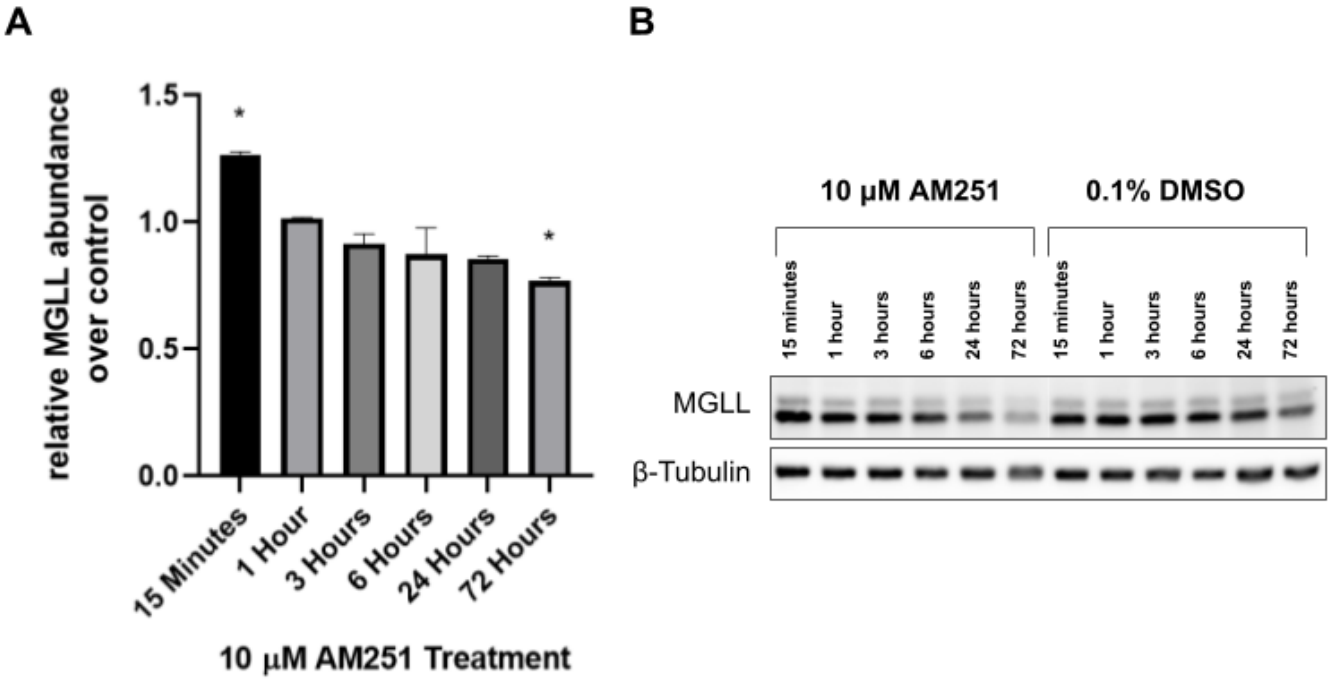


**Supplemental figure 2.12: 10 μM AM251 administration in HuH7.5s demonstrates changes in MGLL abundance over time**

(A) MGLL abundance levels of 10 μM CB1 antagonist AM251 treated HuH7.5s over time. Acutely, MGLL levels are significant up regulated while after 72 hours of treatment, MGLL abundance levels are significantly down regulated. n=3. Significance assessed with two-tailed, unpaired student's t test, *$p < 0.05$.

(B) Representative blot of one of the biological replicates is shown of (A).

# Appendix B – Supplemental tables for Chapter 2

**Supplemental Tables**

**Supplemental Table 2.1**: Antibodies used

| Gene | Antibody Provider | Identifier |
|---|---|---|
| ABHD6 | Abcam | Cat# ab87532; RRID: AB_1951400 |
| ABHD12 | Abcam | Cat# Unknown |
| ACOT1/2 | Santa-Cruz Biotechnologies | Cat# sc-373917; RRID: AB_10918465 |
| AMPK | Cell Signalling Technology | Cat# 2532S; RRID: AB_330331 |
| pAMPK (Thr172) | Cell Signalling Technology | Cat# 2531S; RRID: AB_330330 |
| β-Tubulin | Santa-Cruz Biotechnologies | Cat# sc-9104; RRID: AB_2241191 |
| CPVL | Santa-Cruz Biotechnologies | Cat# sc-376658; RRID: AB_11151401 |
| CTSA | Santa-Cruz Biotechnologies | Cat# sc-73766, |
| FASN | Santa-Cruz Biotechnologies | Cat# sc-483570 |
| HRP goat α-mouse | Jackson Immuno-research | Cat# 115-035-062; RRID: AB_2338504 |
| HRP donkey α-rabbit | Jackson Immuno-research | Cat# 711-035-152; RRID: AB_10015282 |
| MGLL | Santa-Cruz Biotechnologies | Cat# sc-398942 |
| PREP | Abcam | Cat# ab58988; RRID: AB_944973 |
| SREBP1 | Santa-Cruz Biotechnologies | Cat# sc-366; RRID: AB_2194229 |
| Ubiquitin | Cell Signalling Technology | Cat# 3933S; RRID: AB_2180538 |

**Supplemental Table 2.2**: Virus strains used

| Strain | Provider | Reference |
|---|---|---|
| HCV $JFH1_T$ 2a | A kind gift from Dr. Rodney Russell, Memorial University, NFL, CA | [20] (Chapter 3) |

**Supplemental Table 2.3**: Chemicals, peptides, recombinant proteins used

| Product | Provider | Identifier |
|---|---|---|
| ABC110 | A kind gift of Dr. Benjamin Cravatt, Scripps Research Institute | N/A |
| P11 | A kind gift of Dr. Benjamin Cravatt, Scripps Research Institute | CAS Number: 942285-55-4 |
| Yoshio 3 | A kind gift of Dr. Benjamin Cravatt, Scripps Research Institute | N/A |
| JP408 | A kind gift of Dr. Benjamin Cravatt, Scripps Research Institute | N/A |
| HU210 | A kind gift of Dr. Cory Harris, University of Ottawa* | CAS Number: 112830-95-2 |
| WWL113 | Millipore Sigma | Cat #: SML1179, CAS Number: 947669-86-5 |
| KT195 | Millipore Sigma | Cat #: SML1308, CAS Number: 1402612-58-1 |
| AICAR | Millipore Sigma | Cat # A9978, CAS Number: 2627-69-2 |
| AM251 | Millipore Sigma | Cat #: A6226, CAS Number: |

| | | |
|---|---|---|
| | | 183232-66-8 |
| MJN110 | Kind gift of Dr. Benjamin Cravatt, Scripps Research Institute [21 (Chapter 3)], Millipore Sigma | Cat #: SML0872, CAS Number: 1438416-21-7 |
| 2-BP | | CAS Number: 18263-25-7 |
| FP-biotin | Santa Cruz Biotechnologies | Cat.# sc-215056A, CAS Number: 259270-28-5 |
| ActivX TAMRA-FP Serine Hydrolase Probe | Thermo-Fisher Technologies | Cat.# 88318 |
| Streptavidin-agarose beads | ThermoFisher Scientific | Cat.# 20353 |

(*) = Facilities and supervision was provided for the use of this small molecule.

**Supplemental Table 2.4**: Critical commercial assays used

| Product | Provider | Ident |
|---|---|---|
| 10% TGX Stain-Free™ FastCast ™ Acrylamide Gel | BioRad | Cat# 1610183 |
| Trans-Blot® Turbo™ Transfer System | BioRad | Cat# 1704272 |
| Pierce C18 spin columns | Thermo Fischer | Cat# 89873 |
| RNeasy isolation kit | Qiagen | Cat# 74136 |
| iScript cDNA Synthesis Kit | BioRad | Cat# 1708841 |
| SSO advanced SYBR Green Supermix | BioRad | Cat# 1725274 |

**Supplemental Table 2.5**: Experimental models: cell lines used

| Cell line | Provider | RRID |
|---|---|---|
| HuH7.5 | Kind gift from Dr. C.M. Rice, Rockefeller University, NY, USA | RRID: CVCL_7927 |
| HuH7-SGR-Luc (E9) (Huh7 pFK-I389neo/luc/NS3-3'/5.1) | [22 (Chapter 3)] | N/A |
| SHSY-5Y (ATCC® CRL-2266™) | ATCC (American Type Culture Collection) | RRID:CVCL_0019 |

**Supplemental Table 2.6**: Primers used for RT-qPCR analysis

| Gene | Forward primer | Reverse Primer |
|---|---|---|
| 18S | 5'-GCGATGCGGCGGCGTTATTC-3' | 5'-CAATCTGTCAATCCTGTCCGTGTCC-3' |
| CPT1a | 5'-TCCAGTTGGCTTATCGTGGTG-3' | 5'-TCCAGAGTCCGATTGATTTTTGC-3' |
| FASN | 5'-GAAACTGCAGGAGCTGTC-3' | 5'-CACGGAGTTGAGGCGCAT-3' |
| MGLL | 5'-AATGCAGACGGACAGTACCTC-3' | 5'-GAGCCAGCTCTTCATAGCGG-3' |
| PPARα | 5'-CTATCATTTGCTGTGGAGATCG-3' | 5'-AAGATATCGTCCGGGTGGTT-3' |
| SCD1 | 5'- TCTAGCTCCTATACCACCACCA -3' | 5'- TCGTCTCCAACTTATCTCCTCC -3' |
| SREBP1c | 5'- GCCCCTGTAACGACCACTG-3' | 5'- CAGCGAGTCTGCCTTGATG-3' |
| JFH1 | 5'-GTCTGCGGAACCGGTGAGTA-3' | 5'-GCCCAAATGGCCGGGATA-3' |

IRES

**Supplemental Table 2.7**: Software and Algorithms

| Name | Provider | Source Link |
|---|---|---|
| Transcriptome Analysis Console | Affymetrix, ThermoFisher Scientific | https://www.thermofisher.com/ca/en/home/life-science/microarray-analysis/microarray-analysis-instruments-software-services/microarray-analysis-software/affymetrix-transcriptome-analysis-console-software.html |
| GraphPad Prism | GraphPad Prism Software | https://www.graphpad.com/scientific-software/prism/ |
| BioRender | BioRender | https://biorender.com/ |
| Synergy Finder 2.0 | 23 (Chapter 3) | https://synergyfinder.fimm.fi/ |
| ToppGene Suite | Cincinnati Children's Hospital Medical Center | https://toppgene.cchmc.org/ |
| Chemdraw | PerkinElmer | https://perkinelmerinformatics.com/products/research/chemdraw/ |
| Expression Atlas | European Molecular Biology Laboratory-European Bioinformatics Institute | https://www.ebi.ac.uk/ |

**Supplemental Table 2.8**: Changes in transcript abundance of 24 hour 1 µM MGLL inhibitor, MJN110 treated HuH7.5s through microarray; Affymetrix GeneChip™ Human Gene 2.0 ST Array, n = 2. Significance was assessed through analysis of variance (ANOVA) with the empirical Bayes correction. (p vales < 0.05 shown, fold changes less than -1.5, and greater than 1.5 shown)

| Gene Symbol | Fold Change | P-val | Description |
|---|---|---|---|
| ACOT1 | 1.75 | 0.0366 | acyl-CoA thioesterase 1 |
| ADAM5 | 1.68 | 0.0087 | ADAM metallopeptidase domain 5 (pseudogene) |
| ADAMTS19 | 1.51 | 0.0278 | ADAM metallopeptidase with thrombospondin type 1 motif 19 |
| ADGB | 1.55 | 0.0116 | androglobin |
| AHNAK2 | -1.91 | 0.0019 | AHNAK nucleoprotein 2 |
| ALOX12-AS1 | 2.36 | 0.0008 | ALOX12 antisense RNA 1 |
| AMELY | 1.74 | 0.0183 | amelogenin, Y-linked |
| ANKRD30B | 1.54 | 0.0252 | ankyrin repeat domain 30B |
| APOBEC3A_B; APOBEC3A; APOBEC3B | -2.09 | 0.0108 | APOBEC3A and APOBEC3B deletion hybrid; apolipoprotein B mRNA editing enzyme, catalytic polypeptide-like 3A; apolipoprotein B mRNA editing enzyme, catalytic polypeptide-like 3B |
| AQP7P1 | 2 | 0.0059 | aquaporin 7 pseudogene 1 |

| | | | |
|---|---|---|---|
| ASB9P1 | 1.53 | 0.0469 | ankyrin repeat and SOCS box containing 9 pseudogene 1 |
| ATP2A3 | -1.59 | 0.0268 | ATPase, Ca++ transporting, ubiquitous |
| AVP | 1.68 | 0.005 | arginine vasopressin |
| BCL2L15 | -1.97 | 0.0108 | BCL2-like 15 |
| BCRP2 | -1.8 | 0.0022 | breakpoint cluster region pseudogene 2 |
| C1orf146 | 1.59 | 0.0103 | chromosome 1 open reading frame 146 |
| C2orf27B | 1.61 | 0.0146 | chromosome 2 open reading frame 27B |
| C10orf53 | -1.81 | 0.0023 | chromosome 10 open reading frame 53 |
| CBR3-AS1 | -1.59 | 0.0243 | CBR3 antisense RNA 1 |
| CCDC30 | -1.57 | 0.0178 | coiled-coil domain containing 30 |
| CD99 | -1.54 | 0.0163 | CD99 molecule |
| CDHR4 | -1.57 | 0.0176 | cadherin-related family member 4 |
| CDRT15L2 | 1.69 | 0.0302 | CMT1A duplicated region transcript 15-like 2 |
| CEACAM6 | 1.79 | 0.0043 | carcinoembryonic antigen-related cell adhesion molecule 6 (non-specific cross reacting antigen) |
| CEP83 | -1.6 | 0.0058 | centrosomal protein 83kDa |
| CEP295NL | -1.73 | 0.0047 | CEP295 N-terminal like |
| CHORDC1 | 2.06 | 0.0021 | cysteine and histidine rich domain containing 1 |
| CRISP2 | -1.61 | 0.0255 | cysteine-rich secretory protein 2 |
| CROCCP3 | 1.57 | 0.036 | ciliary rootlet coiled-coil, rootletin pseudogene 3 |
| CYCSP52 | 1.53 | 0.0208 | cytochrome c, somatic pseudogene 52 |
| CYP2C19 | 1.55 | 0.019 | cytochrome P450, family 2, subfamily C, polypeptide 19 |
| CYP21A1P | -1.61 | 0.0077 | cytochrome P450, family 21, subfamily A, polypeptide 1 pseudogene |
| DCAF12L2 | 1.82 | 0.0026 | DDB1 and CUL4 associated factor 12-like 2 |
| DCAF13P3 | 1.63 | 0.0102 | DDB1 and CUL4 associated factor 13 pseudogene 3 |
| DEFA3 | 1.5 | 0.0319 | defensin, alpha 3, neutrophil-specific |
| DEFB133 | -1.8 | 0.0064 | defensin, beta 133 |
| DHRSX | -1.54 | 0.0402 | dehydrogenase/reductase (SDR family) X-linked |
| DNM3-IT1 | -1.57 | 0.0139 | DNM3 intronic transcript 1 |
| DPY19L2P3 | -1.53 | 0.0276 | DPY19L2 pseudogene 3 |
| EBLN1 | 1.61 | 0.0104 | endogenous Bornavirus-like nucleoprotein 1 |
| ERVK3-2 | -1.58 | 0.0207 | endogenous retrovirus group K3, member 2 |
| EVPLL | -1.76 | 0.0084 | envoplakin-like |
| F8 | -1.56 | 0.0132 | coagulation factor VIII, procoagulant component |
| FAM53A | -1.53 | 0.0129 | family with sequence similarity 53, member A |
| FAM66D | 1.54 | 0.0148 | family with sequence similarity 66, member D |
| FAM84A | 1.51 | 0.0132 | family with sequence similarity 84, member A |
| FAM85A | 1.58 | 0.0415 | family with sequence similarity 85, member A |
| FAM90A25P | 1.96 | 0.0155 | family with sequence similarity 90, member A7 pseudogene |
| FAM131B | 1.61 | 0.006 | family with sequence similarity 131, member B |

| | | | |
|---|---|---|---|
| FAM223A; FAM223B | 1.85 | 0.0149 | family with sequence similarity 223, member A (non-protein coding); family with sequence similarity 223, member B (non-protein coding) |
| FCGR3A | -2.41 | 0.0005 | Fc fragment of IgG, low affinity IIIa, receptor (CD16a) |
| FLT3 | 1.62 | 0.0138 | fms-related tyrosine kinase 3 |
| FNDC1 | 1.55 | 0.0385 | fibronectin type III domain containing 1 |
| FOXC2 | 1.73 | 0.0088 | forkhead box C2 |
| FUT8 | -1.59 | 0.0121 | fucosyltransferase 8 (alpha (1,6) fucosyltransferase) |
| GATA3-AS1 | 1.51 | 0.0451 | GATA3 antisense RNA 1 |
| GBP1 | 1.76 | 0.0098 | guanylate binding protein 1, interferon-inducible |
| GBP6 | -1.73 | 0.0045 | guanylate binding protein family, member 6 |
| GEMIN8 | 1.57 | 0.0133 | gem nuclear organelle associated protein 8 |
| GK3P | 2.76 | 0.02 | glycerol kinase 3 pseudogene |
| GOLGA2P6; MTPAP | -1.51 | 0.0293 | golgin A2 pseudogene 6; mitochondrial poly(A) polymerase |
| GOLGA6L7P | 1.58 | 0.042 | golgin A6 family-like 7, pseudogene |
| GOLGA8M | -1.51 | 0.0245 | golgin A8 family, member M |
| GPR45 | -1.8 | 0.0061 | G protein-coupled receptor 45 |
| GRIK1 | -1.65 | 0.0129 | glutamate receptor, ionotropic, kainate 1 |
| HAVCR1P1 | -2.13 | 0.0207 | hepatitis A virus cellular receptor 1 pseudogene 1 |
| HEXDC-IT1 | 1.58 | 0.0099 | HEXDC intronic transcript 1 |
| HIST1H4B | -1.7 | 0.0227 | histone cluster 1, H4b |
| HIST3H3 | -1.64 | 0.0169 | histone cluster 3, H3 |
| HLA-H | -1.54 | 0.036 | major histocompatibility complex, class I, H (pseudogene) |
| HMGN5 | 1.55 | 0.0355 | high mobility group nucleosome binding domain 5 |
| HOXB4 | -1.6 | 0.0144 | homeobox B4 |
| HRG | -1.51 | 0.0453 | histidine-rich glycoprotein |
| IFNA5 | -2.07 | 0.0012 | interferon, alpha 5 |
| IFNL2 | -1.78 | 0.0072 | interferon, lambda 2 |
| IGDCC4 | 1.5 | 0.0284 | immunoglobulin superfamily, DCC subclass, member 4 |
| IGHA1; IGHV3-74 | -1.62 | 0.0102 | immunoglobulin heavy constant alpha 1; immunoglobulin heavy variable 3-74 |
| IGHD | -1.76 | 0.0104 | immunoglobulin heavy constant delta |
| IGHD2-8 | 1.8 | 0.015 | immunoglobulin heavy diversity 2-8 |
| IGHD2-15 | -1.93 | 0.0296 | immunoglobulin heavy diversity 2-15 |
| IGHM; IGHV3-30; IGHV3-33 | 1.78 | 0.0147 | immunoglobulin heavy constant mu; immunoglobulin heavy variable 3-30; immunoglobulin heavy variable 3-33 |
| IGHV1-18 | -1.51 | 0.0171 | immunoglobulin heavy variable 1-18 |
| IGHV1-45; IGHM | -1.69 | 0.0109 | immunoglobulin heavy variable 1-45; immunoglobulin heavy constant mu |
| IGHV1-58 | -1.58 | 0.0105 | immunoglobulin heavy variable 1-58 |

| | | | |
|---|---|---|---|
| IGKV1D-42 | -1.61 | 0.0068 | immunoglobulin kappa variable 1D-42 (non-functional) |
| IGLL1 | -1.55 | 0.0121 | immunoglobulin lambda-like polypeptide 1 |
| IGLON5 | -1.54 | 0.02 | IgLON family member 5 |
| IGLV6-57; IGLL5 | 1.63 | 0.0212 | immunoglobulin lambda variable 6-57; immunoglobulin lambda-like polypeptide 5 |
| IL24 | 1.64 | 0.0167 | interleukin 24 |
| ITPKB-IT1 | -1.75 | 0.0148 | ITPKB intronic transcript 1 |
| KIR2DS2 | 1.65 | 0.0437 | killer cell immunoglobulin-like receptor, two domains, short cytoplasmic tail, 2 |
| KLHL38 | 1.52 | 0.0374 | kelch-like family member 38 |
| KRT6B | -2.02 | 0.0265 | keratin 6B, type II |
| KRT7 | -1.83 | 0.0038 | keratin 7, type II |
| KRT75 | -1.53 | 0.0125 | keratin 75, type II |
| KRT77 | -1.86 | 0.0049 | keratin 77, type II |
| KRT83 | -1.61 | 0.0079 | keratin 83, type II |
| KRTAP5-8 | -1.51 | 0.0348 | keratin associated protein 5-8 |
| KRTAP9-4 | -1.52 | 0.0462 | keratin associated protein 9-4 |
| KRTAP19-2 | -1.89 | 0.0016 | keratin associated protein 19-2 |
| KRTAP19-4 | 1.57 | 0.017 | keratin associated protein 19-4 |
| LARGE-AS1 | -1.63 | 0.0134 | LARGE antisense RNA 1 |
| LILRB1 | 2.22 | 0.001 | leukocyte immunoglobulin-like receptor, subfamily B (with TM and ITIM domains), member 1 |
| LINC00184 | 1.64 | 0.0123 | long intergenic non-protein coding RNA 184 |
| LINC00301 | 1.54 | 0.0107 | long intergenic non-protein coding RNA 301 |
| LINC00323 | -1.51 | 0.0162 | long intergenic non-protein coding RNA 323 |
| LINC00363 | 1.56 | 0.0279 | long intergenic non-protein coding RNA 363 |
| LINC00479 | -1.77 | 0.0163 | long intergenic non-protein coding RNA 479 |
| LINC00649 | -1.61 | 0.0078 | long intergenic non-protein coding RNA 649 |
| LINC00996 | -1.64 | 0.0128 | long intergenic non-protein coding RNA 996 |
| LINC01070 | -1.51 | 0.0321 | long intergenic non-protein coding RNA 1070 |
| LINC01410 | 1.54 | 0.0153 | long intergenic non-protein coding RNA 1410 |
| LINC01451 | 1.62 | 0.0096 | long intergenic non-protein coding RNA 1451 |
| LINC01511 | -1.55 | 0.0173 | long intergenic non-protein coding RNA 1511 |
| LINC01549 | 1.65 | 0.0415 | long intergenic non-protein coding RNA 1549 |
| LINC01592 | 1.52 | 0.0425 | long intergenic non-protein coding RNA 1592 |
| LMOD3 | 1.59 | 0.0105 | leiomodin 3 (fetal) |
| LOC84214 | 1.51 | 0.0156 | uncharacterized LOC84214 |
| LOC202181 | 1.95 | 0.0082 | SUMO-interacting motifs containing 1 pseudogene |
| LOC285593 | -1.59 | 0.0136 | uncharacterized LOC285593 |
| LOC389906; LOC441528 | 1.6 | 0.0074 | zinc finger protein 839 pseudogene; zinc finger protein 839-like |
| LOC643387; LOC101927958 | 1.52 | 0.0134 | TAR DNA binding protein pseudogene; uncharacterized LOC101927958 |

| | | | |
|---|---|---|---|
| LOC644172 | 1.99 | 0.0163 | mitogen-activated protein kinase 8 interacting protein 1 pseudogene |
| LOC646762 | -1.65 | 0.02 | uncharacterized LOC646762 |
| LOC729080 | -2.3 | 0.03 | glycine cleavage system protein H (aminomethyl carrier) pseudogene |
| LOC729732 | 1.53 | 0.0124 | uncharacterized LOC729732 |
| LOC100128563 | -2.04 | 0.0275 | uncharacterized LOC100128563 |
| LOC100129291 | 1.81 | 0.0493 | uncharacterized protein CXorf49-like |
| LOC100130268 | 1.7 | 0.0067 | uncharacterized LOC100130268 |
| LOC100130798 | -1.5 | 0.0167 | uncharacterized LOC100130798 |
| LOC100131510 | -1.59 | 0.0452 | uncharacterized LOC100131510 |
| LOC100134868; LOC105372584 | -1.69 | 0.0116 | uncharacterized LOC100134868; uncharacterized LOC105372584 |
| LOC100270804 | -1.52 | 0.0237 | uncharacterized LOC100270804 |
| LOC100420587 | -1.57 | 0.0394 | SHC SH2-domain binding protein 1 pseudogene |
| LOC100505948; LOC102724523 | -1.56 | 0.0155 | uncharacterized LOC100505948; uncharacterized LOC102724523 |
| LOC100506458 | 1.59 | 0.0117 | putative uncharacterized protein LOC65996-like |
| LOC100506688 | -1.59 | 0.03 | uncharacterized LOC100506688 |
| LOC100506766 | -1.56 | 0.0449 | uncharacterized LOC100506766 |
| LOC100996624 | 1.54 | 0.021 | uncharacterized LOC100996624 |
| LOC101927286 | -1.61 | 0.0371 | uncharacterized LOC101927286 |
| LOC101927293 | -1.86 | 0.0229 | uncharacterized LOC101927293 |
| LOC101927468 | -1.81 | 0.0376 | uncharacterized LOC101927468 |
| LOC101927602; LOC105379812 | 1.88 | 0.0014 | uncharacterized LOC101927602; uncharacterized LOC105379812 |
| LOC101927617 | 1.55 | 0.0151 | uncharacterized LOC101927617 |
| LOC101927636 | -1.6 | 0.015 | uncharacterized LOC101927636 |
| LOC101927856 | 1.73 | 0.0062 | uncharacterized LOC101927856 |
| LOC101928195 | 2.58 | 0.0324 | monofunctional C1-tetrahydrofolate synthase, mitochondrial-like |
| LOC101928377 | -1.64 | 0.0185 | uncharacterized LOC101928377 |
| LOC101928597 | 1.53 | 0.0393 | uncharacterized LOC101928597 |
| LOC101928658 | 1.72 | 0.0103 | uncharacterized LOC101928658 |
| LOC101928733 | 1.52 | 0.0138 | uncharacterized LOC101928733 |
| LOC101929504 | 1.93 | 0.0279 | uncharacterized LOC101929504 |
| LOC101929572 | -1.73 | 0.0348 | uncharacterized LOC101929572 |
| LOC101929653 | -1.59 | 0.0094 | uncharacterized LOC101929653 |
| LOC102723516 | -1.54 | 0.015 | uncharacterized LOC102723516 |
| LOC102723906 | -1.61 | 0.0219 | uncharacterized LOC102723906 |
| LOC102724057 | -1.59 | 0.0382 | uncharacterized LOC102724057 |
| LOC102724150 | -1.71 | 0.0067 | uncharacterized LOC102724150 |
| LOC102724220 | 1.77 | 0.0057 | uncharacterized LOC102724220 |
| LOC102724312 | -1.54 | 0.0238 | uncharacterized LOC102724312 |

| | | | |
|---|---|---|---|
| LOC102724587 | 1.66 | 0.0287 | uncharacterized LOC102724587 |
| LOC102724680 | 1.62 | 0.041 | uncharacterized LOC102724680 |
| LOC102724687 | -1.58 | 0.0079 | uncharacterized LOC102724687 |
| LOC102724719 | 1.5 | 0.0142 | uncharacterized LOC102724719 |
| LOC102724849 | -1.65 | 0.0081 | uncharacterized LOC102724849 |
| LOC102724919 | -1.58 | 0.0132 | uncharacterized LOC102724919 |
| LOC102725193; LOC100129048 | -1.53 | 0.0227 | uncharacterized LOC102725193; uncharacterized LOC100129048 |
| LOC104054148 | 1.76 | 0.0026 | uncharacterized LOC104054148 |
| LOC105369328 | -1.62 | 0.0093 | uncharacterized LOC105369328 |
| LOC105369519 | 1.56 | 0.0181 | uncharacterized LOC105369519 |
| LOC105369520 | 1.53 | 0.0143 | uncharacterized LOC105369520 |
| LOC105369576 | -1.53 | 0.0165 | uncharacterized LOC105369576 |
| LOC105369644; LOC105369646 | 1.62 | 0.0135 | uncharacterized LOC105369644; uncharacterized LOC105369646 |
| LOC105369791; LOC105379614 | 1.66 | 0.0221 | uncharacterized LOC105369791; uncharacterized LOC105379614 |
| LOC105369826 | 1.56 | 0.0158 | uncharacterized LOC105369826 |
| LOC105369839 | -1.56 | 0.0265 | uncharacterized LOC105369839 |
| LOC105370201 | -1.52 | 0.0152 | uncharacterized LOC105370201 |
| LOC105370248 | 1.63 | 0.0178 | uncharacterized LOC105370248 |
| LOC105370448; LOC105370449 | -1.5 | 0.017 | uncharacterized LOC105370448; uncharacterized LOC105370449 |
| LOC105370473 | 1.65 | 0.03 | uncharacterized LOC105370473 |
| LOC105370498 | 1.75 | 0.0122 | uncharacterized LOC105370498 |
| LOC105370762 | -1.71 | 0.0364 | uncharacterized LOC105370762 |
| LOC105370817 | 1.6 | 0.0181 | uncharacterized LOC105370817 |
| LOC105371195; LOC105379475 | -1.73 | 0.0038 | uncharacterized LOC105371195; uncharacterized LOC105379475 |
| LOC105371227 | -1.5 | 0.0312 | uncharacterized LOC105371227 |
| LOC105371342 | -2.48 | 0.0399 | uncharacterized LOC105371342 |
| LOC105371550 | -1.53 | 0.0104 | uncharacterized LOC105371550 |
| LOC105371574 | -1.56 | 0.0121 | uncharacterized LOC105371574 |
| LOC105371730 | 1.57 | 0.0152 | uncharacterized LOC105371730 |
| LOC105372551 | -1.51 | 0.0428 | uncharacterized LOC105372551 |
| LOC105372661 | -1.64 | 0.0179 | uncharacterized LOC105372661 |
| LOC105372752 | 1.51 | 0.0345 | uncharacterized LOC105372752 |
| LOC105372890 | -1.58 | 0.0141 | uncharacterized LOC105372890 |
| LOC105373617 | 1.68 | 0.0196 | uncharacterized LOC105373617 |
| LOC105373653 | 1.52 | 0.0307 | uncharacterized LOC105373653 |
| LOC105373737 | -1.59 | 0.0085 | uncharacterized LOC105373737 |
| LOC105373789 | 1.54 | 0.0231 | uncharacterized LOC105373789 |
| LOC105374002 | 1.57 | 0.0176 | uncharacterized LOC105374002 |
| LOC105374122 | -1.87 | 0.0225 | uncharacterized LOC105374122 |

| | | | |
|---|---|---|---|
| LOC105374166 | -1.65 | 0.0219 | uncharacterized LOC105374166 |
| LOC105374661 | 1.51 | 0.0119 | uncharacterized LOC105374661 |
| LOC105374754 | 1.56 | 0.0268 | uncharacterized LOC105374754 |
| LOC105375042 | -1.57 | 0.0103 | uncharacterized LOC105375042 |
| LOC105375716 | -1.59 | 0.0463 | uncharacterized LOC105375716 |
| LOC105375732 | 1.87 | 0.0124 | uncharacterized LOC105375732 |
| LOC105376039 | -1.69 | 0.0046 | uncharacterized LOC105376039 |
| LOC105376093 | -1.63 | 0.0082 | uncharacterized LOC105376093 |
| LOC105376193 | 1.58 | 0.0278 | uncharacterized LOC105376193 |
| LOC105376236 | -1.51 | 0.0423 | uncharacterized LOC105376236 |
| LOC105376347 | -1.55 | 0.0429 | uncharacterized LOC105376347 |
| LOC105376602 | 1.75 | 0.0043 | uncharacterized LOC105376602 |
| LOC105376642 | -1.62 | 0.0375 | uncharacterized LOC105376642 |
| LOC105376774 | 1.65 | 0.0053 | uncharacterized LOC105376774 |
| LOC105377026 | -1.82 | 0.0201 | uncharacterized LOC105377026 |
| LOC105377171 | -1.83 | 0.0089 | uncharacterized LOC105377171 |
| LOC105377343 | -1.54 | 0.02 | uncharacterized LOC105377343 |
| LOC105377456 | 1.5 | 0.0383 | uncharacterized LOC105377456 |
| LOC105377576 | -1.57 | 0.0083 | uncharacterized LOC105377576 |
| LOC105377725 | -1.75 | 0.0445 | uncharacterized LOC105377725 |
| LOC105377740 | -1.52 | 0.0181 | uncharacterized LOC105377740 |
| LOC105378208; LOC105378209 | 1.72 | 0.0053 | uncharacterized LOC105378208; uncharacterized LOC105378209 |
| LOC105378516; LOC105378517 | 1.56 | 0.0131 | uncharacterized LOC105378516; uncharacterized LOC105378517 |
| LOC105378738 | 1.53 | 0.0254 | uncharacterized LOC105378738 |
| LOC105378892 | 2.04 | 0.0275 | uncharacterized LOC105378892 |
| LOC105379132 | 1.58 | 0.0304 | uncharacterized LOC105379132 |
| LOC105379299 | 1.88 | 0.006 | uncharacterized LOC105379299 |
| LRRC32 | 1.62 | 0.041 | leucine rich repeat containing 32 |
| LURAP1L-AS1 | -1.65 | 0.0112 | LURAP1L antisense RNA 1 |
| LYZL1 | 1.56 | 0.0365 | lysozyme-like 1 |
| MAPK8IP1 | 1.75 | 0.0233 | mitogen-activated protein kinase 8 interacting protein 1 |
| MAPK8IP2 | -1.69 | 0.0065 | mitogen-activated protein kinase 8 interacting protein 2 |
| MB21D1 | 1.57 | 0.0276 | Mab-21 domain containing 1 |
| MDGA1 | -1.52 | 0.0248 | MAM domain containing glycosylphosphatidylinositol anchor 1 |
| MGAM2 | 1.55 | 0.0132 | maltase-glucoamylase 2 (putative) |
| MIR16-2 | -1.92 | 0.0024 | microRNA 16-2 |
| MIR30D | -1.59 | 0.0254 | microRNA 30d |
| MIR32 | 1.94 | 0.0023 | microRNA 32 |
| MIR126 | 1.59 | 0.0214 | microRNA 126 |

| | | | |
|---|---|---|---|
| MIR129-1 | 1.63 | 0.0472 | microRNA 129-1 |
| MIR200A | 1.52 | 0.039 | microRNA 200a |
| MIR222 | -1.67 | 0.0188 | microRNA 222 |
| MIR501 | 2.99 | 0.0002 | microRNA 501 |
| MIR516A1 | -1.53 | 0.0127 | microRNA 516a-1 |
| MIR519D | -1.51 | 0.0245 | microRNA 519d |
| MIR519E | -1.94 | 0.0444 | microRNA 519e |
| MIR520D | -1.97 | 0.0498 | microRNA 520d |
| MIR526A1 | 1.58 | 0.0299 | microRNA 526a-1 |
| MIR545 | 2.25 | 0.0032 | microRNA 545 |
| MIR550B1 | 1.58 | 0.0134 | microRNA 550b-1 |
| MIR617 | 1.72 | 0.0087 | microRNA 617 |
| MIR708 | -1.59 | 0.0208 | microRNA 708 |
| MIR1229 | 1.53 | 0.0211 | microRNA 1229 |
| MIR1252 | 1.75 | 0.0279 | microRNA 1252 |
| MIR1972-1; MIR1972-2 | 1.65 | 0.0065 | microRNA 1972-1; microRNA 1972-2 |
| MIR1972-1; MIR1972-2 | 1.65 | 0.0065 | microRNA 1972-1; microRNA 1972-2 |
| MIR2682; MIR137HG | -1.52 | 0.0289 | microRNA 2682; MIR137 host gene |
| MIR3074 | 1.63 | 0.0104 | microRNA 3074 |
| MIR3122 | 1.76 | 0.0033 | microRNA 3122 |
| MIR3130-2 | 1.89 | 0.003 | microRNA 3130-2 |
| MIR3142 | -1.69 | 0.0055 | microRNA 3142 |
| MIR3163 | -1.78 | 0.0158 | microRNA 3163 |
| MIR3191; BBC3 | -1.9 | 0.034 | microRNA 3191; BCL2 binding component 3 |
| MIR3649 | 1.65 | 0.0048 | microRNA 3649 |
| MIR3674 | 1.52 | 0.0167 | microRNA 3674 |
| MIR3690 | 1.71 | 0.0058 | microRNA 3690 |
| MIR3690 | 1.71 | 0.0058 | microRNA 3690 |
| MIR4255 | 1.77 | 0.0297 | microRNA 4255 |
| MIR4266 | -1.87 | 0.0284 | microRNA 4266 |
| MIR4309 | 1.89 | 0.0165 | microRNA 4309 |
| MIR4330 | -1.59 | 0.0076 | microRNA 4330 |
| MIR4432 | 1.8 | 0.0136 | microRNA 4432 |
| MIR4433A | 1.69 | 0.032 | microRNA 4433a |
| MIR4493 | 1.56 | 0.0136 | microRNA 4493 |
| MIR4501 | 1.61 | 0.0099 | microRNA 4501 |
| MIR4527 | -1.67 | 0.0258 | microRNA 4527 |
| MIR4530 | -1.77 | 0.0269 | microRNA 4530 |
| MIR4540 | -2.81 | 0.009 | microRNA 4540 |
| MIR4644 | -1.77 | 0.0271 | microRNA 4644 |
| MIR4655 | -1.58 | 0.0301 | microRNA 4655 |

| | | | |
|---|---|---|---|
| MIR4710 | -1.57 | 0.0336 | microRNA 4710 |
| MIR4771-1; MIR4771-2 | -1.77 | 0.008 | microRNA 4771-1; microRNA 4771-2 |
| MIR4771-1; MIR4771-2 | -1.77 | 0.008 | microRNA 4771-1; microRNA 4771-2 |
| MIR4791 | 1.55 | 0.0087 | microRNA 4791 |
| MIR4803 | 1.55 | 0.0108 | microRNA 4803 |
| MKX-AS1 | 1.73 | 0.0098 | MKX antisense RNA 1 |
| MPLKIP | -1.84 | 0.0225 | M-phase specific PLK1 interacting protein |
| MT1A | 1.94 | 0.002 | metallothionein 1A |
| MT1JP | -1.69 | 0.0054 | metallothionein 1J, pseudogene |
| MYBPH | -1.61 | 0.0136 | myosin binding protein H |
| NANOG | 1.78 | 0.0076 | Nanog homeobox |
| NBPF19; NOTCH2NL; NBPF14 | -1.98 | 0.024 | neuroblastoma breakpoint family, member 19; notch 2 N-terminal like; neuroblastoma breakpoint family, member 14 |
| NIPA1 | -1.53 | 0.0113 | non imprinted in Prader-Willi/Angelman syndrome 1 |
| NUDT4 | 1.63 | 0.0355 | nudix hydrolase 4 |
| ODF1 | 1.56 | 0.0147 | outer dense fiber of sperm tails 1 |
| OR2AG1 | 2.08 | 0.0053 | olfactory receptor, family 2, subfamily AG, member 1 (gene/pseudogene) |
| OR2T12 | -1.77 | 0.0055 | olfactory receptor, family 2, subfamily T, member 12 |
| OR2T34 | 1.66 | 0.0101 | olfactory receptor, family 2, subfamily T, member 34 |
| OR2V2 | -1.98 | 0.0022 | olfactory receptor, family 2, subfamily V, member 2 |
| OR4K1 | 1.59 | 0.0311 | olfactory receptor, family 4, subfamily K, member 1 |
| OR5A2 | -1.83 | 0.0448 | olfactory receptor, family 5, subfamily A, member 2 |
| OR5H2 | 1.54 | 0.0267 | olfactory receptor, family 5, subfamily H, member 2 |
| OR5K1 | 1.92 | 0.022 | olfactory receptor, family 5, subfamily K, member 1 |
| OR6C4; TRAJ41 | -1.56 | 0.0214 | olfactory receptor, family 6, subfamily C, member 4; T cell receptor alpha joining 41 |
| OR8G5; OR8G1 | -1.51 | 0.0179 | olfactory receptor, family 8, subfamily G, member 5; olfactory receptor, family 8, subfamily G, member 1 (gene/pseudogene) |
| OR9A2 | 1.65 | 0.0128 | olfactory receptor, family 9, subfamily A, member 2 |
| OR10A2 | 1.68 | 0.0095 | olfactory receptor, family 10, subfamily A, member 2 |
| OR10H4 | -1.79 | 0.0055 | olfactory receptor, family 10, subfamily H, member 4 |
| OR51B6 | 1.5 | 0.0459 | olfactory receptor, family 51, subfamily B, member 6 |
| OR56B4 | -1.62 | 0.0334 | olfactory receptor, family 56, subfamily B, member 4 |
| OVAAL | -1.74 | 0.0142 | ovarian adenocarcinoma amplified long non-coding RNA |
| P3H2 | -1.65 | 0.0089 | prolyl 3-hydroxylase 2 |
| PCAT2 | -1.52 | 0.023 | prostate cancer associated transcript 2 (non-protein coding) |
| PCNAP1 | -1.51 | 0.0121 | proliferating cell nuclear antigen pseudogene 1 |
| PCSK6 | 1.58 | 0.0161 | proprotein convertase subtilisin/kexin type 6 |

| | | | |
|---|---|---|---|
| PDE12 | 1.72 | 0.0077 | phosphodiesterase 12 |
| PGA5 | -1.65 | 0.0062 | pepsinogen 5, group I (pepsinogen A) |
| PHACTR2-AS1 | -1.54 | 0.0158 | PHACTR2 antisense RNA 1 |
| PLSCR5 | -1.57 | 0.045 | phospholipid scramblase family, member 5 |
| PP13 | -2.68 | 0.016 | vegetative cell wall protein gp1 |
| PRAMEF11 | -1.51 | 0.0215 | PRAME family member 11 |
| PRCAT47 | -1.78 | 0.0058 | prostate cancer-associated 47 |
| PRDM9 | 1.53 | 0.0192 | PR domain containing 9 |
| PRKCH | -1.7 | 0.0044 | protein kinase C, eta |
| PRSS3 | 1.88 | 0.0023 | protease, serine, 3 |
| PRTN3 | -1.51 | 0.0462 | proteinase 3 |
| PSMB11 | -1.68 | 0.0039 | proteasome (prosome, macropain) subunit, beta type, 11 |
| RAB25 | -1.73 | 0.0044 | RAB25, member RAS oncogene family |
| RAX2 | -1.54 | 0.0152 | retina and anterior neural fold homeobox 2 |
| REPS2 | 1.58 | 0.0125 | RALBP1 associated Eps domain containing 2 |
| RFPL2 | -1.7 | 0.0231 | ret finger protein-like 2 |
| RGMB | 1.52 | 0.0221 | repulsive guidance molecule family member b |
| RGS8 | -1.79 | 0.003 | regulator of G-protein signaling 8 |
| RNASE3 | 1.55 | 0.0206 | ribonuclease, RNase A family, 3 |
| RNF165 | 1.86 | 0.0093 | ring finger protein 165 |
| RNVU1-14 | -2.13 | 0.0007 | RNA, variant U1 small nuclear 14 |
| RPRML | 1.52 | 0.0162 | reprimo-like |
| RRAD | 1.6 | 0.0171 | Ras-related associated with diabetes |
| S100A7A | -1.54 | 0.0159 | S100 calcium binding protein A7A |
| SCGB2B3P | -1.52 | 0.0117 | secretoglobin, family 2B, member 3, pseudogene |
| SCN1A | -1.63 | 0.011 | sodium channel, voltage gated, type I alpha subunit |
| SCX | 1.8 | 0.0464 | scleraxis bHLH transcription factor |
| SEMA3E | 1.51 | 0.021 | sema domain, immunoglobulin domain (Ig), short basic domain, secreted, (semaphorin) 3E |
| SERPINA11 | -1.52 | 0.0175 | serpin peptidase inhibitor, clade A (alpha-1 antiproteinase, antitrypsin), member 11 |
| SERPINB3; SERPINB4 | 1.57 | 0.0222 | serpin peptidase inhibitor, clade B (ovalbumin), member 3; serpin peptidase inhibitor, clade B (ovalbumin), member 4 |
| SERPINB8; HMSD | -1.53 | 0.016 | serpin peptidase inhibitor, clade B (ovalbumin), member 8; histocompatibility (minor) serpin domain containing |
| SIRPG-AS1 | 1.74 | 0.0057 | SIRPG antisense RNA 1 |
| SLC13A4 | -1.65 | 0.0452 | solute carrier family 13 (sodium/sulfate symporter), member 4 |
| SLC16A8 | -1.73 | 0.0053 | solute carrier family 16 (monocarboxylate transporter), member 8 |
| SLC30A7 | -1.64 | 0.0171 | solute carrier family 30 (zinc transporter), member 7 |
| SLC35G2 | -1.54 | 0.0112 | solute carrier family 35, member G2 |

| | | | |
|---|---|---|---|
| SMAD5 | -1.77 | 0.011 | SMAD family member 5 |
| SNORA60 | 2.27 | 0.0041 | small nucleolar RNA, H/ACA box 60 |
| SNORA70E | -2.13 | 0.0153 | small nucleolar RNA, H/ACA box 70E |
| SNORA72 | -1.72 | 0.0086 | small nucleolar RNA, H/ACA box 72 |
| SNORA108 | 1.7 | 0.008 | small nucleolar RNA, H/ACA box 108 |
| SNORD72 | -2.29 | 0.0061 | small nucleolar RNA, C/D box 72 |
| SNORD90 | 1.8 | 0.0056 | small nucleolar RNA, C/D box 90 |
| SNORD111 | 2.09 | 0.0022 | small nucleolar RNA, C/D box 111 |
| SNORD113-9 | -2.28 | 0.0007 | small nucleolar RNA, C/D box 113-9 |
| SNORD114-31 | 2.19 | 0.0223 | small nucleolar RNA, C/D box 114-31 |
| SSMEM1 | -1.51 | 0.0136 | serine-rich single-pass membrane protein 1 |
| SSX6 | 1.58 | 0.0206 | synovial sarcoma, X breakpoint 6 (pseudogene) |
| ST3GAL4 | 1.61 | 0.0141 | ST3 beta-galactoside alpha-2,3-sialyltransferase 4 |
| STH | -1.57 | 0.0086 | saitohin |
| SULT1A1 | 1.59 | 0.0063 | sulfotransferase family 1A member 1 |
| SYNPO2 | 2.15 | 0.0145 | synaptopodin 2 |
| SYT2 | 1.58 | 0.007 | synaptotagmin II |
| TAS2R5 | -1.51 | 0.0365 | taste receptor, type 2, member 5 |
| TBX5-AS1 | 1.52 | 0.0286 | TBX5 antisense RNA 1 |
| TINCR | 1.56 | 0.0285 | tissue differentiation-inducing non-protein coding RNA |
| TMEM236 | -1.7 | 0.0444 | transmembrane protein 236 |
| TMIE | -1.54 | 0.0189 | transmembrane inner ear |
| TOMM20L | -1.86 | 0.0104 | translocase of outer mitochondrial membrane 20 homolog (yeast)-like |
| TRAJ17 | 1.65 | 0.0301 | T cell receptor alpha joining 17 |
| TRAV8-6 | -1.83 | 0.0182 | T cell receptor alpha variable 8-6 |
| TRAV9-1 | -1.87 | 0.0058 | T cell receptor alpha variable 9-1 |
| TRAV13-2 | 1.67 | 0.0223 | T cell receptor alpha variable 13-2 |
| TRBV24-1 | 2.01 | 0.0199 | T cell receptor beta variable 24-1 |
| TRIM43 | -1.59 | 0.0315 | tripartite motif containing 43 |
| TRIM49 | 2.1 | 0.0048 | tripartite motif containing 49 |
| TRIM77 | 1.64 | 0.0133 | tripartite motif containing 77 |
| TTTY22 | 1.57 | 0.0083 | testis-specific transcript, Y-linked 22 (non-protein coding) |
| TUBBP5 | 1.76 | 0.0116 | tubulin, beta pseudogene 5 |
| UBAC2-AS1 | -1.59 | 0.0076 | UBAC2 antisense RNA 1 |
| UBXN10-AS1 | -1.54 | 0.0152 | UBXN10 antisense RNA 1 |
| USP17L9P | 1.71 | 0.041 | ubiquitin specific peptidase 17-like family member 9, pseudogene |
| VPS37D | -1.63 | 0.0113 | vacuolar protein sorting 37 homolog D (S. cerevisiae) |
| WNT3A | -1.77 | 0.0026 | wingless-type MMTV integration site family, member 3A |

| | | | |
|---|---|---|---|
| WSCD1 | -1.56 | 0.0126 | WSC domain containing 1 |
| ZCWPW2; IGHV3-23 | 2.02 | 0.0013 | zinc finger, CW type with PWWP domain 2; immunoglobulin heavy variable 3-23 |
| ZFP28 | -1.58 | 0.0141 | ZFP28 zinc finger protein |
| ZG16B | -1.53 | 0.0109 | zymogen granule protein 16B |
| ZNF10 | 1.55 | 0.04 | zinc finger protein 10 |
| ZNF34 | -1.56 | 0.0193 | zinc finger protein 34 |
| ZNF37BP | -1.82 | 0.0154 | zinc finger protein 37B, pseudogene |
| ZNF214 | -1.61 | 0.0339 | zinc finger protein 214 |
| ZNF221 | 1.55 | 0.028 | zinc finger protein 221 |
| ZNF287 | 1.58 | 0.0254 | zinc finger protein 287 |
| ZNF474 | 1.73 | 0.016 | zinc finger protein 474 |
| ZNF491 | -1.56 | 0.0367 | zinc finger protein 491 |
| ZNF808; RPL39P34 | 1.66 | 0.0103 | zinc finger protein 808; ribosomal protein L39 pseudogene 34 |
| ZNF833P | -1.72 | 0.0083 | zinc finger protein 833, pseudogene |
| ZNF883 | -1.54 | 0.0098 | zinc finger protein 883 |

**Supplemental Table 2.9**: Changes in transcript abundance of 72 hour 1 μM MGLL inhibitor, MJN110 treated HuH7.5s through microarray; Affymetrix GeneChip™ Human Gene 2.0 ST Array, n = 2. Significance was assessed through analysis of variance (ANOVA) with the empirical Bayes correction. (p vales < 0.05 shown, fold changes less than -1.5, and greater than 1.5 shown)

| Gene | Fold Change | P-val | Description |
|---|---|---|---|
| ACSS2 | 1.66 | 0.002 | acyl-CoA synthetase short-chain family member 2 |
| ACTR5 | -1.61 | 0.0376 | ARP5 actin-related protein 5 homolog (yeast) |
| ALS2CR11 | -1.55 | 0.0021 | amyotrophic lateral sclerosis 2 chromosome region candidate 11 |
| ANXA13 | -1.52 | 0.0246 | annexin A13 |
| ARGFX | -1.52 | 0.0165 | arginine-fifty homeobox |
| ARHGEF1 | 1.67 | 0.0037 | Rho guanine nucleotide exchange factor 1 |
| ASB5 | 1.55 | 0.0058 | ankyrin repeat and SOCS box containing 5 |
| BDP1 | -1.51 | 0.0021 | B double prime 1, subunit of RNA polymerase III transcription initiation factor IIIB |
| BEGAIN | -1.56 | 0.0098 | brain-enriched guanylate kinase-associated |
| BHLHE40 | 1.58 | 0.01 | basic helix-loop-helix family, member e40 |
| BLVRB | 1.54 | 0.0109 | biliverdin reductase B |
| C8orf4 | -1.58 | 0.0091 | chromosome 8 open reading frame 4 |
| CDH19 | -1.53 | 0.0118 | cadherin 19, type 2 |
| CDRT15L2 | 1.69 | 0.0148 | CMT1A duplicated region transcript 15-like 2 |
| CERS1; GDF1 | 1.53 | 0.0021 | ceramide synthase 1; growth differentiation factor 1 |

| | | | |
|---|---|---|---|
| CHAC1 | 1.71 | 0.0243 | ChaC glutathione-specific gamma-glutamylcyclotransferase 1 |
| CLCN7 | 1.55 | 0.0066 | chloride channel, voltage-sensitive 7 |
| CR1 | 1.54 | 0.0017 | complement component (3b/4b) receptor 1 (Knops blood group) |
| ENPEP | -1.54 | 0.0166 | glutamyl aminopeptidase (aminopeptidase A) |
| EPDR1 | -1.66 | 0.0048 | ependymin related 1 |
| FAM106CP | -1.68 | 0.0116 | family with sequence similarity 106, member C, pseudogene |
| FAM133B | -1.57 | 0.0055 | family with sequence similarity 133, member B |
| FAM182A | -1.54 | 0.0027 | family with sequence similarity 182, member A |
| FAM223A; FAM223B | -1.74 | 0.0332 | family with sequence similarity 223, member A (non-protein coding); family with sequence similarity 223, member B (non-protein coding) |
| GBP3 | 1.58 | 0.0038 | guanylate binding protein 3 |
| GUSBP4 | -1.52 | 0.0404 | glucuronidase, beta pseudogene 4 |
| HCP5 | 1.52 | 0.005 | HLA complex P5 (non-protein coding) |
| HSD17B14 | 2.27 | 0.0004 | hydroxysteroid (17-beta) dehydrogenase 14 |
| IGLJ2 | 1.59 | 0.015 | immunoglobulin lambda joining 2 |
| KRTAP2-1 | 1.64 | 0.018 | keratin associated protein 2-1 |
| LCE3D | 1.55 | 0.0088 | late cornified envelope 3D |
| LINC00264 | 1.51 | 0.0381 | long intergenic non-protein coding RNA 264 |
| LINC00343 | 1.68 | 0.0008 | long intergenic non-protein coding RNA 343 |
| LINC00698 | 1.54 | 0.0016 | long intergenic non-protein coding RNA 698 |
| LINC00923 | -1.56 | 0.0226 | long intergenic non-protein coding RNA 923 |
| LOC100288619 | -1.54 | 0.0331 | uncharacterized LOC100288619 |
| LOC100505824 | 1.5 | 0.0159 | uncharacterized LOC100505824 |
| LOC100507209 | -2 | 0.0382 | uncharacterized LOC100507209 |
| LOC101927650 | 1.59 | 0.0063 | uncharacterized LOC101927650 |
| LOC101928231; LOC101928249 | 1.78 | 0.0013 | uncharacterized LOC101928231; uncharacterized LOC101928249 |
| LOC102724551 | 1.64 | 0.0063 | uncharacterized LOC102724551 |
| LOC105369159 | -1.92 | 0.0026 | uncharacterized LOC105369159 |
| LOC105369482 | -1.57 | 0.0044 | uncharacterized LOC105369482 |
| LOC105369593 | -1.52 | 0.0088 | uncharacterized LOC105369593 |
| LOC105370503 | -1.58 | 0.0377 | uncharacterized LOC105370503 |
| LOC105370741 | 1.5 | 0.0127 | uncharacterized LOC105370741 |
| LOC105370974 | 1.57 | 0.0349 | uncharacterized LOC105370974 |
| LOC105371504 | 1.71 | 0.0054 | uncharacterized LOC105371504 |
| LOC105373696 | -1.85 | 0.0413 | uncharacterized LOC105373696 |
| LOC105373850; LOC105376761 | 1.68 | 0.0121 | uncharacterized LOC105373850; uncharacterized LOC105376761 |
| LOC105373868 | -1.51 | 0.0029 | uncharacterized LOC105373868 |
| LOC105374104 | 1.57 | 0.0082 | uncharacterized LOC105374104 |
| LOC105377265 | 1.55 | 0.0027 | uncharacterized LOC105377265 |

| | | | |
|---|---|---|---|
| LOC105377384 | 1.6 | 0.006 | uncharacterized LOC105377384 |
| LOC105377643 | -1.56 | 0.0182 | uncharacterized LOC105377643 |
| LOC105377656 | 1.73 | 0.0011 | uncharacterized LOC105377656 |
| LOC105378067 | 1.59 | 0.0258 | uncharacterized LOC105378067 |
| LOC105379834 | 1.79 | 0.0056 | uncharacterized LOC105379834 |
| LOC283299 | 1.56 | 0.0018 | uncharacterized LOC283299 |
| LOC441666 | -1.66 | 0.0012 | zinc finger protein 91 pseudogene |
| LOC644669 | 1.6 | 0.0033 | ankyrin repeat domain 30B pseudogene |
| LTB4R2 | 1.53 | 0.0094 | leukotriene B4 receptor 2 |
| MIR1263 | 1.57 | 0.0123 | microRNA 1263 |
| MIR1265 | -1.53 | 0.0198 | microRNA 1265 |
| MIR19B2 | -1.6 | 0.0022 | microRNA 19b-2 |
| MIR302D; MIR302B | -1.59 | 0.002 | microRNA 302d; microRNA 302b |
| MIR3689E | -1.65 | 0.0287 | microRNA 3689e |
| MIR3911 | 1.63 | 0.0073 | microRNA 3911 |
| MIR4295 | -1.58 | 0.0036 | microRNA 4295 |
| MIR4326 | 1.6 | 0.0052 | microRNA 4326 |
| MIR4438 | -1.61 | 0.0049 | microRNA 4438 |
| MIR449A | 1.5 | 0.0096 | microRNA 449a |
| MIR4505 | 1.54 | 0.0043 | microRNA 4505 |
| MIR499B | 1.62 | 0.0186 | microRNA 499b |
| MIR509-3 | -1.82 | 0.0401 | microRNA 509-3 |
| MIR519A1 | 2.04 | 0.0062 | microRNA 519a-1 |
| MIR520C | 1.56 | 0.0014 | microRNA 520c |
| MIR520F | -1.5 | 0.0351 | microRNA 520f |
| MIR548H2 | -1.59 | 0.0079 | microRNA 548h-2 |
| MIR579 | -1.63 | 0.0439 | microRNA 579 |
| MIR708 | 1.72 | 0.0025 | microRNA 708 |
| MIRLET7F1 | -2.14 | 0.0003 | microRNA let-7f-1 |
| MPLKIP | 1.52 | 0.0312 | M-phase specific PLK1 interacting protein |
| MYH4 | -1.77 | 0.012 | myosin, heavy chain 4, skeletal muscle |
| NEU1 | 1.6 | 0.0015 | sialidase 1 (lysosomal sialidase) |
| NEURL3 | 1.54 | 0.0107 | neuralized E3 ubiquitin protein ligase 3 |
| NIPA1 | -1.5 | 0.0022 | non imprinted in Prader-Willi/Angelman syndrome 1 |
| NPC2; MIR4709 | 1.52 | 0.0086 | Niemann-Pick disease, type C2; microRNA 4709 |
| NUP210P1 | 1.65 | 0.0425 | nucleoporin 210kDa pseudogene 1 |
| NUPR1 | 1.77 | 0.0011 | nuclear protein 1, transcriptional regulator |
| OR1F1 | 1.57 | 0.0227 | olfactory receptor, family 1, subfamily F, member 1 |
| OR2A20P; OR2A1-AS1 | 1.55 | 0.0302 | olfactory receptor, family 2, subfamily A, member 20 pseudogene; OR2A1 antisense RNA 1 |
| OR2AE1 | -1.58 | 0.0136 | olfactory receptor, family 2, subfamily AE, member 1 |
| OR2T33 | 1.53 | 0.0275 | olfactory receptor, family 2, subfamily T, member |

| | | | |
|---|---|---|---|
| | | | 33 |
| OR52N5 | 1.91 | 0.0007 | olfactory receptor, family 52, subfamily N, member 5 |
| OR5H6 | 1.69 | 0.0022 | olfactory receptor, family 5, subfamily H, member 6 (gene/pseudogene) |
| PCDH11X | 2.05 | 0.0027 | protocadherin 11 X-linked |
| PLA1A | 1.65 | 0.0137 | phospholipase A1 member A |
| PRAMEF1; PRAMEF28; PRAMEF13 | -1.55 | 0.0344 | PRAME family member 1; PRAME family member 28; PRAME family member 13 |
| PRKAR2B | -1.59 | 0.0441 | protein kinase, cAMP-dependent, regulatory, type II, beta |
| RAB6C-AS1; RAB6C | 1.51 | 0.0255 | RAB6C antisense RNA 1; RAB6C, member RAS oncogene family |
| RHD | 1.52 | 0.0054 | Rh blood group, D antigen |
| S100A4 | -1.53 | 0.0028 | S100 calcium binding protein A4 |
| SAT2 | 1.61 | 0.0046 | spermidine/spermine N1-acetyltransferase family member 2 |
| SGCB | -1.52 | 0.0206 | sarcoglycan beta |
| SHFM1 | -1.58 | 0.0493 | split hand/foot malformation (ectrodactyly) type 1 |
| SNORA11C | -1.74 | 0.0347 | small nucleolar RNA, H/ACA box 11C |
| SNORD114-17 | 1.61 | 0.0118 | small nucleolar RNA, C/D box 114-17 |
| SNORD41 | 1.52 | 0.0087 | small nucleolar RNA, C/D box 41 |
| SPRNP1; SYCE1 | 1.55 | 0.0021 | shadow of prion protein homolog (zebrafish) pseudogene 1; synaptonemal complex central element protein 1 |
| SRGAP2-AS1 | 1.96 | 0.0017 | SRGAP2 antisense RNA 1 |
| STC2 | 1.5 | 0.0095 | stanniocalcin 2 |
| TAS2R30 | -2.24 | 0.0021 | taste receptor, type 2, member 30 |
| TAS2R31 | 1.62 | 0.037 | taste receptor, type 2, member 31 |
| TEX35 | 2.07 | 0.0205 | testis expressed 35 |
| TMEM150B | 1.6 | 0.0033 | transmembrane protein 150B |
| TMEM154 | 1.52 | 0.0067 | transmembrane protein 154 |
| TRDV2; TRAJ29; TRAC | -1.55 | 0.0417 | T cell receptor delta variable 2; T cell receptor alpha joining 29; T-cell receptor alpha constant |
| TRIM48 | 1.91 | 0.0211 | tripartite motif containing 48 |
| UAP1L1 | 2.12 | 0.0021 | UDP-N-acetylglucosamine pyrophosphorylase 1 like 1 |
| UBAP1L | 1.56 | 0.0024 | ubiquitin associated protein 1 like |
| ZCWPW2; IGHV3-23 | 1.78 | 0.0005 | zinc finger, CW type with PWWP domain 2; immunoglobulin heavy variable 3-23 |
| ZNF280D | -1.54 | 0.0034 | zinc finger protein 280D |
| ZNF493 | -1.51 | 0.0163 | zinc finger protein 493 |
| ZNF610 | -1.52 | 0.0042 | zinc finger protein 610 |

**Supplemental Table 2.10**: Changes in transcript abundance of 72 hour 10 μM CB1 Antagonist, AM251 treated HuH7.5s through microarray; Affymetrix GeneChip™ Human Gene 2.0 ST Array, n = 2. Significance was assessed through analysis of variance (ANOVA) with the empirical Bayes correction. (p vales < 0.05 shown, fold changes less than -1.5, and greater than 1.5 shown)

| Gene Symbol | Fold Change | P-val | Description |
|---|---|---|---|
| AIM1 | -2.01 | 0.0002 | absent in melanoma 1 |
| ADAM21P1 | -1.58 | 0.0225 | ADAM metallopeptidase domain 21 pseudogene 1 |
| ADGRD1 | 1.67 | 0.0096 | adhesion G protein-coupled receptor D1 |
| ARL9 | -1.52 | 0.0076 | ADP-ribosylation factor like GTPase 9 |
| ADM2; MIOX | 1.74 | 0.0014 | adrenomedullin 2; myo-inositol oxygenase |
| ANPEP | 1.52 | 0.009 | alanyl (membrane) aminopeptidase |
| ADH6 | -1.56 | 0.006 | alcohol dehydrogenase 6 (class V) |
| ALDH1L2 | 4.65 | 0.0001 | aldehyde dehydrogenase 1 family, member L2 |
| AKR1C4 | -1.67 | 0.0027 | aldo-keto reductase family 1, member C4 |
| AGMO | -1.8 | 0.0007 | alkylglycerol monooxygenase |
| ALPK2 | 1.65 | 0.0489 | alpha kinase 2 |
| AREG | 1.89 | 0.0107 | amphiregulin |
| AREG | 2.27 | 0.0114 | amphiregulin |
| ANKRD26 | -1.55 | 0.0049 | ankyrin repeat domain 26 |
| APOLD1 | -2.05 | 0.0009 | apolipoprotein L domain containing 1 |
| APOL6 | 1.99 | 0.0024 | apolipoprotein L, 6 |
| APOM | -1.55 | 0.013 | apolipoprotein M |
| ARG1 | -2.09 | 0.0023 | arginase 1 |
| ASS1 | 2.42 | 0.0001 | argininosuccinate synthase 1 |
| ASNS | 3.79 | 1.62E-05 | asparagine synthetase (glutamine-hydrolyzing) |
| AKNA | 1.74 | 0.0054 | AT-hook transcription factor |
| ATP11A | 1.98 | 0.0136 | ATPase, class VI, type 11A |
| BMF | 1.83 | 0.004 | Bcl2 modifying factor |
| BTC | 1.55 | 0.0215 | betacellulin |
| BEX2 | 1.72 | 0.0009 | brain expressed X-linked 2 |
| BCRP3 | 1.55 | 0.002 | breakpoint cluster region pseudogene 3 |
| BACH1 | 1.69 | 0.0318 | BTB and CNC homology 1, basic leucine zipper transcription factor 1 |
| CDH1 | 1.59 | 0.0018 | cadherin 1, type 1 |
| CLGN | 1.87 | 0.0005 | calmegin |
| CAPN5 | 1.51 | 0.0043 | calpain 5 |
| CPS1 | -1.65 | 0.0015 | carbamoyl-phosphate synthase 1 |
| CA5A | -1.69 | 0.0099 | carbonic anhydrase VA, mitochondrial |
| CPM | -1.61 | 0.0023 | carboxypeptidase M |

| | | | |
|---|---|---|---|
| CD38 | -2.24 | 0.0004 | CD38 molecule |
| CENPE | -1.8 | 0.0052 | centromere protein E |
| CENPI | -1.62 | 0.0072 | centromere protein I |
| CHAC1 | 4.78 | 7.72E-05 | ChaC glutathione-specific gamma-glutamylcyclotransferase 1 |
| CCR6 | -2.2 | 0.004 | chemokine (C-C motif) receptor 6 |
| C2orf15 | 1.55 | 0.0119 | chromosome 2 open reading frame 15 |
| C9orf91 | 1.78 | 0.0005 | chromosome 9 open reading frame 91 |
| F13B | -1.8 | 0.0007 | coagulation factor XIII, B polypeptide |
| C4BPA | -1.95 | 0.0006 | complement component 4 binding protein, alpha |
| C7 | -1.61 | 0.005 | complement component 7 |
| CTH | 2.45 | 0.0002 | cystathionine gamma-lyase |
| CSTA | 1.7 | 0.0048 | cystatin A (stefin A) |
| CRISP3 | -1.72 | 0.0308 | cysteine-rich secretory protein 3 |
| CYP1A1 | 1.89 | 0.005 | cytochrome P450, family 1, subfamily A, polypeptide 1 |
| CYP1B1 | 1.77 | 0.0254 | cytochrome P450, family 1, subfamily B, polypeptide 1 |
| CYP2B6 | 1.7 | 0.002 | cytochrome P450, family 2, subfamily B, polypeptide 6 |
| CYP2C18 | -1.62 | 0.0326 | cytochrome P450, family 2, subfamily C, polypeptide 18 |
| DDX43 | -1.52 | 0.0396 | DEAD (Asp-Glu-Ala-Asp) box polypeptide 43 |
| DNASE2 | 1.54 | 0.0033 | deoxyribonuclease II, lysosomal |
| DGKK | -3 | 0.0004 | diacylglycerol kinase, kappa |
| DPRXP4 | -1.52 | 0.0026 | divergent-paired related homeobox pseudogene 4 |
| DDIT4 | 4.63 | 2.04E-05 | DNA damage inducible transcript 4 |
| DOC2B | 1.65 | 0.0027 | double C2-like domains, beta |
| DUSP10 | -1.51 | 0.0408 | dual specificity phosphatase 10 |
| EFHD1 | 1.66 | 0.0286 | EF-hand domain family member D1 |
| EPCAM | 1.51 | 0.0106 | epithelial cell adhesion molecule |
| EIF4EBP1 | 1.95 | 0.0005 | eukaryotic translation initiation factor 4E binding protein 1 |
| ELFN1 | 1.51 | 0.0031 | extracellular leucine-rich repeat and fibronectin type III domain containing 1 |
| FAM19A4 | -1.6 | 0.0025 | family with sequence similarity 19 (chemokine (C-C motif)-like), member A4 |
| FAM74A3 | 1.85 | 0.0015 | family with sequence similarity 74, member A3 |
| FAM83D | -1.5 | 0.0041 | family with sequence similarity 83, member D |
| FAM129A | 1.8 | 0.0054 | family with sequence similarity 129, member A |
| FAXDC2 | -1.62 | 0.0099 | fatty acid hydroxylase domain containing 2 |
| FBN1 | 1.76 | 0.0034 | fibrillin 1 |
| FMOD | 2.29 | 0.0025 | fibromodulin |
| FHOD3 | 1.7 | 0.0091 | formin homology 2 domain containing 3 |
| FRAS1 | 1.54 | 0.0085 | Fraser extracellular matrix complex subunit 1 |

| | | | |
|---|---|---|---|
| FRZB | -1.57 | 0.0132 | frizzled-related protein |
| FUT3 | -1.94 | 0.0079 | fucosyltransferase 3 (galactoside 3(4)-L-fucosyltransferase, Lewis blood group) |
| GPR119 | -2.29 | 0.0007 | G protein-coupled receptor 119 |
| GMNC | -1.51 | 0.006 | geminin coiled-coil domain containing |
| GPT2 | 2.07 | 0.0006 | glutamic pyruvate transaminase (alanine aminotransferase) 2 |
| GLTPD2 | -1.54 | 0.0135 | glycolipid transfer protein domain containing 2 |
| GARS | 1.51 | 0.0032 | glycyl-tRNA synthetase |
| GC | -2.68 | 0.0185 | group-specific component (vitamin D binding protein) |
| GDF15 | 1.85 | 0.0348 | growth differentiation factor 15 |
| HP | -3.06 | 8.83E-05 | haptoglobin |
| HAVCR1 | -1.57 | 0.0263 | hepatitis A virus cellular receptor 1 |
| HEXIM1 | -1.56 | 0.0024 | hexamethylene bis-acetamide inducible 1 |
| HRG | -2.27 | 0.0007 | histidine-rich glycoprotein |
| HIST1H2AJ | -1.61 | 0.0116 | histone cluster 1, H2aj |
| HIST1H2BC | -1.96 | 0.0013 | histone cluster 1, H2bc |
| HIST1H2BD | -1.55 | 0.0118 | histone cluster 1, H2bd |
| HIST1H2BF | -1.57 | 0.0021 | histone cluster 1, H2bf |
| HIST1H2BG | -1.75 | 0.016 | histone cluster 1, H2bg |
| HIST1H2BJ | -2.02 | 0.0003 | histone cluster 1, H2bj |
| HIST1H3C | -2.04 | 0.0053 | histone cluster 1, H3c |
| HIST1H3H | -1.7 | 0.0041 | histone cluster 1, H3h |
| HIST1H4H | -2.66 | 3.10E-05 | histone cluster 1, H4h |
| HIST2H2AB | 1.52 | 0.0028 | histone cluster 2, H2ab |
| HOXD1; MIR7704 | -1.83 | 0.002 | homeobox D1; microRNA 7704 |
| HS1BP3-IT1 | 1.52 | 0.0109 | HS1BP3 intronic transcript 1 |
| HSD17B7P2 | -1.6 | 0.0025 | hydroxysteroid (17-beta) dehydrogenase 7 pseudogene 2 |
| HSD17B14 | 1.85 | 0.0042 | hydroxysteroid (17-beta) dehydrogenase 14 |
| IGHV1-45; IGHM | -1.63 | 0.0066 | immunoglobulin heavy variable 1-45; immunoglobulin heavy constant mu |
| INHBE | 2.32 | 0.0001 | inhibin beta E |
| ID4 | -1.59 | 0.0021 | inhibitor of DNA binding 4, dominant negative helix-loop-helix protein |
| INSIG1 | -1.7 | 0.0103 | insulin induced gene 1 |
| IBSP | 1.52 | 0.013 | integrin-binding sialoprotein |
| IFNA5 | 1.53 | 0.0277 | interferon, alpha 5 |
| IL17RB | -1.85 | 0.0014 | interleukin 17 receptor B |
| IL18 | -1.67 | 0.0081 | interleukin 18 |
| KRT24 | 1.52 | 0.0127 | keratin 24, type I |
| KRTAP10-4 | 1.54 | 0.0034 | keratin associated protein 10-4 |

| | | | |
|---|---|---|---|
| KRTAP19-3 | 1.52 | 0.0408 | keratin associated protein 19-3 |
| KLRAP1 | -1.76 | 0.0338 | killer cell lectin-like receptor subfamily A pseudogene 1 |
| KLF7 | 1.63 | 0.0049 | Kruppel-like factor 7 (ubiquitous) |
| KLF11 | 1.54 | 0.0039 | Kruppel-like factor 11 |
| LARS2-AS1 | -1.81 | 0.0373 | LARS2 antisense RNA 1 |
| LTBP1 | 1.62 | 0.0015 | latent transforming growth factor beta binding protein 1 |
| LRP1 | 1.91 | 0.0011 | LDL receptor related protein 1 |
| LRRC31 | 1.74 | 0.0007 | leucine rich repeat containing 31 |
| LRRC63 | 1.75 | 0.0017 | leucine rich repeat containing 63 |
| LGI2 | -1.67 | 0.0013 | leucine-rich repeat LGI family, member 2 |
| LNP1 | -1.51 | 0.0219 | leukemia NUP98 fusion partner 1 |
| LIMD1-AS1 | -1.52 | 0.0045 | LIMD1 antisense RNA 1 |
| LVCAT8 | 1.76 | 0.0102 | liver cancer-associated transcript 8 |
| LINC00312; LMCD1 | 1.71 | 0.0162 | long intergenic non-protein coding RNA 312; LIM and cysteine-rich domains 1 |
| LINC00383 | 1.51 | 0.0106 | long intergenic non-protein coding RNA 383 |
| LINC00501 | -1.52 | 0.0382 | long intergenic non-protein coding RNA 501 |
| LINC00515 | 1.72 | 0.0022 | long intergenic non-protein coding RNA 515 |
| LINC00624 | -1.51 | 0.0063 | long intergenic non-protein coding RNA 624 |
| LINC00641 | -1.89 | 0.0023 | long intergenic non-protein coding RNA 641 |
| LINC00992 | 1.53 | 0.0057 | long intergenic non-protein coding RNA 992 |
| LINC01047 | 1.62 | 0.004 | long intergenic non-protein coding RNA 1047 |
| LINC01314 | -1.62 | 0.0067 | long intergenic non-protein coding RNA 1314 |
| LINC01419 | -1.59 | 0.0314 | long intergenic non-protein coding RNA 1419 |
| LINC01423 | 1.74 | 0.0039 | long intergenic non-protein coding RNA 1423 |
| MB21D1 | 1.5 | 0.0147 | Mab-21 domain containing 1 |
| MAGEA12; CSAG4 | -1.56 | 0.0186 | MAGE family member A12; CSAG family, member 4 (pseudogene) |
| HLA-DRA | -1.66 | 0.006 | major histocompatibility complex, class II, DR alpha |
| MBOAT4 | -1.63 | 0.0377 | membrane bound O-acyltransferase domain containing 4 |
| MT1B | 1.55 | 0.0189 | metallothionein 1B |
| MARS | 1.59 | 0.0025 | methionyl-tRNA synthetase |
| MTHFD2 | 1.98 | 0.0006 | methylenetetrahydrofolate dehydrogenase (NADP+ dependent) 2, methenyltetrahydrofolate cyclohydrolase |
| MCEE | -1.77 | 0.0009 | methylmalonyl CoA epimerase |
| METTL3 | -1.51 | 0.0086 | methyltransferase like 3 |
| MVD | -1.55 | 0.0085 | mevalonate (diphospho) decarboxylase |
| MIR16-2 | 1.61 | 0.0014 | microRNA 16-2 |
| MIR29B2; C1orf132 | 1.82 | 0.0057 | microRNA 29b-2; chromosome 1 open reading frame 132 |

| | | | |
|---|---|---|---|
| MIR103A2 | 1.68 | 0.0035 | microRNA 103a-2 |
| MIR153-2 | 1.66 | 0.0041 | microRNA 153-2 |
| MIR188 | 1.57 | 0.0088 | microRNA 188 |
| MIR302D; MIR302B | -1.81 | 0.0308 | microRNA 302d; microRNA 302b |
| MIR320B2 | 1.68 | 0.0261 | microRNA 320b-2 |
| MIR323B | -1.91 | 0.0004 | microRNA 323b |
| MIR513A1 | 1.76 | 0.003 | microRNA 513a-1 |
| MIR518D | 1.5 | 0.0092 | microRNA 518d |
| MIR520A | 1.92 | 0.0065 | microRNA 520a |
| MIR578 | 1.59 | 0.0136 | microRNA 578 |
| MIR616; DDIT3 | 1.59 | 0.0088 | microRNA 616; DNA-damage-inducible transcript 3 |
| MIR634 | -1.51 | 0.0434 | microRNA 634 |
| MIR668 | 1.59 | 0.0087 | microRNA 668 |
| MIR708 | 1.52 | 0.0493 | microRNA 708 |
| MIR1299 | 1.62 | 0.0188 | microRNA 1299 |
| MIR1321 | 1.57 | 0.0045 | microRNA 1321 |
| MIR3120 | -1.96 | 0.0125 | microRNA 3120 |
| MIR3143 | -1.58 | 0.0017 | microRNA 3143 |
| MIR3671 | 2.68 | 0.0065 | microRNA 3671 |
| MIR3911 | 1.68 | 0.0315 | microRNA 3911 |
| MIR3913-1 | -1.59 | 0.0053 | microRNA 3913-1 |
| MIR4253 | 1.82 | 0.0007 | microRNA 4253 |
| MAP1B | 1.81 | 0.0012 | microtubule associated protein 1B |
| MAP10 | -1.6 | 0.0046 | microtubule-associated protein 10 |
| MIR181A1HG | 1.52 | 0.0199 | MIR181A1 host gene |
| MIR181A2HG | 1.53 | 0.0029 | MIR181A2 host gene |
| MIR217HG | -1.79 | 0.0036 | MIR217 host gene |
| MUC13 | 1.75 | 0.0051 | mucin 13, cell surface associated |
| MSANTD3; MSANTD3-TMEFF1; TMEFF1 | 1.59 | 0.0279 | Myb/SANT-like DNA-binding domain containing 3; MSANTD3-TMEFF1 readthrough; transmembrane protein with EGF-like and two follistatin-like domains 1 |
| MTM1 | -1.52 | 0.0056 | myotubularin 1 |
| N4BP2L2-IT2 | 1.54 | 0.0139 | N4BPL2 intronic transcript 2 |
| NPNT | 2.67 | 0.0133 | nephronectin |
| NES | 1.71 | 0.0037 | nestin |
| NBPF1 | 1.62 | 0.0103 | neuroblastoma breakpoint family, member 1 |
| NBPF7 | -1.6 | 0.0102 | neuroblastoma breakpoint family, member 7 |
| NRCAM | 1.51 | 0.0072 | neuronal cell adhesion molecule |
| NHLRC1 | 1.59 | 0.0117 | NHL repeat containing E3 ubiquitin protein ligase 1 |
| NPIPB1P | 1.69 | 0.0329 | nuclear pore complex interacting protein family, member B1, pseudogene |

| | | | |
|---|---|---|---|
| NR0B2 | 1.9 | 0.0044 | nuclear receptor subfamily 0, group B, member 2 |
| NR4A2 | -1.95 | 0.0004 | nuclear receptor subfamily 4, group A, member 2 |
| NR6A1 | -1.65 | 0.0146 | nuclear receptor subfamily 6, group A, member 1 |
| OR2A20P; OR2A1-AS1 | 1.87 | 0.0007 | olfactory receptor, family 2, subfamily A, member 20 pseudogene; OR2A1 antisense RNA 1 |
| OR2T34 | 1.81 | 0.0074 | olfactory receptor, family 2, subfamily T, member 34 |
| OR4F5 | 1.87 | 0.0329 | olfactory receptor, family 4, subfamily F, member 5 |
| OR4N2 | 1.74 | 0.0045 | olfactory receptor, family 4, subfamily N, member 2 |
| OR13C4 | 1.52 | 0.0026 | olfactory receptor, family 13, subfamily C, member 4 |
| OLMALINC | -1.72 | 0.0134 | oligodendrocyte maturation-associated long intergenic non-coding RNA |
| OGFRL1 | 1.52 | 0.0079 | opioid growth factor receptor-like 1 |
| OAT | -1.51 | 0.0048 | ornithine aminotransferase |
| OLR1 | -1.52 | 0.0061 | oxidized low density lipoprotein (lectin-like) receptor 1 |
| OSBPL10 | 1.58 | 0.0086 | oxysterol binding protein-like 10 |
| PON1 | -1.63 | 0.0049 | paraoxonase 1 |
| PCYT1B-AS1 | 1.53 | 0.0026 | PCYT1B antisense RNA 1 |
| PMAIP1 | 1.61 | 0.002 | phorbol-12-myristate-13-acetate-induced protein 1 |
| PDE9A | 1.62 | 0.0059 | phosphodiesterase 9A |
| PCK2 | 2.36 | 0.0004 | phosphoenolpyruvate carboxykinase 2 (mitochondrial) |
| PHGDH | 1.63 | 0.0018 | phosphoglycerate dehydrogenase |
| PLAC8 | -1.51 | 0.0061 | placenta specific 8 |
| PDGFA | 1.52 | 0.0082 | platelet-derived growth factor alpha polypeptide |
| PDGFRL | -1.52 | 0.0053 | platelet-derived growth factor receptor-like |
| PARP11 | 1.5 | 0.0081 | poly(ADP-ribose) polymerase family member 11 |
| PHC1 | 1.8 | 0.0014 | polyhomeotic homolog 1 (Drosophila) |
| PHC1 | 1.57 | 0.0133 | polyhomeotic homolog 1 (Drosophila) |
| PA2G4P4 | 1.58 | 0.0016 | proliferation-associated 2G4 pseudogene 4 |
| PTGER4 | 1.82 | 0.0068 | prostaglandin E receptor 4 (subtype EP4) |
| PTGFRN | 1.7 | 0.0024 | prostaglandin F2 receptor inhibitor |
| PARM1 | 1.65 | 0.0025 | prostate androgen-regulated mucin-like protein 1 |
| PPM1K | -1.64 | 0.0106 | protein phosphatase, Mg2+/Mn2+ dependent, 1K |
| PNP | -1.51 | 0.0075 | purine nucleoside phosphorylase |
| R3HDM2 | 1.59 | 0.0145 | R3H domain containing 2 |
| RANBP3L | -2.98 | 6.68E-05 | RAN binding protein 3-like |
| RCN1 | 2.66 | 0.0008 | reticulocalbin 1, EF-hand calcium binding domain |
| ARHGEF2 | 1.63 | 0.0013 | Rho/Rac guanine nucleotide exchange factor 2 |
| RPL19P12 | 1.71 | 0.0104 | ribosomal protein L19 pseudogene 12 |
| RPL23AP49 | 1.62 | 0.0172 | ribosomal protein L23a pseudogene 49 |

| | | | |
|---|---|---|---|
| RNF157 | 1.55 | 0.0028 | ring finger protein 157 |
| RNU1-13P | 1.63 | 0.0134 | RNA, U1 small nuclear 13, pseudogene |
| RNU1-13P | 1.63 | 0.0134 | RNA, U1 small nuclear 13, pseudogene |
| RNVU1-6 | -1.54 | 0.003 | RNA, variant U1 small nuclear 6 |
| RNVU1-14 | -1.75 | 0.025 | RNA, variant U1 small nuclear 14 |
| S100P | 1.67 | 0.0132 | S100 calcium binding protein P |
| SEL1L3 | 1.55 | 0.0144 | sel-1 suppressor of lin-12-like 3 (C. elegans) |
| SPTLC3 | -1.53 | 0.0308 | serine palmitoyltransferase, long chain base subunit 3 |
| SPTSSB | -1.67 | 0.0035 | serine palmitoyltransferase, small subunit B |
| SERPINA5 | -1.51 | 0.0476 | serpin peptidase inhibitor, clade A (alpha-1 antiproteinase, antitrypsin), member 5 |
| SERPINA6 | -1.54 | 0.0149 | serpin peptidase inhibitor, clade A (alpha-1 antiproteinase, antitrypsin), member 6 |
| SERPINE2 | 2.14 | 0.0039 | serpin peptidase inhibitor, clade E (nexin, plasminogen activator inhibitor type 1), member 2 |
| SGK2 | 1.76 | 0.0187 | serum/glucocorticoid regulated kinase 2 |
| SARS | 1.61 | 0.0035 | seryl-tRNA synthetase |
| SESN2 | 2.88 | 0.0002 | sestrin 2 |
| SH2B3 | 1.62 | 0.0055 | SH2B adaptor protein 3 |
| SH3BP2 | 1.59 | 0.0055 | SH3-domain binding protein 2 |
| STEAP1 | -1.9 | 0.0107 | six transmembrane epithelial antigen of the prostate 1 |
| SCARNA7 | 1.53 | 0.0106 | small Cajal body-specific RNA 7 |
| SNORD41 | 1.62 | 0.0142 | small nucleolar RNA, C/D box 41 |
| SNORD114-12 | -1.71 | 0.0094 | small nucleolar RNA, C/D box 114-12 |
| SNORD115-27 | -1.59 | 0.02 | small nucleolar RNA, C/D box 115-27 |
| SNCA-AS1 | 1.57 | 0.0112 | SNCA antisense RNA 1 |
| SLC1A4 | 2.62 | 7.25E-05 | solute carrier family 1 (glutamate/neutral amino acid transporter), member 4 |
| SLC1A5 | 1.63 | 0.0011 | solute carrier family 1 (neutral amino acid transporter), member 5 |
| SLC3A2 | 1.55 | 0.0037 | solute carrier family 3 (amino acid transporter heavy chain), member 2 |
| SLC6A6 | -1.5 | 0.0107 | solute carrier family 6 (neurotransmitter transporter), member 6 |
| SLC6A9 | 2.43 | 0.0003 | solute carrier family 6 (neurotransmitter transporter, glycine), member 9 |
| SLC7A5 | 1.59 | 0.0175 | solute carrier family 7 (amino acid transporter light chain, L system), member 5 |
| SLC7A11 | 2.67 | 0.0002 | solute carrier family 7 (anionic amino acid transporter light chain, xc- system), member 11 |
| SLC7A1 | 2.17 | 0.0007 | solute carrier family 7 (cationic amino acid transporter, y+ system), member 1 |
| SLC34A2 | 3.39 | 0.0004 | solute carrier family 34 (type II sodium/phosphate cotransporter), member 2 |
| SLC38A11 | -1.82 | 0.0017 | solute carrier family 38, member 11 |

| | | | |
|---|---|---|---|
| SLC43A1 | 1.53 | 0.015 | solute carrier family 43 (amino acid system L transporter), member 1 |
| SLC48A1 | 1.88 | 0.0047 | solute carrier family 48 (heme transporter), member 1 |
| SLCO1B3 | -1.82 | 0.0368 | solute carrier organic anion transporter family, member 1B3 |
| SLCO2A1 | 1.54 | 0.002 | solute carrier organic anion transporter family, member 2A1 |
| SOS1 | 1.69 | 0.0378 | SOS Ras/Rac guanine nucleotide exchange factor 1 |
| SPANXN4 | -1.52 | 0.034 | SPANX family, member N4 |
| SAT1 | -1.65 | 0.0014 | spermidine/spermine N1-acetyltransferase 1 |
| STC2 | 4.42 | 0.0002 | stanniocalcin 2 |
| STARD4 | -1.65 | 0.0084 | StAR-related lipid transfer domain containing 4 |
| SULT1B1 | -1.58 | 0.0164 | sulfotransferase family 1B member 1 |
| SULT2A1 | -1.77 | 0.0086 | sulfotransferase family 2A member 1 |
| SOCS1 | -1.52 | 0.003 | suppressor of cytokine signaling 1 |
| TRAJ19 | 1.53 | 0.0354 | T cell receptor alpha joining 19 (non-functional) |
| TAS2R19 | 1.61 | 0.0222 | taste receptor, type 2, member 19 |
| TCTEX1D1 | -1.8 | 0.0024 | Tctex1 domain containing 1 |
| TSPAN31 | 1.53 | 0.0022 | tetraspanin 31 |
| TRANK1 | 1.52 | 0.0156 | tetratricopeptide repeat and ankyrin repeat containing 1 |
| TXNIP | 1.64 | 0.0023 | thioredoxin interacting protein |
| TIMP4 | 1.67 | 0.0139 | TIMP metallopeptidase inhibitor 4 |
| TTPA | -1.96 | 0.0141 | tocopherol (alpha) transfer protein |
| TCEB3 | -1.55 | 0.0309 | transcription elongation factor B (SIII), polypeptide 3 (110kDa, elongin A) |
| TM4SF5 | -2.1 | 0.0106 | transmembrane 4 L six family member 5 |
| TMCO4 | 1.53 | 0.0049 | transmembrane and coiled-coil domains 4 |
| TMC7 | 1.5 | 0.0028 | transmembrane channel like 7 |
| TMED10P1 | 1.52 | 0.014 | transmembrane emp24-like trafficking protein 10 (yeast) pseudogene 1 |
| TMEM45B | 1.63 | 0.0084 | transmembrane protein 45B |
| TMEM62 | 1.53 | 0.0058 | transmembrane protein 62 |
| TMEM154 | 1.93 | 0.0213 | transmembrane protein 154 |
| TFF1 | 1.65 | 0.0221 | trefoil factor 1 |
| TRIB3 | 1.98 | 0.0022 | tribbles pseudokinase 3 |
| TRIM31 | -1.82 | 0.006 | tripartite motif containing 31 |
| WARS | 1.52 | 0.013 | tryptophanyl-tRNA synthetase |
| TUBB2A | -1.64 | 0.0036 | tubulin, beta 2A class IIa |
| TUBE1 | 1.9 | 0.001 | tubulin, epsilon 1 |
| TDRD15 | 1.53 | 0.0029 | tudor domain containing 15 |
| USP29 | -1.63 | 0.0241 | ubiquitin specific peptidase 29 |
| UBE2L6 | 1.64 | 0.0027 | ubiquitin-conjugating enzyme E2L 6 |

| | | | |
|---|---|---|---|
| UGT2B15 | 1.72 | 0.0136 | UDP glucuronosyltransferase 2 family, polypeptide B15 |
| B3GALT1 | 1.6 | 0.0014 | UDP-Gal:betaGlcNAc beta 1,3-galactosyltransferase 1 |
| UHRF1BP1 | 1.69 | 0.0013 | UHRF1 binding protein 1 |
| ULBP1 | 4.55 | 4.60E-05 | UL16 binding protein 1 |
| UNC5B | 2.04 | 0.0008 | unc-5 netrin receptor B |
| LOC284014 | -1.59 | 0.0046 | uncharacterized LOC284014 |
| LOC284561 | 1.92 | 0.0014 | uncharacterized LOC284561 |
| FLJ46906 | 1.61 | 0.0093 | uncharacterized LOC441172 |
| LOC642426 | -1.68 | 0.0229 | uncharacterized LOC642426 |
| LOC642648 | -1.5 | 0.0273 | uncharacterized LOC642648 |
| LOC728290 | -1.61 | 0.0029 | uncharacterized LOC728290 |
| LOC100128281 | 1.58 | 0.0019 | uncharacterized LOC100128281 |
| LOC100129046 | -1.55 | 0.0156 | uncharacterized LOC100129046 |
| LOC100507639 | -1.84 | 0.0037 | uncharacterized LOC100507639 |
| LOC101928565 | -1.81 | 0.0023 | uncharacterized LOC101928565 |
| LOC101928663 | -1.55 | 0.0019 | uncharacterized LOC101928663 |
| LOC101929633 | -2.44 | 0.0029 | uncharacterized LOC101929633 |
| LOC102724297 | -1.61 | 0.0016 | uncharacterized LOC102724297 |
| LOC102724422 | 1.67 | 0.0079 | uncharacterized LOC102724422 |
| LOC105370437 | 1.54 | 0.0042 | uncharacterized LOC105370437 |
| LOC105370439 | -1.56 | 0.004 | uncharacterized LOC105370439 |
| LOC105370998 | -1.57 | 0.0022 | uncharacterized LOC105370998 |
| LOC105372290 | -1.53 | 0.0022 | uncharacterized LOC105372290 |
| LOC105372391 | 1.55 | 0.0098 | uncharacterized LOC105372391 |
| LOC105373305 | -1.57 | 0.009 | uncharacterized LOC105373305 |
| LOC105373954 | 1.56 | 0.0034 | uncharacterized LOC105373954 |
| LOC105374990; LOC105374993; LOC105375102 | -1.8 | 0.009 | uncharacterized LOC105374990; uncharacterized LOC105374993; uncharacterized LOC105375102 |
| LOC105376287 | -1.66 | 0.0136 | uncharacterized LOC105376287 |
| LOC105376420 | -1.53 | 0.0067 | uncharacterized LOC105376420 |
| LOC105377172 | -1.67 | 0.0018 | uncharacterized LOC105377172 |
| LOC105379228 | -1.52 | 0.0192 | uncharacterized LOC105379228 |
| UCA1 | -2.01 | 0.0018 | urothelial cancer associated 1 (non-protein coding) |
| USP6NL | 1.57 | 0.045 | USP6 N-terminal like |
| VCAN | 1.77 | 0.0009 | versican |
| VLDLR | 3.44 | 0.0003 | very low density lipoprotein receptor |
| VLDLR-AS1 | 1.63 | 0.0011 | VLDLR antisense RNA 1 |
| WSB1 | -1.51 | 0.0226 | WD repeat and SOCS box containing 1 |
| ZFP69B | 1.74 | 0.0064 | ZFP69 zinc finger protein B |

| | | | |
|---|---|---|---|
| ZNF221 | -1.54 | 0.0196 | zinc finger protein 221 |
| ZNF479 | -1.81 | 0.0009 | zinc finger protein 479 |

**Supplemental Table 2.11**: ToppGene gene ontology transcriptomic analysis of 24 hour 1 µM MGLL inhibitor, MJN110 treated HuH7.5s. Significance was assessed through the probability density function with the Bonferroni correction. p values < 0.05 are displayed.

| Category | ID | Name | p-value | q-value Bonferroni | Hit Count/ Genes in annotation | Hit in Query List |
|---|---|---|---|---|---|---|
| GO: Molecular Function | GO:0034987 | immunoglobulin receptor binding | 9.91E-12 | 4.68E-09 | 12/81 | IGLL5,IGHA1,IGHD,IGHM,IGLL1,IGHV3-74,IGHV3-33,IGHV3-30,IGHV3-23,IGHV1-58,IGHV1-45,IGHV1-18 |
| GO: Molecular Function | GO:0003823 | antigen binding | 8.36E-10 | 3.95E-07 | 14/175 | HLA-H,IGLV6-57,IGLL5,IGHA1,IGHD,IGHM,IGLL1,IGHV3-74,IGHV3-33,IGHV3-30,IGHV3-23,IGHV1-58,IGHV1-45,IGHV1-18 |
| GO: Molecular Function | GO:0004984 | olfactory receptor activity | 2.32E-06 | 1.10E-03 | 16/30 | OR2T12,OR2T34,OR10A2,OR6C4,OR5H2,OR10H4,OR4K1,OR8G5,OR5K1,OR56B4,OR9A2,OR2AG1,OR5A2,OR8G1,OR51B6,OR2V2 |
| GO: Biological Process | GO:0006910 | phagocytosis, recognition | 3.70E-10 | 1.03E-06 | 12/103 | IGLL5,IGHA1,IGHD,IGHM,IGLL1,IGHV3-74,IGHV3-33,IGHV3-30,IGHV3-23,IGHV1-58,IGHV1-45,IGHV1-18 |
| GO: Biological Process | GO:0050853 | B cell receptor signaling pathway | 7.44E-10 | 2.07E-06 | 13/135 | IGLL5,IGHA1,IGHD,IGHM,PRKCH,IGLL1,IGHV3-74,IGHV3-33,IGHV3-30,IGHV3-23,IGHV1-58,IGHV1-45,IGHV1-18 |
| GO: Biological Process | GO:0006958 | complement activation, classical pathway | 1.40E-09 | 3.88E-06 | 13/142 | IGLV6-57,IGLL5,IGHA1,IGHD,IGHM,IGLL1,IGHV3-74,IGHV3-33,IGHV3-30,IGHV3-23,IGHV1-58,IGHV1-45,IGHV1-18 |
| GO: Biological Process | GO:0002455 | humoral immune response mediated by circulating immunoglobulin | 4.79E-09 | 1.33E-05 | 13/157 | IGLV6-57,IGLL5,IGHA1,IGHD,IGHM,IGLL1,IGHV3-74,IGHV3-33,IGHV3-30,IGHV3-23,IGHV1-58,IGHV1-45,IGHV1-18 |
| GO: Biological Process | GO:0006911 | phagocytosis, engulfment | 6.05E-09 | 1.68E-05 | 12/131 | IGLL5,IGHA1,IGHD,IGHM,IGLL1,IGHV3-74,IGHV3-33,IGHV3-30,IGHV3-23,IGHV1-58,IGHV1-45,IGHV1-18 |
| GO: | GO:005087 | positive regulation | 7.01E-09 | 1.95E-05 | 13/162 | IGLL5,IGHA1,IGHD,IGHM,IGLL1,WNT3A,I |

| | | | | | | |
|---|---|---|---|---|---|---|
| Biological Process | 1 | of B cell activation | | | | GHV3-74,IGHV3-33,IGHV3-30,IGHV3-23,IGHV1-58,IGHV1-45,IGHV1-18 |
| GO: Biological Process | GO:0099024 | plasma membrane invagination | 1.29E-08 | 3.58E-05 | 12/140 | IGLL5,IGHA1,IGHD,IGHM,IGLL1,IGHV3-74,IGHV3-33,IGHV3-30,IGHV3-23,IGHV1-58,IGHV1-45,IGHV1-18 |
| GO: Biological Process | GO:0072376 | protein activation cascade | 2.10E-08 | 5.83E-05 | 14/211 | IGLV6-57,IGLL5,F8,IGHA1,IGHD,IGHM,IGLL1,IGHV3-74,IGHV3-33,IGHV3-30,IGHV3-23,IGHV1-58,IGHV1-45,IGHV1-18 |
| GO: Biological Process | GO:0050864 | regulation of B cell activation | 2.36E-08 | 6.57E-05 | 14/213 | IGLL5,FLT3,IGHA1,IGHD,IGHM,IGLL1,WNT3A,IGHV3-74,IGHV3-33,IGHV3-30,IGHV3-23,IGHV1-58,IGHV1-45,IGHV1-18 |
| GO: Biological Process | GO:0006959 | humoral immune response | 2.56E-08 | 7.13E-05 | 19/414 | IGLV6-57,IGLL5,HRG,IFNA5,IGHA1,IGHD,IGHM,IGLL1,PRSS3,PRTN3,DEFA3,IGHV3-74,IGHV3-33,IGHV3-30,IGHV3-23,IGHV1-58,IGHV1-45,IGHV1-18,RNASE3 |
| GO: Biological Process | GO:0006956 | complement activation | 3.68E-08 | 1.02E-04 | 13/186 | IGLV6-57,IGLL5,IGHA1,IGHD,IGHM,IGLL1,IGHV3-74,IGHV3-33,IGHV3-30,IGHV3-23,IGHV1-58,IGHV1-45,IGHV1-18 |
| GO: Biological Process | GO:0045087 | innate immune response | 1.04E-07 | 2.90E-04 | 30/1045 | HLA-H,KIR2DS2,TRIM77,IGLL5,SERPINB4,APOBEC3B,IFNA5,IGHA1,IGHD,IGHM,IGLL1,GBP6,GBP1,LILRB1,APOBEC3A,DEFA3,IGHV3-74,TRIM49,IGHV3-33,IGHV3-30,IGHV3-23,IGHV1-58,IGHV1-45,IGHV1-18,TRIM43,PSMB11,DEFB133,RNASE3,PDE12,IFNL2 |
| GO: Biological Process | GO:0016064 | immunoglobulin mediated immune response | 7.39E-07 | 2.06E-03 | 13/241 | IGLV6-57,IGLL5,IGHA1,IGHD,IGHM,IGLL1,IGHV3-74,IGHV3-33,IGHV3-30,IGHV3-23,IGHV1-58,IGHV1-45,IGHV1-18 |
| GO: Biological Process | GO:0019724 | B cell mediated immunity | 8.90E-07 | 2.48E-03 | 13/245 | IGLV6-57,IGLL5,IGHA1,IGHD,IGHM,IGLL1,IGHV3-74,IGHV3-33,IGHV3-30,IGHV3-23,IGHV1- |

| | | | | | | |
|---|---|---|---|---|---|---|
| | | | | | | 58,IGHV1-45,IGHV1-18 |
| GO: Biological Process | GO:0098542 | defense response to other organism | 8.96E-07 | 2.49E-03 | 32/1285 | HLA-H,KIR2DS2,TRIM77,IGLL5,SERPINB4,HRG,APOBEC3B,IFNA5,IGHA1,IGHD,IGHM,IGLL1,GBP6,GBP1,LILRB1,APOBEC3A,DEFA3,IGHV3-74,TRIM49,IGHV3-33,IGHV3-30,IGHV3-23,IGHV1-58,IGHV1-45,IGHV1-18,TRIM43,PSMB11,MIR708,DEFB133,RNASE3,PDE12,IFNL2 |
| GO: Biological Process | GO:0050851 | antigen receptor-mediated signaling pathway | 1.22E-06 | 3.39E-03 | 15/338 | IGLL5,IGHA1,IGHD,IGHM,PRKCH,IGLL1,GBP1,IGHV3-74,IGHV3-33,IGHV3-30,IGHV3-23,IGHV1-58,IGHV1-45,IGHV1-18,PSMB11 |
| GO: Biological Process | GO:0042742 | defense response to bacterium | 1.22E-06 | 3.39E-03 | 16/384 | IGLL5,IGHA1,IGHD,IGHM,IGLL1,GBP6,DEFA3,IGHV3-74,IGHV3-33,IGHV3-30,IGHV3-23,IGHV1-58,IGHV1-45,IGHV1-18,DEFB133,RNASE3 |
| GO: Biological Process | GO:0002768 | immune response-regulating cell surface receptor signaling pathway | 1.25E-06 | 3.47E-03 | 19/533 | KIR2DS2,IGLV6-57,IGLL5,FCGR3A,IGHA1,IGHD,IGHM,PRKCH,IGLL1,GBP1,LILRB1,IGHV3-74,IGHV3-33,IGHV3-30,IGHV3-23,IGHV1-58,IGHV1-45,IGHV1-18,PSMB11 |
| GO: Biological Process | GO:0002764 | immune response-regulating signaling pathway | 1.39E-06 | 3.87E-03 | 19/537 | KIR2DS2,IGLV6-57,IGLL5,FCGR3A,IGHA1,IGHD,IGHM,PRKCH,IGLL1,GBP1,LILRB1,IGHV3-74,IGHV3-33,IGHV3-30,IGHV3-23,IGHV1-58,IGHV1-45,IGHV1-18,PSMB11 |
| GO: Biological Process | GO:0008037 | cell recognition | 1.66E-06 | 4.61E-03 | 13/259 | IGLL5,IGHA1,IGHD,IGHM,IGLL1,IGHV3-74,IGHV3-33,IGHV3-30,IGHV3-23,IGHV1-58,IGHV1-45,IGHV1-18,ADAM5 |
| GO: Biological Process | GO:0002429 | immune response-activating cell surface receptor signaling pathway | 1.98E-06 | 5.51E-03 | 18/498 | KIR2DS2,IGLV6-57,IGLL5,FCGR3A,IGHA1,IGHD,IGHM,PRKCH,IGLL1,GBP1,IGHV3-74,IGHV3-33,IGHV3-30,IGHV3-23,IGHV1-58,IGHV1-45,IGHV1-18,PSMB11 |
| GO: Biological | GO:0002757 | immune response-activating signal | 2.04E-06 | 5.67E-03 | 18/499 | KIR2DS2,IGLV6-57,IGLL5,FCGR3A,IGHA1,IGHD,IGHM,PRK |

| | | | | | | |
|---|---|---|---|---|---|---|
| Process | | transduction | | | | CH,IGLL1,GBP1,IGHV3-74,IGHV3-33,IGHV3-30,IGHV3-23,IGHV1-58,IGHV1-45,IGHV1-18,PSMB11 |
| GO: Biological Process | GO:0042113 | B cell activation | 2.57E-06 | 7.14E-03 | 15/359 | IGLL5,FLT3,IFNA5,IGHA1,IGHD,IGHM,IGLL1,WNT3A,IGHV3-74,IGHV3-33,IGHV3-30,IGHV3-23,IGHV1-58,IGHV1-45,IGHV1-18 |
| GO: Biological Process | GO:0002449 | lymphocyte mediated immunity | 2.59E-06 | 7.20E-03 | 16/407 | HLA-H,IGLV6-57,IGLL5,SERPINB4,IGHA1,IGHD,IGHM,IGLL1,LILRB1,IGHV3-74,IGHV3-33,IGHV3-30,IGHV3-23,IGHV1-58,IGHV1-45,IGHV1-18 |
| GO: Biological Process | GO:0051707 | response to other organism | 2.83E-06 | 7.86E-03 | 37/1700 | HLA-H,KIR2DS2,TRIM77,IGLL5,SERPINB4,HRG,FLT3,APOBEC3B,IFNA5,IGHA1,IGHD,IGHM,IGLL1,PRSS3,GBP6,PRTN3,GBP1,LILRB1,APOBEC3A,DEFA3,IGHV3-74,IL24,TRIM49,IGHV3-33,IGHV3-30,IGHV3-23,IGHV1-58,IGHV1-45,IGHV1-18,TRIM43,PSMB11,MIR708,DEFB133,RNASE3,PDE12,IFNL2,TRAV13-2 |
| GO: Biological Process | GO:0043207 | response to external biotic stimulus | 2.90E-06 | 8.08E-03 | 37/1702 | HLA-H,KIR2DS2,TRIM77,IGLL5,SERPINB4,HRG,FLT3,APOBEC3B,IFNA5,IGHA1,IGHD,IGHM,IGLL1,PRSS3,GBP6,PRTN3,GBP1,LILRB1,APOBEC3A,DEFA3,IGHV3-74,IL24,TRIM49,IGHV3-33,IGHV3-30,IGHV3-23,IGHV1-58,IGHV1-45,IGHV1-18,TRIM43,PSMB11,MIR708,DEFB133,RNASE3,PDE12,IFNL2,TRAV13-2 |
| GO: Biological Process | GO:0050778 | positive regulation of immune response | 4.34E-06 | 1.21E-02 | 23/809 | HLA-H,KIR2DS2,IGLV6-57,IGLL5,FCGR3A,HRG,IGHA1,IGHD,IGHM,PRKCH,IGLL1,GBP1,LILRB1,HMSD,IGHV3-74,IGHV3-33,IGHV3-30,IGHV3-23,IGHV1-58,IGHV1-45,IGHV1-18,PSMB11,IFNL2 |

| | | | | | | |
|---|---|---|---|---|---|---|
| GO: Biological Process | GO:0009607 | response to biotic stimulus | 4.90E-06 | 1.36E-02 | 37/1741 | HLA-H,KIR2DS2,TRIM77,IGLL5,SERPINB4,HRG,FLT3,APOBEC3B,IFNA5,IGHA1,IGHD,IGHM,IGLL1,PRSS3,GBP6,PRTN3,GBP1,LILRB1,APOBEC3A,DEFA3,IGHV3-74,IL24,TRIM49,IGHV3-33,IGHV3-30,IGHV3-23,IGHV1-58,IGHV1-45,IGHV1-18,TRIM43,PSMB11,MIR708,DEFB133,RNASE3,PDE12,IFNL2,TRAV13-2 |
| GO: Biological Process | GO:0050907 | detection of chemical stimulus involved in sensory perception | 5.20E-06 | 1.45E-02 | 17/481 | OR2T12,OR2T34,TAS2R5,OR10A2,OR6C4,OR5H2,OR10H4,OR4K1,OR8G5,OR5K1,OR56B4,OR9A2,OR2AG1,OR5A2,OR8G1,OR51B6,OR2V2 |
| GO: Biological Process | GO:0050911 | detection of chemical stimulus involved in sensory perception of smell | 5.22E-06 | 1.45E-02 | 16/430 | OR2T12,OR2T34,OR10A2,OR6C4,OR5H2,OR10H4,OR4K1,OR8G5,OR5K1,OR56B4,OR9A2,OR2AG1,OR5A2,OR8G1,OR51B6,OR2V2 |
| GO: Biological Process | GO:0002253 | activation of immune response | 6.47E-06 | 1.80E-02 | 19/597 | KIR2DS2,IGLV6-57,IGLL5,FCGR3A,IGHA1,IGHD,IGHM,PRKCH,IGLL1,GBP1,HMSD,IGHV3-74,IGHV3-33,IGHV3-30,IGHV3-23,IGHV1-58,IGHV1-45,IGHV1-18,PSMB11 |
| GO: Biological Process | GO:0006909 | phagocytosis | 9.18E-06 | 2.55E-02 | 15/399 | IGLV6-57,IGLL5,FCGR3A,IGHA1,IGHD,IGHM,IGLL1,PRTN3,IGHV3-74,IGHV3-33,IGHV3-30,IGHV3-23,IGHV1-58,IGHV1-45,IGHV1-18 |
| GO: Biological Process | GO:0050906 | detection of stimulus involved in sensory perception | 1.24E-05 | 3.45E-02 | 18/569 | OR2T12,OR2T34,TAS2R5,SCN1A,OR10A2,OR6C4,OR5H2,OR10H4,OR4K1,OR8G5,OR5K1,OR56B4,OR9A2,OR2AG1,OR5A2,OR8G1,OR51B6,OR2V2 |
| GO: Biological Process | GO:0007608 | sensory perception of smell | 1.24E-05 | 3.46E-02 | 16/461 | OR2T12,OR2T34,OR10A2,OR6C4,OR5H2,OR10H4,OR4K1,OR8G5,OR5K1,OR56B4,OR9A2,OR2AG1,OR5A2,OR8G1,OR51B6,OR2V2 |
| GO: | GO:000959 | detection of | 1.44E-05 | 3.99E-02 | 17/520 | OR2T12,OR2T34,TAS2R5,OR10A2,OR6C4 |

| | | | | | | |
|---|---|---|---|---|---|---|
| Biological Process | 3 | chemical stimulus | | | | ,OR5H2,OR10H4,OR4K1,OR8G5,OR5K1,OR56B4,OR9A2,OR2AG1,OR5A2,OR8G1,OR51B6,OR2V2 |
| GO: Biological Process | GO:0002460 | adaptive immune response based on somatic recombination of immune receptors built from immunoglobulin superfamily domains | 1.78E-05 | 4.94E-02 | 15/422 | HLA-H,IGLV6-57,IGLL5,IGHA1,IGHD,IGHM,IGLL1,LILRB1,IGHV3-74,IGHV3-33,IGHV3-30,IGHV3-23,IGHV1-58,IGHV1-45,IGHV1-18 |
| GO: Cellular Component | GO:0042571 | immunoglobulin complex, circulating | 8.96E-12 | 2.74E-09 | 12/77 | IGLL5,IGHA1,IGHD,IGHM,IGLL1,IGHV3-74,IGHV3-33,IGHV3-30,IGHV3-23,IGHV1-58,IGHV1-45,IGHV1-18 |
| GO: Cellular Component | GO:0019814 | immunoglobulin complex | 8.08E-10 | 2.47E-07 | 14/167 | IGLV6-57,IGLL5,IGKV1D-42,IGHA1,IGHD,IGHM,IGLL1,IGHV3-74,IGHV3-33,IGHV3-30,IGHV3-23,IGHV1-58,IGHV1-45,IGHV1-18 |
| GO: Cellular Component | GO:0009897 | external side of plasma membrane | 1.63E-05 | 4.99E-03 | 16/480 | HLA-H,IGLL5,FCGR3A,FLT3,IGHA1,IGHD,IGHM,IGLL1,LILRB1,IGHV3-74,IGHV3-33,IGHV3-30,IGHV3-23,IGHV1-58,IGHV1-45,IGHV1-18 |
| GO: Cellular Component | GO:0045095 | keratin filament | 4.38E-05 | 1.34E-02 | 7/98 | KRTAP9-4,KRTAP5-8,KRT77,KRT6B,KRT7,KRT83,KRT75 |
| GO: Cellular Component | GO:0005882 | intermediate filament | 6.00E-05 | 1.84E-02 | 10/223 | KRTAP19-2,KRTAP19-4,KRTAP9-4,KRTAP5-8,KRT77,KRT6B,KRT7,KRT83,KRT75,EVPLL |
| Pathway | M14091 | Olfactory transduction | 2.60E-07 | 7.18E-05 | 16/389 | OR2T12,OR2T34,OR10A2,OR6C4,OR5H2,OR10H4,OR4K1,OR8G5,OR5K1,OR56B4,OR9A2,OR2AG1,OR5A2,OR8G1,OR51B6,OR2V2 |
| Pathway | M3468 | Genes encoding | 4.65E-05 | 1.28E-02 | 10/238 | ADAMTS19,SERPINB8,SERPINB3,SERPIN |

| | | | | | | |
|---|---|---|---|---|---|---|
| | | enzymes and their regulators involved in the remodeling of the extracellular matrix | | | | B4,HRG,SERPINA11,PRSS3,HMSD,P3H2, PCSK6 |
| Pubmed | 16381832 | miRBase: microRNA sequences, targets and gene nomenclature. | 5.14E-13 | 6.69E-09 | 49 | MIR526A1,MIR519D,MIR520D,MIR516A1, MIR545,MIR501,MIR3674,MIR1972-1,MIR3690,MIR550B1,MIR3163,MIR4266,MIR3130-2,MIR3649,MIR1229,MIR1252,MIR4309,MIR3122,MIR3142,MIR4432,MIR4330,MIR1972-2,MIR2682,MIR4255,MIR4644,MIR3074,MIR4803,MIR3191,MIR4771-1,MIR4493,MIR129-1,MIR126,MIR4710,MIR4791,MIR16-2,MIR4540,MIR4433A,MIR4527,MIR200A, MIR222,MIR32,MIR30D,MIR4771-2,MIR4530,MIR4655,MIR4501,MIR708,MIR617,MIR519E |
| Pubmed | 16407327 | APOBEC3A and APOBEC3B are potent inhibitors of LTR-retrotransposon function in human cells. | 5.00E-07 | 6.51E-03 | 3 | APOBEC3B,APOBEC3A_B,APOBEC3A |
| Pubmed | 17447845 | Population stratification of a common APOBEC gene deletion polymorphism. | 5.00E-07 | 6.51E-03 | 3 | APOBEC3B,APOBEC3A_B,APOBEC3A |
| Pubmed | 14983052 | The human olfactory receptor gene family. | 7.32E-07 | 9.54E-03 | 15 | OR2T12,OR2T34,OR10A2,OR6C4,OR5H2, OR10H4,OR4K1,OR8G5,OR5K1,OR56B4, OR9A2,OR2AG1,OR5A2,OR8G1,OR2V2 |
| Pubmed | 17604727 | A mammalian | 7.32E-07 | 9.54E-03 | 15 | MIR526A1,MIR519D,MIR520D,MIR516A1, |

| | | | | | | |
|---|---|---|---|---|---|---|
| | | microRNA expression atlas based on small RNA library sequencing. | | | | MIR545,MIR501,MIR129-1,MIR126,MIR16-2,MIR200A,MIR222,MIR32,MIR30D,MIR708,MIR519E |
| Pubmed | 18403710 | Evidence for editing of human papillomavirus DNA by APOBEC3 in benign and precancerous lesions. | 1.97E-06 | 2.57E-02 | 3 | APOBEC3B,APOBEC3A_B,APOBEC3A |

**Supplemental Table 2.12**: ToppGene gene ontology transcriptomic analysis of 72 hour 1 µM MGLL inhibitor, MJN110 treated HuH7.5s. Significance was assessed through the probability density function with the Bonferroni correction. p values < 0.05 are displayed.

| Category | ID | Name | p-value | q-value Bonferroni | Hit Count/ Genes in annotation | Hit in Query List |
|---|---|---|---|---|---|---|
| GO: Biological Process | GO:0035195 | gene silencing by miRNA | 1.65E-05 | 2.10E-02 | 12/719 | MIR520C,MIR302B,MIR520F,MIR302D,MIR519A1,MIR499B,MIR548H2,MIRLET7F1,MIR708,MIR19B2,MIR1265,MIR449A |
| GO: Biological Process | GO:0035194 | post-transcriptional gene silencing by RNA | 1.87E-05 | 2.37E-02 | 12/728 | MIR520C,MIR302B,MIR520F,MIR302D,MIR519A1,MIR499B,MIR548H2,MIRLET7F1,MIR708,MIR19B2,MIR1265,MIR449A |
| GO: Biological Process | GO:0016441 | posttranscriptional gene silencing | 2.00E-05 | 2.54E-02 | 12/733 | MIR520C,MIR302B,MIR520F,MIR302D,MIR519A1,MIR499B,MIR548H2,MIRLET7F1,MIR708,MIR19B2,MIR1265,MIR449A |
| GO: Biological Process | GO:0031047 | gene silencing by RNA | 2.61E-05 | 3.31E-02 | 12/753 | MIR520C,MIR302B,MIR520F,MIR302D,MIR519A1,MIR499B,MIR548H2,MIRLET7F1,MIR708,MIR19B2,MIR1265,MIR449A |
| Pubmed | 16381832 | miRBase: microRNA sequences, targets | 9.28E-09 | 2.94E-05 | 22/1918 | MIR4295,MIR520C,MIR302B,MIR520F,MIR302D,MIR4505,MIR519A1,MIR499B,MIR4438,MIR548H2,MIRLET7F1,MIR3911,MIR50 |

| | | | | | | |
|---|---|---|---|---|---|---|
| | | and gene nomenclature. | | | | 9-3,MIR708,MIR579,MIR1263,MIR19B2,MIR4326,MIR1265,MIR4709,MIR449A,MIR3689E |
| Pubmed | 17604727 | A mammalian microRNA expression atlas based on small RNA library sequencing. | 1.37E-07 | 4.33E-04 | 10/393 | MIR520C,MIR302B,MIR302D,MIR519A1,MIRLET7F1,MIR509-3,MIR708,MIR579,MIR19B2,MIR449A |
| Pubmed | 21037258 | miRBase: integrating microRNA annotation and deep-sequencing data. | 6.18E-07 | 1.96E-03 | 12/713 | MIR302B,MIR520F,MIR302D,MIR4505,MIR519A1,MIRLET7F1,MIR3911,MIR509-3,MIR19B2,MIR4326,MIR4709,MIR449A |
| Pubmed | 25238166 | Low expression of miR-449 in gynecologic clear cell carcinoma. | 7.42E-06 | 2.35E-02 | 2/2 | MIR302D,MIR449A |
| Pubmed | 28423501 | Epigenetic silencing of miR-520c leads to induced S100A4 expression and its mediated colorectal cancer progression. | 7.42E-06 | 2.35E-02 | 2/2 | MIR520C,S100A4 |
| Pubmed | 2034669 | Expression of growth/differentiation factor 1 in the nervous system: conservation of a bicistronic structure. | 7.42E-06 | 2.35E-02 | 2/2 | GDF1,CERS1 |
| Pubmed | 1704486 | Identification of a | 7.42E-06 | 2.35E-02 | 2/2 | GDF1,CERS1 |

| | | | | | | |
|---|---|---|---|---|---|---|
| | | novel member (GDF-1) of the transforming growth factor-beta superfamily. | | | | |
| Pubmed | 9872981 | Homologs of the yeast longevity gene LAG1 in Caenorhabditis elegans and human. | 7.42E-06 | 2.35E-02 | 2/2 | GDF1,CERS1 |

**Supplemental Table 2.13**: ToppGene gene ontology transcriptomic analysis of 72 hour 10 µM CB1 antagonist, AM251 treated HuH7.5s. Significance was assessed through the probability density function with the Bonferroni correction. p values < 0.05 are displayed.

| Category | ID | Name | p-value | q-value Bonferroni | Hit Count/ Genes in annotation | Hit in Query List |
|---|---|---|---|---|---|---|
| GO: Molecular Function | GO:0015175 | neutral amino acid transmembrane transporter activity | 5.32E-09 | 3.90E-06 | 8/36 | SLC7A11,SLC43A1,SLC1A4,SLC1A5,SLC3A2,SLC6A6,SLC6A9,SLC7A5 |
| GO: Molecular Function | GO:0015171 | amino acid transmembrane transporter activity | 3.62E-08 | 2.66E-05 | 10/84 | SLC7A11,SLC38A11,SLC43A1,SLC1A4,SLC1A5,SLC3A2,SLC6A6,SLC6A9,SLC7A1,SLC7A5 |
| GO: Molecular Function | GO:0046943 | carboxylic acid transmembrane transporter activity | 2.79E-07 | 2.05E-04 | 12/160 | SLCO1B3,AKR1C4,SLC7A11,SLC38A11,SLC43A1,SLC1A4,SLC1A5,SLC3A2,SLC6A6,SLC6A9,SLC7A1,SLC7A5 |
| GO: Molecular Function | GO:0005342 | organic acid transmembrane transporter activity | 2.99E-07 | 2.19E-04 | 12/161 | SLCO1B3,AKR1C4,SLC7A11,SLC38A11,SLC43A1,SLC1A4,SLC1A5,SLC3A2,SLC6A6,SLC6A9,SLC7A1,SLC7A5 |
| GO: Molecular Function | GO:0015179 | L-amino acid transmembrane transporter activity | 4.06E-07 | 2.98E-04 | 8/61 | SLC7A11,SLC43A1,SLC1A4,SLC1A5,SLC3A2,SLC6A9,SLC7A1,SLC7A5 |
| GO: | GO:0005319 | lipid transporter | 7.33E-07 | 5.38E-04 | 12/175 | SLCO1B3,AKR1C4,SLC7A11,TTPA,APOM, |

| | | | | | | |
|---|---|---|---|---|---|---|
| Molecular Function | | activity | | | | OSBPL10,ATP11A,GLTPD2,STARD4,SLC1A4,SLC1A5,SLCO2A1 |
| GO: Molecular Function | GO:0008514 | organic anion transmembrane transporter activity | 4.50E-05 | 3.30E-02 | 10/183 | SLCO1B3,SLC7A11,SLC1A4,SLC1A5,SLC3A2,SLC6A6,SLC6A9,SLC7A1,SLCO2A1,SLC7A5 |
| GO: Biological Process | GO:0089718 | amino acid import across plasma membrane | 3.49E-09 | 1.44E-05 | 9/48 | SLC7A11,SLC43A1,SLC1A4,SLC1A5,SLC3A2,SLC6A6,SLC6A9,SLC7A1,SLC7A5 |
| GO: Biological Process | GO:0043090 | amino acid import | 1.46E-08 | 5.99E-05 | 9/56 | SLC7A11,SLC43A1,SLC1A4,SLC1A5,SLC3A2,SLC6A6,SLC6A9,SLC7A1,SLC7A5 |
| GO: Biological Process | GO:0009636 | response to toxic substance | 5.35E-08 | 2.20E-04 | 16/257 | CYP1A1,CYP1B1,MAP1B,SLC7A11,TTPA,APOM,HP,SESN2,NR4A2,PON1,CPS1,ARG1,MT1B,ASNS,ASS1,CDH1 |
| GO: Biological Process | GO:0003333 | amino acid transmembrane transport | 3.16E-07 | 1.30E-03 | 10/103 | SLC7A11,SLC38A11,SLC43A1,SLC1A4,SLC1A5,SLC3A2,SLC6A6,SLC6A9,SLC7A1,SLC7A5 |
| GO: Biological Process | GO:0008202 | steroid metabolic process | 3.34E-07 | 1.37E-03 | 18/371 | CYP1A1,CYP1B1,CYP2B6,INSIG1,FAXDC2,GC,AKR1C4,SULT1B1,SULT2A1,UGT2B15,NR0B2,VLDLR,STARD4,PON1,SERPINA6,LRP1,HSD17B14,MVD |
| GO: Biological Process | GO:0006082 | organic acid metabolic process | 8.34E-07 | 3.43E-03 | 33/1130 | CYP1A1,CYP1B1,CYP2B6,CYP2C18,MTHFD2,INSIG1,GARS1,AKR1C4,SLC7A11,PHGDH,ADH6,SULT1B1,SARS1,SULT2A1,ALDH1L2,UGT2B15,SESN2,MCEE,GPT2,PNP,DDIT4,WARS1,STARD4,PON1,OAT,PPM1K,CPS1,ARG1,TRIB3,ASNS,ASS1,CTH,PCK2 |
| GO: Biological Process | GO:0015804 | neutral amino acid transport | 9.02E-07 | 3.71E-03 | 7/46 | SLC43A1,SLC1A4,SLC1A5,SLC3A2,SLC6A6,SLC6A9,SLC7A5 |
| GO: Biological Process | GO:1902475 | L-alpha-amino acid transmembrane transport | 1.26E-06 | 5.19E-03 | 8/69 | SLC7A11,SLC43A1,SLC1A4,SLC1A5,SLC3A2,SLC6A9,SLC7A1,SLC7A5 |
| GO: Biological | GO:0061107 | seminal vesicle development | 1.53E-06 | 6.29E-03 | 3/3 | SERPINE2,ID4,SERPINA5 |

| | | | | | | |
|---|---|---|---|---|---|---|
| Process | | | | | | |
| GO: Biological Process | GO:0015807 | L-amino acid transport | 1.57E-06 | 6.47E-03 | 8/71 | SLC7A11,SLC43A1,SLC1A4,SLC1A5,SLC3A2,ARG1,SLC7A1,SLC7A5 |
| GO: Biological Process | GO:0043436 | oxoacid metabolic process | 3.73E-06 | 1.53E-02 | 31/1098 | CYP1A1,CYP1B1,CYP2B6,CYP2C18,MTHFD2,INSIG1,GARS1,AKR1C4,SLC7A11,PHGDH,ADH6,SULT1B1,SARS1,SULT2A1,ALDH1L2,UGT2B15,SESN2,MCEE,GPT2,DDIT4,WARS1,STARD4,PON1,OAT,CPS1,ARG1,TRIB3,ASNS,ASS1,CTH,PCK2 |
| GO: Biological Process | GO:0006629 | lipid metabolic process | 3.73E-06 | 1.53E-02 | 38/1503 | B3GALT1,CYP1A1,SPTLC3,CYP1B1,CYP2B6,CYP2C18,PDGFA,INSIG1,FAXDC2,GC,AKR1C4,TTPA,APOM,ADH6,SULT1B1,SULT2A1,OSBPL10,UGT2B15,SESN2,MCEE,NR0B2,VLDLR,STARD4,SPTSSB,PON1,CPS1,SERPINA6,MBOAT4,TRIB3,MTM1,DGKK,AGMO,LRP1,SOCS1,FUT3,HSD17B14,PCK2,MVD |
| GO: Biological Process | GO:1901652 | response to peptide | 3.89E-06 | 1.60E-02 | 21/579 | IL18,MAP1B,INSIG1,FBN1,SESN2,KLF11,GDF15,NR4A2,CPS1,TFF1,ARG1,TRIB3,STC2,TIMP4,EIF4EBP1,ASS1,LRP1,SOCS1,ARHGEF2,PCK2,SOS1 |
| GO: Biological Process | GO:0019752 | carboxylic acid metabolic process | 5.57E-06 | 2.29E-02 | 30/1064 | CYP1A1,CYP1B1,CYP2B6,CYP2C18,MTHFD2,INSIG1,GARS1,AKR1C4,SLC7A11,PHGDH,ADH6,SARS1,SULT2A1,ALDH1L2,UGT2B15,SESN2,MCEE,GPT2,DDIT4,WARS1,STARD4,PON1,OAT,CPS1,ARG1,TRIB3,ASNS,ASS1,CTH,PCK2 |
| GO: Biological Process | GO:0006869 | lipid transport | 8.28E-06 | 3.40E-02 | 19/512 | SLCO1B3,AKR1C4,SLC7A11,TTPA,APOM,APOLD1,OSBPL10,ATP11A,GLTPD2,NR0B2,VLDLR,STARD4,PON1,SLC1A4,SLC1A5,SLCO2A1,APOL6,LRP1,SERPINA5 |
| GO: Biological Process | GO:1901615 | organic hydroxy compound metabolic process | 9.31E-06 | 3.83E-02 | 21/613 | CYP1A1,SPTLC3,CYP1B1,INSIG1,FAXDC2,GC,AKR1C4,SLC7A11,TTPA,ADH6,SULT1B1,SULT2A1,NR0B2,VLDLR,STARD4,MIOX,NR4A2,PON1,LRP1,PCK2,MVD |

| | | | | | | |
|---|---|---|---|---|---|---|
| GO: Biological Process | GO:1901653 | cellular response to peptide | 1.08E-05 | 4.44E-02 | 17/429 | IL18,MAP1B,INSIG1,FBN1,KLF11,GDF15,NR4A2,CPS1,ARG1,TRIB3,EIF4EBP1,ASS1,LRP1,SOCS1,ARHGEF2,PCK2,SOS1 |
| GO: Biological Process | GO:0006865 | amino acid transport | 1.16E-05 | 4.76E-02 | 11/187 | SLC7A11,SLC38A11,SLC43A1,SLC1A4,SLC1A5,SLC3A2,ARG1,SLC6A6,SLC6A9,SLC7A1,SLC7A5 |
| GO: Cellular Component | GO:0009986 | cell surface | 3.58E-05 | 1.51E-02 | 27/1053 | PDGFA,HLA-DRA,SLC7A11,PTGFRN,HAVCR1,SERPINE2,HRG,CCR6,CAPN5,IL17RB,VLDLR,NRCAM,ANPEP,IGHV1-45,CPM,SLC1A4,AREG,SLC3A2,IGHM,VCAN,CD38,LRP1,ULBP1,SLC7A5,CDH1,EPCAM,SERPINA5 |
| GO: Cellular Component | GO:0009925 | basal plasma membrane | 9.31E-05 | 3.94E-02 | 12/291 | SLCO1B3,SLC1A5,SLC3A2,SLC6A6,SLC6A9,SLC7A1,CD38,LRP1,SLC7A5,CDH1,EPCAM,ALPK2 |
| Mouse Phenotype | MP:0005308 | abnormal circulating ammonia level | 4.37E-07 | 1.15E-03 | 5.0/14 | CA5A,OAT,CPS1,ARG1,ASS1 |
| Mouse Phenotype | MP:0005309 | increased circulating ammonia level | 4.37E-07 | 1.15E-03 | 5/14 | CA5A,OAT,CPS1,ARG1,ASS1 |
| Mouse Phenotype | MP:0030604 | abnormal ammonia homeostasis | 4.15E-06 | 1.09E-02 | 5/21 | CA5A,OAT,CPS1,ARG1,ASS1 |
| Pathway | M39570 | Amino Acid metabolism | 5.30E-05 | 3.74E-02 | 8/91 | GPT2,WARS1,OAT,CPS1,ARG1,ASNS,ASS1,CTH |
| Pathway | M16794 | Metabolism of xenobiotics by cytochrome P450 | 6.91E-05 | 4.87E-02 | 7/70 | CYP1A1,CYP1B1,CYP2B6,CYP2C18,AKR1C4,ADH6,UGT2B15 |
| Pubmed | 18195088 | Amino acid transport across mammalian intestinal and renal epithelia. | 5.25E-11 | 1.50E-06 | 8/31 | SLC7A11,SLC43A1,SLC1A4,SLC1A5,SLC3A2,SLC6A6,SLC7A1,SLC7A5 |

| | | | | | | |
|---|---|---|---|---|---|---|
| Pubmed | 31789450 | Wnt regulates amino acid transporter Slc7a5 and so constrains the integrated stress response in mouse embryos. | 1.89E-09 | 5.42E-05 | 7/30 | DDIT3,ALDH1L2,CHAC1,SLC3A2,TRIB3,SLC7A5,PCK2 |
| Pubmed | 23376485 | Proteomic analysis of podocyte exosome-enriched fraction from normal human urine. | 2.64E-08 | 7.57E-04 | 36/1744 | IL18,HLA-DRA,GARS1,GC,CRISP3,PHGDH,APOM,ADH6,S100P,FBN1,HP,HRG,CAPN5,C7,DNASE2,PNP,MIOX,ANPEP,GDF15,PON1,CPM,MUC13,SERPINA6,OLR1,SLC3A2,ARG1,ELFN1,EFHD1,IGHM,MTM1,ASS1,CSTA,CDH1,EPCAM,SERPINA5,PCK2 |
| Pubmed | 16335952 | Human plasma N-glycoproteome analysis by immunoaffinity subtraction, hydrazide chemistry, and mass spectrometry. | 7.07E-08 | 2.02E-03 | 13/257 | F13B,APOM,HP,HRG,C4BPA,C7,NRCAM,ANPEP,PON1,SERPINA6,SLC3A2,LRP1,SERPINA5 |
| Pubmed | 26590417 | Establishment and Dysfunction of the Blood-Brain Barrier. | 1.08E-07 | 3.10E-03 | 7/52 | SLC1A4,SLC1A5,SLC6A6,SLC6A9,SLC7A1,LRP1,SLC7A5 |
| Pubmed | 27106802 | Embryonic cardiomyocytes can orchestrate various cell protective mechanisms to survive mitochondrial stress. | 7.84E-07 | 2.24E-02 | 5/24 | MTHFD2,DDIT3,CHAC1,TRIB3,ASNS |

| | | | | | | |
|---|---|---|---|---|---|---|
| Pubmed | 14760718 | Screening for N-glycosylated proteins by liquid chromatography mass spectrometry. | 1.24E-06 | 3.56E-02 | 6/47 | HP,C7,PON1,SERPINA6,IGHM,SERPINA5 |
| Pubmed | 23533145 | In-depth proteomic analyses of exosomes isolated from expressed prostatic secretions in urine. | 1.56E-06 | 4.46E-02 | 24/1070 | GC,AKR1C4,PHGDH,KRT24,SARS1,HP,ALDH1L2,HRG,CAPN5,C7,DNASE2,PNP,WARS1,ANPEP,GDF15,PON1,CPM,SERPINA6,SLC3A2,IGHM,CD38,ASS1,CDH1,SERPINA5 |
| Pubmed | 17197568 | Ornithine transport via cationic amino acid transporter-1 is involved in ornithine cytotoxicity in retinal pigment epithelial cells. | 1.56E-06 | 4.47E-02 | 3/4 | SLC3A2,SLC7A1,SLC7A5 |
| Pubmed | 18638388 | Association study of polymorphisms in the neutral amino acid transporter genes SLC1A4, SLC1A5 and the glycine transporter genes SLC6A5, SLC6A9 with schizophrenia. | 1.56E-06 | 4.47E-02 | 3/4 | SLC1A4,SLC1A5,SLC6A9 |
| Pubmed | 24816252 | An atlas of genetic influences on human blood metabolites. | 1.63E-06 | 4.66E-02 | 10/190 | SPTLC3,AKR1C4,PHGDH,SULT2A1,ANPEP,SH2B3,PPM1K,CPS1,SLC1A4,SLC7A5 |
| Disease | C0025517 | Metabolic Diseases | 7.97E-09 | 3.52E-05 | 33/937 | CYP1B1,CYP2B6,METTL3,IL18,CYP2C18,GC,APOM,FBN1,SAT1,HP,SESN2,MCEE,N |

| | | | | | | |
|---|---|---|---|---|---|---|
| | | | | | | R0B2,CA5A,PNP,DDIT4,KLF11,WARS1,ANPEP,GDF15,PON1,CPS1,MBOAT4,OLR1,ARG1,SLC6A9,KLF7,TRIB3,STC2,CD38,ASS1,GPR119,PCK2 |
| Disease | C0004153 | Atherosclerosis | 6.85E-08 | 3.03E-04 | 50/1998 | CYP1A1,NES,CYP2B6,IL18,PDE9A,PDGFA,MTHFD2,UNC5B,ADM2,GC,NR6A1,DDIT3,APOM,HAVCR1,FBN1,TSPAN31,SAT1,SULT2A1,HP,UCA1,SESN2,CCR6,NR0B2,PNP,VLDLR,FMOD,ANPEP,SH2B3,GDF15,PON1,OLR1,HEXIM1,SLC3A2,ARG1,TXNIP,TRIB3,STC2,MIR188,VCAN,ASS1,APOL6,LRP1,SOCS1,SLC7A5,CTH,FUT3,ARHGEF2,GPR119,MIR29B2,SOS1 |
| Disease | C0003850 | Arteriosclerosis | 1.71E-07 | 7.53E-04 | 49/1995 | CYP1A1,NES,CYP2B6,IL18,PDGFA,MTHFD2,UNC5B,ADM2,GC,NR6A1,DDIT3,APOM,HAVCR1,FBN1,TSPAN31,SAT1,SULT2A1,HP,UCA1,SESN2,CCR6,NR0B2,PNP,VLDLR,FMOD,ANPEP,SH2B3,GDF15,PON1,OLR1,HEXIM1,SLC3A2,ARG1,TXNIP,TRIB3,STC2,MIR188,VCAN,ASS1,APOL6,LRP1,SOCS1,SLC7A5,CTH,FUT3,ARHGEF2,GPR119,MIR29B2,SOS1 |
| Disease | C0023893 | Liver Cirrhosis, Experimental | 2.53E-07 | 1.12E-03 | 27/774 | IL18,PDGFA,GC,PLAC8,FBN1,SULT2A1,ALDH1L2,C7,NR0B2,INHBE,BMF,RCN1,ID4,OAT,R3HDM2,CPS1,SERPINA6,HEXIM1,SGK2,SLC7A1,TRIB3,ASNS,CD38,SOCS1,LTBP1,EPCAM,PCK2 |
| Disease | C0007222 | Cardiovascular Diseases | 3.26E-07 | 1.44E-03 | 41/1551 | CYP1A1,CYP1B1,NES,CYP2B6,IL18,CYP2C18,ADM2,GC,APOM,HAVCR1,FBN1,SAT1,HP,UCA1,SESN2,CAPN5,NR0B2,ANPEP,SH2B3,GDF15,NR4A2,PON1,PPM1K,OLR1,SLC1A5,ARG1,TXNIP,MT1B,SLC7A1,TRIB3,TIMP4,MIR188,VCAN,CD38,APOL6,LRP1,SOCS1,CTH,EPCAM,SERPINA5,SOS1 |
| Disease | C0085207 | Gestational Diabetes | 1.95E-06 | 8.60E-03 | 22/608 | CYP1B1,MIR518D,IL18,UNC5B,INSIG1,GC,PTGFRN,DDIT3,PLAC8,FBN1,TSPAN31,S |

| | | | | | | |
|---|---|---|---|---|---|---|
| | | | | | | AT1,HP,ANPEP,GDF15,PON1,OLR1,TXNIP,SLC7A1,MIR323B,MIR29B2,SOS1 |
| Disease | C0023418 | leukemia | 2.23E-06 | 9.85E-03 | 46/1984 | CYP1A1,CYP1B1,NES,CYP2B6,METTL3,IL18,UBE2L6,MTHFD2,BCRP3,AKR1C4,PTGER4,PHGDH,SULT2A1,HP,UCA1,C4BPA,CCR6,DDX43,NR0B2,PMAIP1,DDIT4,FMOD,ANPEP,SH2B3,ANKRD26,PON1,ID4,PPM1K,HEXIM1,PHC1,TXNIP,TRIB3,IGHM,FRZB,ASNS,CD38,EIF4EBP1,ASS1,LRP1,ULBP1,SOCS1,FUT3,CDH1,EPCAM,MIR29B2,SOS1 |
| Disease | C1956346 | Coronary Artery Disease | 2.82E-06 | 1.25E-02 | 38/1504 | CYP1A1,NES,CYP2B6,IL18,CYP2C18,PDGFA,MAP1B,MTHFD2,INSIG1,GC,DDIT3,APOM,SERPINE2,FBN1,HP,HRG,SESN2,PMAIP1,VLDLR,ANPEP,SH2B3,GDF15,PON1,CPS1,OLR1,TFF1,ARG1,TXNIP,TRIB3,TIMP4,LRP1,SOCS1,CTH,LTBP1,FUT3,ARHGEF2,SERPINA5,MVD |
| Disease | C0027051 | Myocardial Infarction | 3.68E-06 | 1.63E-02 | 39/1582 | CYP1A1,CYP1B1,NES,IL18,PDGFA,ADM2,GARS1,BACH1,GC,PTGER4,DDIT3,PHGDH,APOM,HAVCR1,FBN1,HP,HRG,SESN2,VLDLR,DDIT4,WARS1,ANPEP,SH2B3,GDF15,PON1,OLR1,AREG,ARG1,TXNIP,SLC6A6,TRIB3,TIMP4,MIR188,VCAN,EIF4EBP1,LRP1,SOCS1,SERPINA5,MIR29B2 |
| Disease | C0015695 | Fatty Liver | 6.36E-06 | 2.81E-02 | 24/757 | NES,IL18,INSIG1,GC,SLC7A11,APOM,HAVCR1,NR0B2,DNASE2,VLDLR,MIOX,ANPEP,NR4A2,PON1,PPM1K,SLC3A2,TXNIP,MT1B,STC2,ASS1,LRP1,SLC7A5,GPR119,PCK2 |
| Disease | C0011854 | Diabetes Mellitus, Insulin-Dependent | 6.44E-06 | 2.84E-02 | 37/1497 | NES,IL18,HLA-DRA,GC,PTGER4,APOM,HAVCR1,FBN1,SARS1,SAT1,HP,BTC,CCR6,GPT2,IL17RB,CA5A,DOC2B,DDIT4,WARS1,MIOX,ANPEP,SH2B3,GDF15,PON1,FHOD3,SERPINA6,TXNIP,SLC6A6,TRIB3,IGHM,VCAN,CD38, |

| | | | | | | |
|---|---|---|---|---|---|---|
| Disease | C1168401 | Squamous cell carcinoma of the head and neck | 8.94E-06 | 3.95E-02 | 37/1519 | LRP1,SOCS1,ARHGEF2,TUBE1,LINC00641 CYP1A1,SPTLC3,CYP1B1,IL18,PDGFA,SLCO1B3,SLC7A11,SERPINE2,TSPAN31,SAT1,HP,HRG,SESN2,PMAIP1,CHAC1,PNP,DDIT4,GDF15,NR4A2,OAT,SLC1A5,AREG,SLC3A2,ARG1,TXNIP,STC2,SLCO2A1,EIF4EBP1,CSTA,LRP1,ULBP1,SOCS1,SLC7A5,CDH1,EPCAM,SERPINA5,MVD |